HIGH-RESOLUTION THREE-DIMENSIONAL PLUME MODELING WITH EULERIAN ATMOSPHERIC CHEMISTRY AND TRANSPORT MODELS

A Dissertation
Presented to
The Academic Faculty

by

Fernando García Menéndez

In Partial Fulfillment
of the Requirements for the Degree
Doctor of Philosophy in the
School of Civil and Environmental Engineering

Georgia Institute of Technology
December, 2013

HIGH-RESOLUTION THREE-DIMENSIONAL PLUME MODELING WITH EULERIAN ATMOSPHERIC CHEMISTRY AND TRANSPORT MODELS

Approved by:

Dr. M. Talat Odman, Advisor
School of Civil and Environmental Engineering
Georgia Institute of Technology

Dr. Armistead G. Russell, Advisor
School of Civil and Environmental Engineering
Georgia Institute of Technology

Dr. Athanasios Nenes
School of Earth & Atmospheric Sciences
Georgia Institute of Technology

Dr. Michael H. Bergin
School of Civil and Environmental Engineering
Georgia Institute of Technology

Dr. Michael Chang
Brook Byers Institute for Sustainable Systems
Georgia Institute of Technology

Date Approved: August 7th, 2013

To Adriana,

ACKNOWLEDGEMENTS

I would like to express my very great appreciation to Dr. Talat Odman for his support and guidance throughout my doctoral studies. Participating in Dr. Odman's scientific research has been very rewarding and hopefully we will continue to collaborate in the future. I would also like to thank Dr. Ted Russell for his advising and the opportunity to join an excellent research group. Working alongside the members of the Russell group has been a great experience. I am particularly grateful for the help provided by Dr. Yongtao Hu. Additionally, I appreciate the valuable assistance of Dr. Michael Chang, Dr. Athanasios Nenes and Dr. Michael Bergin as members of the thesis committee. Finally, I would like to thank my family for their encouragement and love during these years.

TABLE OF CONTENTS

LIST OF TABLES

Page

LIST OF FIGURES

Page

SUMMARY

Eulerian chemical transport models are extensively used to steer environmental policy, forecast air quality and study atmospheric processes. However, the ability of these models to simulate concentrated atmospheric plumes, including fire-related smoke, may be limited. Wildland fires are important sources of air pollutants and can significantly affect air quality. Emissions released in wildfires and prescribed burns have been known to substantially increase the air pollution burden at urban locations across large regions.

Air quality forecasts generated with numerical models can provide valuable information to environmental regulators and land managers about the potential impacts of fires. Eulerian models present an attractive framework to simulate the transport and transformation of fire emissions. Still, the limitations inherent to chemical transport models when applied to replicate smoke plumes must be identified and well understood to adequately interpret results and further improve the models' predictive skills. Through this work, the capability of current chemical transport models to replicate fire-related air quality impacts was evaluated, key research needs to achieve effective simulations were identified, and numerical tools designed to improve model performance were developed.

A modeling framework centered on the Community Multiscale Air Quality modeling system (CMAQ) was used to simulate several fire episodes that occurred in the Southeastern U.S. and investigate the sensitivity of fine particulate matter concentration ($PM_{2.5}$) predictions to various model inputs and parameters. Significant uncertainties associated with fire emissions estimates and their distribution on gridded modeling domains were identified. $PM_{2.5}$ concentrations predicted by a regional-scale air quality

model in simulations attempting to replicate fire-related episodes were highly sensitive to plume rise and responsive to the horizontal and temporal distribution of fire emissions. In addition to realistic estimates of emitted mass, effectively modeling smoke transport with chemical transport models depends on an accurate spatiotemporal allocation of emissions. The predictions from a regional-scale air quality model also proved to be extremely sensitive to meteorological fields. Normalized errors in model predictions attempting to forecast the regional impacts of fires on $PM_{2.5}$ levels could be as high as 100% due to inaccuracies in wind data, suggesting that fire-related regional-scale air quality simulations are limited by the performance of existing numerical weather models.

To investigate the influence of grid resolution on model predictions, adaptive grid modeling is explored as a strategy to simulate fire-related plumes. An adaptive version of CMAQ, capable of dynamically restructuring the grid on which solution fields are estimated and providing refinement at the regions where accuracy is most dependent on resolution was developed. In an evaluation simulation aiming to reproduce smoke transport from two prescribed fires, the adaptive grid algorithm reduced artificial diffusion, produced better defined plumes and led to more accurate $PM_{2\,5}$ concentration predictions. Additionally, a three-dimensional adaptive grid algorithm capable of simultaneously refining horizontal and vertical grid resolution is presented. Extremely high levels of grid resolution can be achieved using this grid refinement method. The fully adaptive three-dimensional modeling technique can be applied to gain insight into plume dynamics unattainable with static grid models.

CHAPTER 1

INTRODUCTION

Atmospheric pollution is a major global concern. The most recent Global Burden of Disease Study finds that in 2010 over 3 million deaths and nearly 80 million disability-adjusted life-years were attributable to ambient particulate matter and ozone pollution (Lim et al., 2012). Accordingly, ambient particulate matter pollution ranked ninth among risk factors by attributable burden of disease in 2010. Multiple studies have identified associations between air pollution and increased mortality (Pope and Dockery, 2006). For instance, one study finds that a 10 $\mu g\ m^{-3}$ decrease in fine particulate matter concentration is associated with an increase in mean life expectancy of approximately 0.6 years (Pope et al., 2009). Furthermore, no consensus has been reached regarding the existence of a threshold for major pollutants under which concentrations would cease to have health effects (Brunekreef and Holgate, 2002).

Anthropogenic emissions have significantly increased the air pollution burden across vast regions, impacting public health and leading to a diverse set of problems which include damage to property, disruption of ecosystems and climate change. In response, legislation has been enacted throughout the world setting standards and regulations designed to limit the emissions of atmospheric pollutants and pollutant precursors and maintain pollution below concentrations selected to protect public health and welfare. In the United States, for example, the Clean Air Act was promulgated to protect air quality. The benefits and costs associated with implementing the legislation are significant. For the 1990 Clean Air Act Amendments alone, the annual costs and benefits of implementation, relative to a baseline maintained at the control levels defined by the 1970 and 1977 Clean Air Act Amendments, are estimated to reach approximately $65 billion and $2 trillion respectively in 2020 (2006 dollars) (U.S. Environmental

Protection Agency, 2011). Not surprisingly, extensive scientific research has centered on better understanding the sources, transport, and transformations of pollutants in the atmosphere.

The complexity of the physical processes and reaction kinetics associated with air pollution make its understanding highly dependent on computational models. Air quality modeling is the computational science of developing mathematical models that describe the behavior of pollutants in the atmosphere. Pollutants are emitted from various sources, including natural and anthropogenic. Once introduced into the atmosphere, they are subject to dynamics and chemistry that transport and transform them continuously. Among the transport processes are advection, turbulent diffusion, convection, and deposition. Transformation processes include gas and aqueous phase chemistry, phase changes, and particle nucleation and growth. Additionally, transformation processes can couple pollutants to each other and create secondary pollutants that are not emitted but formed in the atmosphere from other precursor species that are emitted. Air quality models aim to represent all these processes in the most comprehensive manner. Initially, analysis of control strategies designed to manage air quality stimulated the development of air quality models. However, at present air quality models serve much broader purposes and are vital to advance our understanding of atmospheric processes.

Different approaches exist to modeling air pollution, including Lagrangian dispersion models, Eulerian chemical transport models, and statistical receptor models. The applicability of each method depends on a simulation's scale, chemical species of interest, and computational resources. The transport and transformation of emissions are best described by Lagrangian or Eulerian models. Additionally, these models provide an opportunity to forecast the air quality resulting from specific emission scenarios, making them important tools in air quality management. Between them, Eulerian air quality models are the most powerful and least restricted by assumptions (Russell, 1997). They are also the most complex air quality models and have the highest computational demand.

However, as the power of computational systems has continued to escalate, most current operational photochemical air quality models have adopted the Eulerian framework and are capable of providing multi-pollutant predictions across complete regional domains. Today Eulerian regional air-quality models are extensively applied in North America and Europe to design environmental policy, generate air quality forecasts, and study atmospheric chemistry and processes (Rao et al., 2010).

Nevertheless, comprehensive Eulerian air quality models continue to be restricted by computational resources. Their limitations become apparent as simulations call for increasing levels of grid resolution to adequately replicate atmospheric phenomena. Computational requirements typically restrict regional-scale chemical transport models to a few kilometers. Still, emissions can be released by localized sources into concentrated plumes with dimensions below the grid resolutions typically used in chemical transport models. Eulerian air quality models have been applied to simulate concentrated plumes from a diverse set of emissions sources, including industrial point sources, biomass burning, dust and volcanoes, among others (e.g., Colette et al., 2011; Galanter et al., 2000; Tang et al., 2004; Zhou et al., 2012). In chemical transport models, the assumption of complete mixing within each grid cell may lead to artificial dilution and errors in chemical transformation rates. Upon injection into a coarse grid, small-scale features of pollutant plumes may be immediately lost. In spite of these shortcomings, the detailed treatments of atmospheric processes and spatiotemporal coverage available to Eulerian air quality models make gridded chemical transport models an attractive choice to simulate atmospheric plumes.

In this work, air quality simulations are undertaken to explore whether existing regional-scale chemical transport models operating with high spatial resolution are able to effectively replicate the transport and dispersion of atmospheric plumes without embedded subgrid scale models. Specifically, the study centers on smoke plumes from wildland fires. The influence of wildland fires on atmospheric pollutant concentrations

and the potential of fires to bring about acute air pollution episodes are further discussed in Chapter 2. Fire-related smoke plumes are an important example of an atmospheric phenomenon that involves relatively fine-scale characteristics and air quality impacts that may transition into larger, regional scales downwind. For emissions from industrial stacks, operational Eulerian grid models may offer subgrid scale plume treatments (Karamchandani et al., 2011). However, these are generally not available for fire-related plumes. In addition, as the resolution of current chemical transport models continues to increase, it may be possible to adequately simulate the transport and transformation of fire-related emissions within a single modeling framework without the restrictions imposed by embedded subgrid-scale models. Here, the ability of a present-day operational regional-scale air quality model to replicate smoke plumes is examined. Simulations of past air quality events and systematic evaluations of model predictions are discussed. Sources of uncertainty and important research needs to better replicate fire-related air quality impacts with regional Eulerian models are identified. Significant attention is given to the influence of spatial resolution in simulations focused on smoke plumes. A brief description of the objectives for each ensuing chapter is given below.

Chapter 2: Modeling smoke transport from wildland fires with chemical transport models

The modeling framework used to simulate the air quality impacts of wildland fires within this work is presented. Simulations aiming to reproduce smoke transport from fires are carried out to evaluate the modeling system described. The simulations cover particularly different spatial and temporal scales to assess the system's performance and diagnose modeling results. Important research needs to better simulate the air quality impacts of wildland fires with regional-scale Eulerian chemical transport models are identified.

Chapter 3: Simulating smoke transport from wildland fires with a regional-scale air quality model: sensitivity to spatiotemporal allocation of fire emissions

The sensitivity of fine particulate matter ($PM_{2.5}$) concentrations predicted with a regional-scale Eulerian air quality model to the spatial and temporal allocation of fire-related emissions is explored. A fire-related urban smoke event which severely impacted air quality throughout the Atlanta metropolitan area is simulated to assess the potential uncertainties associated with the distribution of fire emissions on gridded modeling domains. A series of sensitivity analyses were completed to evaluate the influence of emissions distributions among a model's vertical layers, along the horizontal plane, and into hourly inputs on predicted $PM_{2.5}$ concentrations at downwind locations.

Chapter 4: Simulating smoke transport from wildland fires with a regional-scale air quality model: sensitivity to uncertain wind fields

Within simulations attempting to reproduce smoke plumes with chemical transport models, the sensitivity of predicted $PM_{2.5}$ concentrations to wind field inputs is investigated. Using a simulation of the air quality impacts of two fires on an urban area, brute-force sensitivity analyses are undertaken to weigh the responsiveness of modeled pollutant concentrations to variations in wind speed and direction. Additionally, wind fields produced with the Weather Research and Forecasting model (WRF) are evaluated against surface and upper air meteorological observations to assess potential uncertainty in model predictions.

Chapter 5: Adaptive grid use in air quality modeling

Adaptive gridding as a strategy to improve the accuracy of air quality simulations with chemical transport models is reviewed. Reported adaptive grid methods in air quality models are analyzed and categorized. Common challenges faced by adaptive grid

algorithms and findings shared by developers are discussed. The use of adaptive grids in weather and climate models and connections to air quality modeling are also examined.

Chapter 6: An adaptive grid version of CMAQ for improving the resolution of plumes

An adaptive grid version of the Community Multiscale Air Quality Model (CMAQ) is presented. The adaptation algorithm used to achieve dynamic grid refinement is described and implementation into CMAQ's chemical transport model is discussed. The adaptive grid model is evaluated by simulating an air quality incident in which air quality at an urban location was impacted by a fire-related smoke plume. $PM_{2.5}$ concentrations predicted by adaptive and fixed grid simulations are compared to monitoring station observations during the incident.

Chapter 7: A **three-dimensional refinement adaptive grid algorithm for Eulerian air quality models**

A full three-dimensional adaptive grid algorithm intended for Eulerian regional-scale air quality models is introduced. The algorithm enables horizontal and vertical refinement of the modeling grid while retaining its original structure. Tests evaluating the functionality of the algorithm and exploring its potential to reduce numerical diffusion due to coarse grid resolution in chemical transport models are discussed. Recommendations to achieve full three-dimensional adaptation in existing operational air quality models are presented.

Chapter 8: Summary of conclusions and future research

The principal conclusions of the dissertation are summarized. Future research directions are identified and discussed.

1.1 References

Brunekreef, B., Holgate, S.T. (2002) Air pollution and health. Lancet 360, 1233-1242.

Colette, A., Favez, O., Meleux, F., Chiappini, L., Haeffelin, M., Morille, Y., et al. (2011) Assessing in near real time the impact of the April 2010 Eyjafjallajokull ash plume on air quality. Atmospheric Environment 45, 1217-1221.

Galanter, M., Levy, H., Carmichael, G.R. (2000) Impacts of biomass burning on tropospheric CO, NOx, and O3. Journal of Geophysical Research-Atmospheres 105, 6633-6653.

Karamchandani, P., Vijayaraghavan, K., Yarwood, G. (2011) Sub-Grid Scale Plume Modeling. Atmosphere 2, 389-406.

Lim, S.S., Vos, T., Flaxman, A.D., Danaei, G., Shibuya, K., Adair-Rohani, H., et al. (2012) A comparative risk assessment of burden of disease and injury attributable to 67 risk factors and risk factor clusters in 21 regions, 1990-2010: a systematic analysis for the Global Burden of Disease Study 2010. The Lancet 380, 2224-2260.

Pope, C.A., Dockery, D.W. (2006) Health effects of fine particulate air pollution: Lines that connect. Journal of the Air & Waste Management Association 56, 709-742.

Pope, C.A., Ezzati, M., Dockery, D.W. (2009) Fine-Particulate Air Pollution and Life Expectancy in the United States. New England Journal of Medicine 360, 376-386.

Rao, S.T., Galmarini, S., Puckett, K. (2010) Air Quality Model Evaluation International Initiative (AQMEII): Advancing the State of the Science in Regional Photochemical Modeling and Its Applications. Bulletin of the American Meteorological Society 92, 23-30.

Russell, A. (1997) Regional photochemical air quality modeling: Model Formulations, History, and State of the Science. Annual Review of Energy and the Environment 22, 537-588.

Tang, Y., Carmichael, G.R., Kurata, G., Uno, I., Weber, R.J., Song, C.-H., et al. (2004) Impacts of dust on regional tropospheric chemistry during the ACE-Asia experiment: A model study with observations. Journal of Geophysical Research: Atmospheres 109, D19S21.

U.S. Environmental Protection Agency, (2011) The Benefits and Costs of the Clean Air Act from 1990 to 2020. Office of Air and Radiation.

Zhou, W., Cohan, D.S., Pinder, R.W., Neuman, J.A., Holloway, J.S., Peischl, J., et al. (2012) Observation and modeling of the evolution of Texas power plant plumes. Atmospheric Chemistry and Physics 12, 455-468.

CHAPTER 2

MODELING SMOKE TRANSPORT FROM WILDLAND FIRES WITH CHEMICAL TRANSPORT MODELS

Abstract

Wildland fires can significantly deteriorate air quality and lead to unhealthy air pollution levels. Eulerian air quality models are an attractive option to simulate the impacts of fire-related emissions. A modeling framework to simulate the air quality impacts of fires based on the Community Air Quality modeling system is presented. The system's ability to replicate smoke transport is evaluated by simulating the emissions from a prescribed burn and a series of wildfires. Large discrepancies between predicted and observed pollutant concentrations indicate that ability of current regional-scale air quality modeling systems to forecast the impacts of fire-related smoke may be limited. Components of the modeling system significantly contributing to the error in model predictions are identified, including emission estimates, meteorological drivers, grid resolution, and plume rise representations.

2.1 Introduction

Wildland fires have been identified as important emissions sources which can significantly impact air quality (DeBell et al., 2004; Wotawa and Trainer, 2000). The emissions released by wildfires have been known to substantially increase the air pollution burden at urban locations across extensive regions downwind (Amiridis et al., 2012; Lee et al., 2005a; Miranda et al., 2009; Phuleria et al., 2005; Witham and Manning, 2007). Similarly, controlled prescribed burns can heavily influence local and regional air

---

*A part of this chapter has been published in *Modeling Smoke Plume-Rise and Dispersion from Southern United States Prescribed Burns with Daysmoke*, Atmosphere **2011**, 2, 358-388.

quality (Reisen et al., 2013; Zeng et al., 2008). The impacts of fires on atmospheric composition are apparent in the concentrations of trace gases and aerosols, including carbon monoxide, nitrogen oxides, ozone, black carbon, and particulate matter.

Increased pollution from wildland fires may pose a significant threat to public health. The adverse effects of smoke from wildfires and prescribed burns on air pollution concentrations and visibility have been investigated in several studies (Fox and Riebau, 2009; Johnston et al., 2012). Several epidemiological analyses exploring the health impacts of wildland fires have identified statistically significant associations between fire-related smoke and respiratory- and asthma-related hospital admissions (Kochi et al., 2010). The influence of fires on fine particulate matter ($PM_{2.5}$) concentrations deserves special attention; fire-related impacts on monitored air pollutants are strongest for $PM_{2.5}$ and may lead to unhealthy air quality (Delfino et al., 2009; Henderson et al., 2011; Rappold et al., 2011). Significant reductions to visibility brought about by wildland fires can also be important (Park et al., 2006; Wise, 2008).

Wildland fires can account for a substantial fraction of $PM_{2.5}$ pollution (Mueller and Mallard, 2011). In the U.S. for instance, Park et al. (2007) estimate that wildland fires contribute 10-24% of total $PM_{2.5}$ concentrations. Wildfires largely drive the variability in summertime organic carbon aerosol concentrations in the western U.S. (Spracklen et al., 2007). In the southeast U.S., prescribed burning can be a major contributor to $PM_{2.5}$ pollution (Tian et al., 2009). As air quality standards become more stringent and emissions from anthropogenic sources are better controlled, the significance of fires to air pollution concentrations is expected to grow. Furthermore, wildfire activity may strengthen under a changing climate. Studies suggest that a warmer and drier climate will increase the area burned by wildfires and their severity (Flannigan et al., 2005; Rogers et al., 2011; Westerling et al., 2011). As a result, considerable increases to organic and elemental carbon aerosol concentrations have been predicted to occur by midcentury as fire-related emissions intensify (Spracklen et al., 2009).

In the U.S., controlled forest fires, or prescribed burns, are used as a land management strategy. Prescribed burns are frequently carried out throughout the southeastern U.S. and have proven to be effective towards accomplishing different objectives, such as habitat restoration, wildfire prevention, endangered species protection, site preparation for seeding and planting, disease control, and appearance enhancement, among others. However, pollutants and pollution precursors emitted by prescribed burns may be transported and transformed, contributing to poor air quality at downwind urban areas. In the southeastern U.S., prescribed burns are a major source of primary $PM_{2.5}$ and gaseous pollutants (Lee et al., 2005b). The popularity of prescribed burning as a land management practice is also on the rise. Over the past ten years, more than 30% of the area burned by fires within the contiguous U.S. corresponded to prescribed burns (NIFC, 2013).

Air quality forecasts produced with numerical models can provide valuable information to environmental regulators and land-managers about the potential impacts of fires on pollutant concentrations. Commonly, fire-related smoke plumes have been simulated using various dispersion models. Simple Gaussian plume models have been developed to assist land managers in planning prescribed burns, such as VSMOKE and the Simple Approach Smoke Estimation Model (Lavdas et al., 1996; Riebau et al., 1988). Puff models, which simulate fire emissions as a series of continuously emitted parcels, can be used to model dispersion under space- and time-varying meteorological fields over detailed terrain. Calpuff is a widely used puff model that has been previously applied to simulate smoke transport (Henderson et al., 2010; Jain et al., 2007). The Hybrid Single Particle Lagrangian Integrated Trajectory Model (HYSPLIT) is a component of the Smoke Forecasting System used by the U.S. National Weather Service to produce daily smoke forecasts (Rolph et al., 2009). Additionally, Lagrangian particle models, such as FLEXPART, have been used to simulate fire pollution plumes (Lapina et al., 2008; Stohl

et al., 2006; Warneke et al., 2006). In this work, Daysmoke (Achtemeier et al., 2011), a Lagrangian particle model, is used to generate vertical plume structures.

While less commonly used than plume models, Eulerian chemical transport models are an attractive option to simulate the transport and transformation of fire emissions. The multiscale capabilities of gridded three-dimensional air quality models allow the transition of fire-related air pollution from local scales into larger regional scales to be adequately reproduced. Complex atmospheric transformations affecting fire emissions can be simulated through state-of-the science representations of chemical and physical processes included in chemical transport models. Additionally, comprehensive emissions inventories and weather inputs available for these models facilitate more representative reproductions of pollutants' interactions with complex meteorological fields and the background atmosphere. Simulations aimed at reproducing the effects of wildland fires with chemical transport models have been previously reported (Chen et al., 2008; Hodzic et al., 2007; Strand et al., 2012). Greater insight into the atmospheric transformation of fire-related emissions is often achieved with Eulerian air quality models.

However, there are limitations associated with applying the current generation of chemical transport models to simulate smoke transport and atmospheric plumes in general. A number of these stem from the coarse grid resolution normally used in gridded air quality models. Eulerian chemical transport models operate by dividing an atmospheric domain into a number of discrete cells and simulating atmospheric processes for every cell. Emissions are immediately diluted upon injection into a cell, potentially losing information about the subgrid-scale structure of a plume. As pollutants are dispersed within the modeling domain, coarse grid resolution causes numerical diffusion by uniformly mixing pollutants within each cell. The numerical diffusion can lead to a loss of accuracy in the nonlinear transformations included in the model. Processes occurring at scales smaller than those captured by grid resolution must be parameterized.

Additionally, plume-rise algorithms must be included to account for the buoyancy of fire-related emissions.

The objective of this chapter is to describe the modeling framework and process applied within this work to simulate the air quality impacts of wildland fires. The modeling system is evaluated by simulating fire plumes occurring on vastly different spatial and temporal scales. A diagnostic assessment of the modeling results is undertaken to better understand the system's ability to simulate regional-scale transport of fire-related smoke and identify important areas of research that must be investigated to attain accurate air quality forecasts with chemical transport models. Research needs identified are further explored in subsequent chapters.

2.2 Modeling Framework

In this section the components of the numerical modeling system used to carry out the simulations included in this work are briefly described. In simulations attempting to replicate the transport and transformation of fire-related emissions, multiple tools must be applied to model the processes related to the phenomenon, including pollutant emission rates, plume rise, meteorology, smoke transport, and emissions transformations. The tools included in the modeling framework described below vary in complexity and scope. However, each element models key processes that must be included in atmospheric simulations aimed at reproducing fire-related plumes. Figure 2.1 shows the most important modeling components applied, as well as their interconnections.

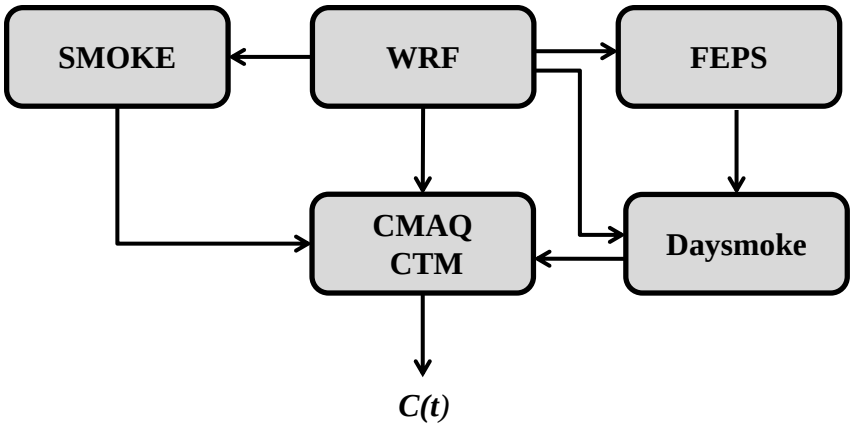

Figure 2.1. Major components of the modeling framework used to simulate fire-related emissions.

2.2.1 Community Multiscale Air Quality Modeling System

Air quality simulations undertaken as part of this work used the Community Multiscale Air Quality (CMAQ) modeling system (Byun and Schere, 2006). CMAQ is a third-generation air quality model maintained by the U.S. Environmental Protection Agency which has been widely applied for regulatory and policy analysis purposes, as well as atmospheric research. The principal components of the modeling system are a numerical weather prediction system, an emissions processor, and a chemical transport model. Meteorological and emissions fields generated by the system are used as inputs to CMAQ, which includes state-of-the-science representations of the chemical and physical processes that determine gaseous and particulate air pollutant concentrations. CMAQ considers several processes that are necessary to model the transport and transformation of fire-related emissions including three-dimensional advection and diffusion, atmospheric chemistry and aerosol dynamics. In addition, the system was designed with multiscale capabilities, enabling air quality simulations that range from urban to regional spatial scales and extend across a few days or multiple years.

2.2.2 Weather Research and Forecasting Model

The Weather Research and Forecasting Model (WRF) is a mesoscale numerical weather prediction system extensively used for atmospheric research and forecasting purposes (Skamarock et al., 2008). The model has been previously applied to simulate weather at scales varying from less than a kilometer to thousands of kilometers. The model is fully compressible and nonhydrostatic, and includes different physics options to simulate the planetary boundary layer, land-surface processes, atmospheric and surface radiation, microphysics, and cumulus convection. Meteorological fields produced with WRF are treated with interface processors to prepare CMAQ-ready inputs used to drive air quality modeling in the chemical transport model. In the past, the CMAQ modeling system has generally been operated using one-way coupling between WRF and the system's chemical transport model. Under this methodology, meteorological modeling is completed offline without feedback from the air quality simulations. In this work, atmospheric simulations were carried out using the traditional, one-way coupling approach. Recently, CMAQ version 5 was designed to allow online meteorological modeling by implementing two-way coupling between WRF and the system's chemical transport model (Wong et al., 2012). The ability to include the effects of atmospheric aerosol and gaseous concentrations estimated within CMAQ in WRF's numerical weather predictions may be of great interest in simulations attempting to replicate fire-related plumes and should be further explored.

2.2.3 Sparse Matrix Operator Kernel Emissions Modeling System

The Sparse Matrix Operator Kernel Emissions Modeling System (SMOKE) is a processor developed to simulate the emission rates used by Eulerian air quality models (Coats, 1996). In this work, SMOKE is used to process emissions from all sources with the exception of emissions released by the wildland fires specifically targeted in the simulations. Emissions considered by SMOKE include area, mobile, biogenic, and point

sources and are derived from emissions inventories and land use data. In addition, processing of biogenic emissions, mobile sources, and plume rise for point sources requires meteorological inputs, which are typically derived from the same weather fields used to drive the chemical transport model.

2.2.4 Fire Emission Production Simulator

The Fire Emission Production Simulator (FEPS) is an emissions model designed to replicate emissions, heat release, and fuel consumption patterns for prescribed burns and wildland fires (Anderson et al., 2004). FEPS can be used to generate hourly emission and heat release data from prescribed and wildland fires involving a large variety of forest, shrub, and grassland types. The model simualtes fire emission rates by processing user-supplied fire characteristics including burn area, fuel type, moisture, and weather. Fuels can be selected from a database of typical fuels included within the model. FEPS uses this data to estimate flaming and smoldering phase fire-related emissions, as well as fuel consumption rates. Although hourly emissions rates are only provided for a few pollutants (CO, CH_4, and $PM_{2.5}$), emission factors available for different species along with the fuel consumption estimates provided by FEPS can be used to calculate a larger array of fire-related emissions. In addition, plume rise is also calculated by the model based on theoretical and empirical formulations.

2.2.5 Daysmoke

Daysmoke is an empirical-statistical fire impact model developed by the U.S. Forest service to simulate plume rise and dispersion of smoke from prescribed burns (Achtemeier et al., 2011). Daysmoke simulates fire emissions as a series of dimensionless smoke particles, and uses an array of parameters to model their transport while attempting to capture the stochastic nature of the fire plume processes. The model relies on meteorological fields generated by a numerical weather prediction system and fire

emissions provided by an emissions processor. In addition, Daysmoke can be used as a subgrid-scale model to inject fire emissions into regional-scale chemical transport models. Here, smoke plume structures simulated by Daysmoke are used to vertically distribute fire-related emissions among the chemical transport model's vertical layers. Vertical smoke profiles are taken from Daysmoke after a plume reaches full development and used to inject and distribute fire-related emissions within the modeling domain at the appropriate locations and heights.

2.3 Smoke Plume Simulations

In this section, two simulations attempting to replicate smoke transport from wildland fires with an Eulerian chemical transport model are described. The simulations focus on smoke plumes from markedly different fires. The first simulation described below seeks to reproduce a single weak plume formed from a short-lived prescribed burn. The burn's impact on air quality is mostly local and relatively brief. In contrast, a simulation attempting to model a series of large wildfires which burned for over a month and consumed several thousand square kilometers was also completed. In this case, the fires affected air quality at regional scale and their impacts were observed throughout the southeastern U. S. The fire episodes were selected to evaluate CMAQ's multiscale abilities applied to reproduce smoke transport over significantly different temporal and spatial scales.

2.3.1 Fort Benning Prescribed Burn: April 9, 2008

In this air quality modeling application, the impacts of a prescribed burn at the Fort Benning, GA military base on $PM_{2.5}$ concentrations on April 9, 2008 are simulated. During this day, 300 acres of wildland were treated by prescribed burning. Ignition occurred at 12:30 local time (LT) and flaming lasted until 14:45 LT, smoldering emissions continuing thereafter. This episode is of special interest as a large increase in

$PM_{2.5}$ concentrations, likely due to the impact from the burn, was recorded at the Columbus, GA airport air quality monitoring site. The burning episode provides an opportunity to compare modeled results to pollutant concentrations observed at a regulatory air quality monitoring station.

Hourly emissions from the prescribed burn were estimated with FEPS, using information provided by land managers at the site. Non-fire emissions for the CMAQ simulation were prepared using SMOKE and a 2002 "typical year" emissions inventory (MACTEC, 2008) projected to 2008 using growth factors generated from the Economic Growth Analysis System (Bollman, 2001). Meteorological fields were generated using WRF at 1.33 km horizontal grid resolution and 34 vertical layers of increasing in depth from the surface upwards. Initialization, boundary conditions constraining, and nudging at 6-hour intervals were performed using analysis products from the North American Mesoscale (NAM) model. The CMAQ domain covered 120 × 124 km over southwestern Georgia and southeastern Alabama with 1.33 km horizontal grid spacing and 34 vertical layers, analogous to the meteorological modeling.

Daysmoke simulations were undertaken using 6 updraft cores. For injection into CMAQ, the plume profile estimated by Daysmoke 4 km downwind of the fire was used to vertically distribute fire emissions at the location of the fire within the CMAQ domain. This downwind distance provided sufficient time for full plume development without becoming excessively separated from the source (3 grid cells downwind). The vertical distribution of $PM_{2.5}$ fire emissions for the entire episode is shown in Figure 2.2. The largest fraction of emissions is injected into layer 8, which ranges from approximately 500 to 680 m above the ground. Nearly 70 % of fire emissions were distributed into layers 6, 7, and 8, extending from 335 to 680 m above the ground.

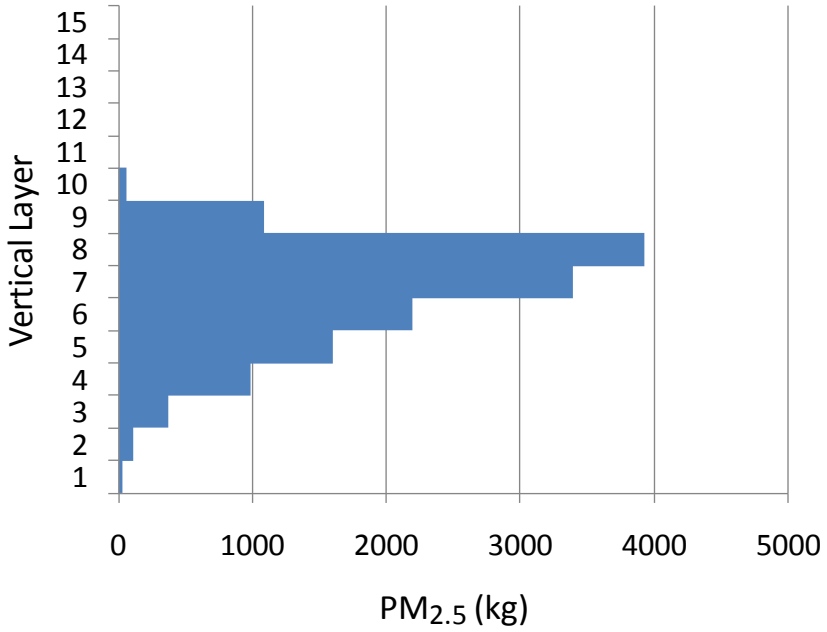

Figure 2.2. Vertical distribution of prescribed burn $PM_{2.5}$ emissions by layer used in CMAQ simulations.

Figure 2.3 shows the evolution of CMAQ-predicted $PM_{2.5}$ concentrations at the Columbus Airport monitoring site, 30 km from the location of the prescribed burn, along with the station's recorded pollutant concentrations. A sharp increase in $PM_{2.5}$ concentration is apparent from the observations after 17:00 LT. Similarly, a rapid increment is evident in the concentration predictions, although occurring at an earlier time. CMAQ overestimates the maximum $PM_{2.5}$ concentration by approximately 4 µg m^{-3}. A mismatch in the timing of observed and modeled peak pollutant concentrations is also clear. The fact that emissions estimates generated by FEPS are hourly, while in reality fire ignition occurred 30 minutes past 12:00 LT, may partially explain the discrepancy.

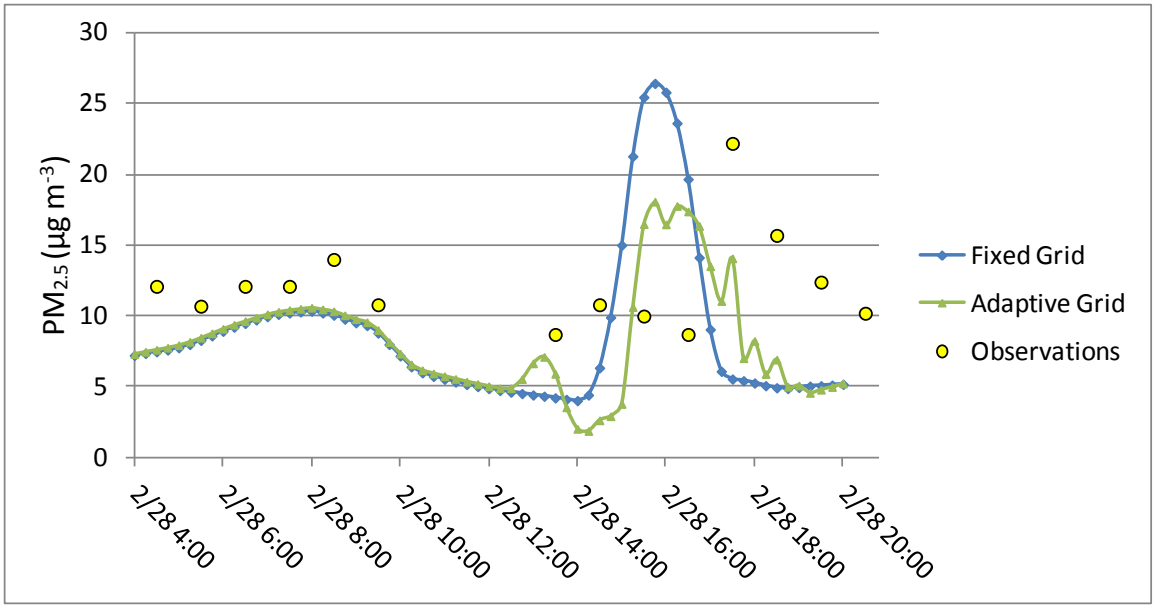

Figure 2.3. Hourly averaged $PM_{2.5}$ concentrations (µg m^{-3}) observed at the Columbus airport air quality monitoring site and predicted by fixed and adaptive grid CMAQ simulations on April 9, 2008 (LT).

A major concern related to modeling atmospheric plumes with chemical transport models is the adequacy of a model's spatial resolution to simulate the phenomenon. As plumes are transported within gridded modeling domains, emissions are numerically diluted due to coarse grid resolution and the assumption of perfect mixing within each cell's volume. Here, a simulation completed with an adaptive grid algorithm in CMAQ was carried out to assess the influence of horizontal grid resolution on concentration predictions. The adaptive grid version of CMAQ is described in depth in Chapter 5. In brief, the algorithm is designed to dynamically increase grid resolution at the locations by clustering grid nodes at the locations where solution accuracy most heavily depends on grid spacing. By doing so, grid resolution in the vicinity of the smoke plume targeted by the simulation is refined well below 1 km.

Concentration predictions generated with the adaptive grid are included in Figure 2.3 along with the results of the 1.33 km fixed grid simulation. Although at 1.33 km grid spacing the fixed grid simulation was carried out using a resolution close to the finest

resolutions typically applied in CMAQ, significant differences are apparent between the static and adaptive simulations. The finest horizontal resolution attained by the adaptive grid was approximately 100 m. In contrast to the fixed grid prediction, the adaptive grid simulation, underestimates the maximum $PM_{2.5}$ concentration at the Columbus airport with respect to observations, although the magnitude of the error is similar for both simulations. However, modeled $PM_{2.5}$ concentrations fall abruptly after peaking in the static grid simulation, while the decrease is gentler when the adaptive grid is applied and more closely resembles the observations. Overall, the mean fractional error in the modeled results relative to station observations was reduced by 17 % with the adaptive grid compared to the fixed grid simulation.

A better understanding of the modeling results can be attained by visualizing pollutant concentration fields for each simulation. The $PM_{2.5}$ surface-level concentration fields depicted in Figure 2.4 correspond to the time when maximum concentrations were predicted at the Columbus airport by both simulations. The smoke plume generated by the static grid simulation undergoes greater diffusion compared to the one obtained using grid adaptation. It is also apparent that the predicted impact at the airport site is not direct, but rather a tangential plume hit. In the adaptive grid simulation, the $PM_{2.5}$ concentration field displays a concentrated smoke plume with high concentrations at the plume's core persisting longer into the simulation. Figure 2.5 further contrasts the plumes produced with static and adaptive grids. The iso-surfaces included in Figure 2.5, show three-dimensional plume volumes defined by $PM_{2.5}$ concentrations equal to 30 $\mu g\ m^{-3}$. The viewer position has been rotated in the figure to better appreciate the plume volumes. The three-dimensional visualizations reflect the differences in plume structure brought about by significantly increasing grid resolution beyond the levels typically applied to regional-scale chemical transport models.

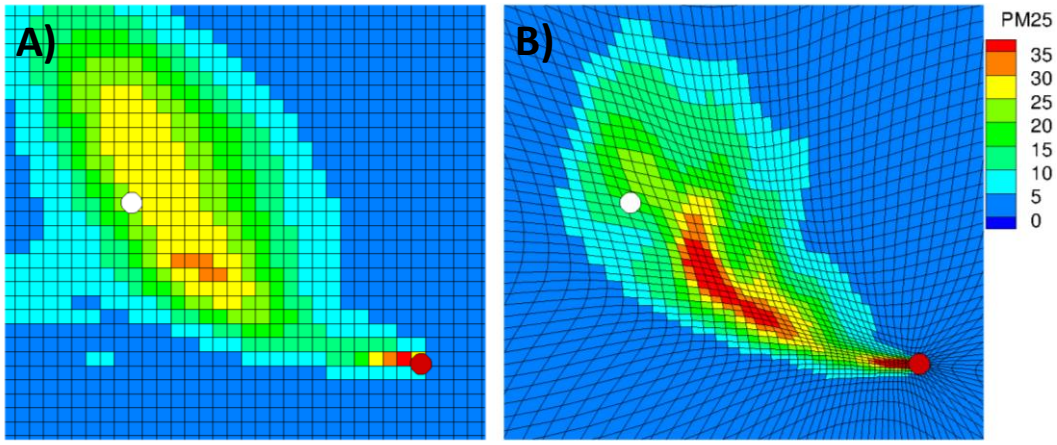

Figure 2.4. CMAQ-predicted $PM_{2.5}$ concentrations (μg m^{-3}) on April 9, 2008 at 15:45 LT generated using (A) 4-km fixed grid CMAQ simulation; and (B) adaptive grid CMAQ simulation. Locations of the prescribed fire at Ft. Benning and the Columbus airport air quality monitoring site are indicated by red and white circles respectively.

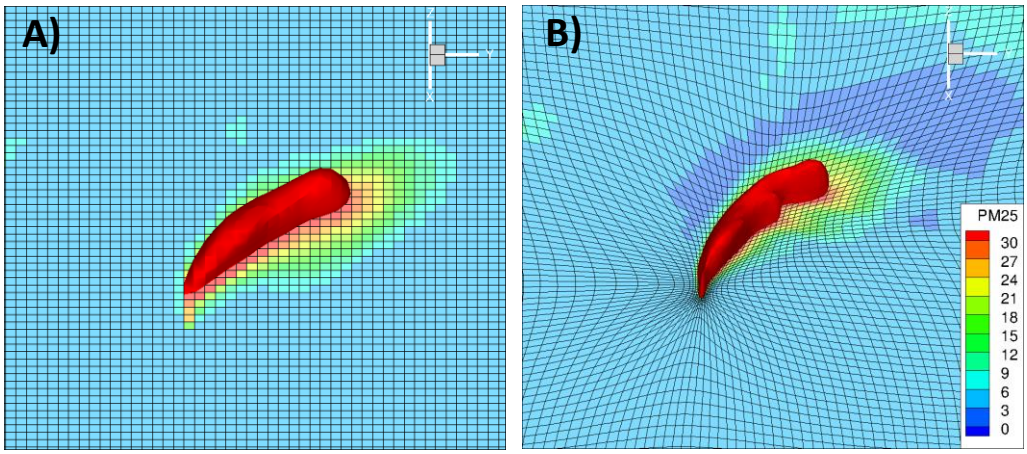

Figure 2.5. Three-dimensional iso-surfaces defined by $PM_{2.5}$ concentration equal to 30 μg m^{-3} on April 9, 2008 at 15:15 LT generated using (A) 4-km fixed grid CMAQ simulation and (B) adaptive grid CMAQ simulation.

2.3.2 Georgia-Florida Wildfires: May, 2007

The simulation described in this section attempts to model smoke transport from a series of wildfires which occurred in southeast Georgia and northeast Florida during the spring of 2007. The wildfires burned for several months, beginning as two separate fires in Georgia and Florida which converged and became the Georgia Bay Complex. The

magnitude of the wildfires was unprecedented in these states, burning over 500,000 acres (GFC, 2007). Severe drought and excessive accumulation of forest fuels led to favorable fire conditions. The event would later prompt wider use of prescribed burning, such as the fire described in section 2.2.1, as a land management strategy to reduce the risk of uncontrolled wildfires. Smoke from the fires impacted air quality at urban areas throughout Georgia, Alabama, and Florida, leading to health warnings and road closures.

In contrast to the Fort Benning prescribed burn simulation previously discussed, the simulation attempting to model the smoke plumes from the Georgia-Florida wildfires of 2007 involved significantly larger spatial and temporal scales. CMAQ was used to model air quality across the southeastern U.S. during the entire month of May. A nested domain covering the state of Georgia and fractions of Florida, Alabama, and South Carolina was used to simulate smoke transport using 4 km horizontal grid resolution. As in the Fort Benning simulation, emissions from all sources other than the wildfires of interest were estimated through SMOKE and a projected 2002 "typical year" emissions inventory. Meteorological fields were prepared with WRF using 4 km grid resolution and 34 vertical layers. Due to the characteristics and extent of the wildfires, modeling fire emissions and plume rise with FEPS and Daysmoke was unfeasible. Here wildfire emissions were estimated using the Satellite Mapping Automated Reanalysis Tool for Fire Incident Reconciliation (SMARTFIRE) information system and the Bluesky modeling framework (Sullivan et al., 2008). SMARTFIRE combines fire-related field observations with satellite-derived fire data to estimate burn areas and locations which were processed with the Bluesky framework to quantify pollutant emissions.

To assess CMAQ's ability to simulate smoke transport from the Georgia-Florida wildfires, a series of stations in which air quality recorded by observational networks at urban locations was clearly impacted by fire-related emission were selected to evaluate and diagnose model performance. The episodes selected include smoke-related air quality impacts recorded at Macon, Atlanta, and Savannah in Georgia, as well as Birmingham,

Alabama. During these days maximum hourly $PM_{2.5}$ concentrations recorded at air quality monitoring stations within these cities ranged from 80 to 340 µg m^{-3}. Figure 2.6 shows the date and location of the periods selected for model evaluation along with peak $PM_{2.5}$ concentrations observed and the approximate location of the Georgia Bay Complex.

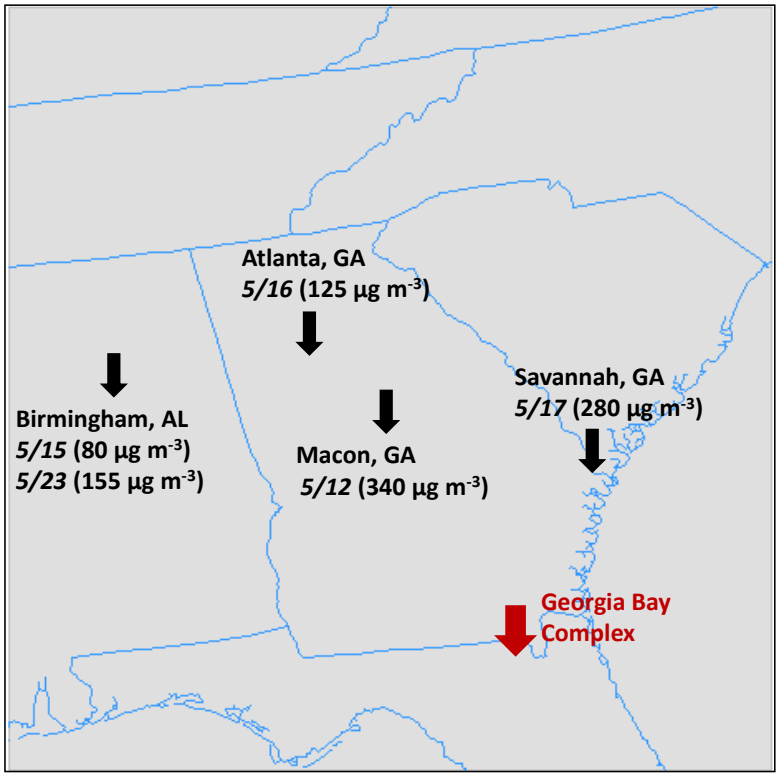

Figure 2.6. Location of Georgia Bay Complex and urban smoke episodes selected for model evaluation. Incident dates and maximum observed hourly $PM_{2.5}$ concentrations are also included.

Figure 2.7 shows the surface-level $PM_{2.5}$ concentrations predicted by CMAQ on May 17th at the time high $PM_{2.5}$ concentrations were observed in Savannah. During this period, a smoke plume extending from the location of the wildfires to the city of Savannah is apparent in the modeled pollutant concentrations. Moreover, the simulated smoke plume followed a trajectory corresponding to the increase in pollutant concentrations observed within the city. Similarly, for most of the smoke episodes

analyzed, CMAQ produced relatively accurate plume trajectories, predicting well-timed hits at the expected locations. However, the Macon, GA incident on May 12 was an exception. On this day the simulation did not predict any significant impact on pollutant concentrations that would match the increase in observed $PM_{2.5}$ concentrations of almost 350 µg m^{-3}. In this case, the trajectory traveled by the smoke plume narrowly missed the city of Macon.

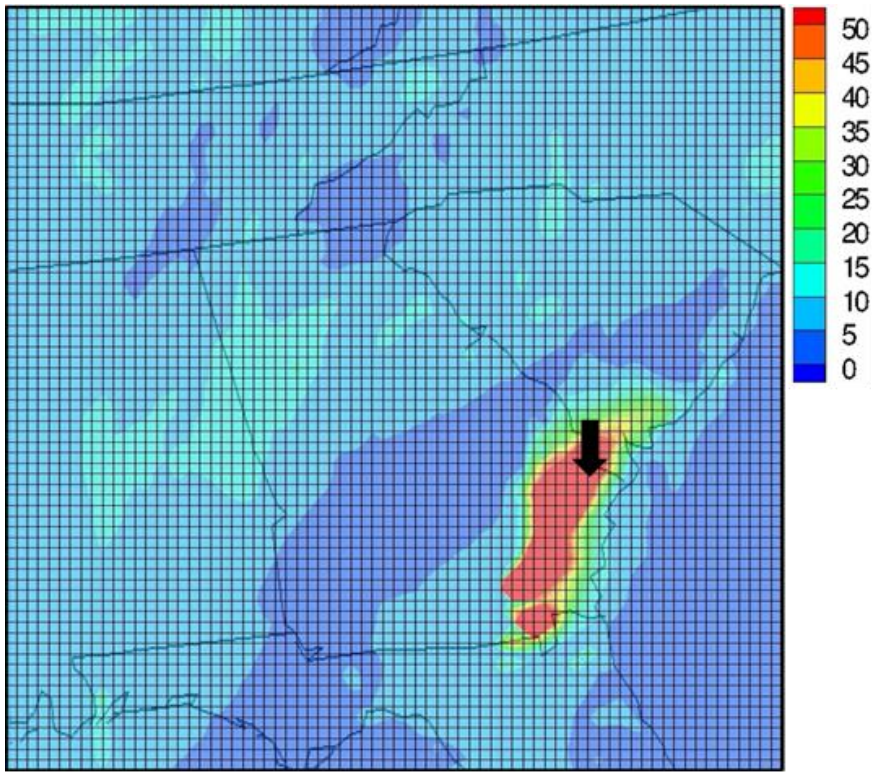

Figure 2.7. Predicted surface-level $PM_{2.5}$ concentrations (µg m^{-3}) over the southeastern U.S. during the Savannah smoke incident of May 17, 2007 at 14:00 LT. The location of Savannah is indicated by the black marker.

Although CMAQ-predicted smoke trajectories largely agreed with the timing of recorded peaks in monitored pollutant concentrations, the simulation usually underestimated the maximum $PM_{2.5}$ impacts. Figure 2.8 shows CMAQ-predicted and observed $PM_{2.5}$ concentrations at Savannah on May 17. Compared to observations, simulated concentrations reflect a substantial underestimation of high pollutant concentrations at Savannah. In all smoke incidents analyzed, peak $PM_{2.5}$ concentrations

were significantly underestimated by the model. Additionally, the discrepancies between observed and modeled concentrations heightened as distance between the wildfires and receptors increased.

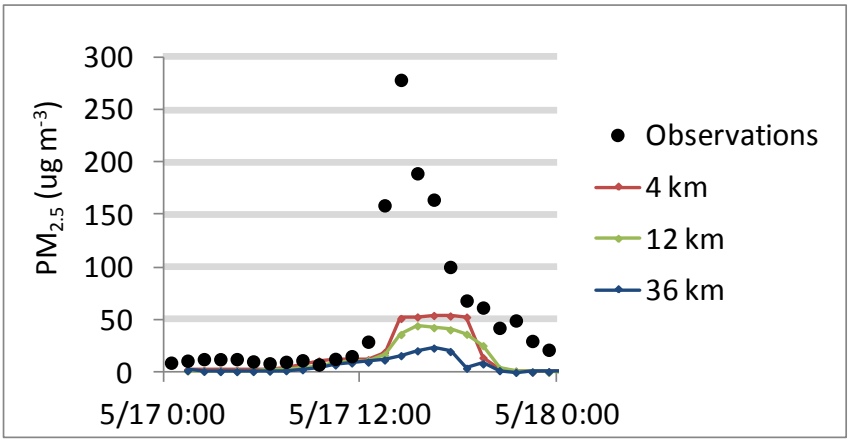

Figure 2.8. Hourly $PM_{2.5}$ concentrations observed and predicted by CMAQ with 4, 12, and 36 km resolutions at the Savannah-Lathrop Monitoring Site on May 17, 2007 (UT).

To assess the influence of grid resolution on modeled concentrations, predictions from the 4 km simulation were compared to those obtained using 12 and 36 km grid spacing. Figure 2.8 includes $PM_{2.5}$ concentrations simulated at each level of horizontal grid resolution and exposes a significant sensitivity in CMAQ predictions to grid spacing. At Savannah, the maximum $PM_{2.5}$ concentrations predicted using a 4 km grid was over twice as large as that produced under 36 km resolution. In all smoke episodes explored, significant sensitivity in concentration predictions to grid resolution was demonstrated. In general, higher resolution led to less diffusion, better structured plumes, and higher pollutant concentrations.

Three-dimensional visualization of modeled plumes reveals additional details related to smoke transport in the simulations. Figure 2.9A shows the structure of the plume that impacted air quality in Savannah on May 17 when the maximum $PM_{2.5}$ concentration was observed within the city. In Figure 2.9, smoke plumes are depicted as

iso-surfaces defined by $PM_{2.5}$ concentrations equal to 50 µg m^{-3}. The visualization shows that during the Savannah incident a significant fraction of the fire-related $PM_{2.5}$ is transported aloft in the models upper layers. Surface concentrations were unaffected by a substantial amount of $PM_{2.5}$ concentrated at higher altitudes. Similarly, the visualization of the smoke plume that impacted air quality in Atlanta on May 16 (Figure 2.9B) exposes significant $PM_{2.5}$ transport within the model's upper layers. During the Macon and Birmingham episodes, only weak and highly diffused smoke plumes were present in the simulation. In these cases, the three-dimensional visualizations of smoke transport suggest an underestimation of fire-related emissions.

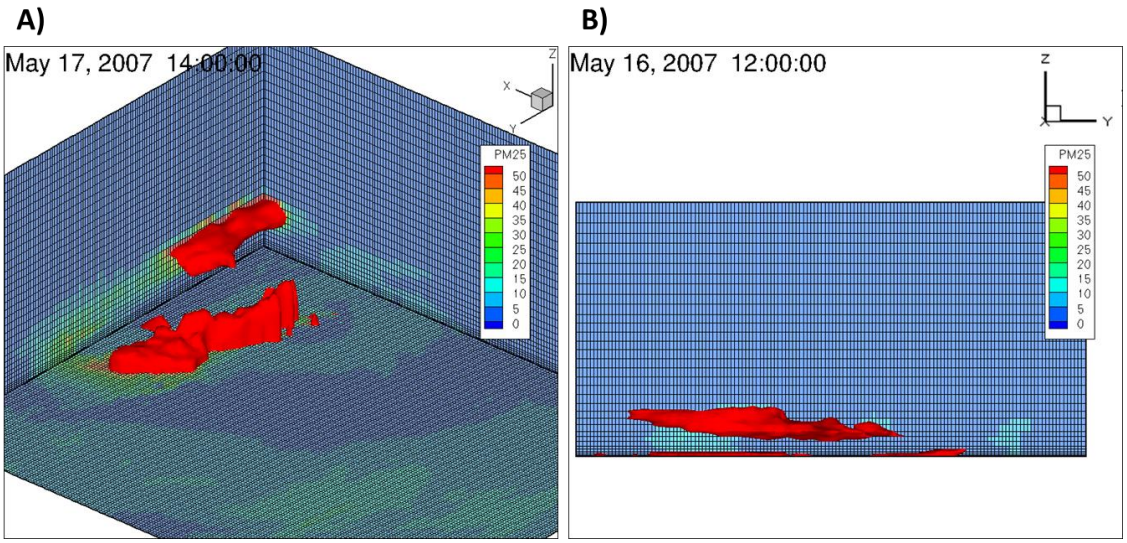

Figure 2.9. Three-dimensional iso-surfaces defined by $PM_{2.5}$ concentration equal to50 µg m^{-3}: (A) Savannah smoke incident of May 17, 2007 and (B) Atlanta smoke incident of May 16, 2007. Viewer position is from the upper north-west corner of the domain in (A) and from the eastern domain boundary in (B).

2.4 Discussion

At a local-scale, the modeling system was able to predict the impact of a single prescribed burn smoke plume on air quality at a downwind receptor with reasonable accuracy. However, when applied to simulate regional-scale smoke transport from multiple wildfires over a prolonged period the system did not perform as well for

simulating air quality. Specifically, CMAQ severely underestimated the impact of wildfires on $PM_{2.5}$ concentrations at urban locations downwind. Similarly,Yang et al. (2011) found in their simulation of the 2007 Georgia-Florida wildfires that CMAQ was able to capture smoke transport reasonably well but systematically underestimated observed $PM_{2.5}$ concentrations during the fires. Several elements of the modeling system likely contribute to the underprediction of pollutant concentrations. However, in the Georgia Bay Complex simulation weak plumes and large discrepancies between modeled and observed $PM_{2.5}$ concentrations strongly suggest a significant underestimation of fire-related emissions in the satellite-derived estimates. Emission rates generated by fire emission processors such as FEPS seem more reliable but require a substantial amount of information describing a fire's characteristics and may be limited to smaller and better controlled events. In addition, studies have recommended the inclusion of fire-related secondary organic aerosol production in air quality simulations (Lee et al., 2008). However, improved emissions estimates of secondary organic aerosol precursors and formation mechanisms are needed to realistically simulate the process within the model.

The simulated plumes also reflect the importance of meteorological drivers in modeling applications attempting to reproduce the transport of fire-related smoke. The influence of wind fields on predicted pollutant concentrations is evident in the long-range transport of fire-relate emissions within the Georgia-Florida wildfires simulation. Although predicted smoke trajectories agreed with observed concentration peaks during most of the urban air quality incidents explored, in at least one of the locations selected sizable discrepancies between observed and modeled pollutant concentrations seem to be mainly attributable to errors in wind-driven smoke transport. Even at considerably smaller spatial and temporal scales, such as those pertaining to the Fort Benning simulation, a strong influence of meteorological inputs on air quality modeling results is apparent; the severity of predicted impacts at downwind receptors is largely dependent on the meteorological fields used to drive dispersion. If models are used to forecast fire-

related air quality, it is important to recognize that the ability of chemical transport models to predict the air quality impacts of wildland fires is significantly constrained by the uncertainties inherent to numerical weather modeling. Additionally, the vertical distribution of fire emissions appears to be an essential component of air quality simulations centered on smoke transport. Plume rise has been previously identified as an important model input (Liu et al., 2008). Subgrid scale models may be a practical method to vertically allocate buoyant emissions in chemical transport models operating on predetermined flow fields. The accumulation of fire-related emissions above the atmospheric boundary layer observed in the Georgia-Florida wildfires simulation signals a need to accurately represent the vertical structure of smoke plumes and the fraction of emissions penetrating into the free troposphere.

Finally, the effect of grid resolution on predicted pollutant concentrations was demonstrated in both simulations. By increasing horizontal grid resolution, simulated plumes from the Georgia Bay Complex were subjected to significantly less numerical diffusion and produced substantially larger air quality impacts at downwind receptors. The influence of grid resolution was also appreciable at a local scale in the prescribed burn plume simulation. In this case, a fixed grid simulation was carried out at relatively fine resolution. Still, the air quality predictions obtained at higher resolution through an adaptive grid proved to be appreciably different to those estimated under a 1.33 km grid.

The results of the simulations included in this chapter and the performance of the modeling system call for additional research exploring the sources of error and uncertainty in fire-related simulations with Eulerian regional-scale models. Key features of the modeling process used to simulate the impacts of fires on air quality identified from the simulations described herein are further explored in subsequent chapters. Chapter 3 centers on fire-related emissions and specifically analyzes the spatiotemporal allocation of emissions on gridded domains, including representations of plume rise. Chapter 4 explores the sensitivity of model predictions to meteorological fields in the

context of fire-related air quality modeling. Chapter 6 describes the development of the adaptation algorithm used to carry out the adaptive grid simulation described in Section 2.2.1 and further explores the influence of grid resolution in atmospheric simulations of smoke plumes from wildland fires.

2.5 References

Achtemeier, G.L., Goodrick, S.A., Liu, Y., Garcia-Menendez, F., Hu, Y., Odman, M.T. (2011) Modeling smoke plume-rise and dispersion from southern United States prescribed burns with Daysmoke. Atmosphere 2, 358-388.

Amiridis, V., Zerefos, C., Kazadzis, S., Gerasopoulos, E., Eleftheratos, K., Vrekoussis, M., Stohl, A., Mamouri, R.E., Kokkalis, P., Papayannis, A., Eleftheriadis, K., Diapouli, E., Keramitsoglou, I., Kontoes, C., Kotroni, V., Lagouvardos, K., Marinou, E., Giannakaki, E., Kostopoulou, E., Giannakopoulos, C., Richter, A., Burrows, J.P., Mihalopoulos, N. (2012) Impact of the 2009 Attica wild fires on the air quality in urban Athens. Atmospheric Environment 46, 536-544.

Anderson, G., Sandberg, D., Norheim, R. (2004) Fire Emission Production Simulator (FEPS) User's Guide (version 1.0). Prepared by the USDA Forest Service, Pacific Northwest Research Station, Seattle, WA.

Bollman, A.D., and G. M. Stella, (2001) Economic Growth Analysis System (EGAS) Version 4.0, International Emission Inventory Conference: One Atmosphere, One Inventory, Many Challenges, Denver, Colo.

Byun, D., Schere, K.L. (2006) Review of the governing equations, computational algorithms, and other components of the models-3 Community Multiscale Air Quality (CMAQ) modeling system. Applied Mechanics Reviews 59, 51-77.

Chen, J., Vaughan, J., Avise, J., O'Neill, S., Lamb, B. (2008) Enhancement and evaluation of the AIRPACT ozone and PM2.5 forecast system for the Pacific Northwest. Journal of Geophysical Research 113, D14305.

Coats, C.J., (1996) High-performance algorithms in the Sparse Matrix Operator Kernel Emissions (SMOKE) modeling system, Proc. Ninth AMS Joint Conference on Applications of Air Pollution Meteorology with A&WMA, Amer. Meteor. Soc., Atlanta, GA, pp. 584-588.

DeBell, L.J., Talbot, R.W., Dibb, J.E., Munger, J.W., Fischer, E.V., Frolking, S.E. (2004) A major regional air pollution event in the northeastern United States caused by extensive forest fires in Quebec, Canada. Journal of Geophysical Research: Atmospheres 109, D19305.

Delfino, R.J., Brummel, S., Wu, J., Stern, H., Ostro, B., Lipsett, M., Winer, A., Street, D.H., Zhang, L., Tjoa, T., Gillen, D.L. (2009) The relationship of respiratory and cardiovascular hospital admissions to the southern California wildfires of 2003. Occupational and Environmental Medicine 66, 189-197.

Flannigan, M.D., Logan, K.A., Amiro, B.D., Skinner, W.R., Stocks, B.J. (2005) Future Area Burned in Canada. Climatic Change 72, 1-16.

Fox, D.G., Riebau, A.R., (2009) Effects of forest fires on visibility and air quality, in: Bytnerowicz, A., Arbaugh, M.J., Riebau, A.R., Andersen, C. (Eds.), Wildland Fires and Air Pollution. Elsevier, pp. 171-195.

GFC, (2007) Georgia Wildfires of 2007 Summary of Facts and Costs for Recovery. Georgia Forestry Commission.

Henderson, S.B., Brauer, M., MacNab, Y.C., Kennedy, S.M. (2011) Three Measures of forest fire smoke exposure and their associations with respiratory and cardiovascular health outcomes in a population-based cohort. Environmental Health Perspectives 119, 1266-1271.

Henderson, S.B., Ichoku, C., Burkholder, B.J., Brauer, M., Jackson, P.L. (2010) The validity and utility of MODIS data for simple estimation of area burned and aerosols emitted by wildfire events. International Journal of Wildland Fire 19, 844-852.

Hodzic, A., Madronich, S., Bohn, B., Massie, S., Menut, L., Wiedinmyer, C. (2007) Wildfire particulate matter in Europe during summer 2003: meso-scale modeling of smoke emissions, transport and radiative effects. Atmospheric Chemistry and Physics 7, 4043-4064.

Jain, R., Vaughan, J., Kyle, H., Ramosa, C., Clalborn, C., Maarten, S., Schaaf, M., Lamb, B. (2007) Development of the ClearSky smoke dispersion forecast system for agricultural field burning in the Pacific Northwest. Atmospheric Environment 41, 6745-6761.

Johnston, F.H., Henderson, S.B., Chen, Y., Randerson, J.T., Marlier, M., DeFries, R.S., Kinney, P., Bowman, D., Brauer, M. (2012) Estimated global mortality attributable to smoke from landscape fires. Environmental Health Perspectives 120, 695-701.

Kochi, I., Donovan, G.H., Champ, P.A., Loomis, J.B. (2010) The economic cost of adverse health effects from wildfire-smoke exposure: a review. Int. J. Wildland Fire 19, 803-817.

Lapina, K., Honrath, R.E., Owen, R.C., Val Martín, M., Hyer, E.J., Fialho, P. (2008) Late summer changes in burning conditions in the boreal regions and their implications for NOx and CO emissions from boreal fires. Journal of Geophysical Research: Atmospheres 113, D11304.

Lavdas, L.G., Jackson, W.A., Harms, M.F., Amer Meteorol, S.O.C. (1996) VSMOKE - A forestry smoke dispersion algorithm with GIS interface. 22nd Conference on Agricultural & Forest Meteorology with Symposium on Fire & Forest Meteorology/12th Conference on Biometeorology & Aerobiology, 292-295.

Lee, K.H., Kim, J.E., Kim, Y.J., Kim, J., von Hoyningen-Huene, W. (2005a) Impact of the smoke aerosol from Russian forest fires on the atmospheric environment over Korea during May 2003. Atmospheric Environment 39, 85-99.

Lee, S., Baumann, K., Schauer, J.J., Sheesley, R.J., Naeher, L.P., Meinardi, S., Blake, D.R., Edgerton, E.S., Russell, A.G., Clements, M. (2005b) Gaseous and particulate emissions from prescribed burning in Georgia. Environmental Science & Technology 39, 9049-9056.

Lee, S., Kim, H.K., Yan, B., Cobb, C.E., Hennigan, C., Nichols, S., Chamber, M., Edgerton, E.S., Jansen, J.J., Hu, Y., Zheng, M., Weber, R.J., Russell, A.G. (2008) Diagnosis of Aged Prescribed Burning Plumes Impacting an Urban Area. Environmental Science & Technology 42, 1438-1444.

Liu, Y., Achtemeier, G., Goodrick, S. (2008) Sensitivity of air quality simulation to smoke plume rise. Journal of Applied Remote Sensing 2, 021503.

Miranda, A.I., Marchi, E., Ferretti, M., Millán, M.M., (2009) Forest fires and air quality issues in southern Europe, in: Bytnerowicz, A., Arbaugh, M.J., Riebau, A.R., Andersen, C. (Eds.), Developments in Environmental Science, 8 ed. Elsevier, pp. 209-231.

Mueller, S.F., Mallard, J.W. (2011) Contributions of natural emissions to ozone and PM2.5 as simulated by the Community Multiscale Air Quality (CMAQ) model. Environmental Science & Technology 45, 4817-4823.

NIFC, (2013) Wildland Fire Summary and Statistics Annual Report 2012. National Interagency Coordination Center.

Park, R.J., Jacob, D.J., Kumar, N., Yantosca, R.M. (2006) Regional visibility statistics in the United States: Natural and transboundary pollution influences, and implications for the Regional Haze Rule. Atmospheric Environment 40, 5405-5423.

Park, R.J., Jacob, D.J., Logan, J.A. (2007) Fire and biofuel contributions to annual mean aerosol mass concentrations in the United States. Atmospheric Environment 41, 7389-7400.

Phuleria, H.C., Fine, P.M., Zhu, Y.F., Sioutas, C. (2005) Air quality impacts of the October 2003 Southern California wildfires. Journal of Geophysical Research 110, D07s20.

Rappold, A.G., Stone, S.L., Cascio, W.E., Neas, L.M., Kilaru, V.J., Carraway, M.S., Szykman, J.J., Ising, A., Cleve, W.E., Meredith, J.T., Vaughan-Batten, H., Deyneka, L., Devlin, R.B. (2011) Peat bog wildfire smoke exposure in rural North Carolina is associated with cardiopulmonary emergency department visits assessed through syndromic surveillance. Environmental Health Perspectives 119, 1415-1420.

Reisen, F., Meyer, C.P., Keywood, M.D. (2013) Impact of biomass burning sources on seasonal aerosol air quality. Atmospheric Environment 67, 437-447.

Riebau, A.R., Fox, D.G., Sestak, M.L., Dailey, B., Archer, S.F. (1988) Simple approach smoke estimation model. Atmospheric Environment 22, 783-788.

Rogers, B.M., Neilson, R.P., Drapek, R., Lenihan, J.M., Wells, J.R., Bachelet, D., Law, B.E. (2011) Impacts of climate change on fire regimes and carbon stocks of the U.S. Pacific Northwest. Journal of Geophysical Research: Biogeosciences 116, G03037.

Rolph, G.D., Draxler, R.R., Stein, A.F., Taylor, A., Ruminski, M.G., Kondragunta, S., Zeng, J., Huang, H.C., Manikin, G., McQueen, J.T., Davidson, P.M. (2009) Description and verification of the NOAA Smoke Forecasting System: The 2007 fire season. Weather and Forecasting 24, 361-378.

Skamarock, W.C., Klemp, J.B., Dudhia, J., Gill, D.O., Barker, D.M., Duda, M.G., Huang, X.-Y., Wang, W., Powers, J.G., (2008) A description of the Advanced Research WRF version 3, Tech. Note, NCAR/TN-475+STR. Natl. Cent. for Atmos. Res., Boulder, Colorado, USA.

Spracklen, D.V., Logan, J.A., Mickley, L.J., Park, R.J., Yevich, R., Westerling, A.L., Jaffe, D.A. (2007) Wildfires drive interannual variability of organic carbon aerosol in the western U.S. in summer. Geophysical Research Letters 34, L16816.

Spracklen, D.V., Mickley, L.J., Logan, J.A., Hudman, R.C., Yevich, R., Flannigan, M.D., Westerling, A.L. (2009) Impacts of climate change from 2000 to 2050 on wildfire activity and carbonaceous aerosol concentrations in the western United States. Journal of Geophysical Research: Atmospheres 114, D20301.

Stohl, A., Andrews, E., Burkhart, J.F., Forster, C., Herber, A., Hoch, S.W., Kowal, D., Lunder, C., Mefford, T., Ogren, J.A., Sharma, S., Spichtinger, N., Stebel, K., Stone, R., Ström, J., Tørseth, K., Wehrli, C., Yttri, K.E. (2006) Pan-Arctic enhancements of light absorbing aerosol concentrations due to North American boreal forest fires during summer 2004. Journal of Geophysical Research: Atmospheres 111, D22214.

Strand, T.M., Larkin, N., Craig, K.J., Raffuse, S., Sullivan, D., Solomon, R., Rorig, M., Wheeler, N., Pryden, D. (2012) Analyses of BlueSky Gateway PM2.5 predictions during the 2007 southern and 2008 northern California fires. J. Geophys. Res. 117.

Sullivan, D.C., Raffuse, S.M., Pryden, D.A., Craig, K.J., Reid, S.B., Wheeler, N.J., Chinkin, L.R., Larkin, N.K., Solomon, R., Strand, T., (2008) Development and applications of systems for modeling emissions and smoke from fires: the BlueSky smoke modeling framework and SMARTFIRE, 17th International Emissions Inventory Conference, pp. 2-5.

Tian, D., Hu, Y.T., Wang, Y.H., Boylan, J.W., Zheng, M., Russell, A.G. (2009) Assessment of biomass burning emissions and their impacts on urban and regional PM2.5: A Georgia case study. Environmental Science & Technology 43, 299-305.

Warneke, C., de Gouw, J.A., Stohl, A., Cooper, O.R., Goldan, P.D., Kuster, W.C., Holloway, J.S., Williams, E.J., Lerner, B.M., McKeen, S.A., Trainer, M., Fehsenfeld, F.C., Atlas, E.L., Donnelly, S.G., Stroud, V., Lueb, A., Kato, S. (2006) Biomass burning and anthropogenic sources of CO over New England in the summer 2004. Journal of Geophysical Research-Atmospheres 111.

Westerling, A.L., Turner, M.G., Smithwick, E.A.H., Romme, W.H., Ryan, M.G. (2011) Continued warming could transform Greater Yellowstone fire regimes by mid-21st century. Proceedings of the National Academy of Sciences.

Wise, E.K. (2008) Meteorologically influenced wildfire impacts on urban particulate matter and visibility in Tucson, Arizona, USA. International Journal of Wildland Fire 17, 214-223.

Witham, C., Manning, A. (2007) Impacts of Russian biomass burning on UK air quality. Atmospheric Environment 41, 8075-8090.

Wong, D.C., Pleim, J., Mathur, R., Binkowski, F., Otte, T., Gilliam, R., Pouliot, G., Xiu, A., Young, J.O., Kang, D. (2012) WRF-CMAQ two-way coupled system with aerosol feedback: software development and preliminary results. Geosci. Model Dev. 5, 299-312.

Wotawa, G., Trainer, M. (2000) The Influence of Canadian Forest Fires on Pollutant Concentrations in the United States. Science 288, 324-328.

Yang, E.S., Christopher, S.A., Kondragunta, S., Zhang, X.Y. (2011) Use of hourly Geostationary Operational Environmental Satellite (GOES) fire emissions in a Community Multiscale Air Quality (CMAQ) model for improving surface particulate matter predictions. Journal of Geophysical Research 116, D04303.

Zeng, T., Wang, Y.H., Yoshida, Y., Tian, D., Russell, A.G., Barnard, W.R. (2008) Impacts of Prescribed Fires on Air Quality over the Southeastern United States in Spring Based on Modeling and Ground/Satellite Measurements. Environmental Science & Technology 42, 8401-8406.

CHAPTER 3

SIMULATING SMOKE TRANSPORT FROM WILDLAND FIRES WITH A REGIONAL-SCALE AIR QUALITY MODEL: SENSITIVITY TO SPATIOTEMPORAL ALLOCATION OF FIRE EMISSIONS

Abstract

Air quality simulations produced with comprehensive atmospheric chemistry and transport models can provide valuable information about the impacts of fires on pollutant concentrations. However, significant uncertainties are associated with fire-related emissions estimates as well as their distribution on gridded modeling domains. In this study, we explore the sensitivity of fine particulate matter ($PM_{2.5}$) concentrations simulated with a three-dimensional gridded air quality model to the spatial and temporal allocation of fire emissions. The assessment was completed by using the Community Multiscale Air Quality modeling system (CMAQ) to simulate a fire-related urban smoke event which severely impacted air quality throughout the Atlanta metropolitan area on 28 February 2007. Sensitivity analyses were undertaken to evaluate the significance of emissions distribution among a model's vertical layers, along the horizontal plane, and into hourly inputs. Results show that predicted $PM_{2.5}$ concentrations are highly sensitive to emissions injection altitude relative to planetary boundary layer height. Simulations were responsive to the horizontal allocation of fire emissions and their distribution into single or multiple grid cells. Additionally, modeled $PM_{2.5}$ concentrations proved to be greatly sensitive to the temporal distribution of fire-related emissions. The analyses completed in this study demonstrate that, in addition to representative estimates of

emitted mass, successfully modeling the impacts of wildland fires on air quality with gridded models depends on an accurate spatiotemporal allocation of emissions.

3.1 Introduction

Air quality simulations produced with numerical models can provide valuable information to environmental regulators and land-managers about the potential impacts of fires on pollution levels. Comprehensive chemical transport models are well-suited to simulate the atmospheric dispersion and transformation of emissions released in wildland fires across different spatial scales. Previous studies have attempted to simulate the air quality impacts of wildland fires using chemical transport models (Junquera et al., 2005; Konovalov et al., 2011; Zeng et al., 2008). Only a few of these simulations attempted to replicate distinct smoke plumes and evaluated model predictions against measured or satellite-derived pollutant concentrations. Such evaluations have reported mixed results when aiming to reproduce observed particle loads downwind of specific fires. Often, gridded air quality models significantly underpredict $PM_{2.5}$ concentrations (Liu et al., 2009; Strand et al., 2012; Yang et al., 2011). A considerable amount of research pertaining to the effects of wildland fires on air pollution has focused on determining accurate fire-related emissions and emission factors (Akagi et al., 2011; Lee et al., 2005; Wiedinmyer et al., 2006). However, the distribution of fire emissions in space and time on gridded modeling domains is also subject to significant uncertainty (Tian, 2006). Beyond evaluating the magnitude of fire-related emissions inputs, the methodologies applied to include fire emissions in air quality simulations must be assessed.

Sensitivity analyses can be used to quantify the responsiveness of modeling results to specific inputs or parameters. By doing so, they provide information about the relative importance of each input variable to select model outputs. Furthermore, sensitivity analyses are a key step in the process of improving model performance and achieving successful simulations. In this study, we explore the sensitivities of $PM_{2.5}$

concentrations simulated with a three-dimensional gridded air quality model to the spatial and temporal allocation of fire emissions for a severe urban smoke event. Sensitivity analyses were performed to evaluate the significance of plume rise approximations, or the distribution of fire emissions among a model's vertical layers. The implications of emissions allocation along the horizontal plane are also assessed by comparing $PM_{2.5}$ concentration sensitivities to injection into discrete grid cells and assessing the effect of treating fires as point sources or distributing fire-related emissions into multiple cells. Additionally, a sensitivity analysis of simulated pollutant concentrations to the temporal partitioning of fire emissions into hourly model inputs is presented. Numerical simulations were performed with CMAQ and a "brute-force" method was applied to complete the necessary sensitivity analyses. The results of this study weigh the potential benefits of better characterizing fire emissions in gridded air quality models beyond the traditional emphasis placed on emissions strength.

3.2 Methods

3.2.1 Air Quality Modeling Framework

Numerical air quality simulations undertaken as part of this work were done through the modeling framework described in Chapter 2. Meteorological fields were produced with the Weather Research and Forecasting model (WRF version 2.2, http://www.wrf-model.org/index.php). WRF modeling was carried out using 3 nested domains with increasing horizontal grid resolutions of 36, 12, and 4 km. Analysis products from the North American Mesoscale model (nomads.ncdc.noaa.gov) were used to initialize weather simulations, constrain boundary conditions, and nudge meteorological fields at 6-hour intervals. Additional details about the WRF configuration applied are included in Chapter 4.

Pollutant emission rates for non-fire sources were prepared through the Sparse Matrix Operator Kernel Emissions modeling system (SMOKE version 2.1, http://www.smoke-model.org/index.cfm). Emissions were projected from a 2002 "typical year" emissions inventory (MACTEC, 2005). Fire-related emissions were estimated with the Fire Emission Production Simulator (FEPS version 1.1.0, http://www.fs.fed.us/pnw/fera/feps/). Distribution of fire emissions into vertical layers was derived from plume rise estimates produced with the Daysmoke model (Achtemeier et al., 2011).

Chemical transport modeling was done with the Community Multiscale Air Quality modeling system (CMAQ version 4.5, http://www.cmaq-model.org/). For all CMAQ simulations, modeling domains were divided into 34 sigma-pressure vertical layers increasing in depth from the ground up. Layer thickness increases from approximately 20 m at the surface to over 3 km at the domain's upper edge approximately 20 km above ground. The first 1000 m of the atmosphere are contained within the lower 10 vertical layers. Analogous to the WRF simulations, CMAQ air quality modeling was performed using 3 levels of nested grids at 36, 12, and 4 km horizontal resolutions. Coarser-resolution simulations were carried out to define initial and boundary conditions for fine-resolution modeling. All sensitivity analyses and necessary air quality simulations were done at 4 km grid resolution.

3.2.2 Base Case Simulation

Fire-related smoke severely impacted air quality across metro Atlanta on 28 February 2007. The dramatic increase in pollutant concentrations was caused by two prescribed burns roughly 80 km southwest of Atlanta at the Oconee National Forrest and Piedmont National Wildlife Refuge (henceforth referred to as Oconee and Piedmont). Approximately 12 km^2 of wildland were affected by these fires. Hourly $PM_{2.5}$ concentrations observed throughout Atlanta escalated to around 150 $\mu g\ m^{-3}$ a few hours

after ignition. Figure 3.1 shows the locations of prescribed burns and air quality monitoring stations considered in this study.

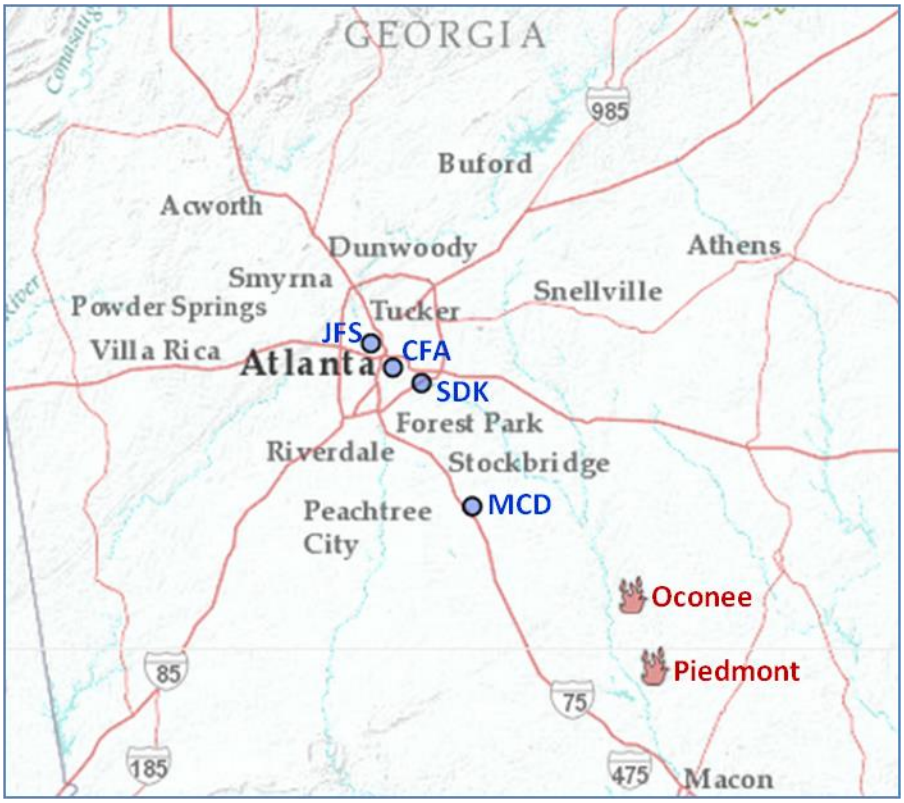

Figure 3.1 Location of Oconee and Piedmont fires, and Confederate Ave. (CFA), South DeKalb (SDK), Jefferson St. (JFS), and McDonough (MCD) air quality monitoring stations.

This smoke incident was selected as a case study and is the focus of this work. The episode has also been modeled with CMAQ in previous studies. Hu et al. (2008) compared an air quality forecast executed with preburn information to a series of "hindcasts" that incorporated additional details about fire evolution and observed meteorology. Liu et al. (2009) analyzed smoke transport from these prescribed burns and compared simulated trajectories to satellite observations. In Chapter 6, an adaptive grid version of CMAQ capable of dynamically refining grid resolution is used to simulate this

smoke episode and demonstrate the significance of horizontal grid resolution in atmospheric plume modeling.

Figure 3.2 shows hourly $PM_{2.5}$ emissions estimates for each burn. Emissions processing with FEPS requires approximations of burned area and fuel consumption, as well as appropriate emission factors. Reported uncertainties for bottom-up estimates of $PM_{2.5}$ emissions from fires in the Southeastern U.S. such as these range from 15-50% (Odman, 2011; Tian, 2006). One recent study, for instance, quantified emissions from a series of prescribed burns in northern Florida using the same approach applied here found $PM_{2.5}$ emissions estimates were underpredicted by 15% with respect to field measurements (Odman, 2012). Hourly plume structures simulated by Daysmoke were used to distribute fire emissions among the CMAQ domain's vertical layers. Figure 3.3 shows $PM_{2.5}$ injected into each layer from the Oconee and Piedmont fires for the entire simulation. Generally, upper layer injection corresponds to flaming combustion while emissions distributed closer to the surface correspond to the fire's smoldering phase.

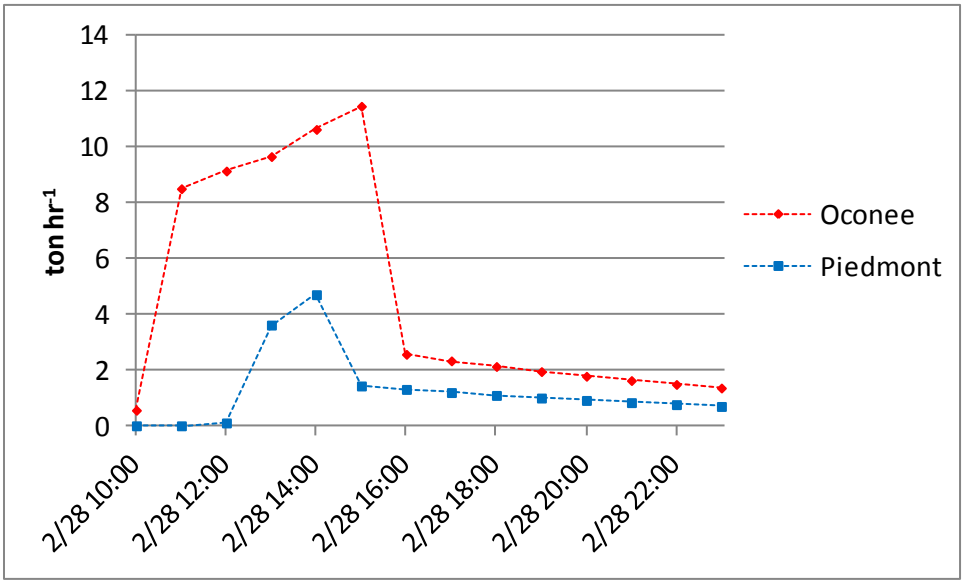

Figure 3.2 Total fire-related $PM_{2.5}$ emissions by vertical layer for Oconee and Piedmont fires. Approximate full layer heights (m AGL) are also included.

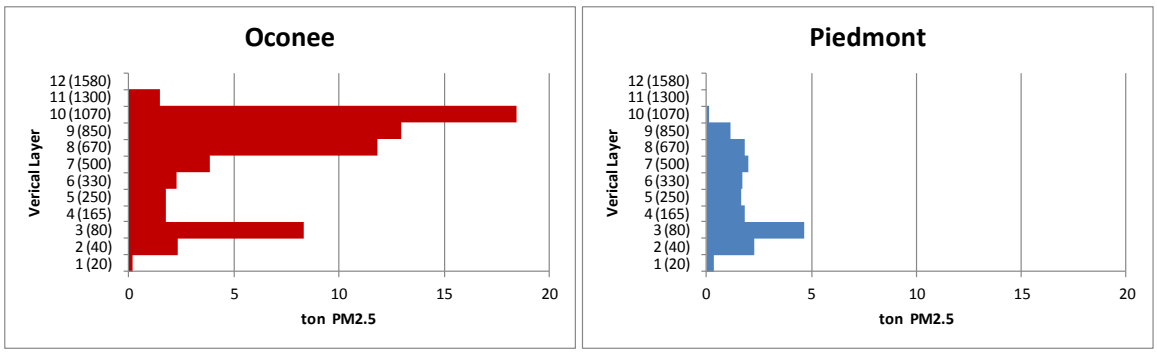

Figure 3.3 Total fire-related $PM_{2.5}$ emissions by vertical layer for Oconee and Piedmont fires. Approximate full layer heights (m AGL) are also included.

3.2.3 Sensitivity Analyses

Sensitivities of CMAQ-modeled concentrations to emission inputs were quantified by calculating the difference between two simulations in which a parameter was perturbed,

$$s_x = \frac{C_{x+\Delta x} - C_{x-\Delta x}}{2\Delta x} \tag{3.1}$$

where s_x is the first-order sensitivity coefficient of concentration C response to parameter x, and $C_{x+\Delta x}$ and $C_{x-\Delta x}$ are the concentrations resulting from simulations under $+\Delta x$ and $-\Delta x$ perturbations to x. These sensitivity estimates, also known as "brute-force" sensitivities, can be applied to any simulated variable and model parameter or input (Hwang et al., 1997). Similar to first-order sensitivity approximations, higher-order sensitivity coefficients can also be estimated using finite differencing methods. Extending on Equation (3.1), second-order sensitivity coefficients can be approximated from three simulations as

$$s_x^2 = \frac{C_{x+\Delta x} - C_x + C_{x-\Delta x}}{\Delta x^2} \tag{3.2}$$

where s_x^2 is the second-order sensitivity coefficient and base-case concentration C_x is included. In this study, first-order sensitivity analyses were used to quantify the response of modeled $PM_{2.5}$ concentrations to variations in the temporal and spatial allocation of fire emissions. Each sensitivity estimate requires two additional CMAQ simulations

beyond the base case. With the exception of fire-related emissions, model configuration and other inputs in the sensitivity runs remain identical to those used in the base case simulation. In the sensitivity simulations, fire emissions are perturbed by increasing and decreasing base-line emissions by an equal percentage. When sensitivities are intended to quantify the response to emissions from a specific grid cell, vertical layer, or period of time, only emissions within that subset are perturbed.

Using the brute-force method to estimate sensitivities of modeled concentrations and project air quality impacts entails several considerations. First, brute-force sensitivity estimates may be heavily influenced by numerical errors if small perturbations are used (Hakami et al., 2004). Equation (3.1) provides first-order sensitivity coefficients estimated from the model's response to specific perturbations. The ability of these sensitivity coefficients to replicate response to larger or smaller perturbations is dependent on the response's linearity. Although many atmospheric aerosol-phase processes included in CMAQ are linear, some, such as thermodynamic aerosol interactions, cloud processes, and secondary aerosol formation, are not (Napelenok et al., 2006). For concentrations involving significant nonlinearities, higher-order sensitivity coefficients are required to accurately reproduce model response across a broad range of perturbations. The analyses of $PM_{2.5}$ concentration sensitivity to fire emissions conducted for this study focus on primary carbonaceous emissions. While secondary formation may contribute to fire-related $PM_{2.5}$, most of the impacts can typically be attributed to primary fine particle emissions (Tian et al., 2009). For many primary pollutants, the response of atmospheric concentrations to emissions perturbations can be expected to be mostly linear (Cohan et al., 2005). Previous sensitivity analyses have in fact shown a nearly linear source-receptor relationship for primary emissions (Koo et al., 2009). Furthermore, although fire-related $PM_{2.5}$ impacts may not be entirely linear, the response to fire emissions in air quality modeling applications commonly is (Liu et al., 2009; Tian et al., 2008). Limited information about fire-associated emission of secondary aerosol

precursors and nonlinear atmospheric transformations affecting fire-related particle pollution generally constrains smoke simulations to primary sources and linear response. The adequacy of linear extrapolation for this study is discussed in Section 3.3.2. Additionally, $PM_{2.5}$ sensitivity estimates can be scaled to other primary pollutants dominated by advection and diffusion, and provide information about the dispersion-related response of all species.

3.3 Results and Discussion

3.3.1 Base Case Model Performance

CMAQ performance was evaluated for the base case simulation by comparing predicted $PM_{2.5}$ concentrations to concurrent observations at air quality monitoring stations downwind of fires where evident increases in $PM_{2.5}$ concentrations were recorded during the smoke episode. Sites used for evaluation and sensitivity analyses are operated by the Georgia Department of Natural Resources (Confederate Ave., South DeKalb, and McDonough stations) and Southeastern Aerosol Research and Characterization (Jefferson St. station) networks. Figure 3.4a shows a visualization of the smoke plume simulated by CMAQ.

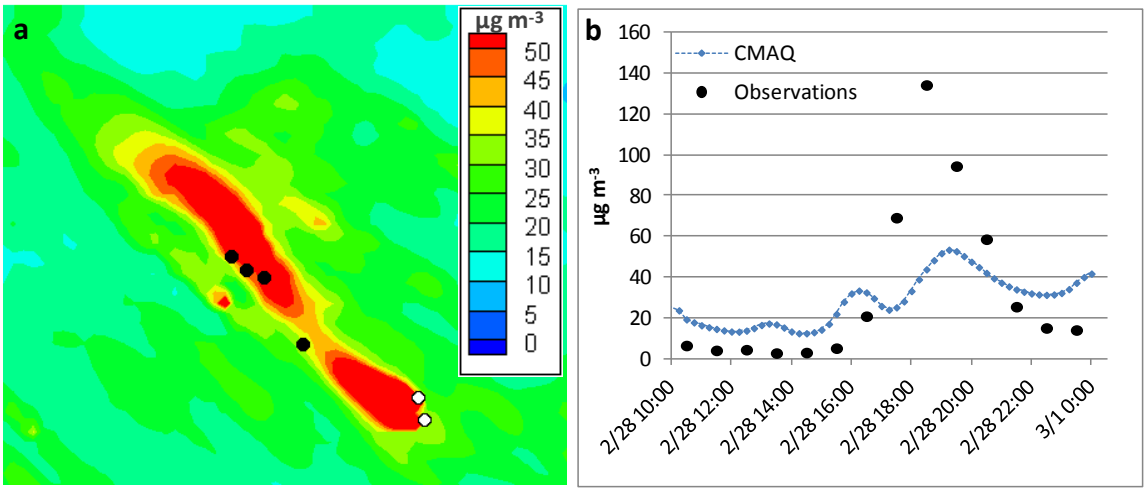

Figure 3.4 (a) CMAQ predicted $PM_{2.5}$ ground-level concentrations at 1900 LT on 28 February 2007. Black and white circles indicate monitoring station and fire locations respectively. (b) Observed 1-hour average and CMAQ-predicted $PM_{2.5}$ concentrations at the Jefferson St. monitoring site on 28 February 2007.

Figure 3.4b compares modeled and observed $PM_{2.5}$ concentrations at the Jefferson St. monitoring station in downtown Atlanta. A large underprediction in simulated $PM_{2.5}$ concentrations compared to measurements is evident. Similarly, CMAQ-estimated $PM_{2.5}$ concentrations are lower than recorded observations at all monitoring sites significantly impacted by smoke. At sites within Atlanta's urban core (Confederate Ave., Jefferson St., and South DeKalb) CMAQ underestimates maximum observed 1-hour average $PM_{2.5}$ concentrations by 58-67%. For these locations, the model's mean fractional error ($2|C_{modeled}-C_{observed}|/(C_{observed}+C_{modeled})$) ranges from 64-73% during the 8-hour interval with the highest observed $PM_{2.5}$ concentrations. However, the simulation does result in relatively well-timed peaks at downwind receptors and produces a reasonable pollutant plume trajectory. At the McDonough station, about halfway between downtown Atlanta and the prescribed burns, CMAQ underpredicts the maximum observed $PM_{2.5}$ concentration by 33%. Still, an 8-hour mean fractional error of 67% for modeled $PM_{2.5}$ could indicate that the error at the site is due to poor timing relative to observations.

Additional CMAQ performance metrics are included in Chapter 6 for a similar simulation. The analyses included therein also showed that increasing horizontal grid resolution may lead to substantially higher $PM_{2.5}$ concentration predictions; by applying an adaptive grid version of CMAQ that dynamically refines grid resolution at the smoke plumes to less than 1km, peak simulated $PM_{2.5}$ concentrations in Atlanta were increased by up to 40%. Still, underpredictions persist in the adaptive grid simulations. Other studies have also reported CMAQ-modeled $PM_{2.5}$ concentrations far lower than ground-based observations when attempting to simulate fire-related air quality impacts. For instance, Yang et al. (2011) modeled a series of wildfires occurring along the Georgia-Florida boundary using CMAQ and found that predicted $PM_{2.5}$ concentrations were

underestimated when compared to monitoring station observations even after increasing fire emissions by a factor of three. Assessing the contribution of uncertainty in spatiotemporal allocation of fire emissions to this error is the objective of the sensitivity analyses undertaken below.

3.3.2 Linear Response to Fire Emissions

As previously discussed, linearity is an important assumption if the brute-force sensitivity approximations are used to estimate model response across a range of perturbations. Linear response enables accurate approximations of impacts and source contributions using first-order sensitivity coefficients as

$$C = C_0 + s_x \Delta x \tag{3.3}$$

where C_0 is a base case concentration and C is the concentration resulting from Δx. For the air quality simulations included in this study, the response of $PM_{2.5}$ concentrations to fire emissions can be expected to be predominantly linear. Fire-related particle emissions are determined from $PM_{2.5}$ emission factors and speciated mostly into primary organic aerosol (90%) and primary elemental carbon (6%). For these species, no significant indirect effects are anticipated.

To evaluate the accuracy of the linear response assumption several tests were carried out. First, a series of CMAQ simulations were performed varying the magnitude of base case fire emissions by ±10%, ±30%, and ±50%. Throughout the full simulation, linear response was evident for predicted $PM_{2.5}$ concentrations at all downwind receptors. Additionally, the relationship between concentrations and emissions intensity was nearly linear across the complete variation range from -50% to +50%. As expected, first-order sensitivity coefficients to fire emissions estimated using Equation (3.1) proved to be practically equal whether applying ±10%, ±30%, or ±50% perturbations. Next, second-order sensitivity coefficients were estimated for the base case simulation and compared to first-order coefficients. The importance of higher-order sensitivity coefficients to

replicate the response of pollutants affected by nonlinearities was discussed in Section 3.2.3. Second-order coefficients calculated using Equation (3.2) proved to be minor compared to first-order ones. In fact, inclusion of second-order coefficients into response calculations only changed total estimated $PM_{2.5}$ impacts by less than 2%. The results further demonstrate that for the analyses included in this study modeled $PM_{2.5}$ concentration response to fire emissions can be effectively captured by first-order sensitivity coefficients.

3.3.3 Fire Contributions to $PM_{2.5}$ Concentrations

Fire contributions to modeled $PM_{2.5}$ concentrations at each downwind site were quantified using brute-force sensitivity estimates. Figure 3.5a shows the first-order sensitivity coefficient for $PM_{2.5}$ concentration response to fire emissions at South DeKalb during the smoke episode. The sensitivity coefficient quantifies change in modeled concentration per ton of fire-emitted $PM_{2.5}$ as a function of time. It is important to mention that estimates at each instant represent sensitivity to all prior $PM_{2.5}$ emissions (i.e. cumulative fire-emitted $PM_{2.5}$). Fire and non-fire contributions to simulated $PM_{2.5}$ concentrations at South DeKalb are shown in figure 3.5b. The non-fire contribution, which includes all sources other than the two fires of interest, was estimated from a CMAQ simulation without Oconee and Piedmont fire emissions. The fire contribution to $PM_{2.5}$ concentrations was calculated using the first-order sensitivity coefficients. Figure 3.5b also includes results from a simulation including all emission sources and shows these concentrations closely match the sum of estimated fire and non-fire contributions. A significant fraction of the CMAQ-predicted $PM_{2.5}$ pollution is attributable to fire emissions. For sites near downtown Atlanta, fire-attributable $PM_{2.5}$ impact increases to 20-31 $\mu g\ m^{-3}$ and can contribute up to 56-67% of total modeled $PM_{2.5}$. At McDonough, the maximum fire contribution to modeled $PM_{2.5}$ concentration is 78% and the largest impact from fires is 70 $\mu g\ m^{-3}$. However, contributions from non-fire sources are also

significant throughout the simulation and display large variations characteristic of the daily fluctuation in urban pollutant concentrations. The importance of non-fire contributions to simulated $PM_{2.5}$ concentrations has been acknowledged in previous air quality modeling efforts exploring the air quality impacts of wildland fires (Christopher et al., 2009; Yang et al., 2011).

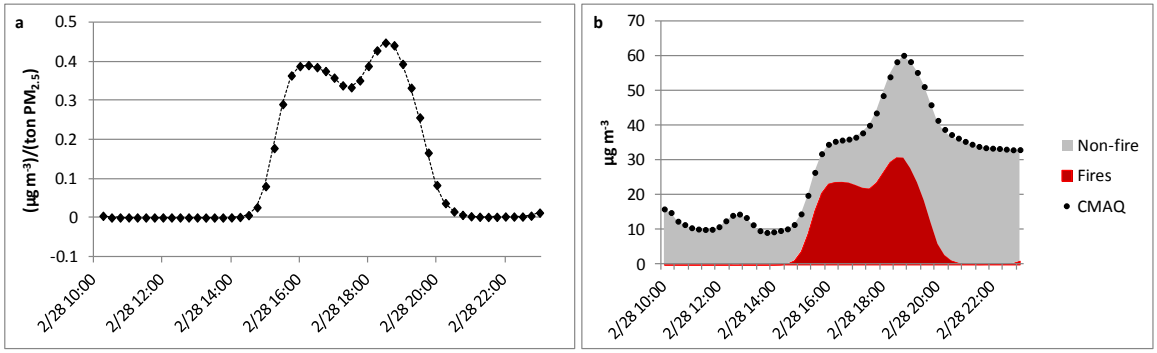

Figure 3.5. (a) Brute-force first-order sensitivity coefficient for $PM_{2.5}$ concentration response to fire emissions and (b) fire and non-fire contributions to modeled $PM_{2.5}$ concentrations at South DeKalb on 28 February 2007 (LT). Base-case CMAQ predictions are also included in (b).

First-order sensitivity coefficients were also used to determine the increase to fire emissions that would match maximum simulated $PM_{2.5}$ concentrations and peak observations. Figure 3.6 shows the effect, approximated with Equation (3.3), of intensifying base-line fire emissions by a factor of 5.1 at Jefferson St. and 3.7 at South DeKalb (additional results are included in the auxiliary material). Overall, base-line fire emissions would have to be increased by a factor of 4-6 for CMAQ predictions to reach the highest observed concentrations within Atlanta. Increments of this magnitude seem unrealistic and suggest that underpredicted downwind impacts cannot be fully explained by underestimated emissions. The projections also indicate that while modeled maxima are generally well-timed relative to peak observations, important differences exist between the complete evolution of predicted fire impacts and observed $PM_{2.5}$ increments throughout the episode. As discussed in Chapter 2, and later in this thesis, the

underestimate is found to be due not only to emission rates, but model resolution and plume dynamics.

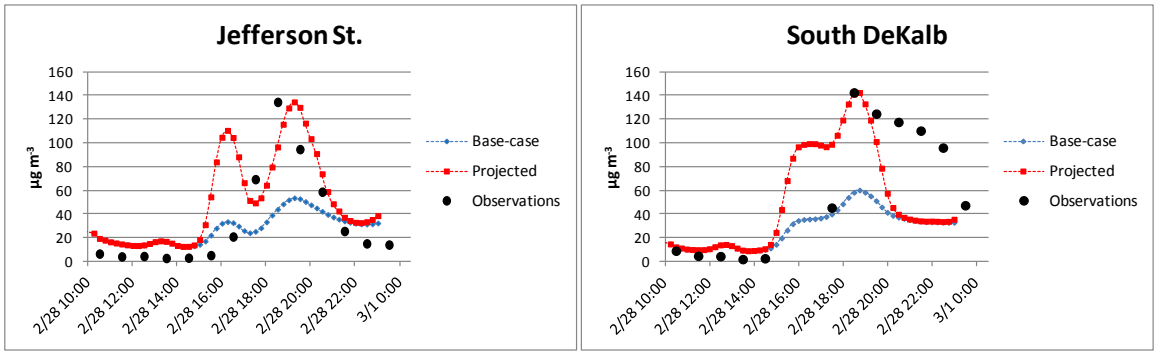

Figure 3.6. Base-case and projected $PM_{2.5}$ concentrations along with monitoring site observations on 28 February 2007 (LT). Projections estimate the effect of increasing fire emissions by factors of 5.1 (Jefferson St.) and 3.7 (South DeKalb).

Sensitivity coefficients were calculated for each individual prescribed burn and used to quantify and compare $PM_{2.5}$ concentration contributions specific to the Oconee and Piedmont fires. $PM_{2.5}$ impacts broken down by fire at South DeKalb are included in Figure 3.7a. Although contributions from both fires are significant, at all sites considered about 75% of the total fire-related $PM_{2.5}$ impact is attributable to the Oconee burn. The disparity in contributions is brought about by unequal emissions and differences in concentration sensitivities to each fire. Figure 3.7b shows hourly first-order sensitivity coefficients for each burn. It is clear that stronger emissions from the Oconee burn largely drive pollution impacts. However, it is interesting to note that sensitivity coefficients can be significantly higher for Piedmont burn emissions. While the added impact of Oconee emissions is larger, on average each ton of $PM_{2.5}$ emitted by the Piedmont burn leads to a greater increase in concentrations at downwind locations. Moreover, the timing of peak sensitivity coefficients for the Piedmont fire better agrees with maximum simulated and observed concentrations. Sensitivity coefficients for individual fires are different because of dissimilar spatial and temporal emissions

distribution for each. The difference corroborates that allocation of fire emissions into hourly rates and gridded three-dimensional domains may significantly influence predicted pollutant concentrations. Sensitivities related to emissions allocation are further explored in Section 3.3.4.

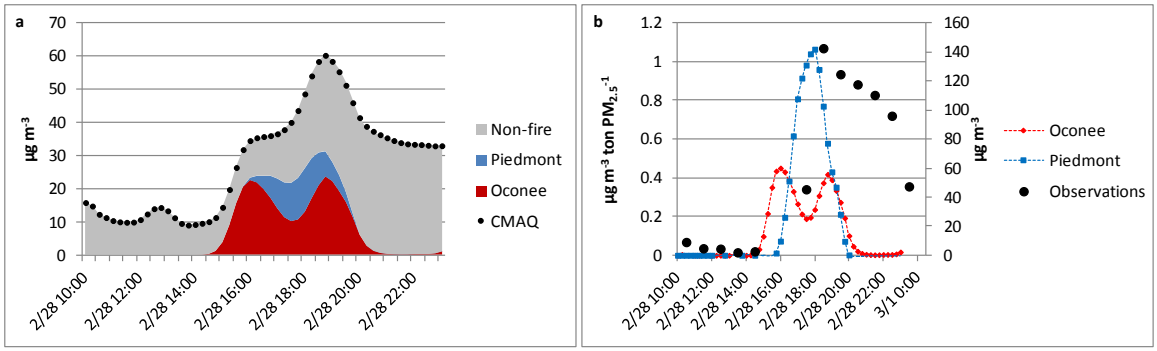

Figure 3.7. (a) Contributions to modeled $PM_{2.5}$ concentrations at South DeKalb from the Oconee and Piedmont fires on 28 February 2007 (LT). Non-fire contribution and base-case CMAQ predictions are also included. (b) First-order sensitivity coefficients for $PM_{2.5}$ concentration response to fire emissions from each fire at South DeKalb (left axis) and site observations (right axis).

3.3.4 Sensitivity Analyses

3.3.4.1 Horizontal allocation of fire emissions

It is common to treat fires as point sources, with all of the emissions in the same horizontal grid cell, in episodic air quality simulations with gridded regional-scale models. This assumption may limit accuracy by injecting fire emissions into a single horizontal grid cell and ignoring details about burned area and fire spread. In our base-case air quality simulation, emissions from each fire were horizontally allocated to a single cell at the centroid of burned areas. Errors associated with this simplification grow as grid resolution is increased. The Oconee and Piedmont fires each consumed approximately 6.2 and 5.9 km^2 of wildland, an area roughly equivalent to a 2.5 km × 2.5 km quadrilateral. On a 4 km horizontal resolution grid, it is possible that each fire might

extend across multiple cells. Furthermore, fire locations may include significant uncertainties. Information on fire extent and evolution may be limited, especially for wildfires. Satellite-based methods of determining fire locations and sizes may introduce additional uncertainty (Giglio et al., 2006; Henderson et al., 2010). Hu et al. (2008) determined that modifying the horizontal allocation of fire emissions had a small effect on predicted downwind concentrations. For major events, satellite information has also been used to spatially refine coarse fire characterizations (Roy et al., 2007). The sensitivity analysis described below was completed to assess the potential gains of more accurately pinpointing fires or distributing their emissions across multiple grid cells.

For the Oconee and Piedmont burns, sensitivity estimates were used to compare $PM_{2.5}$ concentration impacts at downwind receptors for all 4 km × 4 km grid cells horizontally adjacent to the cell into which fire-related emissions were originally injected. Figure 3.8 shows total $PM_{2.5}$ contributions at Jefferson St. attributable to the Oconee fire relative to the base-case fire location (center cell). Additionally, simulated peak $PM_{2.5}$ concentrations are compared to the base-case maximum (54 μg m^{-3}) across the nine cell area. It is evident from Figure 3.8 that small changes to the horizontal allocation of fire emissions may significantly affect modeled $PM_{2.5}$ concentrations downwind. For the urban sites considered, reallocation of emissions from the Oconee fire into a neighboring grid cell can increase total $PM_{2.5}$ impact up to 28% or lower it by as much as 21%. A single cell shift in the horizontal allocation of Oconee fire emissions, which only account for a fraction of total $PM_{2.5}$ pollution, can also cause peak concentrations at these receptors to escalate or fall by up to 20%. At McDonough, closer to the prescribed burns, the sensitivity of $PM_{2.5}$ concentration to horizontal allocation of fire emissions is even larger.

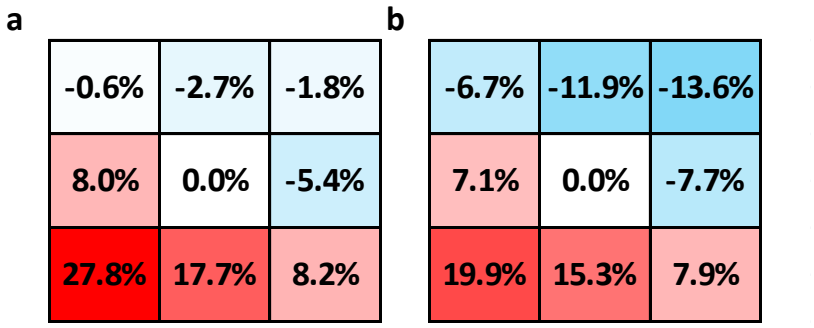

Figure 3.8. Change in (a) Oconee fire $PM_{2.5}$ contribution and (b) maximum simulated $PM_{2.5}$ concentration relative to base-case at Jefferson St. after relocating Oconee fire emissions into grid cells adjacent to original injection cell.

Changes in total $PM_{2.5}$ impacts brought about by reallocating fire emissions do not necessarily correspond to changes in peak concentrations. For example, shifting emissions from the Oconee burn one cell northeast will increase total fire-attributable $PM_{2.5}$ at Confederate Av. by 8%, but decrease the maximum simulated $PM_{2.5}$ concentration by 12%. Furthermore, the response may be completely different for individual downwind receptors close to each other; while the reallocation operation described above leads to an 8% increase in fire-related $PM_{2.5}$ impact at Confederate Av., it causes a concurrent 20% reduction at South DeKalb 7 km away. Sensitivities are also markedly dissimilar for the Oconee and Piedmont burns. Figure 3.9 is equivalent to Figure 3.8, but shows the effects of altering emissions injection for the Piedmont fire. Significant differences exist between the magnitudes and patterns of $PM_{2.5}$ concentration response to equivalent changes in horizontal distribution of Oconee and Piedmont fire emissions. However, the sensitivities of CMAQ-predicted $PM_{2.5}$ pollution concentrations to the horizontal allocation of emissions from the Piedmont fire are also large; a single cell shift can change total $PM_{2.5}$ contribution and peak concentration at Atlanta sites by up to 35% and 9% respectively.

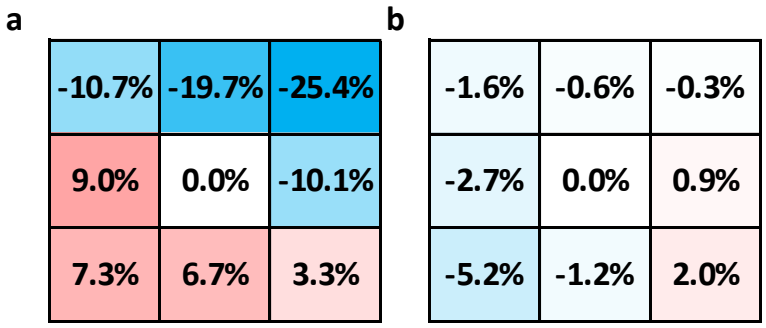

Figure 3.9. Change in (a) Piedmont fire $PM_{2.5}$ contribution and (b) maximum simulated $PM_{2.5}$ concentration relative to base-case at Jefferson St. after relocating Piedmont fire emissions into grid cells adjacent to original injection cell.

Additional uncertainty regarding the horizontal positioning of fire emissions stems from the plume rise representations applied to account for buoyancy. In the air quality simulations completed, plume structure was modeled to distribute fire emissions across the domain's vertical layers. Using a subgrid scale dispersion model, plume rise was approximated as the vertical distribution of fire-related particulate matter at a fixed downwind distance for a fully developed plume. For the episode simulated, vertical plume structure was determined 10 km downwind of fires but used to vertically distribute fire emissions at the source. To evaluate the implications of applying a downwind plume rise estimate at the original fire location, $PM_{2.5}$ impacts were compared for emissions injection into cells 10 km downwind of fires (i.e. two grid cells northwest). Figure 3.10 shows how contributions to $PM_{2.5}$ at Jefferson St. would change if Oconee and Piedmont fire emissions were injected downwind of the burns. Again, it is clear that reallocating emissions can have an important effect on predicted concentrations. Relocating emissions 10 km downwind can alter fire-attributable $PM_{2.5}$ impacts and maximum simulated concentrations at the sites near downtown Atlanta by up to 15%. As before, there is no evident correspondence between total $PM_{2.5}$ contributions and peak concentrations, different downwind sites, or the Oconee and Piedmont burns.

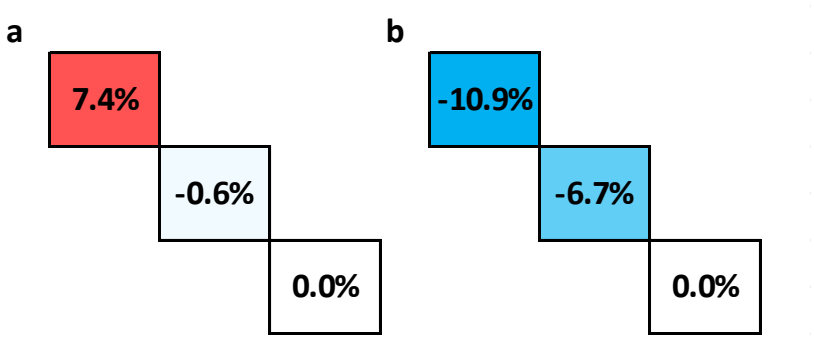

Figure 3.10. Change in (a) Oconee fire $PM_{2.5}$ contribution and (b) Piedmont fire $PM_{2.5}$ contribution relative to base-case at Jefferson St. after relocating each fire's emissions into grid cells downwind (northwest) of fire location.

3.3.4.2 Vertical allocation of fire emissions

Plume rise approximations are an important component of air quality simulations involving buoyant emissions. As previously discussed, when fires are included in gridded domains, their emissions must be distributed among the domain's vertical layers. Frequently, vertical distribution profiles for fire-related emissions are determined from simplified theoretical or empirical plume rise approximations (Hodzic et al., 2007; Junquera et al., 2005). Fire emissions processors (e.g. FEPS) or subgrid scale models may be able to provide hourly maximum and minimum plume height estimates (Freitas et al., 2007; Sessions et al., 2011). Emissions can then be uniformly distributed among vertical layers from the maximum plume height down to the ground or minimum height. Fire emissions have also been simply homogeneously distributed within the planetary boundary layer (PBL) or below a fixed altitude (Hu et al., 2008; Yang et al., 2011). Alternatively, Lagrangian particle models can produce complete vertical plume structures that may also be used to allocate fire emissions on gridded domains and provide additional information about the true vertical distribution of pollutants (Liu et al., 2008). As previously described in Section 3.2.2, the hourly vertical distributions of fire emissions used in this study were determined with Daysmoke, a pollutant transport model developed for prescribed burns. To assess the significance of vertical emissions allocation

in successfully modeling the air quality impacts of wildland fires, brute-force sensitivities of CMAQ-predicted $PM_{2.5}$ concentrations to fire emissions were compared for each vertical layer included in our base-case simulation. Sensitivity approximations were then used to quantify the $PM_{2.5}$ impacts attributable to each layer. Figure 3.11 shows estimated fire contributions to $PM_{2.5}$ concentration at South DeKalb by vertical layer. In the base-case simulation emissions were injected into the lower eleven layers. The contribution from non-fire sources, determined from a simulation without fire emissions, and base-case CMAQ concentrations are also included. The strongest fire contributions come from layers 8-10, accounting for over 65% of the fire-related impact on $PM_{2.5}$ concentrations. Not surprisingly, these layers also receive the largest fractions of fire emissions. Additionally, Figure 3.11 shows that the sum of non-fire and individual contributions to $PM_{2.5}$ closely matches base-case predicted concentrations. This agreement, observed at all downwind sites, further supports a linear response to fire emissions and the adequacy of brute-force sensitivities in this analysis.

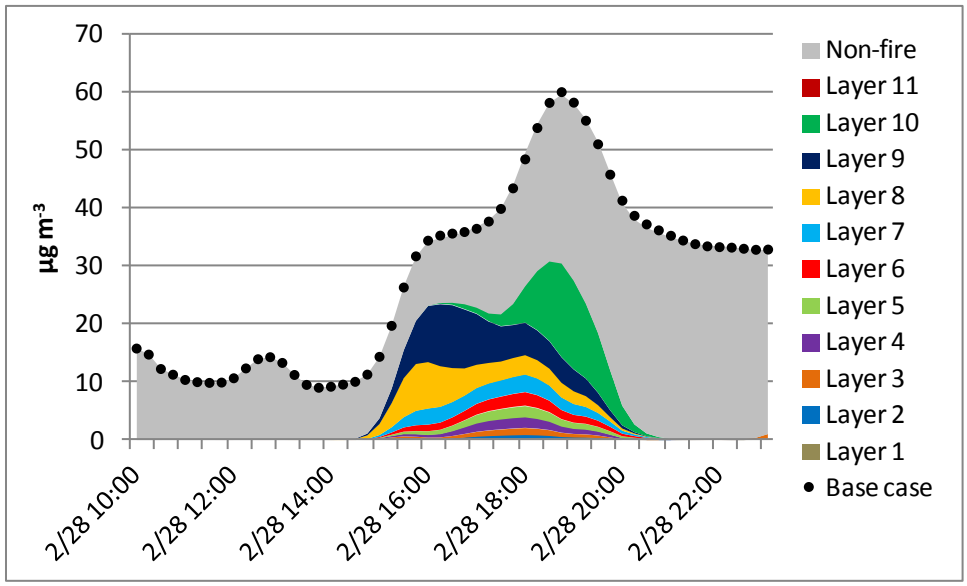

Figure 3.11. Fire contributions to modeled $PM_{2.5}$ concentrations at South DeKalb by vertical CMAQ layer on 28 February 2007 (LT). Non-fire contribution and base-case CMAQ results are also included.

Layer-specific contributions to simulated $PM_{2.5}$ concentrations are largely dependent on the magnitude of emissions injected into each layer. Sensitivity estimates, which quantify the response of concentration predictions per unit of emitted mass, are of greater value to determine the significance of vertical distribution profiles in air quality modeling. 3.12 compares $PM_{2.5}$ concentration sensitivities to fire emissions from each vertical layer at South Dekalb and includes hourly-averaged monitoring station observations. Sensitivity coefficients vary significantly between different vertical layers at all the sites considered. As observed concentrations peak at South DeKalb, the sensitivity to fire emissions is clearly largest for layer 10. These results might seem to indicate that CMAQ-predicted $PM_{2.5}$ concentrations are significantly sensitive to the vertical allocation of fire emissions. However, it is important to note that two distinct components of individual vertical layer emissions make sensitivities to them differ: injection altitude and emissions timing. If time-varying vertical profiles are applied, simulated concentrations may be more responsive to emissions from a specific vertical layer due to the timing of injection rather that layer altitude. To isolate the influence of spatial or temporal allocation in brute-force sensitivity calculations, only a single component of fire emissions should be perturbed. Sensitivity to temporal allocation of emissions is discussed in Section 3.3.4.3.

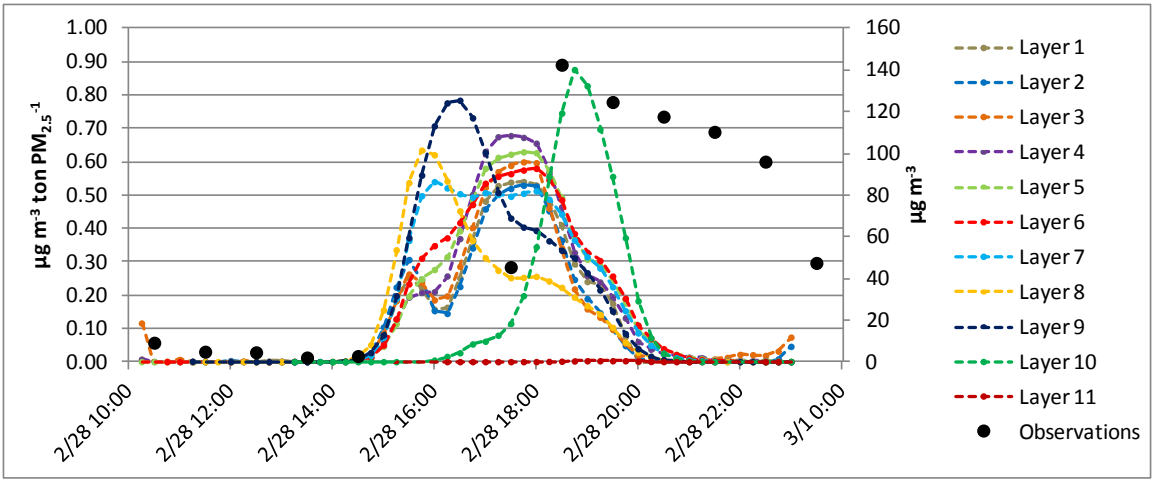

Figure 3.12. Brute-force first-order sensitivity coefficients for $PM_{2.5}$ concentration response to fire emissions by vertical CMAQ layer at South DeKalb (left axis) and site observations (right axis) on 28 February 2007 (LT).

To remove the temporal variability between different layers, brute-force sensitivities were quantified using a constant vertical emissions profile. An accurate assessment of the sensitivity of modeled $PM_{2.5}$ concentrations to injection height was achieved by equally dividing fire emissions into all layers considered throughout the full episode. Further, allocating the same amount of hourly fire emissions to each layer allows for a fair comparison of their respective impacts. Figure 3.13 shows $PM_{2.5}$ concentration sensitivities to fire emissions by vertical layer at South DeKalb after applying a constant and layer-uniform vertical emissions distribution covering the lower 16 layers. Contrary to the comparison previously presented in Figure 3.12, these results indicate that after eliminating the temporal variation in layer emissions, sensitivities are similar for all vertical layers below layer 10. Sensitivity to layer 10 emissions is markedly lower and modeled $PM_{2.5}$ concentrations are not responsive at all to emissions injected above layer 10 or approximately 1000 m. The same conclusions can be drawn from sensitivity estimates at other downwind sites.

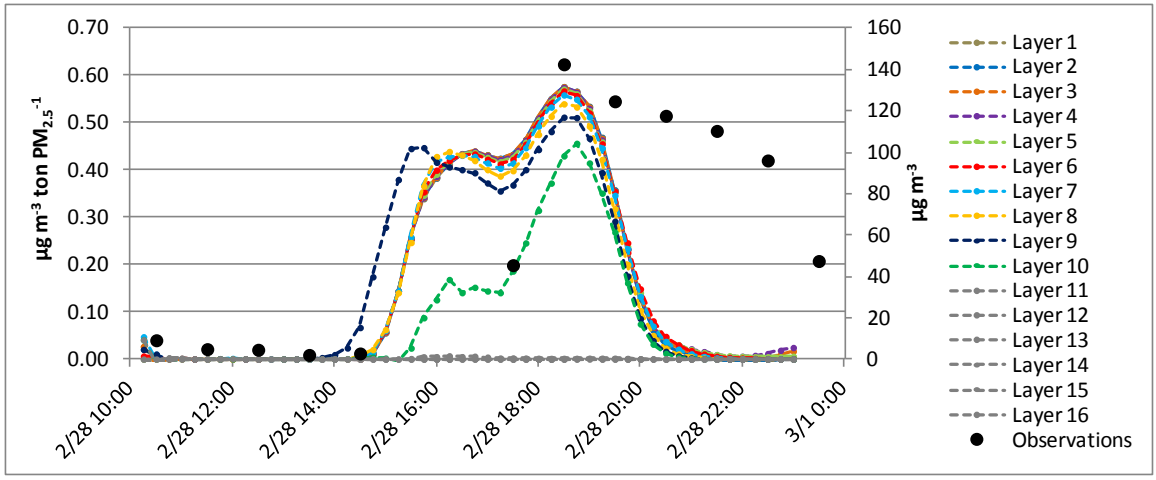

Figure 3.13. Brute-force first-order sensitivity coefficients for $PM_{2.5}$ concentration response to fire emissions by vertical CMAQ layer at South DeKalb for uniform distribution into 16 lowest layers (left axis), and site observations (right axis) on 28 February 2007 (LT).

The analysis reveals that CMAQ-predicted $PM_{2.5}$ concentrations are not exceedingly sensitive to the vertical distribution of fire emissions other than injection above or below a specific altitude. These results can be explained by analyzing the evolution of PBL height in meteorological input data. Figure 3.14 shows WRF-predicted PBL height during the episode at the Oconee fire location along with full-layer heights for the lower 11 vertical layers. In Section 3.3.4.3 below, we demonstrate that simulated $PM_{2.5}$ concentrations at South DeKalb are mostly sensitive to fire emissions released between 1200 and 1600 LT. During this lapse the PBL partially extends into layer 10 for only a fraction of the time and does not reach layers above. The analysis indicates that modeled $PM_{2.5}$ concentrations respond similarly to all fire emissions injected within the PBL and are not affected by emissions released into the free atmosphere. Previous studies have reported similar findings. Yang et al. (2011) conclude that modifying the vertical distribution of fire emissions injection did not significantly affect performance for their CMAQ simulations. Sensitivity analyses performed on the National Oceanic and Atmospheric Administration's Smoke Forecasting System determined that model effectiveness is dependent on accurately determining whether smoke injection height

occurred within or above the PBL (Stein et al., 2009). Although Liu et al. (2008) assert that CMAQ $PM_{2.5}$ predictions are highly sensitive to plume rise approximations, concentration differences are most evident between their simulations with emissions distributed within the PBL and that with injection at much higher altitudes. The results may change for plumes concentrated at the top of the PBL.

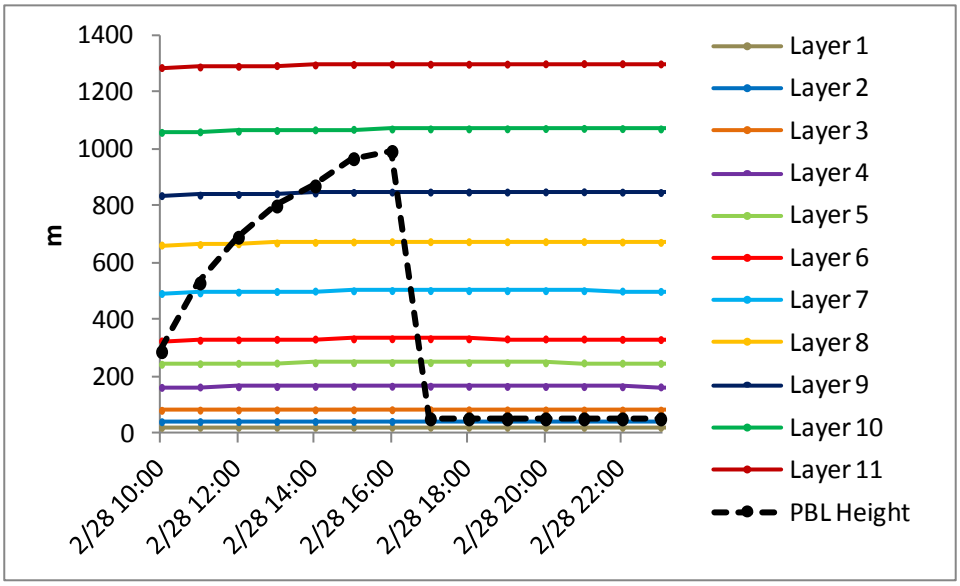

Figure 3.14. PBL height and full-layer altitudes for lower 11 vertical layers at Oconee fire site on 28 February 2007 (LT).

3.3.4.3 Temporal allocation of fire emissions

While important uncertainties related to the spatial allocation of fire emissions on gridded domains may exist, additional uncertainty associated with the temporal allocation of emissions may affect an air quality model's ability to simulate the impacts of wildland fires. Emissions are generally input into comprehensive air quality models as hourly emission rates. Similarly, fire emissions processors typically provide hourly estimates. Partitioning of fire emissions into hourly rates may be complicated by limited information about ignition time, duration, and evolution.

In this study, hourly rates for all fire emissions were prepared through FEPS. Hourly $PM_{2.5}$ emissions were previously shown in Figure 3.2. To compare the responsiveness of CMAQ-predicted $PM_{2.5}$ concentrations at Atlanta sites to hour-by-hour fire emissions, brute-force sensitivities were estimated for each hour. Perturbations were applied to single hour emissions in order to quantify first-order sensitivity coefficients and individual contributions to $PM_{2.5}$ concentrations at downwind receptors. Figure 3.15 shows estimated fire contributions to $PM_{2.5}$ concentration at South DeKalb for each hour of emissions. At this site, it is clear that most of the fire-related $PM_{2.5}$ pollution is attributable to fire emissions released during a 4 hour span. Emissions released from 1200 to 1600 LT are accountable for over 85% of the simulated fire contribution to $PM_{2.5}$ concentration.

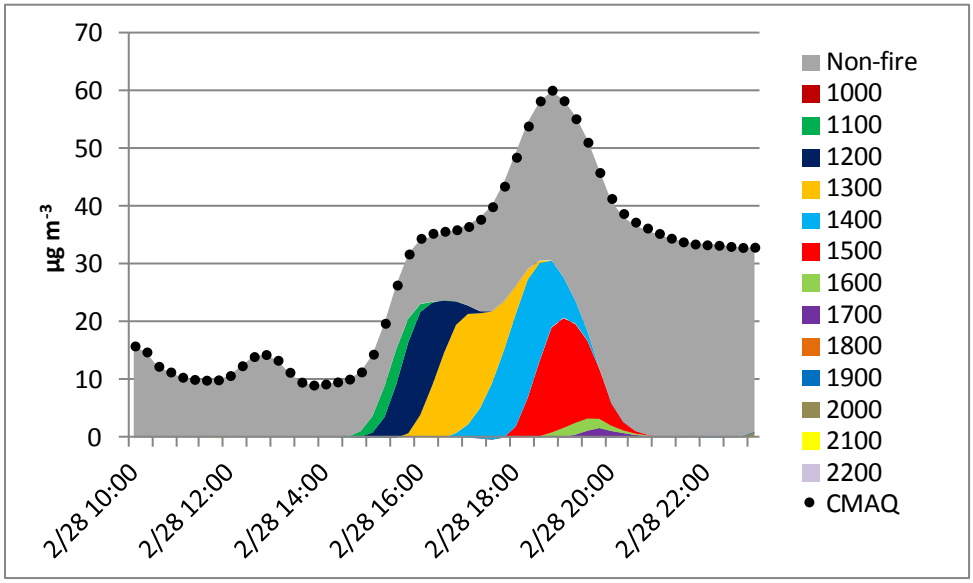

Figure 3.15. Fire contributions to modeled $PM_{2.5}$ concentration at South DeKalb by hour of emissions on 28 February 2007 (LT). Emissions are labeled at the start of the hour. Non-fire contribution and base-case CMAQ results are also included.

Differences between fire-related impacts for each hour of emissions are driven by both emissions timing and mass. Sensitivity estimates reflecting concentration

responsiveness to fire emissions are more informative. However, an objective comparison between sensitivities to hour-by-hour emission rates must account for the temporal variation in vertical distribution of emissions as described in Section 3.3.4.2. Here again, a constant vertical emissions distribution was applied to remove the influence of time-varying plume rise profiles and allow sensitivity calculations to solely focus on the temporal allocation of fire emissions. Figure 3.16 shows $PM_{2.5}$ concentration sensitivities to hour-by-hour fire emissions at South DeKalb after equally distributing fire emissions into the lower 10 vertical layers during the entire simulation. Results at all sites considered demonstrate that sensitivities of modeled $PM_{2.5}$ concentrations to hour-specific emissions can be substantially different. In Atlanta, $PM_{2.5}$ concentrations are influenced to varying degrees by emissions released between 1000 and 1800 LT with specific locations responding more intensely to emissions from distinct hours. The analysis also shows that each hour's fire-related emissions only influence concentrations at downwind receptors during a 2-3 hour period starting approximately 3 hours after release. Overall, sensitivity estimates illustrate that altering the temporal allocation of fire emissions can significantly change the timing of fire-related impacts and peak simulated concentrations. Hu et al. (2008) conclude from their "hindcast" simulations of this same episode that enhanced CMAQ performance is more readily achieved by improving hourly emissions profiles rather than refining fire location or emitted mass. The sensitivity analysis of modeling results to diurnal variability in wildfire emissions reported by Hodzic et al. (2007) finds that hourly resolved smoke emissions can greatly improve simulations compared to daily emissions inventories. Additionally, satellite information has been applied to temporally refine coarse fire emissions data and achieve superior model predictions (Roy et al., 2007).

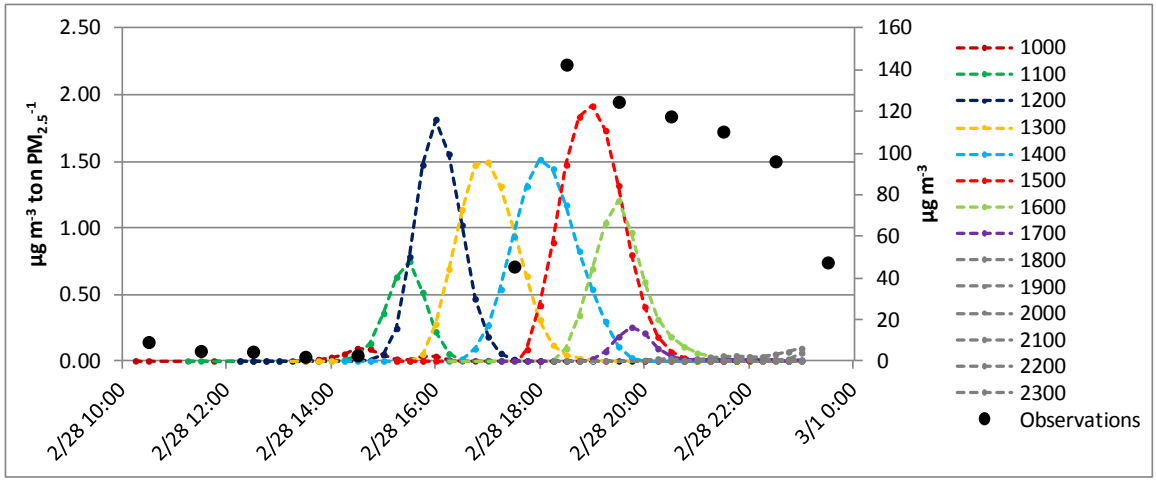

Figure 3.16. Brute-force first-order sensitivity coefficients for $PM_{2.5}$ concentration response to fire emissions by hour of emissions at South DeKalb for uniform distribution into 10 lower layers (left axis), and site observations (right axis) on 28 February 2007 (LT). Emissions are labeled at the start of the hour.

3.4 Conclusions

The sensitivity analyses completed in this study demonstrate that successful modeling of wildland fires impacts on air quality with gridded models is dependent on effective spatiotemporal allocation of emissions. Furthermore, the results indicate that shortcomings observed in previously reported simulations cannot be overcome by solely focusing on fire emissions magnitude. The horizontal and vertical distributions of emissions on gridded domains and their timing are key inputs that must also be carefully addressed.

In this study, analyses exploring the influence of plume rise show that modeled $PM_{2.5}$ concentrations are mostly sensitive to the fraction of emissions injected into the PBL. The vertical distribution of emissions within the PBL had little effect on downwind concentrations, at least under unstable atmospheric conditions. For the simulations completed, CMAQ-modeled vertical mixing of fire emissions within the PBL was extremely rapid and efficient. While correctly determining plume penetration into the free atmosphere is crucial to model results, only marginal gains in performance should be

expected from applying more detailed representations of vertical plume structure unless the approach also accounts for warm plume caught at the top of the PBL.

Sensitivity estimates related to the horizontal allocation of emissions on a gridded domain indicate that model performance could significantly benefit from more accurately positioning emissions. Predicted $PM_{2.5}$ concentrations are sensitive to the horizontal allocation of emissions. Additionally, model results are clearly responsive to whether fire emissions are horizontally distributed into single or multiple grid cells. Improving the horizontal allocation of fire emissions may be especially important in relation to plume rise approximations. Using downwind ascent approximations but then injecting fire emissions at the initial position of release is clearly an error that may significantly affect results. Optimum model performance necessitates injection at the correct downwind location. The responsiveness of predicted $PM_{2.5}$ concentrations to small variations in the horizontal allocation of fire emissions also reflects a strong influence from meteorological inputs. Sensitivities may be primarily driven by variability in meteorological fields. Yang et al. (2011) find that errors in CMAQ predictions of the air quality impacts of wildfires may be dominated by uncertainty in wind fields. The degree to which simulations are constrained by uncertainties in meteorological fields produced by weather forecasting models is further investigated in Chapter 4.

Perhaps the largest potential gains in model accuracy lie in better characterizing the temporal distribution of fire-related emissions. For the smoke episode simulated sensitivity analysis show that fire-related $PM_{2.5}$ impacts are primarily attributable to emissions injected within a specific time frame. The analyses also demonstrate that each individual hour's fire emissions produce a response at downwind receptors lasting 2-3 hours. Reducing the uncertainties associated with distributing emissions into discontinuous inputs and better approximating the timing and progression of pollutant releases is a practical approach to improve model performance. Here again ensuring the adequacy of meteorological inputs is essential.

Beyond spatiotemporal allocation of emissions, additional concerns must be considered to successfully simulate the air quality impacts of wildland fires with comprehensive modeling systems. Grid resolution may be especially significant in smoke plume modeling. Fire-related emissions estimates must still be further improved. Representative estimates of secondary aerosol formation and precursor emissions may also be important. Furthermore, the response of pollutants subject to strong nonlinearities may be different to the dispersion-related response explored in this study. A substantial improvement in the ability of photochemical air quality models to forecast the impacts of wildland fires would require jointly addressing these research needs.

3.5 References

Achtemeier, G.L., Goodrick, S.A., Liu, Y., Garcia-Menendez, F., Hu, Y., Odman, M.T. (2011) Modeling smoke plume-rise and dispersion from southern United States prescribed burns with Daysmoke. Atmosphere 2, 358-388.

Akagi, S.K., Yokelson, R.J., Wiedinmyer, C., Alvarado, M.J., Reid, J.S., Karl, T., Crounse, J.D., Wennberg, P.O. (2011) Emission factors for open and domestic biomass burning for use in atmospheric models. Atmospheric Chemistry and Physics 11, 4039-4072.

Christopher, S.A., Gupta, P., Nair, U., Jones, T.A., Kondragunta, S., Wu, Y.L., Hand, J., Zhang, X.Y. (2009) Satellite remote sensing and mesoscale modeling of the 2007 Georgia/Florida fires. IEEE Journal of Selected Topics in Applied Earth Observations and Remote Sensing 2, 163-175.

Cohan, D.S., Hakami, A., Hu, Y.T., Russell, A.G. (2005) Nonlinear response of ozone to emissions: Source apportionment and sensitivity analysis. Environmental Science & Technology 39, 6739-6748.

Freitas, S.R., Longo, K.M., Chatfield, R., Latham, D., Silva Dias, M.A.F., Andreae, M.O., Prins, E., Santos, J.C., Gielow, R., Carvalho Jr, J.A. (2007) Including the sub-grid scale plume rise of vegetation fires in low resolution atmospheric transport models. Atmospheric Chemistry and Physics 7, 3385-3398.

Giglio, L., van der Werf, G.R., Randerson, J.T., Collatz, G.J., Kasibhatla, P. (2006) Global estimation of burned area using MODIS active fire observations. Atmospheric Chemistry and Physics 6, 957-974.

Hakami, A., Odman, M.T., Russell, A.G. (2004) Nonlinearity in atmospheric response: A direct sensitivity analysis approach. Journal of Geophysical Research 109, D15303.

Henderson, S.B., Ichoku, C., Burkholder, B.J., Brauer, M., Jackson, P.L. (2010) The validity and utility of MODIS data for simple estimation of area burned and aerosols emitted by wildfire events. International Journal of Wildland Fire 19, 844-852.

Hodzic, A., Madronich, S., Bohn, B., Massie, S., Menut, L., Wiedinmyer, C. (2007) Wildfire particulate matter in Europe during summer 2003: meso-scale modeling of smoke emissions, transport and radiative effects. Atmospheric Chemistry and Physics 7, 4043-4064.

Hu, Y.T., Odman, M.T., Chang, M.E., Jackson, W., Lee, S., Edgerton, E.S., Baumann, K., Russell, A.G. (2008) Simulation of air quality impacts from prescribed fires on an urban area. Environmental Science & Technology 42, 3676-3682.

Hwang, D., Byun, D.W., Talat Odman, M. (1997) An automatic differentiation technique for sensitivity analysis of numerical advection schemes in air quality models. Atmospheric Environment 31, 879-888.

Junquera, V., Russell, M.M., Vizuete, W., Kimura, Y., Allen, D. (2005) Wildfires in eastern Texas in August and September 2000: Emissions, aircraft measurements, and impact on photochemistry. Atmospheric Environment 39, 4983-4996.

Konovalov, I.B., Beekmann, M., Kuznetsova, I.N., Yurova, A., Zvyagintsev, A.M. (2011) Atmospheric impacts of the 2010 Russian wildfires: integrating modelling and measurements of an extreme air pollution episode in the Moscow region. Atmospheric Chemistry and Physics 11, 10031-10056.

Koo, B., Wilson, G.M., Morris, R.E., Dunker, A.M., Yarwood, G. (2009) Comparison of source apportionment and sensitivity analysis in a particulate matter air quality model. Environmental Science & Technology 43, 6669-6675.

Lee, S., Baumann, K., Schauer, J.J., Sheesley, R.J., Naeher, L.P., Meinardi, S., Blake, D.R., Edgerton, E.S., Russell, A.G., Clements, M. (2005) Gaseous and particulate emissions from prescribed burning in Georgia. Environmental Science & Technology 39, 9049-9056.

Liu, Y., Achtemeier, G., Goodrick, S. (2008) Sensitivity of air quality simulation to smoke plume rise. Journal of Applied Remote Sensing 2, 021503.

Liu, Y., Goodrick, S., Achtemeier, G., Jackson, W.A., Qu, J.J., Wang, W. (2009) Smoke incursions into urban areas: simulation of a Georgia prescribed burn. Int. J. Wildland Fire 18, 336-348.

MACTEC, (2005) Documentation of the revised 2002 base year, revised 2018, and initial 2009 emission inventories for VISTAS. Visibility Improvement State and Tribal Association of the Southeast, Forest Park, GA.

Napelenok, S.L., Cohan, D.S., Hu, Y.T., Russell, A.G. (2006) Decoupled direct 3D sensitivity analysis for particulate matter (DDM-3D/PM). Atmospheric Environment 40, 6112-6121.

Odman, M.T., (2011) Evaluation of smoke models and sensitivity analysis for determining their emission related uncertainties. Joint Fire Science Program, Atlanta, GA.

Odman, M.T., (2012) Characterization of emissions and air quality modeling for predicting the impacts of prescribed burns at DoD lands. Strategic Environmental Research and Development Program, Atlanta, GA.

Roy, B., Pouliot, G.A., Gilliland, A., Pierce, T., Howard, S., Bhave, P.V., Benjey, W. (2007) Refining fire emissions for air quality modeling with remotely sensed fire counts: A wildfire case study. Atmospheric Environment 41, 655-665.

Sessions, W.R., Fuelberg, H.E., Kahn, R.A., Winker, D.M. (2011) An investigation of methods for injecting emissions from boreal wildfires using WRF-Chem during ARCTAS. Atmospheric Chemistry and Physics 11, 5719-5744.

Stein, A.F., Rolph, G.D., Draxler, R.R., Stunder, B., Ruminski, M. (2009) Verification of the NOAA Smoke Forecasting System: Model sensitivity to the injection height. Weather and Forecasting 24, 379-394.

Strand, T.M., Larkin, N., Craig, K.J., Raffuse, S., Sullivan, D., Solomon, R., Rorig, M., Wheeler, N., Pryden, D. (2012) Analyses of BlueSky Gateway PM2.5 predictions during the 2007 southern and 2008 northern California fires. J. Geophys. Res. 117.

Tian, D., (2006) Evaluation of emission uncertainties and their impacts on air quality modeling: applications to biomass burning. Georgia Institute of Technology, Atlanta, GA.

Tian, D., Hu, Y.T., Wang, Y.H., Boylan, J.W., Zheng, M., Russell, A.G. (2009) Assessment of biomass burning emissions and their impacts on urban and regional PM2.5: A Georgia case study. Environmental Science & Technology 43, 299-305.

Tian, D., Wang, Y.H., Bergin, M., Hu, Y.T., Liu, Y.Q., Russell, A.G. (2008) Air quality impacts from prescribed forest fires under different management practices. Environmental Science & Technology 42, 2767-2772.

Wiedinmyer, C., Quayle, B., Geron, C., Belote, A., McKenzie, D., Zhang, X.Y., O'Neill, S., Wynne, K.K. (2006) Estimating emissions from fires in North America for air quality modeling. Atmospheric Environment 40, 3419-3432.

Yang, E.S., Christopher, S.A., Kondragunta, S., Zhang, X.Y. (2011) Use of hourly Geostationary Operational Environmental Satellite (GOES) fire emissions in a Community Multiscale Air Quality (CMAQ) model for improving surface particulate matter predictions. Journal of Geophysical Research 116, D04303.

Zeng, T., Wang, Y.H., Yoshida, Y., Tian, D., Russell, A.G., Barnard, W.R. (2008) Impacts of Prescribed Fires on Air Quality over the Southeastern United States in Spring Based on Modeling and Ground/Satellite Measurements. Environmental Science & Technology 42, 8401-8406.

CHAPTER 4

SIMULATING SMOKE TRANSPORT FROM WILDLAND FIRES WITH A REGIONAL-SCALE AIR QUALITY MODEL: SENSITIVITY TO UNCERTAIN WIND FIELDS

Abstract

Uncertainties associated with meteorological inputs which are propagated through atmospheric chemical transport models may constrain their ability to replicate the effects of wildland fires on air quality. Here we investigate the sensitivity of predicted fine particulate matter ($PM_{2.5}$) concentrations to uncertain wind fields by simulating the air quality impacts of two fires on an urban area with the Community Multiscale Air Quality modeling system (CMAQ). Brute-force sensitivity analyses show that modeled concentrations at receptors downwind from the fires are highly sensitive to variations in wind speed and direction. Additionally, uncertainty in wind fields produced with the Weather Research and Forecasting model (WRF) was assessed by evaluating meteorological predictions against surface and upper air observations. Significant differences between predicted and observed wind fields were identified. Simulated $PM_{2.5}$ concentrations at urban sites displayed large sensitivities to wind perturbations within the error range of meteorological inputs. The analyses demonstrate that normalized errors in CMAQ predictions attempting to model the regional impacts of fires on $PM_{2.5}$ concentrations could be as high as 100% due to inaccuracies in wind data. Meteorological drivers may largely account for the considerable discrepancies between monitoring site observations and predicted concentrations. The results of this study demonstrate that

*A modified version of this chapter has been published in *Simulating smoke transport from wildland fires with a regional-scale air quality model: Sensitivity to uncertain wind fields*, Journal of Geophysical Research: Atmospheres **2013**, 118, 6493–6504.

limitations in fire-related air quality simulations cannot be overcome by solely improving emission rates.

4.1 Introduction

Wildland fires may greatly impact air quality and pose a significant threat to public health. Air quality models can serve as tools to quantify exposure to fire-related pollution and provide important information to fire and land managers. However, the limitations inherent to numerical models when used to replicate the air quality impacts of fires must be identified and well understood to adequately interpret results and further improve the models' predictive skills. Multiscale atmospheric chemical transport models provide an appealing framework to simulate the effects of wildland fires on air quality: complex chemical and physical processes are represented; local and regional scales can be jointly treated; and detailed emissions and meteorological fields can be used to drive air quality modeling. Multiple attempts to replicate the impacts of fires on air quality with Eulerian models have been reported (Goodrick et al., 2012). Commonly, model performance in these simulations, assessed by comparing modeled and observed pollutant concentrations, has been unsatisfactory and a need to improve predictions has been recognized.

Air quality models require two fundamental inputs: meteorological fields and emission rates. The importance of meteorological input fields in air quality simulations has long been acknowledged (Seaman, 2000). However, prior studies seeking to simulate the impacts of wildland fires with Eulerian air quality models have generally focused on better characterizing fire-related emissions as a strategy to strengthen model performance (Konovalov et al., 2011; Tian et al., 2009; Yang et al., 2011). In contrast, little attention has been given to the implications uncertain meteorological inputs may have on model predictions. Still, weather conditions determine the principal physical driving forces in the atmosphere, making gridded representations of meteorology the foundation of all

three-dimensional air quality simulations. While enhanced fire emissions estimates can improve the accuracy of air quality simulations, errors associated with weather data continue to affect model results. Therefore, determining the degree to which uncertainties in meteorological inputs might hinder fire-related simulations is an important step towards successfully modeling the impacts of wildland fires on pollutant concentrations with atmospheric chemical transport models.

Sensitivity analyses are an important diagnostic tool to evaluate the influence individual inputs may have on specific model outputs. Here we use a regional-scale chemical transport model to simulate smoke transport from wildland fires in an urban smoke episode which severely deteriorated air quality throughout the Atlanta metropolitan area in 2007. The simulation results show a significant response in predicted $PM_{2.5}$ concentrations to small variations in the spatial allocation of fire emissions, suggesting a potentially strong influence from wind inputs. In fact, errors in model-predicted $PM_{2.5}$ concentrations could be dominated by the uncertainty in wind fields rather than emission estimates (Yang et al., 2011). In this chapter, the Atlanta 2007 simulation is used as a base case episode to investigate the sensitivities of model predictions to the meteorological fields used to drive air quality simulations.

A series of sensitivity analyses were applied to explore the responsiveness of $PM_{2.5}$ concentrations predicted by the air quality model to uncertainties in three-dimensional wind fields. We focus on primary fine carbonaceous particle emissions from fires, the main component of fire-related smoke, and wind, the meteorological variable most clearly associated with fire-attributable impacts on $PM_{2.5}$ concentrations. The results of this work indicate the extent to which simulations may be constrained by inaccuracies in meteorological data produced by numerical weather prediction models. Additionally, the analysis described in this study investigates whether the errors in predicted concentrations can be abated by exclusively focusing on better estimation of fire-related emissions. The air quality modeling framework used is described in Section 4.2. Section

4.3 presents the methodology applied to carry out the sensitivity analyses and evaluate the wind field inputs. The results of the sensitivity analyses and wind field uncertainty assessment are included in Section 4.4. Finally, our conclusions are presented in Section 4.5.

4.2 Numerical Modeling Framework

4.2.1 Meteorology

Meteorological data are used to capture atmospheric conditions throughout modeling domains and play a vital role in determining pollutant concentrations predicted by air quality models. Although air quality simulations, particularly those performed with plume or puff models, can rely on observed or simplified weather data, comprehensive Eulerian models require detailed three-dimensional meteorological fields. Meteorological fields used by atmospheric chemical transport models are typically prepared with mesoscale numerical weather prediction systems such as the fifth-generation Pennsylvania State University/National Center for Atmospheric Research Mesoscale Model (MM5) (Grell et al., 1994) and the Weather Research and Forecasting model (WRF) (Skamarock et al., 2008). For retrospective air quality simulations, reanalysis fields and data assimilation of observed meteorology can be applied.

Most reported simulations attempting to replicate the impacts of wildland fires on air quality with Eulerian models have relied on meteorological fields produced with MM5 (Chen et al., 2008; Junquera et al., 2005; Strand et al., 2012). The choice is consistent with the initial application of current models, originally designed to use MM5-derived meteorological inputs. More recently, air quality modeling has incorporated meteorological fields generated with WRF (Appel et al., 2010). Studies comparing MM5 and WRF performance and assessing the sensitivity of air quality predictions to weather model selection indicate that, although differences exist in model results, meteorological

and air quality fields based on either are of comparable qualities (Appel et al., 2010; Gilliam and Pleim, 2010).

For this study, meteorological fields produced with WRF (version 2.1.2) were used to drive all air quality modeling. Meteorology was simulated on three nested domains with 36, 12, and 4 km horizontal grid spacing and 34 vertical layers extending up to 50 hPa. The simulations used the Yonsei University (YSU) planetary boundary layer scheme (Hong et al., 2006), Noah land surface model (Ek et al., 2003), Dudhia shortwave radiation scheme (Dudhia, 1989), Rapid Radiative Transfer Model (RRTM) longwave radiation scheme (Mlawer et al., 1997), Kain-Fritsch cumulus parameterization scheme (Kain, 2004), and the Lin et al. microphysics scheme (Chen and Sun, 2002; Lin et al., 1983; Rutledge and Hobbs, 1984). The options selected correspond to the configuration of an operational air quality forecasting system in Atlanta which has been used by forecasters in the state of Georgia (USA) since 2006 (Hu et al., 2010). Simulations were initialized, constrained at the boundaries, and nudged at 6-hour intervals using reanalysis fields from the North American Mesoscale model (nomads.ncdc.noaa.gov).

4.2.2 Air Quality

A description of the emissions of and chemical transport models used to numerically simulate the transport and transformation of pollutant emissions is included in Chapter 3. Briefly, the Multiscale Air Quality Modeling system (CMAQ version 4.5, http://www.cmaq-model.org/) was used to simulate fire-related emissions. Sensitivity analyses relied on CMAQ simulations carried out with 4 km resolution. Emission inputs from non-fire sources were processed with the Sparse Matrix Operator Kernel Emission processor (SMOKE version 2.1, http://www.smoke-model.org/index.cfm), while the emission rates for featured wildland fires were prepared through the Fire Emissions Production Simulator (FEPS version 1.1.0, http://www.fs.fed.us/pnw/fera/feps/). Plume

rise estimates from the Daysmoke model (Achtemeier et al., 2011) were used to vertically distribute fire emissions.

4.3 Methodology

4.3.1 Base case simulation

The sensitivity analyses performed were based on a CMAQ simulation of a fire-related smoke episode which occurred on 28 February 2007 and was previously described in Chapter 3. The base case air quality simulation intends to replicate the impact of two prescribed burns on $PM_{2.5}$ concentrations throughout the Atlanta metropolitan area. The fires occurred at the Oconee National Forest and Piedmont National Wildlife Refuge (henceforth referred to as Oconee and Piedmont), approximately 80 km southeast of Atlanta. Transport of fire-related emissions by southeasterly winds throughout the day is believed to have led to large increases in pollutant concentrations recorded at urban monitoring sites.

Measured $PM_{2.5}$ concentrations from the Georgia Department of Natural Resources' Ambient Monitoring Program and the Southeastern Aerosol Research and Characterization (SEARCH) Network were used to assess model performance. Air quality records from three Atlanta sites (Confederate Ave., Jefferson St., and South DeKalb) and one additional site (McDonough), located approximately midway between Atlanta and the Oconee and Piedmont fires, were considered. Figure 4.1 shows observed and CMAQ-predicted $PM_{2.5}$ concentrations at the Confederate Ave. station. Simulated $PM_{2.5}$ concentrations were much lower than observed peaks at monitoring sites. It should be noted that a simulation without the fires predicts about 20 $\mu g\ m^{-3}$ of $PM_{2.5}$ at the Atlanta sites considered, leaving only about 30 $\mu g\ m^{-3}$ associated with the burns. Consistent with previously reported efforts to replicate the air pollution impacts of wildland fires with Eulerian chemical transport models, the base case CMAQ simulation

significantly underpredicts the impacts of prescribed burns on $PM_{2.5}$ concentrations observed at urban monitoring stations (Liu et al., 2009; Strand et al., 2012; Yang et al., 2011). For predicted $PM_{2.5}$ concentrations to match maximum observed concentrations throughout Atlanta fire emissions would have to be increased by more than 400%, as demonstrated in the sensitivity analyses related to fire emissions included in Chapter 2. Uncertainties in fire-related emission rates may play a significant role in the underestimation of $PM_{2.5}$ concentrations. However, an increment of this magnitude does not seem reasonable. In addition, significant sensitivities of CMAQ predictions to the spatiotemporal allocation of fire-related emissions on gridded domains were observed. These are suggestive of potentially important sensitivities to meteorological inputs and in particular to wind fields.

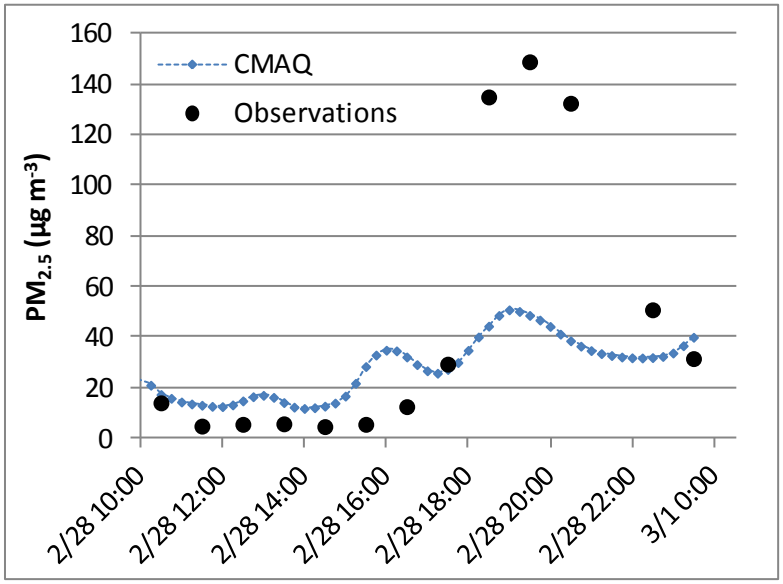

Figure 4.1. Observed 1-hour average and CMAQ-predicted 15-minute $PM_{2.5}$ concentrations at the Confederate Ave. monitoring site on 28 February 2007 (LT).

4.3.2 Brute-force sensitivity analyses

A brute-force method was applied to carry out sensitivity analyses. The method relies on successively simulating the same system of interest while varying a specific model input and holding others constant to observe the response of model outputs (Hwang et al., 1997). In air quality modeling, brute-force sensitivity analyses have been frequently used to quantify the responsiveness of simulated concentrations to changes in emissions. The response of modeled $PM_{2.5}$ concentrations to changes in primary emissions should be nearly linear (Koo et al., 2009). Here, the brute-force method is used to assess the sensitivity of simulated $PM_{2.5}$ concentrations to perturbations in wind inputs, namely wind speed and direction. In this case, the response of concentrations to changes in winds is not expected to be linear as there are complex nonlinear relationships between the winds and concentrations at downwind receptors. Nevertheless, sensitivity analyses were performed to observe the degree to which simulations are affected by variations, or uncertainty, in wind fields.

A series of simulations under perturbed wind fields were carried out to examine the responsiveness of CMAQ-predicted $PM_{2.5}$ concentrations at specific downwind receptors. Wind fields were modified within the Meteorology-Chemistry Interface Processor (MCIP, version 3.4.1) (Otte and Pleim, 2010) used to convert WRF output fields into CMAQ-compatible inputs. The magnitude and direction of wind vectors read in from WRF-generated fields were perturbed to varying extents to produce modified CMAQ inputs, as illustrated in Figure 4.2. In this manner, perturbations are reflected in all wind-associated variables included in the meteorological input data used to drive the air quality model. It is also important to note that in CMAQ 4.5, mass conservation is ensured by adjusting vertical winds (Hu et al., 2006). Perturbations to wind direction and wind speed are accompanied by changes to the vertical winds as mass conservation is obeyed within the model. In general we find that perturbing horizontal wind speeds leads

to proportional changes in the vertical speeds, while the effect of altering wind direction on the vertical wind field is nonlinear and spatially complex.

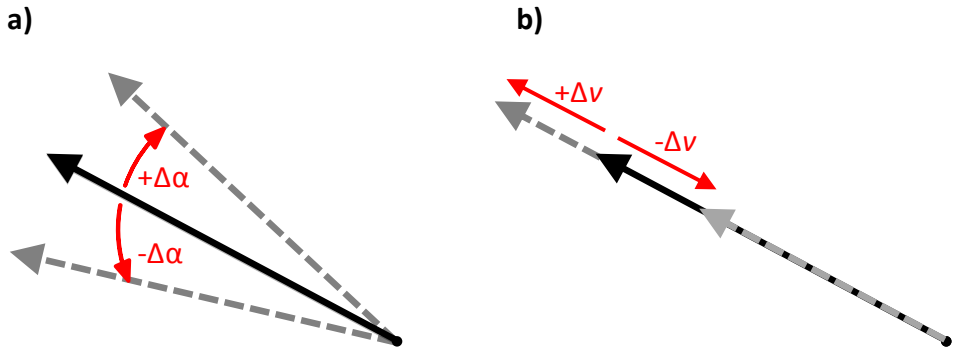

Figure 4.2. Representation of perturbations applied to (a) wind direction and (b) wind speed in brute-force sensitivity analysis.

4.3.3 Meteorological uncertainty

Meteorological model performance was evaluated to assess the level of uncertainty in weather fields used to drive air quality simulations. Hourly surface observations from the Research Data Archive of the National Center for Atmospheric Research (http://rda.ucar.edu/datasets/ds472.0/) were used to compute model performance metrics by comparing surface-layer observations and predictions. Bias and error in WRF-derived ground-level predictions were estimated for wind direction, wind speed, temperature, and humidity. Additionally, upper air model predictions were evaluated against atmospheric soundings launched from Peachtree City, GA, approximately 45 km southwest of Atlanta and 80 km northwest from the Oconee and Piedmont fires. Sounding observations were available every 12 hours at 0000 and 1200 UT.

4.4 Results

4.4.1 Sensitivity Analyses

4.4.1.1 Wind Direction

To examine the sensitivity of CMAQ-predicted $PM_{2.5}$ concentrations to wind direction, the Atlanta 2007 smoke episode was modeled under a series of perturbed wind fields. Modified fields were produced by uniformly perturbing wind direction by ±5°, ±15°, and ±30° across the entire domain. The changes were applied at each grid point by rotating all wind vectors from WRF by the same angle during MCIP processing, as described in Section 4.3.2. At selected downwind monitoring sites, predicted $PM_{2.5}$ concentrations for each perturbed wind field and the base case were compared to observe the responsiveness to variations in wind direction. Figure 4.3 shows $PM_{2.5}$ concentrations simulated by CMAQ at the Jefferson St. monitoring site with both perturbed and unperturbed fields. The sensitivity of predicted $PM_{2.5}$ concentrations to wind direction is extremely high at Jefferson St., as well as at all other sites considered. The results indicate that small variations in wind direction can lead to large changes in predicted pollutant concentrations at specific receptors downwind. At Jefferson St., for instance, a -5° rotation to wind vectors increases the maximum predicted $PM_{2.5}$ concentration by more than 13 μg m^{-3}, a 26% increase. At different urban locations, sensitivities to wind direction are likewise large and nonlinear. Peak $PM_{2.5}$ concentrations predicted at sites within Atlanta increased by as much as 8 to 30% with perturbed wind fields, although remaining well below observed levels. However, the effect of the wind direction variations at each receptor may vary significantly. Figure 4.4 shows the change in predicted $PM_{2.5}$ concentrations relative to the base case simulation at different monitoring sites after applying a -5° perturbation to wind direction. Although the responses are quite similar at the Confederate Ave. and Jefferson St. sites 8 km apart, appreciable differences

exist between the sensitivities at these locations and South DeKalb, 7 km from Confederate Ave., where the maximum change in predicted $PM_{2.5}$ concentration is significantly lower. At McDonough, approximately 40 km closer to the fires, the response is larger and, compared to the Atlanta sites, appears to reflect a 2-hour advance consistent with expected differences in transport time.

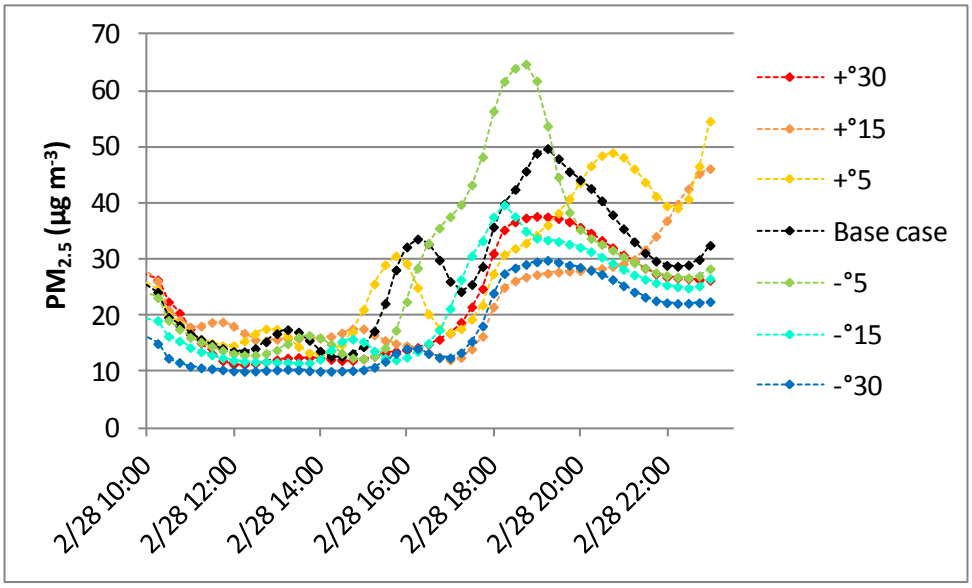

Figure 4.3. CMAQ-predicted $PM_{2.5}$ concentrations at the Jefferson St. monitoring site using wind direction perturbations on 28 February 2007 (LT). Base case simulation results are also included.

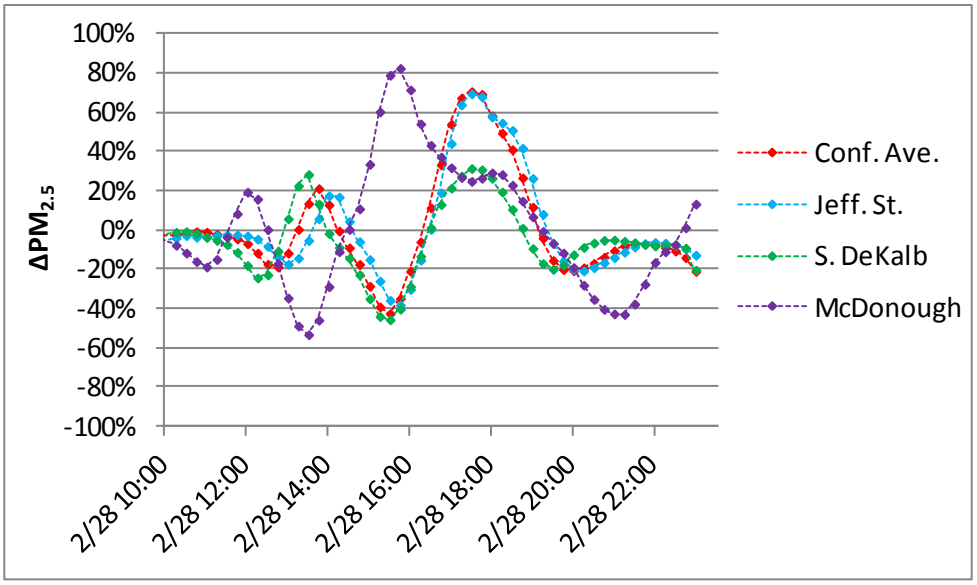

Figure 4.4. Change in CMAQ-predicted $PM_{2.5}$ concentrations on 28 February 2007 (LT) relative to base case simulation at the Confederate Ave., Jefferson St., South DeKalb, and McDonough monitoring sites after applying a -5° perturbation to wind direction.

The influence of wind direction on air quality modeling results can be observed in Figure 4.5 which compares ground-level $PM_{2.5}$ concentration predictions after perturbing wind direction by -5° and +5°. The figure shows how a 10° difference in wind direction can completely change a smoke plume's predicted impact at downwind receptors. Within this 10° wind direction variation range, predicted $PM_{2.5}$ concentrations at Atlanta may vary by more than 30 μg m^{-3}. It is important to note that although errors in wind direction may partially explain the discrepancy between modeled and observed concentrations, simply inducing a directional adjustment on wind fields should not be considered a robust strategy to strengthen model performance. While it was possible to reduce the gap between observed and predicted peak $PM_{2.5}$ concentrations in Atlanta by modifying wind direction in meteorological inputs, perturbed wind fields decreased the root mean squared error (RMSE), estimated from the differences between modeled and observed values, only at Jefferson St. and McDonough. Still, the sensitivity analysis demonstrates that wind direction in meteorological inputs is a key element of air quality simulations

attempting to replicate the impacts of fires and accurate wind directions are essential to produce realistic predictions.

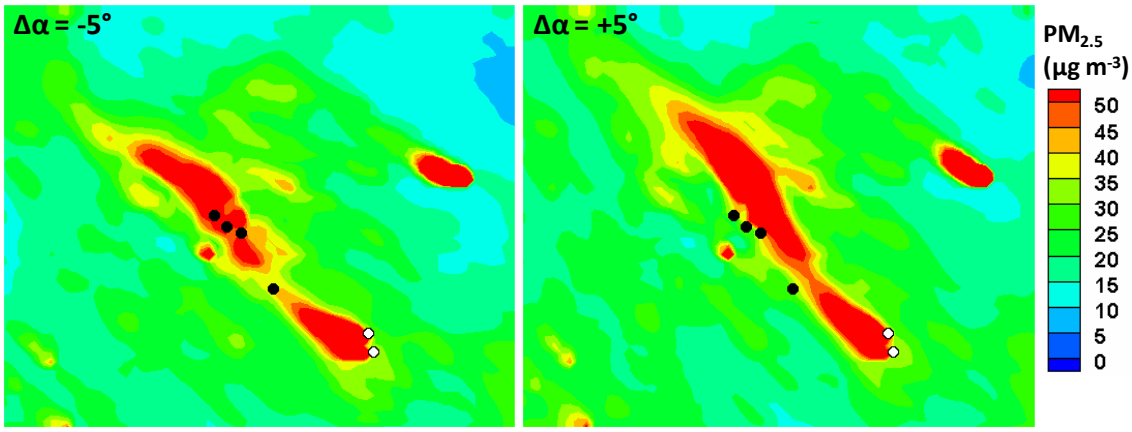

Figure 4.5. CMAQ-predicted $PM_{2.5}$ concentrations (μg m^{-3}) over northern Georgia at 1900 LT on 28 February 2007 using -5° and +5° perturbations to wind direction. Black shaded circles indicate monitoring station locations. The Oconee and Piedmont fire sites are denoted by white shaded markers.

4.4.1.2 Wind Speed

The methodology previously described in Section 4.3.2 was also used to explore the sensitivity of CMAQ-predicted $PM_{2.5}$ concentrations to wind speed. Similarly to the perturbations on wind direction, modified wind fields were produced by uniformly changing wind speeds by ±10%, ±20%, and ±30% across meteorological inputs. Large differences exist between predicted concentrations at downwind receptors under different modified fields. In Figure 4.6, simulated $PM_{2.5}$ concentrations at the South DeKalb monitoring site are shown for each perturbation. A strong response to variations in wind speed is evident: at South DeKalb a 30% decrease in wind speed elevated the peak $PM_{2.5}$ concentration by more than 40 μg m^{-3}, an increase of nearly 75% with respect to the base case simulation. The responses are similar at all receptors considered; $PM_{2.5}$ concentrations significantly increased and experienced a growing delay with decreasing wind speeds. Unlike the response to wind direction, response to wind speed can be

relatively linear. Figure 4.7 shows maximum $PM_{2.5}$ concentrations predicted by CMAQ at different downwind receptors as wind speed is perturbed from -50% to +50%. Response to wind speed is highly linear for negative perturbations but flattens out as magnitude is increased beyond a +10% perturbation.

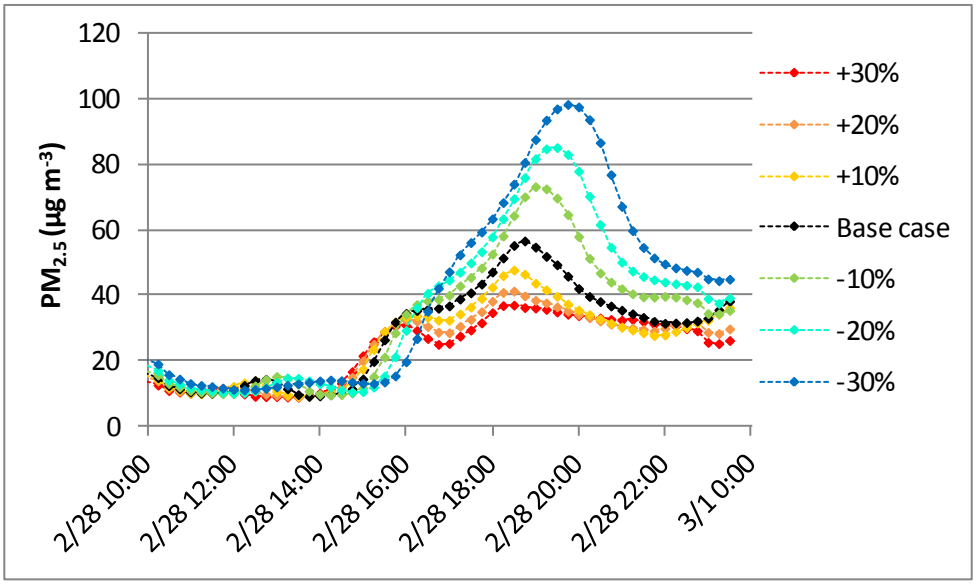

Figure 4.6. CMAQ-predicted $PM_{2.5}$ concentrations on 28 February 2007 (LT) at the South DeKalb monitoring site with wind speed perturbations. Base case simulation results are also included.

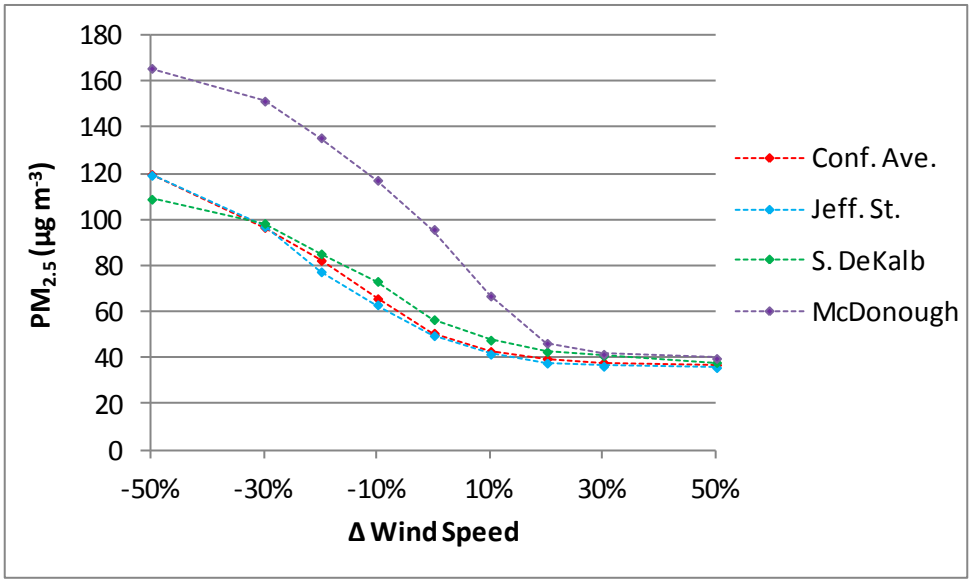

Figure 4.7. Maximum CMAQ-predicted $PM_{2.5}$ concentrations at the Confederate Ave., Jefferson St., South DeKalb, and McDonough monitoring sites with wind speed perturbations ranging from -50% to +50%.

Several factors contribute to the large differences in $PM_{2.5}$ concentration predictions obtained applying different perturbations. Most importantly, changes to wind speed bring about significant differences in the dispersion of fire-related emissions. While larger wind speeds intensify advective dispersion, decreasing wind speed allows $PM_{2.5}$ emissions to accumulate within a smaller volume and reach higher concentrations. The effect wind speeds can have on smoke plume dispersion in Eulerian models is depicted in Figure 4.8. Here, smoke plumes are shown as three-dimensional iso-surfaces bounded by $PM_{2.5}$ concentration equal to 35 µg m^{-3}. As wind speed increases, dispersion of smoke occurs at a higher rate. The effect becomes more evident as winds strengthen with increasing altitude. Variations in wind speed also result in changes to the vertical winds within CMAQ. Generally, the perturbations to horizontal wind speeds yield a proportional increase or decrease in the vertical winds. This may further affect dispersion, enhancing it when wind speed is intensified and suppressing it when wind speed is reduced. In addition, wind speed perturbations may alter the trajectory traveled by the

smoke plume and change the likelihood that it will directly impact a specific downwind receptor. Another factor leading to differences in predicted concentrations is the PBL height at the time of smoke arrival to the receptor. Finally, it is apparent that wind speed perturbations may also influence the dispersion of emissions from non-fire sources, including urban emissions. Therefore, the changes to $PM_{2.5}$ concentrations predicted under modified wind fields are due to the combined response of both fire-related impacts and the impacts from all other sources included in the simulation.

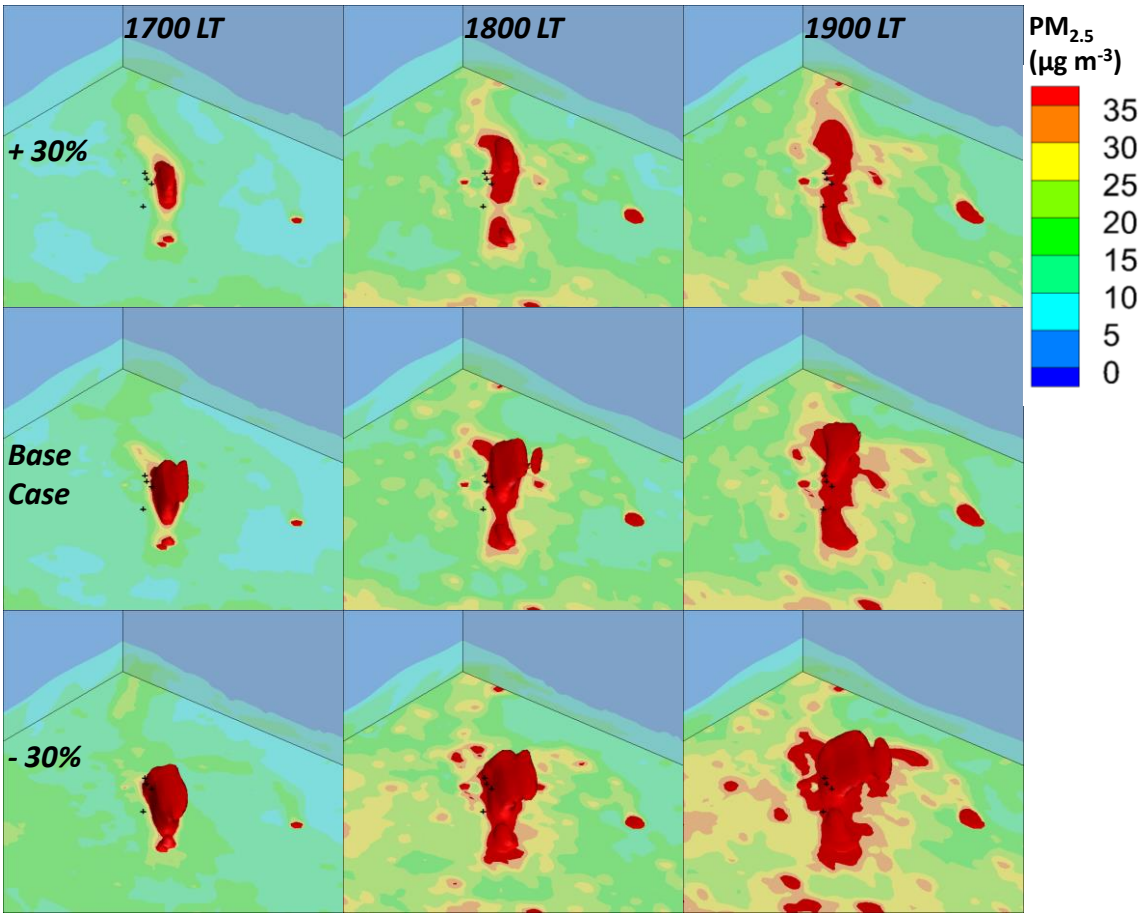

Figure 4.8. Modeled pollution plumes on 28 February 2007 (LT) shown as three-dimensional iso-surfaces bounded by $PM_{2.5}$ concentration equal to 35 µg m^{-3} for base case and simulations carried out with ±30% perturbations to wind speed. Ground-level $PM_{2.5}$ concentrations (µg m^{-3}) are also shown. Air quality monitoring sites are indicated by black markers.

Although errors related to wind speed cannot fully explain the difference between modeled and observed $PM_{2.5}$ concentrations, the sensitivity analyses suggest that uncertain wind speed estimates may play an important role in the underpredictions commonly associated with simulations attempting to replicate the air quality impacts of fires. In the smoke episode simulated for this study, reduced wind speeds led to higher peak $PM_{2.5}$ concentrations and prolonged air quality impacts, consistent with observations at downwind receptors. At the Atlanta locations considered, a 30% decrease in wind speed significantly improved model performance, reducing RMSE, estimated from the differences between modeled and observed $PM_{2.5}$ concentrations, at Confederate Ave., Jefferson St., and South DeKalb by 37%, 12%, and 36% respectively. No gains in model performance were achieved at McDonough, GA, indicating that the prediction error at this location closer to the fires is more likely related to wind direction or the spatiotemporal allocation of fire emissions.

4.4.1.3 Relation to grid resolution

The importance of grid resolution in simulations attempting to replicate the air quality impacts of fires with chemical transport models was closely investigated using the base case considered for this study in Chapter 6. The analyses described therein showed that CMAQ-predicted $PM_{2.5}$ concentrations at sites downwind of fires are significantly affected by horizontal grid resolution of the model domain. In assessing the responsiveness of modeled concentrations to wind field inputs, it is important to consider the influence of model resolution on sensitivity estimates. Increased grid resolution can reduce numerical diffusion and produce better defined atmospheric plumes. Additionally, simulations carried out with coarser resolution become less sensitive to the spatial allocation of fire emissions on a gridded domain. This is especially true if emissions are allocated into a single coarse cell and concentration gradients are spatially smoothed

immediately upon injection. Under these conditions, the sensitivities of air quality model predictions to uncertain wind fields may be greatly enhanced.

To explore the relationship between grid resolution and the sensitivities of CMAQ-predicted $PM_{2.5}$ concentrations, the Atlanta 2007 smoke episode was modeled under coarser 12 km horizontal grid resolution. Sensitivities to wind direction and speed were then evaluated by repeating the simulations under modified wind fields using the same perturbations described in Sections 4.4.1.1 and 4.4.1.2. The analyses showed that simulated $PM_{2.5}$ concentrations at the downwind receptors considered were significantly less sensitive to wind field perturbations under coarser grid resolution. Figure 4.9 compares the standard deviation of predicted $PM_{2.5}$ concentrations at Confederate Ave. for all simulations carried out under perturbed wind fields using 12 km horizontal grid resolution to that of simulations using 4 km resolution, after fire-related emissions have begun. The values reflect the spread of CMAQ predictions within the perturbation range applied to wind direction (±5°, ±15°, ±30°, and base case) and wind speed (±10%, ±20%, and ±30%, and base case). At Confederate Ave. the average standard deviation for $PM_{2.5}$ concentrations within both the wind direction and wind speed simulation sets decreases by approximately 35% when horizontal grid resolution is coarsened from 4 to 12 km. Maximum hourly standard deviations fall by nearly 50% when grid spacing is increased. The impact of coarser resolution is similar at other sites within the city of Atlanta; average standard deviation decreases by 25% and 38% at Jefferson St. and South DeKalb respectively, while peak values drop by more than 40% at both locations. The effect is stronger at McDonough where reductions greater than 50% and 70% to average and the maximum standard deviations, respectively, are observed after coarsening resolution. At this site the enhanced impact of grid resolution is brought about by decreased diffusion at shorter range and how denser smoke plumes react to changes in winds.

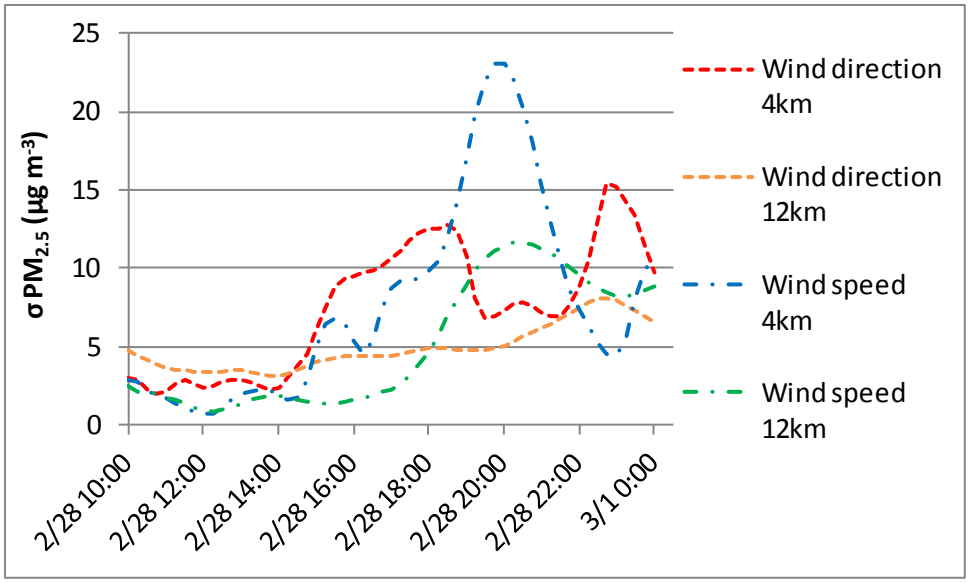

Figure 4.9. Standard deviation of $PM_{2.5}$ concentration from CMAQ predictions on 28 February 2007 (LT) at Confederate Ave. for all simulations within the perturbation range applied to wind direction (±5°, ±15°, ±30°, and base case) and wind speed (±10%, ±20%, and ±30%, and base case) under 4 km and 12 km horizontal grid resolutions.

The differences between the sensitivities of $PM_{2.5}$ concentrations to wind fields using 4 and 12 km horizontal grid spacing demonstrate a strong connection between the potential impact of meteorological uncertainty and model resolution. As fire-related air quality simulations undertaken with Eulerian models move towards even finer levels of resolution, the sensitivity of predicted pollutant concentrations to wind fields can be expected to increase. Under such conditions, errors associated with meteorological inputs may strongly propagate to air quality predictions and offset some of the gains achieved from increased grid resolution.

4.4.1.4 Relation to PBL Height

Winds are a major meteorological driver associated with fire-related air quality impacts and the focus of this study. However, planetary boundary layer (PBL) height is a fundamental parameter that shapes the turbulent atmospheric volume in which pollutants are readily dispersed. Previous analyses have identified the vertical allocation of fire-

related emissions as a key element of smoke forecasting (Stein et al., 2009). In CMAQ 4.5, the similarity theory option was used to parameterize eddy diffusivity according to the PBL data produced by meteorological models. PBL heights influence the wind flow used to transport fire-related emissions and may significantly affect the predictions of air quality models. However, large discrepancies between PBL heights estimated by different meteorological models and observational data have been reported (Vautard et al., 2012). Uncertainty in PBL height fields may propagate in model results and influence their sensitivity to winds.

To explore the sensitivity of CMAQ-predicted $PM_{2.5}$ concentrations at downwind receptors to PBL height, the Atlanta 2007 smoke episode was simulated with modified meteorological inputs. Similar to the sensitivity analyses centered on wind fields, PBL heights produced by WRF were perturbed by ±10%, ±20%, and ±30% to evaluate the responsiveness of predicted $PM_{2.5}$ concentrations to these variations. Significant sensitivities to PBL heights were evident at all downwind receptors considered. Figure 4.10 shows modeled $PM_{2.5}$ concentrations at Jefferson St. for each simulation carried out under perturbed PBL heights. Initially, and for much of the simulation, $PM_{2.5}$ concentrations at all sites are inversely related to PBL height. However, the correlation is not permanently negative and reflects the continual interaction between PBL height, plume rise, and emissions transport. While lowering the PBL height constrains pollutants within to a smaller volume, therefore increasing ground-level concentrations, it may also allow a greater fraction of the fire emissions to reach the free troposphere and be transported above the PBL, reducing their impact on surface air quality. In Figure 4.11, the standard deviation of predicted $PM_{2.5}$ concentrations at Confederate Ave. is shown for all simulations carried out with different PBL height fields. Also included are the base case PBL height predicted by WRF at the site and the fire-related contribution to $PM_{2.5}$ concentration estimated by comparing the results of simulations with and without fire emissions. Figure 4.11 shows how the sensitivity of $PM_{2.5}$ concentrations to PBL height,

reflected in the standard deviation, evolves throughout the episode. At Confederate Ave., the strongest sensitivity to PBL height occurs at the confluence of elevated PBL height and large fire-attributable $PM_{2.5}$ impacts. Similarly, at all receptors considered, the variation among model predictions is greatest when fire-related emissions contribute significantly to $PM_{2.5}$ concentrations and their injection into the atmospheric boundary layer is most susceptible to changes in PBL height.

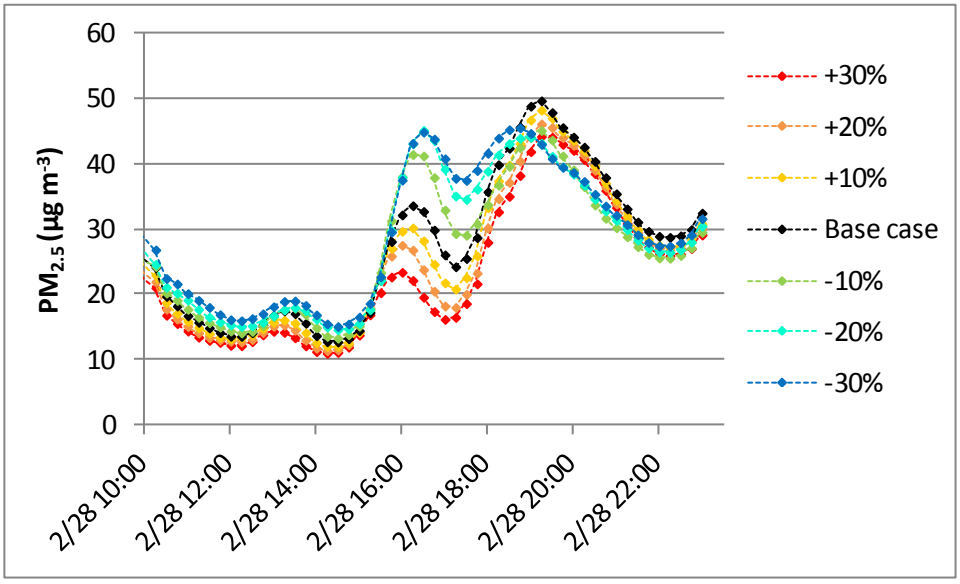

Figure 4.10. CMAQ-predicted $PM_{2.5}$ concentrations on 28 February 2007 (LT) at the Jefferson St. monitoring site under perturbed PBL heights. Base case simulation results are also included.

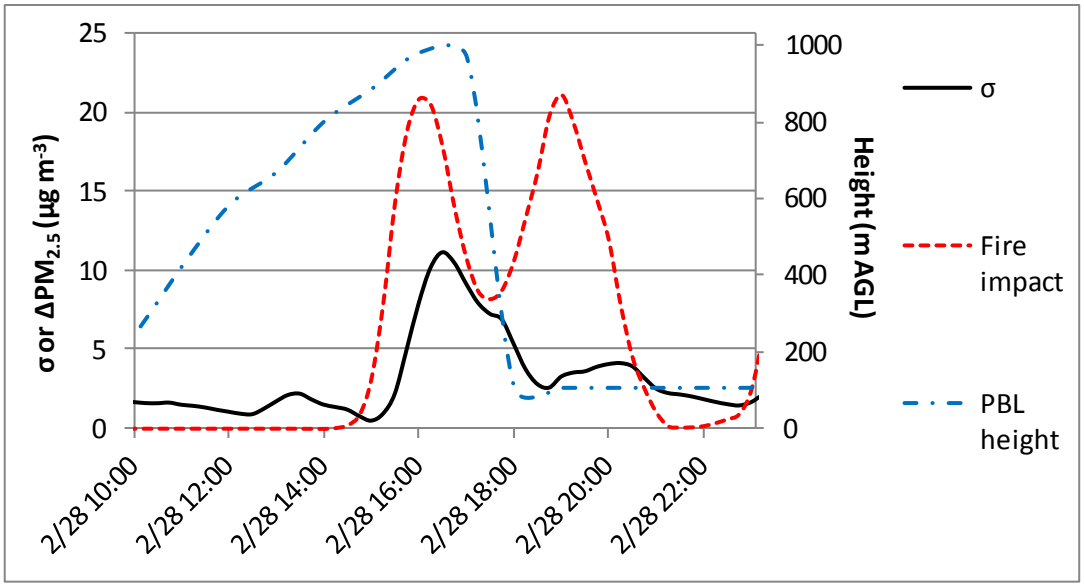

Figure 4.11. Standard deviation (σ) of CMAQ-predicted $PM_{2.5}$ concentrations on 28 February 2007 (LT) at Confederate Ave. for all simulations carried out under different PBL heights (±10%, ±20%, and ±30%, and base case) and base case PBL height prediction at Confederate Ave. (right vertical axis). The estimated fire-related contribution to $PM_{2.5}$ concentration ($\Delta PM_{2.5}$) is also included.

4.4.2 Wind field and meteorological uncertainty

4.4.2.1 Ground-level observations and model comparison

Wind fields generated by WRF were evaluated against surface-layer hourly observations from weather stations located within the base case modeling domain. Observations and predictions from 33 stations were spatially and temporally paired to calculate episode-mean performance metrics for key meteorological variables. Table 4.1 includes estimated statistical metrics as well as suggested performance benchmarks for meteorological models in air quality modeling applications (Emery et al., 2001). For this simulation, the metrics generally reflect adequate performance by WRF. Additionally, the statistics are comparable to those reported by annual evaluations of meteorological model performance in air quality modeling applications (Gilliam et al., 2006; Gilliam and Pleim,

2010; Hu et al., 2010). However, the evaluation does expose a significant positive bias in ground-level wind speed predictions that is outside the recommended range.

Table 4.1. Daily performance benchmarks for air quality modeling applications suggested by Emery et al. (2001) and episode-mean performance metrics for the base case meteorological modeling.

	Recommended Benchmark	Base case Simulation
Temperature Bias (*K*)	±0.5	-0.6
Temperature Error (*K*)	2.0	1.5
Mixing Ratio Bias (*g/kg*)	±1.0	1.0
Mixing Ratio Error (*g/kg*)	2.0	1.0
Wind Direction Bias (°)	±10 °	8.5
Wind Direction Error (°)	30 °	9.6
Wind Speed Bias ($m\ s^{-1}$)	±0.5	1.3
Wind Speed RMSE ($m\ s^{-1}$)	2	2.1

To focus on the meteorology driving fire emissions transport, observations and predictions were compared spatially and temporally within a 150 km x 150 km window centered over plume trajectories for the Atlanta 2007 smoke episode. The window includes hourly weather observations from a subset of 12 weather stations. Figure 4.12 compares mean predicted and observed temperature, humidity, wind direction, and wind speed within the evaluation window from the initial release of fire-related emissions until the end of the simulation. During fire emissions transport, the mean bias and error in temperature predictions compared to observation were -1.5 K and 1.6 K respectively. Simulated humidity displayed a consistent positive bias equal to 1.3 g kg^{-1}. The uncertainties associated with predicted wind fields are of greater significance to simulations attempting to replicate the impacts of fires on downwind $PM_{2.5}$ concentrations. The mean bias and error in wind direction predictions with respect to observations were +5.8° and 6.9° respectively. Nevertheless, the maximum hourly wind direction error is nearly 15°. During the episode, the mean bias and error in simulated

wind speeds were +1.1 m s^{-1} and 1.2 m s^{-1} respectively. Wind speed predictions closely agree with observations during the first half of the episode and exhibit a positive bias of approximately 2 m s^{-1} thereafter. Similarly, discrepancies between surface-layer observations and WRF-predicted wind speed and direction have been reported by other studies (Borge et al., 2008; de Foy et al., 2009). The uncertainties in WRF-generated surface-layer winds, especially wind speeds , are relevant to air quality modeling involving smoke plume transport given the large sensitivities to variations in winds described in Sections 4.4.1.1 and 4.4.1.2. However, fire-related emissions are largely transported above the surface-layer and a stronger response to wind flow at higher altitude should be expected.

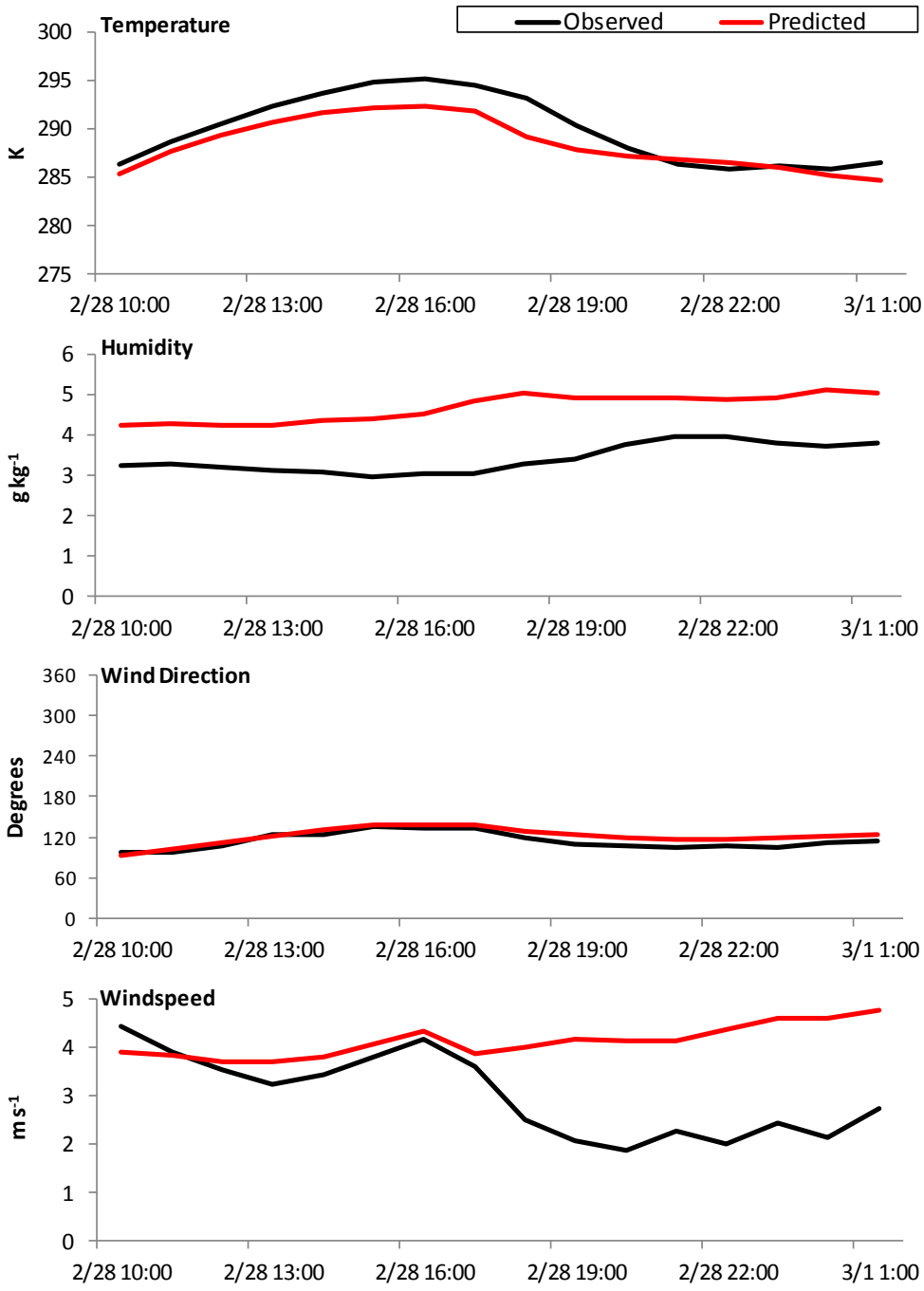

Figure 4.12. Mean observed and WRF-predicted ground-level temperature, humidity, wind direction, and wind speed over northern Georgia for 15 hours starting at 1000 LT on 28 February 2007.

4.4.2.2 Atmospheric soundings and model comparison

Atmospheric soundings provide an opportunity to evaluate upper air meteorological predictions. Within the simulation domain used for this study, sounding balloons were launched every 12 hours from Peachtree City, GA, approximately 45 km southeast of Atlanta. Sounding data was paired spatially and temporally with WRF predictions to assess uncertainty in the meteorological fields used to drive the simulations. Figure 4.13 compares wind speed and wind direction data from the rawinsonde launched at 1900 LT on 28 February 2007 with WRF-predicted wind fields. This sounding provides the closest available record of upper air measurements, spatially and temporally, to the peak $PM_{2.5}$ concentrations observed in Atlanta during the 2007 smoke episode. Across the full vertical modeling domain, WRF-predicted wind fields display good agreement with the sounding observations. Overall, wind speed predictions compared to observations show a +0.5 m/s mean bias, a 7.4% mean normalized bias, and a mean normalized error equal to 14.1%. Model performance is similarly strong for wind direction. When compared to sounding data across the vertical plane, WRF wind direction predictions show a mean bias of +1.82° and a mean error equal to 5.4°.

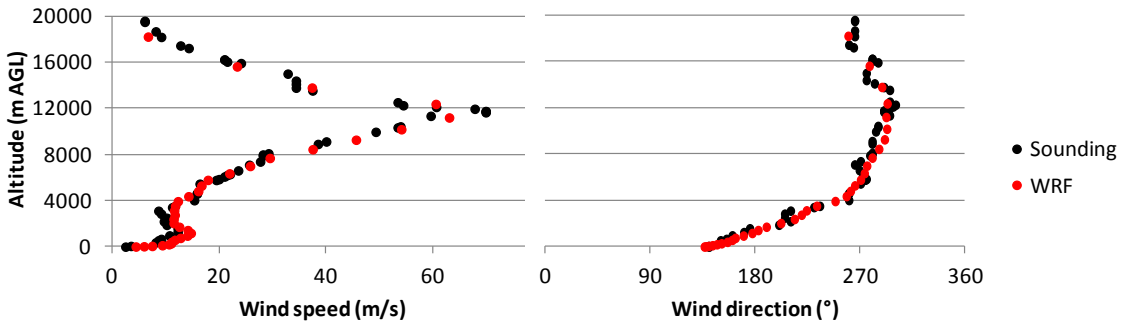

Figure 4.13. Wind speed and direction predicted by WRF (red) upper air observations (black) from the rawinsonde launched from Peachtree City, GA at 1900 LT on 28 February 2007.

However, fire emissions transport only occurs within a fraction of the modeling domain. In our base case simulation, fire-related emissions are injected into the modeling domain up to 1300 m above ground-level (AGL) and pollutant concentrations at downwind receptors are most sensitive to emissions released and transported within the PBL. Likewise, other studies suggest that low and middle PBL winds dominate the local and regional transport of fire related emissions (Stohl, 1998). Figure 4.14 focuses on the lower domain and again compares WRF-predicted winds to sounding observations. It becomes clear that at lower altitudes, where wind flow drives the transport of fire-related emissions, the model significantly overpredicts wind velocity. A bias in wind direction persists in the lower layers as well. Within the lowest 1500 m of the modeling domain, the WRF simulation overestimates wind speed by 40.2% with respect to sounding observations and displays a 6.8° bias in wind direction.

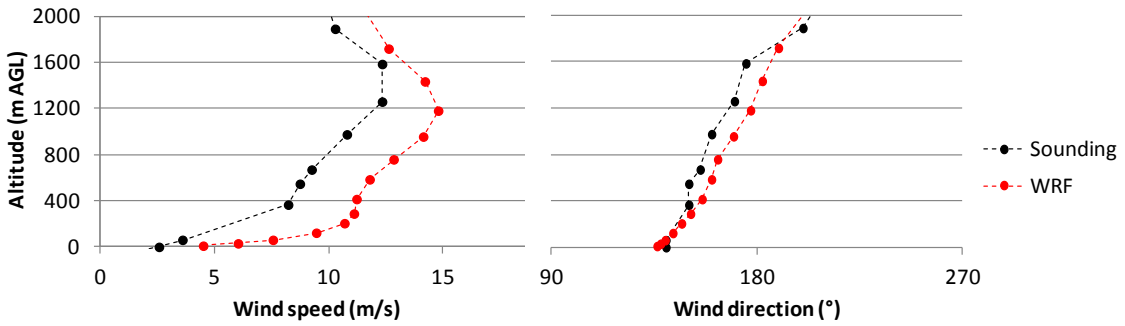

Figure 4.14. WRF-predicted wind speed and direction and observations from the rawinsonde launched from Peachtree City, GA at 1900 LT on 28 February 2007 for lower 2000 m of the atmosphere.

The discrepancies between sounding data and WRF-generated wind fields demonstrate that significant uncertainties exist in the meteorological inputs used to drive air quality modeling. During the full 36-hour CMAQ base case simulation, modeled wind speed and direction can differ significantly with concurrent upper air soundings within the lower levels of the modeling domain. Wind speeds near the surface are consistently

overestimated by WRF. Discrepancies between predicted and observed wind directions are mostly lower than 10° and do not reflect a clear model bias for this episode. Similarly, other comparisons of WRF-predicted boundary layer winds speed and direction to wind profiler and aircraft observations have identified significant discrepancies (Gilliam and Pleim, 2010). Furthermore, systematic positive biases for boundary-layer wind speed were also revealed in a collective evaluation of mesoscale meteorological models within the framework of the Air Quality Model Evaluation Initiative (Vautard et al., 2012).

4.4.3 Wind-associated error in $PM_{2.5}$ predictions

Meteorological fields are a key driver in air quality modeling. Errors associated with meteorological inputs propagate through air quality models and affect the accuracy of pollutant concentration predictions. Therefore, it is essential to evaluate the extent to which the performance of air quality models may be limited by uncertain meteorological input data. The process entails (1) determining the output variables most relevant to the modeling application, (2) identifying the input variables that significantly influence the values of the outputs of interest, (3) assessing the range of uncertainty in these model inputs, and (4) quantifying the sensitivity of output variables to input variable perturbations within their uncertainty range. In simulations attempting to replicate the impacts of wildland fires on air quality, ground-level pollutant concentrations at downwind locations are the output variables of greatest interest. Furthermore, in this study we focus on $PM_{2.5}$, the atmospheric pollutant most commonly associated with fire-related air quality impacts. Typically, a few input variables control the value of specific model outputs. For air quality simulations involving wildland fires, wind inputs are clearly among the variables dominating predicted $PM_{2.5}$ concentration. Here, uncertainties in wind inputs were explored by comparing meteorological predictions and

observations. Finally, brute force sensitivity analyses were used to determine the potential response of modeled $PM_{2.5}$ concentrations to errors in wind field inputs.

The sensitivity analyses described in Section 4.4.1 show that CMAQ-predicted $PM_{2.5}$ concentrations could respond strongly to wind field variations well within their uncertainty bounds. Previous studies have compared pollutant trajectories projected from wind profiler observations and model predictions and have revealed that large deviations (100-200 km) may develop over a 24-hour period within the lower 1000 m of the atmosphere (Gilliam et al., 2006; Godowitch et al., 2011). These transport errors, largely attributed to wind speed differences, could significantly influence air quality predictions. In this study's base case simulation, we revealed a positive bias in wind speed predictions with respect to both ground-level and upper air observations. The comparisons to weather data also revealed errors in wind direction predictions, generally smaller than 10°. The uncertainties in weather forecasts should not come as a surprise. However, it is clear that even small errors in wind flow can lead to large variations in $PM_{2.5}$ concentration predictions. Across the lowest 1500 m of the modeling domain, wind speed in meteorological inputs would need an average reduction of 27% to match observed values from the available atmospheric sounding. Likewise, an average adjustment of -6.8° to wind direction is needed to equate predicted and observed values across the same vertical range.

Figure 4.15 compares base case $PM_{2.5}$ concentration predictions at Atlanta to results from simulations in which wind speed was systematically reduced by 27% and wind direction was uniformly modified by -6.8°. The differences among predictions exemplify how errors associated with wind fields in meteorological inputs propagate into the output fields thereby limiting model performance. The reduction in wind speed increased the maximum predicted $PM_{2.5}$ concentrations within Atlanta by 47-52 $\mu g\ m^{-3}$ (82-103%) and delayed peak concentrations by approximately 1 hour. Modifying wind direction resulted in earlier peak $PM_{2.5}$ concentrations and an 8-24 $\mu g\ m^{-3}$ (15-47%)

increase to maximum predicted concentrations. Additionally, Figure 4.15 shows the combined effect of simultaneously modifying wind speed and wind direction in meteorological input fields. The impacts of different perturbations on simulated concentrations are not additive, but rather each wind field produces a unique solution. Under specific conditions, the influence of errors associated with either wind speed or wind direction can dominate concentration estimates. Nevertheless, the analyses show that CMAQ-predicted $PM_{2.5}$ concentrations in simulations attempting to replicate the air quality impacts of fires may carry normalized errors as high as 100% due to uncertain wind inputs.

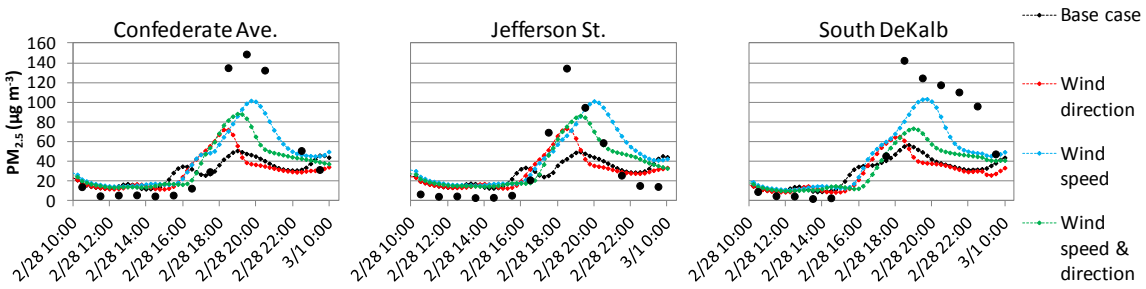

Figure 4.15. $PM_{2.5}$ concentration predictions on 28 February 2007 (LT) at Atlanta monitoring sites for base case CMAQ simulation, simulations with perturbed wind speed (-27%) and wind direction (-6.8°), and simulation with combined wind speed and wind direction perturbations. Monitoring station observations are also included.

4.5 Conclusions

The results of this study show that air quality estimates from chemical transport models attempting to replicate the impacts of wildland fires are extremely sensitive to meteorological fields. For such an application, model performance largely depends on the accuracy of wind inputs. More importantly, simulated pollutant concentrations displayed large sensitivities to variations in wind fields well within the uncertainty range of numerical weather prediction. Errors associated with wind data may largely account for considerable discrepancies frequently detected between observed and predicted $PM_{2.5}$

concentrations. Overestimated wind speeds in the lower atmosphere may be especially significant.

However, shortcomings in model performance can only be partially explained by meteorology. Additional parameters and inputs have been identified as sources of error. Fire-related emissions remain uncertain, especially for precursors of secondary organic aerosol. The spatiotemporal allocation of fire emissions on gridded domains may also impact model predictions. The significance of grid resolution in air quality simulations involving wildland fires is ascertained in Chapter 6. However, in the episode modeled for this study, the influence of uncertainty in wind inputs on concentration predictions substantially outweighed the effect all other sources of error identified, including uncertain emission rates. This suggests that fire-related simulations with chemical transport models are limited by the performance of existing numerical weather prediction systems. Additionally, as air quality modeling moves towards finer grid resolution, errors associated with meteorological inputs can be expected to constrain model accuracy even further.

The response of $PM_{2.5}$ concentration predictions to wind flow perturbations signals a need to include meteorological inputs in any strategy designed to improve fire-related air quality simulations. Furthermore, it is important to recognize the limitations inherent to weather forecasts in the context of air quality modeling. Uncertain wind fields are an intrinsic component of numerical weather prediction and mitigating errors in short term and small scale wind forecasts produced by existing models is a challenging task. Concerns about the ability of meteorological models to capture intraday wind variations have been previously raised (Hogrefe et al., 2001). Additionally, substantial variability exists in meteorological predictions from different models and different configurations of the same model (Vautard et al., 2012). In light of this, air quality forecasts predicting the impact of fires on air quality produced by atmospheric chemistry and transport models

must be considered substantially uncertain. These uncertainties must be considered when air quality modeling is used to steer fire management decision-making.

4.6 References

Achtemeier, G.L., Goodrick, S.A., Liu, Y., Garcia-Menendez, F., Hu, Y., Odman, M.T. (2011) Modeling smoke plume-rise and dispersion from southern United States prescribed burns with Daysmoke. Atmosphere 2, 358-388.

Appel, K.W., Roselle, S.J., Gilliam, R.C., Pleim, J.E. (2010) Sensitivity of the Community Multiscale Air Quality (CMAQ) model v4.7 results for the eastern United States to MM5 and WRF meteorological drivers. Geosci. Model Dev. 3, 169-188.

Borge, R., Alexandrov, V., del Vas, J.J., Lumbreras, J., Rodriguez, E. (2008) A comprehensive sensitivity analysis of the WRF model for air quality applications over the Iberian Peninsula. Atmospheric Environment 42, 8560-8574.

Chen, J., Vaughan, J., Avise, J., O'Neill, S., Lamb, B. (2008) Enhancement and evaluation of the AIRPACT ozone and PM2.5 forecast system for the Pacific Northwest. Journal of Geophysical Research 113, D14305.

Chen, S.H., Sun, W.Y. (2002) A one-dimensional time dependent cloud model. Journal of the Meteorological Society of Japan 80, 99-118.

de Foy, B., Zavala, M., Bei, N., Molina, L.T. (2009) Evaluation of WRF mesoscale simulations and particle trajectory analysis for the MILAGRO field campaign. Atmospheric Chemistry and Physics 9, 4419-4438.

Dudhia, J. (1989) Numerical study of convection observed during the winter monsoon experiment using a mesoscale two-dimensional model. J. Atmos. Sci. 46, 3077-3107.

Ek, M.B., Mitchell, K.E., Lin, Y., Rogers, E., Grunmann, P., Koren, V., Gayno, G., Tarpley, J.D. (2003) Implementation of Noah land surface model advances in the National Centers for Environmental Prediction operational mesoscale Eta model. J. Geophys. Res. 108, 8851.

Emery, C., Tai, E., Yarwood, G., (2001) Enhanced meteorological modeling and performance evaluation for two Texas ozone episodes. Tex. Nat. Resour. Conserv. Comm., Novato, California, USA.

Gilliam, R.C., Hogrefe, C., Rao, S.T. (2006) New methods for evaluating meteorological models used in air quality applications. Atmospheric Environment 40, 5073-5086.

Gilliam, R.C., Pleim, J.E. (2010) Performance assessment of new land surface and planetary boundary layer physics in the WRF-ARW. Journal of Applied Meteorology and Climatology 49, 760-774.

Godowitch, J.M., Gilliam, R.C., Rao, S.T. (2011) Diagnostic evaluation of ozone production and horizontal transport in a regional photochemical air quality modeling system. Atmospheric Environment 45, 3977-3987.

Goodrick, S.L., Achtemeier, G.L., Larkin, N.K., Liu, Y., Strand, T.M. (2012) Modelling smoke transport from wildland fires: a review. Int. J. Wildland Fire.

Grell, G.A., Dudhia, J., Stauffer, D.R., (1994) A description of the fifth-generation Penn State/NCAR Mesoscale Model (MM5), NCAR Tech. Note NCAR/TN-398+STR. Mesoscale and Microscale Meteorol. Div., Natl. Cent. for Atmos, Boulder, Colorado, USA.

Hogrefe, C., Rao, S.T., Kasibhatla, P., Kallos, G., Tremback, C.J., Hao, W., Olerud, D., Xiu, A., McHenry, J., Alapaty, K. (2001) Evaluating the performance of regional-scale photochemical modeling systems: Part I—meteorological predictions. Atmospheric Environment 35, 4159-4174.

Hong, S.Y., Noh, Y., Dudhia, J. (2006) A new vertical diffusion package with an explicit treatment of entrainment processes. Monthly Weather Review 134, 2318-2341.

Hu, Y.T., Chang, M.E., Russell, A.G., Odman, M.T. (2010) Using synoptic classification to evaluate an operational air quality forecasting system in Atlanta. Atmospheric Pollution Research 1, 280-287.

Hu, Y.T., Odman, M.T., Russell, A.G. (2006) Mass conservation in the Community Multiscale Air Quality model. Atmospheric Environment 40, 1199-1204.

Hwang, D., Byun, D.W., Talat Odman, M. (1997) An automatic differentiation technique for sensitivity analysis of numerical advection schemes in air quality models. Atmospheric Environment 31, 879-888.

Junquera, V., Russell, M.M., Vizuete, W., Kimura, Y., Allen, D. (2005) Wildfires in eastern Texas in August and September 2000: Emissions, aircraft measurements, and impact on photochemistry. Atmospheric Environment 39, 4983-4996.

Kain, J.S. (2004) The Kain-Fritsch convective parameterization: An update. J. Appl. Meteor. 43, 170-181.

Konovalov, I.B., Beekmann, M., Kuznetsova, I.N., Yurova, A., Zvyagintsev, A.M. (2011) Atmospheric impacts of the 2010 Russian wildfires: integrating modelling and measurements of an extreme air pollution episode in the Moscow region. Atmospheric Chemistry and Physics 11, 10031-10056.

Koo, B., Wilson, G.M., Morris, R.E., Dunker, A.M., Yarwood, G. (2009) Comparison of source apportionment and sensitivity analysis in a particulate matter air quality model. Environmental Science & Technology 43, 6669-6675.

Lin, Y.L., Farley, R.D., Orville, H.D. (1983) Bulk parameterization of the snow field in a cloud model. J. Climate Appl. Meteor. 22, 1065-1092.

Liu, Y., Goodrick, S., Achtemeier, G., Jackson, W.A., Qu, J.J., Wang, W. (2009) Smoke incursions into urban areas: simulation of a Georgia prescribed burn. Int. J. Wildland Fire 18, 336-348.

Mlawer, E.J., Taubman, S.J., Brown, P.D., Iacono, M.J., Clough, S.A. (1997) Radiative transfer for inhomogeneous atmospheres: RRTM, a validated correlated-k model for the longwave. J. Geophys. Res. 102, 16663-16682.

Otte, T.L., Pleim, J.E. (2010) The Meteorology-Chemistry Interface Processor (MCIP) for the CMAQ modeling system: updates through MCIPv3.4.1. Geosci. Model Dev. 3, 243-256.

Rutledge, S.A., Hobbs, P.V. (1984) The mesoscale and microscale structure and organization of clouds and precipitation in midlatitude cyclones. XII: A diagnostic modeling study of precipitation development in narrow cold-frontal rainbands. J. Atmos. Sci. 41, 2949-2972.

Seaman, N.L. (2000) Meteorological modeling for air-quality assessments. Atmospheric Environment 34, 2231-2259.

Skamarock, W.C., Klemp, J.B., Dudhia, J., Gill, D.O., Barker, D.M., Duda, M.G., Huang, X.-Y., Wang, W., Powers, J.G., (2008) A description of the Advanced Research WRF version 3, Tech. Note, NCAR/TN-475+STR. Natl. Cent. for Atmos. Res., Boulder, Colorado, USA.

Stein, A.F., Rolph, G.D., Draxler, R.R., Stunder, B., Ruminski, M. (2009) Verification of the NOAA Smoke Forecasting System: Model sensitivity to the injection height. Weather and Forecasting 24, 379-394.

Stohl, A. (1998) Computation, accuracy and applications of trajectories - A review and bibliography. Atmospheric Environment 32, 947-966.

Strand, T.M., Larkin, N., Craig, K.J., Raffuse, S., Sullivan, D., Solomon, R., Rorig, M., Wheeler, N., Pryden, D. (2012) Analyses of BlueSky Gateway PM2.5 predictions during the 2007 southern and 2008 northern California fires. J. Geophys. Res. 117.

Tian, D., Hu, Y.T., Wang, Y.H., Boylan, J.W., Zheng, M., Russell, A.G. (2009) Assessment of biomass burning emissions and their impacts on urban and regional PM2.5: A Georgia case study. Environmental Science & Technology 43, 299-305.

Vautard, R., Moran, M.D., Solazzo, E., Gilliam, R.C., Matthias, V., Bianconi, R., Chemel, C., Ferreira, J., Geyer, B., Hansen, A.B., Jericevic, A., Prank, M., Segers, A., Silver, J.D., Werhahn, J., Wolke, R., Rao, S.T., Galmarini, S. (2012) Evaluation of the meteorological forcing used for the Air Quality Model Evaluation International Initiative (AQMEII) air quality simulations. Atmospheric Environment 53, 15-37.

Yang, E.S., Christopher, S.A., Kondragunta, S., Zhang, X.Y. (2011) Use of hourly Geostationary Operational Environmental Satellite (GOES) fire emissions in a Community Multiscale Air Quality (CMAQ) model for improving surface particulate matter predictions. Journal of Geophysical Research 116, D04303.

CHAPTER 5

ADAPTIVE GRID USE IN AIR QUALITY MODELING

Abstract

The predictions from air quality models are subject to many sources of uncertainty; among them, grid resolution has been viewed as one that is limited by the availability of computational resources. A large grid size can lead to unacceptable errors for many pollutants formed via nonlinear chemical reactions. Further, insufficient grid resolution limits the ability to perform accurate exposure assessments. To address this issue in parallel to increasing computational power, modeling techniques that apply finer grids to areas of interest and coarser grids elsewhere have been developed. Techniques using multiple grid sizes are called nested grid or multiscale modeling techniques. These approaches are limited by uncertainty in the placement of finer grids since pertinent locations may not be known *a priori*, loss in solution accuracy due to grid boundary interface problems, and inability to adjust to changes in grid resolution requirements.

A different approach to achieve local resolution involves using dynamic adaptive grids. Various adaptive mesh refinement techniques using structured grids as well as mesh enrichment techniques on unstructured grids have been explored in atmospheric modeling. Recently, some of these techniques have been applied to full blown air quality models. In this chapter, adaptive grid methods used in air quality modeling are reviewed and categorized. The advantages and disadvantages of each adaptive grid method are discussed. Advances made in air quality simulation owing to the use of adaptive grids are summarized. Relevant connections to adaptive grid modeling in weather and climate modeling are also described.

---

* A modified version of this chapter has been published in *Adaptive Grid Use in Air Quality Modeling*, Atmosphere **2011**, 2, 484-509.

5.1 Introduction

Air quality modeling provides a valuable means to reproduce the behavior of atmospheric pollutants. Air quality models are either of Eulerian grid type or Lagrangian models with underlying grids. Cell size is the measure of the scales that can be explicitly resolved by a grid model. Smaller-scale phenomenon can only be represented through subgrid scale parameterizations. The dynamic and chemical processes involved in the transport and transformation of atmospheric pollutants encompass a wide range of scales. Complex interactions between processes occurring at different scales make it necessary to resolve the finest relevant scales. For example, it is well known that emissions from urban and industrial centers are responsible for regional or global air quality problems. On the other hand, if emission plumes are injected into relatively coarse grid cells in a regional or global scale model, they are immediately diluted with the contents of the cell and the details of their chemical interaction with the surrounding atmosphere are lost. In the early days of regional modeling 100 km resolution was typical; today, models are pushing the 1 km barrier and the quest for higher resolution continues. With higher grid resolution come increased resolution of complex terrain topography, land use, land cover, cloud cover, and other data used in subgrid scale parameterizations, enabling an increase to the overall resolution of the models.

Historically, the motivation for air pollution modeling has been air quality management. Development of control strategies has been the initial driving force behind modeling research and advancement. With the confidence gained in describing historic pollution events, models were applied in air quality forecasting. Today, models are used for much broader purposes that connect air quality to other fields. The feedback of pollution on meteorology is receiving more attention with a focus on problems such as smoke from wildfires and volcanic ash, leading to the coupling of air quality models with numerical weather prediction models that were historically used to provide meteorological inputs only. Along with the study of climate and global-scale air quality

problems, air quality models are beginning to merge with global circulation and global chemistry models. These trends considerably expand the domains of the models from their original dimensions.

Modeling large geographic regions with high resolution is a challenging computational problem. The models' demand for computational resources escalates rapidly with increasing resolution. For example, consider the changes to the operation count in a model that uses an explicit numerical scheme. An explicit scheme advances a system from its current state $Y(t)$ to a future state $Y(t + \Delta t)$ at time $t + \Delta t$ as follows:

$$Y(t + \Delta t) = F(Y(t)) . \tag{5.1}$$

$Y(t + \Delta t)$ can be obtained by direct substitution of the current state $Y(t)$ into the right-hand-side of this equation. The operation count in substitution is $O(N)$ where N is the number of grid cells. If N increases, the operation count and computational resource demands, such as memory and CPU time, increase linearly with it. Doubling the horizontal grid resolution (e.g., reducing linear grid size from 1 km to 500 m) quadruples the number of grid cells. If the number of vertical layers is also doubled, the total number of grid cells increases by a factor of 8. In addition, there is a computational cost experienced with explicit schemes related to time-stepping; as N is increased, the length scales decrease and a smaller time step, Δt, is required due to stability considerations encountered with explicit schemes. Advancing the system using shorter time steps makes the overall increase in computational cost super-linear and typically further augments it by another factor of two when the resolution is doubled.

For models that use implicit schemes, the computational resource demand grows more rapidly with increasing resolution. In an implicit scheme, both the current and future states of the system appear in an equation of the following form:

$$G(Y(t), Y(t + \Delta t)) = 0 . \tag{5.2}$$

This equation can be solved directly or iteratively. Direct solutions involve a matrix inversion and are typically more expensive than iterative solutions. Depending on the

selected solution method, the operation count of an implicit scheme is generally between $O(N \log N)$ and $O(N^2)$. Therefore, doubling the resolution, which increases the number of grid cells by a factor of 8 as described above, may result in an operation count 64 times larger. One advantage of implicit schemes is that they are not subject to stability limits; thus, it is not necessary to decrease the time step if N is increased. However, it may still be desirable to reduce the time steps, as characteristic times of certain processes are shortened (e.g., the time it takes to advect emissions by the winds over the length scale Δx). This obviously increases the computational cost even further.

Multiscale modeling techniques emerged as a solution to this gargantuan computational challenge. The goal is to develop models capable of applying the appropriate scale or sufficient resolution where and when it is needed. The goal of multiscale models is to encompass different scales (e.g., local, urban, regional, global) in a unified modeling system to better capture the interactions among the processes relevant at each scale. There are various multiscale modeling techniques; two methods applied in air quality models are described here. The first features grids that can be nested multiple levels deep for better resolution of finer scale processes. The second involves grid adaptation in response to the needs of a particular simulation, either by refining a structured mesh or by locally enriching an unstructured mesh with added cells. This chapter will focuses on the adaptive grid method and continues with a review of its use in air quality modeling. It ends with remarks on the prospect of growing use of adaptive grids in atmospheric modeling.

5.2 Nested Grid Methods

Nested-grid modeling techniques have been and still are very popular in atmospheric modeling (e.g., (Clark and Farley, 1984; Jones, 1977; Miyakoda and Rosati, 1977; Phillips and Shukla, 1973; Pleim et al., 1991; Zhang et al., 1986)). In static grid nesting, finer grids (FGs) are placed or “nested” inside coarser grids (CGs). The domain

and resolution of each nest are specified prior to the simulation and remain fixed throughout. The nested grid method targets higher resolution for domain features that remain stationary (e.g., terrain, coastline, the location of a power plant or urban area). A fixed FG near such features is a simple and practical solution to locally increase resolution. The grid size of the CG is usually an integer multiple of the FG's grid size. Typically, the temporal resolution of the FG is also higher, as its time step is set to be shorter than that of the CG. It is customary, although not necessary, to set the time step ratio equal to the grid size ratio.

While static grid nesting is a practical multiscale modeling technique, it has limitations. The domains and resolutions of nests are selected either arbitrarily or based on conceptual models that may not be very accurate. The quality and accuracy of the solution obtained greatly depends on the initial selections. Once the grids are set, it may not be simple to change them since input data must be reprocessed for the new grid settings. This is the case, for example, in forecasting operations. A common problem associated with grid nesting methods is that they often lead to spurious oscillations at grid interfaces. This is particularly problematic when an interface coincides with an area of large physical gradients because the filters used to remove the oscillations can also reduce the amplitudes of resolvable waves. Large refinement ratios between CG and FG amplify the oscillations and necessitate more vigorous filtering (Odman and Russell, 1994).

5.3 Adaptive Grid Methods

The objective of an adaptive grid method is to increase solution accuracy by providing dynamic refinement at regions and instances where accuracy is most dependent on resolution. This can be achieved by restructuring the grid on which solution fields are estimated to better fit the needs of the system being numerically described. Adaptive

gridding techniques can be classified as h-refinement or r-refinement depending on the type of grid restructuring employed.

H-refinement relies on increasing the total number of grid elements (e.g., nodes or cells) within a base grid for which the original structure remains fixed. The technique, also known as mesh enrichment or local refinement, modifies the grid at regions tagged for increased resolution. Frequently, the method is carried out by subdividing grid elements into smaller self-similar components. In Figure 5.1, the example depicting h-refinement shows a single refinement level. A second level of refinement could involve subdividing the refined cells at the center of the domain into four even smaller cells. Generally, a maximum number of refinement levels allowed must be defined.

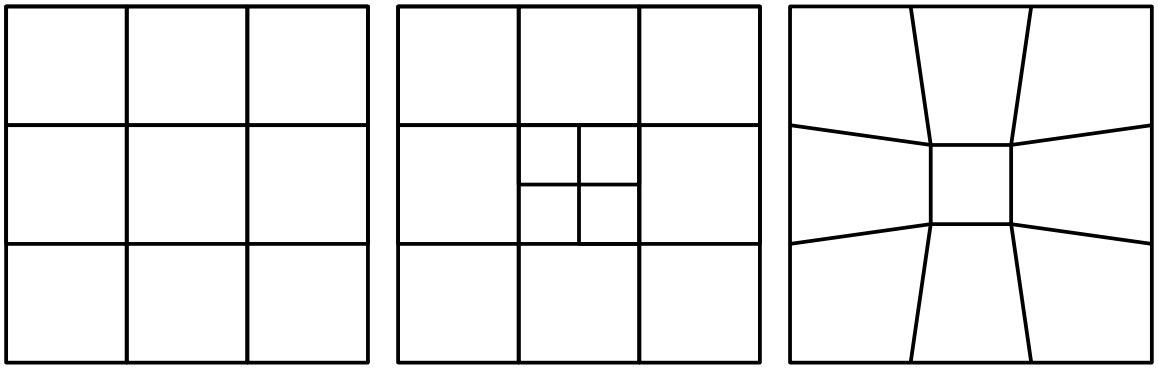

Figure 5.1. Uniform grid (left) and examples of h-refinement (center) and r-refinement (right).

H-refinement can be realized by applying two distinct methodologies. One approach is to include added grid elements directly into the original base grid; all elements are solved on a single grid throughout the simulation. This method requires data storage procedures and solvers capable of handling unstructured grids. Alternatively, h-refinement can be achieved by considering the additional elements at increased resolution levels as distinct grids that are dynamically created or removed. In this manner, each refined grid can remain structured and be individually solved using algorithms developed

exclusively for uniform or rectangular grids. Here, communication among different levels of refinement takes the form of boundary and initial conditions setting for the different grids.

R-refinement techniques, commonly referred to as mesh moving or global refinement, relocate mesh nodes to regions warranting increased resolution and subsequently increase grid element concentration at the areas with the greatest inaccuracies. However, the total number of grid points is maintained constant. Unlike h-refinement, r-refinement around a region is necessarily accompanied by coarsening at another. Figure 5.1 shows simple schematics of h-refinement and r-refinement at the center of a simple nine element quadrilateral grid.

Both adaptive gridding techniques have advantages and drawbacks associated with them. An advantageous distinguishing feature of r-refinement is smoother transitions in grid resolution. In contrast, h-refinement ordinarily operates on grids with abrupt discontinuities among the different refinement levels allowed. Acute disruptions in resolution are undesirable and may lead to interface problems. The constant number of grid elements maintained throughout a simulation using r-refinement could prove beneficial; a fixed number of elements simplifies solution algorithms and is helpful in parallel computing implementations. It could appear that the achievable improvement to solution accuracy with r-refinement is limited by the total number of grid elements or nodes, and that such a restraint is not inherent to h-refinement. However, it is important to note that the available computational resources, and not the number of nodes, are the true limitation to accuracy. At the limit of computational capacity, both h- and r-refinement can only increase local refinement at the expense of coarsening elsewhere. More accurately, r-refinement's disadvantage lies in its need to determine global resolution (i.e., total number of grid elements) *a priori*. A poorly selected domain-wide number of elements will limit solution accuracy if too low and hinder efficiency if overly large. The requirement may be especially important when dealing with multiple and

concurrent calls for increased resolution within different regions of a domain. This prerequisite is not essential to h-refinement. Additionally, h-refinement can guarantee a minimum solution accuracy level for all fields throughout the full domain by disallowing coarsening beyond a base grid resolution. R-refinement can be thought of as an optimization problem; the technique attempts to determine the best grid configuration possible under user-defined computational constraints. In h-refinement an optimal grid is not necessarily sought or possible. Typically, the discrete and bounded refinement levels used for adaptation with h-refinement schemes negate optimization. H-refinement is more frequently applied as a simple technique to identify regions that would likely benefit from increased resolution and readily refine at these locations if additional computational resources are available. The procedure may lead to an acceptable increase in solution accuracy by utilizing simpler adaptive algorithms that may be significantly less burdensome than those invoked by r-refinement methods. Neither refinement technique can be labeled as superior. While mesh movement seems better equipped to optimize resolution and computational workload, achieving an optimal grid may not be straightforward. Under such conditions the advantages of mesh enrichment could be of greater value.

5.3.1. Grid Structuring

Grid structures applied in numerical modeling may be categorized as structured or unstructured. The distinguishing feature between them refers to the data structure associated with each, rather than visual traits. Data on a structured grid can be arranged into a rectangular matrix; cells and nodes can be identified through integer indices (e.g., i, j, k). The requirement brings forth regular grid patterns and most often quadrilateral or hexahedral elements. Additionally, the data arrangement in structured grids reduces memory requirements compared to unstructured ones.

In contrast to structured grids, data from unstructured grids cannot be arranged by applying simple integer indexing and full connectivity must be defined and stored for each node. Unstructured grid cells are defined as a group of nodes that encompass an element of any geometry. These grids can be built using triangles, quadrilaterals, tetrahedra, hexahedra, or any polygon or polyhedron, including combinations of elements with different geometries. The irregularity of unstructured grids allows greater versatility in their assembly compared to structured grids. This flexibility in domain discretization has made unstructured meshes popular in simulations dealing with complex geometries and a common choice to model fluid mechanics (Morgan and Peraire, 1998).

Typically, finite-difference methods are used with structured grids and finite-element (or finite-volume) methods are used with unstructured grids. Both methods are well developed for the solution of hyperbolic partial differential equations of the type encountered in atmospheric models. Higher-order spatial approximations are available for both types of methods; therefore, the desired level of accuracy can be achieved with either. In general, higher-order methods in atmospheric models must be used together with flux-correction or filtering algorithms to avoid the generation of spurious oscillations that may lead to undesirable effects such as nonmonotonic and unphysical solutions (e.g., negative concentrations in air quality models) or even instabilities. Using higher-order difference approximations or higher-order elements is known as p-refinement, an alternative to the adaptive grid h- or r-refinement techniques described above for increasing solution accuracy. The decision of using an explicit or an implicit scheme must be made for time integration; it does not depend on the spatial grid and whether it is structured or unstructured. Hence, either option is available both with finite-difference and finite-element methods.

Mesh enrichment (i.e., h-refinement) can be implemented into both structured and unstructured grids. Often, refinement involves subdividing cells into equal self-similar elements; quadrilaterals and hexahedra are divided into four or eight smaller elements

respectively. Likewise, techniques are available to systematically divide triangular and tetrahedral grid elements. For structured grids, mesh enrichment may decimate the regularity in grid elements and render original solution algorithms inapplicable, unless refinements are treated as distinct grids, similar to nested grid methods. H-refinement is more compatible with unstructured grids. Given the arbitrary arrangement of cells within an unstructured domain, initial solution algorithms will generally also be applicable to the refined grid.

Mesh movement (i.e., r-refinement) can also be achieved regardless of grid structure. The technique is clearly well suited to structured grids; despite node movement, the regularity and connectivity of grid elements remains intact. Nevertheless, solution algorithms designed for structured grids may have been also developed assuming uniformity and be invalid under a nonuniform grid. Solver incompatibility can be addressed by applying a coordinate transformation to the governing equations and grid, from nonuniform in physical space to uniform in computational space. The transformation must be applied each time the grid is restructured and may significantly increase the method's overhead. Mesh movement on unstructured grids can be simpler if the solution algorithms available are capable of handling irregular, nonuniform grids from the start.

5.3.2. Error Estimation

The objective of increasing solution accuracy through adaptive gridding can only be met if adaptation is driven by an efficient indicator of the solution error in a spatial field. The concept of error equidistribution has been used to describe the adaptive grid process; grids are reconfigured to result in an equal amount of error for all grid elements (Baker, 1997). However, directly quantifying error is not a straightforward task. Quantitative analysis of resolution-induced error in advection algorithms has been previously investigated. For advection schemes, a Fourier method can estimate error (i.e.,

numerical diffusion) as a function of grid resolution (Odman, 1997). The estimation becomes much more complex after integrating other physical and chemical processes into the system, particularly nonlinear transformations. Additionally, exact error quantification cannot be used as a refinement driver *a priori*, as the error itself depends on grid structure after adaptation.

Typically, adaptive grids use an error indicator in place of solution error to drive refinement. The error indicator may be a rudimentary calculation related to the error. For instance, estimates of the truncation or interpolation error may be applied. It is also common to rely on physical features that are known to efficiently signal locations where the error is most sensitive to grid resolution. In air quality modeling, for example, concentration gradients or curvatures can be used to trigger refinement and effectively increase solution accuracy. The selection of an error indicator to drive refinement is more critical to r-refinement than h-refinement. For mesh moving refinement, adaptation acts as an optimization processes by which error is minimized with a fixed amount of available resolution. Since refinement at one region necessitates coarsening at another, effective adaptation criteria truly representative of solution error are crucial. In mesh enrichment, base-level solution accuracy is generally guaranteed. Refinement augments resolution at selected locations and increases total grid resolution. An optimal grid configuration is not necessarily achieved nor pursued. Instead, mesh enrichment may simply allocate additional resolution in an attempt to sufficiently increase solution accuracy.

5.4. Antecedents of Adaptive Grid Air Quality Modeling

Research efforts investigating adaptive gridding in meteorological modeling precede those exploring the technique as an option for air quality simulation. The motivations and methodologies for adaptive grid refinement in both atmospheric realms are very much alike. The earliest attempt to simulate atmospheric flows using an adaptive

grid was reported by Jones (1977). In the model described, two levels of nested grids were allowed to move within a larger domain while tracking a tropical cyclone identified from the surface pressure field.

Subsequent applications of adaptive gridding in atmospheric modeling were described by Skamarock et al.(Skamarock et al., 1989; Skamarock and Klemp, 1993). In these simulations, grid refinement was based on the method of Berger and Oliger (1984). This approach to adaptive gridding achieves dynamic refinement by nesting rectangular subgrids of arbitrary orientation at regions necessitating enhanced resolution within a coarse-resolution base grid. Subgrids may overlap and multiple grid levels with increasing resolution can coexist. Estimates of truncation error at each grid point are used to flag the locations requiring improved resolution. Flagged points are clustered and rectangular subgrids encompassing each cluster are created. The procedure is performed at each level of resolution until no further refinement is required or a user-defined maximum level is reached.

An alternative strategy to adaptive gridding in meteorological modeling was reported by Dietachmayer and Droegemeier (Dietachmayer, 1992; Dietachmayer and Droegemeier, 1992). This method utilizes r-refinement driven by a weight function calculated from the spatial fields of selected physical properties, typically based on gradients and curvatures. Similar to other r-refinement algorithms, a coordinate transformation from irregular physical space to uniform computational space is applied to the governing system of equations.

5.5. Adaptive Grids in Air Quality Models

Application of adaptive grids in air quality modeling has been explored for over 10 years. Three distinct efforts to implement adaptive gridding techniques into Eulerian air pollution models can be identified. These undertakings can each be traced back to Tomlin et al. (1997), Srivastava et al. (2000), and Constantinescu et al. (2008). The

techniques presented by Tomlin et al. (1997) and Srivastava et al. (2000) have undergone substantial development thereafter, and evolved from simple exercises designed to prove the worthiness of adaptive gridding in air pollution modeling to elements of regional air quality models applied to realistic simulations. The aforementioned approaches to adaptive grid modeling are vastly different; methods applied to achieve improved results are unique to each. However, the goal and many of the conclusions reached from analysis of modeled results are common to all. In this section the main characteristics of each of these adaptive grid modeling techniques are described, as well as common challenges encountered and shared conclusions. A summary of the methods' characteristics is also presented in Table 5.1.

Table 5.1. Adaptive Grid Methods in Air Quality Modeling.

Original Publication	**Grid Structure**	**Refinement method**	**Refinement criteria applied**	**Implementation into operational air quality model**	**Vertical adaptivity**
Tomlin et al. (1997)	Unstructured triangular or tetrahedral	Single grid h-refinement	1st and 2nd order solution difference; concentration gradient	Eulerian grid model	Yes
Srivastava et al. (2000)	Structured quadrilateral	R-refinement	Interpolation error; concentration curvature	CMAQ	No
Constantinescu et al. (2008)	Uniform quadrilateral with nested refinements	Multigrid h-refinement	Concentration curvature	STEM	No

5.5.1. Reported Adaptive Grid Methods in Air Quality Modeling

An adaptive grid method applicable to air pollution modeling using unstructured grids is described by Tomlin et al. (1997). The method is applied to an unstructured triangular grid model which solves the discretized atmospheric diffusion equation using a finite-volume approach. Grid refinement is achieved through mesh enrichment (i.e., h-

refinement). Original grid nodes remain fixed and refinement is accomplished by splitting each triangle into 4 smaller, similar triangles. The process can be extended to any user-determined level of refinement and derefinement simply involves merging elements contained within the same parent triangle. The refinement technique is illustrated in Figure 5.2. Adaptation is driven by the spatial error estimated as the difference between solutions calculated using first- and second-order methods. A test case simulated dispersion of a concentrated NO_x plume within background atmospheres with varying degrees of pollution. The NO concentration field was selected to estimate spatial error and drive refinement limited to a maximum of two levels. In the simulation, refinement winds up concentrated around pronounced spatial gradients. The adaptive grid captures features in the ozone and NO_2 concentration structures unseen in a simulation without refinement, near the point source and further downwind. Additionally, a significant difference in total NO_2 mass is observed between adapted and unadapted simulations. The authors attribute the discrepancy to nonlinear chemistry, which renders ozone and NO_x concentrations grid resolution dependent.

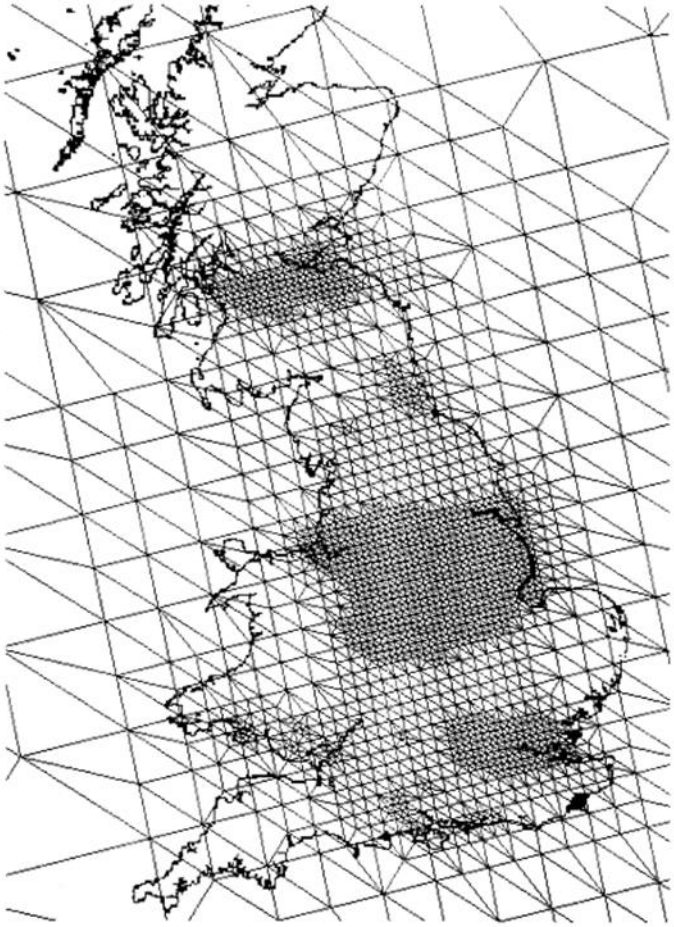

Figure 5.2. Refined unstructured triangular grid covering the United Kingdom. Reprinted with permission from Tomlin et al. (2000).

The adaptive gridding method of Tomlin et al. (1997) has been subsequently applied to model the dispersion of nuclear contamination (Lagzi et al., 2004) and air pollution formation across central Europe (Lagzi et al., 2009). These simulations extended into the regional scale and incorporated vertical layering and mixing, space-and-time-varying three-dimensional meteorological fields, dry deposition, and pollutant transformations (e.g., nuclear decay or chemical reactivity). In these studies, concentrations estimated using adaptive grids exhibited closer agreement to concentrations calculated under fine resolution than those attainable using coarse grids or nested grids placed over main pollutant sources. Furthermore, adaptive grids required only a fraction of the computer time necessary for the fine resolution simulations.

Implementation of adaptive gridding along the vertical domain has also been reported (Ghorai et al., 2000; Tomlin et al., 2000). The three-dimensional adaptive grid method uses an unstructured tetrahedral grid. Refinement is based on the same strategy previously described for the horizontal adaptation and is achieved by subdividing tetrahedral elements into 6 to 14 smaller tetrahedra depending on cell location and the number of edges tagged for refinement. In one test case, the adaptive grid method was used to model an elevated NO point source under conditions representative of different stability classes (Ghorai et al., 2000). Adaptation was driven by node-to-node concentration gradients. The results demonstrate the significance of vertical resolution in estimating accurate pollutant concentrations. This is especially true downwind of sources and under neutral-to-stable atmospheric conditions, which frequently lead to limited mixing and large gradients at inversion layers.

The use of mesh movement (r-refinement) as an adaptive grid strategy in air quality modeling was first reported by Srivastava et al. (2000). The proposed adaptive grid algorithm maintains the number of grid cells fixed throughout the simulation and operates on a structured grid. Nodes are allowed to relocate across the domain in an attempt to minimize solution error. However, grid topology remains unaltered. Use of nonuniform grid elements requires that a transformation from Cartesian to curvilinear coordinates be applied to governing equations and node positions. This transforms the grid from nonuniform in physical space to uniform in computational space, and allows the finite-volume solution procedures designed for a physically uniform grid to be applied to a nonuniform dynamic grid. Adaptation (i.e., grid movement) is controlled by a weight function based on an error estimate defined as the difference between the values at each cell and those obtained by interpolation of values in neighboring cells. A combination of species' concentrations may be selected as values used in the weight estimation. Weights are normalized, smoothed, and integrate several parameters that can be used to control the degree of adaptation. During adaptation, grid nodes are relocated

and clustered around areas bearing large weights. After the grid is modified, it is necessary to reorganize solution fields onto the new grid applying a redistribution procedure. The newly generated solution fields can then be used to recalculate spatial error (i.e., weights) in an iterative procedure that continues until a grid convergence criterion, defined as a maximum node movement relative to initial grid spacing, is met.

Several tests were performed using this adaptive grid algorithm to evaluate its performance including simulations of rotating conical concentration distributions (Srivastava et al., 2000), a reacting pollutant puff (Srivastava et al., 2000, 2001a), and dispersion of a power plant plume (Srivastava et al., 2001b). The simulation of single and multiple rotating conical distributions confirmed a significant increase in solution accuracy compared to static grid simulations and demonstrated the adaptive grid's ability to better resolve features involving steep gradients or discontinuities. An important observation is mentioned by the authors; while the adaptive grid provides an improvement over fixed grids, solution accuracy may still be limited by the total number of grid nodes in the simulation. A closer approximation to the exact solution may require that the number of grid nodes (i.e., cells) be increased, especially if multiple features simultaneously require increased resolution to be well resolved. The results from tests that modeled a reactive pollutant puff demonstrated that the adaptive grid algorithm better simulates nonlinear chemical transformations of pollutant distributions compared to static grid models. Srivastava et al. (2001b) modeled a plume from an elevated point source resembling a power plant stack with a simplified chemical mechanism using adaptive and static grids. The authors find that the adaptive grid method decreases plume dispersion and has a significant effect on modeled ozone concentrations. The adaptive simulation was able to capture the small scale ozone plume structure near the source as well as high ozone concentrations at large distances downwind. These features are not observed when using a static grid. The test further demonstrates that the transport and nonlinear chemical processes relevant to an ozone plume's "early", "intermediate", and

"mature" stages can only be adequately modeled by adaptive gridding or drastically increasing the number of cells in a much more computationally expensive simulation.

To demonstrate the computational expense and accuracy gained, CPU times with static and adaptive grids were compared for the reactive pollutants puff test (Srivastava et al., 2000). The solution with an adaptive grid took 9 times longer than the solution on a static grid with the same number of grid cells. However, the accuracy of the adaptive grid solution was far superior as the minimum grid cell size around the puffs was 30–40 times smaller than the static grid cell size. The CPU time of a refined static grid solution using 9 times more cells was also measured. Note that this solution falls short of providing the minimum cell size and the accuracy achieved by the adaptive grid solution, yet its CPU time was 63 times longer than the adaptive grid's. These comparisons show that adaptive grids have the potential to offer accurate solutions at significant cost savings.

Implementation of r-refinement into a comprehensive regional chemical-transport model was first reported by Odman et al. (2002). Later, Garcia-Menendez et al. (2010) developed an adaptive grid version of the Community Multiscale Air Quality modeling system (CMAQ) (Byun and Schere, 2006) using the adaptive grid algorithm proposed by Srivastava et al. (2000). This model is extensively discussed in Chapter 6. CMAQ integrates advection, diffusion, deposition, gas-phase chemistry, aqueous-phase reactions, aerosol dynamics, and cloud processes into air quality modeling. The adaptive grid version of CMAQ (AG-CMAQ) performs a transformation of the original governing equations in curvilinear coordinates, which allows the existing numerical schemes to be applied on a nonuniform grid. Two-dimensional grid refinement is driven by a weight function estimated from a numerical approximation of the curvature in selected model variables. The weight function can incorporate concentrations of different species or alternative atmospheric variables and adjust the relative importance of each.

AG-CMAQ performance was evaluated by applying the model to simulate the air pollution impacts from an actual biomass burning event affecting air quality over a large

urban area. Figure 5.3 illustrates the application. The focus was placed on fine particulate matter. This differs from most adaptive grid plume simulations previously reported, centered on ozone photochemistry. Additionally, results were compared to measurements at air quality monitoring sites, an assessment approach that had only been previously reported for adaptive grids by Lagzi et al. (2009). Three-dimensional meteorological and emissions data were prepared by a numerical weather prediction model and emissions processors. The evaluation showed that AG-CMAQ reduced diffusion and produced better refined plumes compared to fixed grid CMAQ results. The mean fractional error relative to measurements was also reduced when using AG-CMAQ. Furthermore, the developers believe that AG-CMAQ may provide insight into atmospheric processes beyond that which can be gained from fixed grid CMAQ simulations.

The adaptive grid method described by Constantinescu et al. (2008) has also been implemented into a comprehensive chemical and transport model. The authors developed a mesh enrichment (i.e., h-refinement) technique based on a structured quadrilateral grid and limited to the horizontal plane. The technique is illustrated in Figure 5.4. In this method, coarse level cells are grouped into equilateral blocks, each containing an equal number of cells. Refinement is achieved by subdividing a block into smaller blocks. Each refined block maintains the same structure and number of cells as the original block from which they were derived. Refinement can continue up to a specified maximum level; smaller cells are produced and the total number of cells across the domain is increased. Derefining involves merging several blocks into a single coarser-level block. The block structure and number of cells enclosed within each block, remain constant throughout the simulation. Adaptation is driven by the curvature in horizontal concentration fields. The normalized root mean square concentration curvature is estimated for each block, and the maximum estimate among all vertical layers is compared to user-defined tolerances to indicate refinement or derefinement. Simplified tests simulating atmospheric dispersion

indicated that the adaptive grid is capable of producing more accurate results than coarse and nested grids.

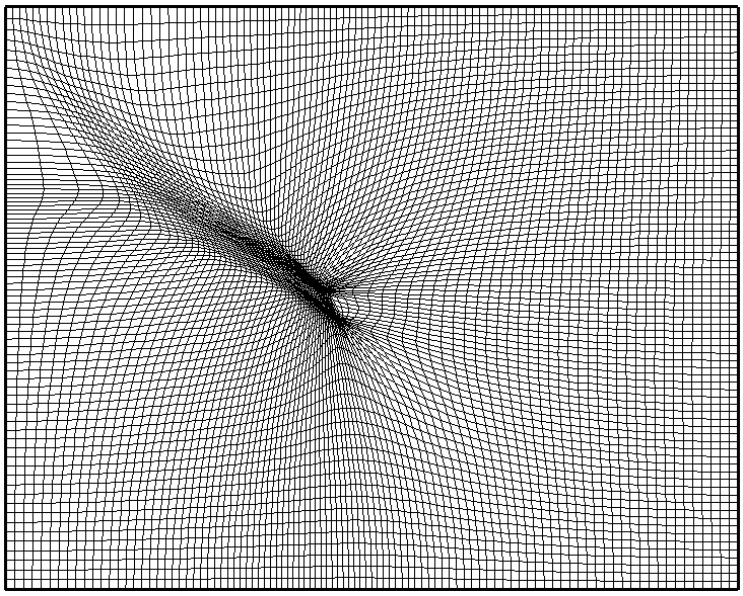

Figure 5.3. Adapted grid during a biomass burning plume simulation with AG-CMAQ.

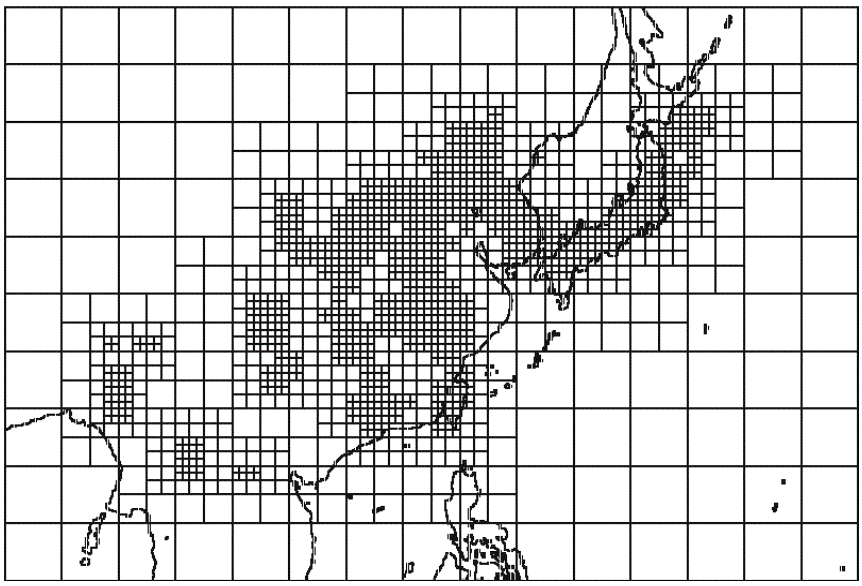

Figure 5.4. Block-structured dynamically refined grid over East Asia. Reprinted with permission from Constantinescu et al. (2008).

The adaptive grid methodology of Constantinescu et al. (2008) was integrated into the Sulfur Transport and dEposition Model (STEM) (Carmichael et al., 1991). STEM includes three-dimensional representations of dispersion, deposition, chemical transformation, and cloud processes. An adaptive grid simulation focused on ozone formation over East Asia during one week was carried out using four levels of refinement. Over 100 chemical species and 200 chemical reactions are considered in the model. Yearly averaged emissions inventories and prognostic weather simulation results were included as inputs. Different species were used to estimate concentration curvature and drive adaptation. The curvature in ozone proved least useful, while curvature estimates accounting for ozone precursors (NO, NO_2, and HCHO) produced better results. An increase in accuracy was observed when applying an adaptive grid relative to coarse resolution results. Two interesting observations are also discussed: (1) the increase in solution accuracy is highly dependent on the user defined refinement tolerances, and (2) the total number of grid cells decreases with time until becoming fairly stable. Special attention was given to implementation of the adaptive grid method into parallel computing systems, facilitated by the domain's division into self-similar blocks. A computational cost is acknowledged for adaptive gridding. However, the computational requirements were significantly lower than those necessary for simulations performed at the finest grid resolution allowed in the adaptive grid application. For the application described, wall-clock times of STEM runs with static and adaptive grids were compared. An adaptive grid run of comparable accuracy required only a quarter of the time spent in a static fine grid run.

5.5.2. Common Challenges

The methodologies described in Section 5.5.1 follow different approaches to adaptive grid integration into air pollution modeling. However, all attempts have

encountered common challenges. These common obstacles and the strategies applied to overcome them merit attention and are discussed in this subsection.

5.5.2.1. Refinement Criterion

We have previously mentioned that an essential component of any grid refinement technique is an error estimation that serves as a refinement criterion. All applications of adaptive gridding to air quality modeling previously reported have relied on atmospheric concentration spatial fields. An error estimate calculated from the difference in first-order and second-order approximations of local concentrations was described in Tomlin et al. (1997). A simpler error calculation based on the gradient between neighboring concentration values was applied in Ghorai et al. (2000). A numerical approximation of the curvature of concentration fields was introduced by Srivastava et al. (2000) and has been used in later studies (Constantinescu et al., 2008; Garcia-Menendez et al., 2010). The different error estimations have all proven adequate. For simulations analyzing secondary pollutant fields, results indicate that spatial error calculations that consider precursor species outperform those that focus solely on the secondary pollutant.

5.5.2.2. Refinement Control

A need to constrain refinement intensity has also been identified in all previous investigations. Uncontrolled adaptation may lead to excessive refinement. Control parameters are implemented into the refinement criteria estimates previously described to normalize and smooth spatial error calculations. Mesh enrichment methods additionally require that user-defined upper and lower tolerances be set to trigger adaptation, directly controlling the degree to which grids are reconfigured. Furthermore, mesh enrichment techniques constrain adaptation to a maximum number of refinement levels. In the iterative mesh moving method previously described, a maximum number of relocation

operations and minimum node movement relative to initial grid spacing are defined to stop adaptation.

Some concern about abrupt transitions in grid resolution has been expressed in past adaptive gridding exercises. The existence of neighboring grid elements refined to very different degrees may lead to errors and the loss of features resolved under the fine resolution if advection transports the features into coarse resolution regions prior to adaptation. A safety layer encompassing high resolution regions is proposed as a solution by Tomlin et al. (2000). The problem has also been addressed by significantly smoothing the error estimation driving adaptation (Srivastava et al., 2000). In r-refinement no boundaries between different resolution levels are created and smoothing can guarantee changes in grid size are gradual. Special care must be given to refinement along domain borders, as boundary conditions are generally only available at coarser resolution. Domain design should consider maintaining features that will call forth considerable refinement distanced from the domain edges. The moving mesh algorithm developed by Srivastava et al. (2000) only allows node movement along the lateral domain boundaries, limiting the refinement attainable along these edges. The same strategy is applied in AG-CMAQ. In the adaptive grid model developed by Constantinescu et al. (2008) the cell blocks along lateral domain boundaries are maintained at the coarsest level throughout the simulation, and each subsequent cell block is only allowed to adapt to one additional refinement level.

5.5.2.3. Adaptation Frequency

As adaptability is integrated into more complex atmospheric systems, the grid refinement process may become increasingly taxing, especially when applied to comprehensive chemical-transport models. Therefore, it may be necessary or desirable to apply grid adaptation at intervals greater than solution frequency. Ghorai et al. (2000) found that performing grid adaptation every 20 minutes is sufficient to produce accurate

results and reduces the computational requirements of a three-dimensional elevated plume simulation. A 5 minute adaptation interval is used in the regional air quality case presented in Lagzi et al. (2009). In their simulation of air quality over East Asia, Constantinescu et al. (2008) tested adaptation intervals from 1 to 6 hours and determined that 3 hours provided an adequate balance between solution accuracy and computational cost. The reactive plume simulation of Srivastava et al. (2001b) applies grid adaptation at a frequency equivalent to every 4 solution time steps. The adaptive grid version of CMAQ developed by Garcia-Menendez et al. (2010), carries out adaptation once every output time step, set to 15 minutes in the application described. A related concern is the existing lag between adaptation and solution; error calculations that drive adaptation are estimated using the solution at the end of a time step, but the grid generated is applied towards solution of the following time step. To address this issue, quadratic interpolants have been used to predict the evolution of spatial error at a future time step and determine refinement (Tomlin et al., 1997). Such an approach may become increasingly useful as adaptability is implemented into more complex models and the frequency of adaptation must be reduced.

5.5.2.4. Preadaptation

Preadaptation has also been identified as a process that might be important in effective grid refinement. The strategy is of particular relevance to point sources which might immediately dilute into coarse cells and lose plume features prior to any adaptation. The plume simulation carried out by Tomlin et al. (2000) addressed the issue by placing the modeled stack within a subdomain and using the subdomain concentration as an internal boundary condition, an approach similar to grid nesting. Subsequent applications of this adaptive grid method have commenced from grids initially refined around major pollutant sources (e.g., point sources (Ghorai et al., 2000), cities (Lagzi et al., 2004; Lagzi et al., 2009)). A grid preadaptation step was proposed by Srivastava et al.

(2000). Under this procedure, a grid is adapted from the initial concentration field using the same error weight function estimation applied throughout the simulation. For sources that begin to emit at the start of the simulation, emissions are assumed to occur prior to initiating the run. Although preadaptation was not considered in the simulations discussed in Constantinescu et al. (2008), the authors acknowledge that a transient phase characterized by heavier refinement and observed during the initial stages of all runs might be attributable to coarse resolution around major sources at the onset.

5.5.2.5. Interpolation

Interpolation of coarse or uniformly distributed data onto adapted grids is an important component of all adaptive air quality modeling methods reported. The operation is essential during three processes of an adaptive grid air quality model: emissions, meteorology, and solution redistribution. The procedure for processing emissions must be applied after each grid adaptation operation. Different interpolation schemes have been used to interpolate area sources onto adapted nonuniform grids. Additionally, point sources must be relocated to appropriate cells after grid reconfiguration. Emissions processing can become taxing, especially for mesh moving methods that use cells with irregular geometries (Garcia-Menendez et al., 2010). Meteorological inputs, whether from numerical weather prediction models or synoptic observations, are typically uniformly spaced and provided at a resolution coarser than that of refined grids. Ideally, meteorological inputs should be provided on the same adaptive grids. A system with adaptive grid capability that attempts to couple simple air pollutant dispersion models with meteorology models was reported by Bacon et al. (2000) and is further described in Section 5.6. Mapping of meteorological fields onto required locations on an adapted grid is necessary and can be achieved through interpolation techniques. Nonetheless, the interpolation should ensure conservation and produce minimally modified fields (Tomlin et al., 2000). The most recurrent interpolation

operation in an adaptive grid algorithm is redistribution of solution fields onto modified grids after applying adaptation. Here, conservation is paramount. With grid enrichment methods, the operation may be as simple as linear interpolation (Constantinescu et al., 2008). More elaborate interpolation techniques have been applied to solution interpolation onto unstructured triangular and tetrahedral based grids, including a conservative rezoning algorithm and cell-vertex method (Tomlin et al., 2000). Under mesh moving techniques, the movement of nodes over solution fields can be considered as equivalent to advective fluxes crossing cell boundaries. Solution redistribution procedures using a conservative interpolation equation or monotonic advection scheme have been previously described (Garcia-Menendez et al., 2010; Srivastava et al., 2000). It is likely that a significant fraction of the computational cost associated with adaptive grid air quality modeling is attributable to solution redistribution operations. This is especially true for iterative procedures. The overhead from adaptation must be kept in check by defining appropriate adaptation intervals and refinement parameters. Finding an adequate balance between adaptation efficiency and computational workload is important to achieve an effective operational model.

5.5.2.6. Time-Stepping

One characteristic of adaptive grid air quality models that can severely hinder performance is excessively small process time steps applied uniformly throughout the domain. It is common practice in air pollution models to apply the domain-minimum time step, typically fixed by the characteristic time for advection, at every point (Constantinescu et al., 2008; Ghorai et al., 2000). Therefore, the domain-wide solution time step is determined by the grid cells subjected to the highest resolution and greatest wind speeds. This guarantees that the Courant stability condition is met. However, as grids are refined solution time steps become increasingly small. Applying the minimum solution time step across the entire grid regardless of the individual needs at each location

is an inefficiency typically encountered in air quality models that may render adaptive gridding prohibitive. This concern is especially relevant when applying adaptive grid algorithms to comprehensive air quality models. The problem can be controlled by constraining the degree of refinement allowed as previously described. Alternatively, a variable time step algorithm was implemented into the adaptive grid version of CMAQ to address the issue (Garcia-Menendez et al., 2010). Under this technique, a local solution time step is assigned to each grid cell and the computational cost associated with adaptive gridding can be notably reduced. The local time steps are all integer divisors of a synchronization time step used to advance in time a synchronized global solution (Hu and Odman, 2010).

5. 5.2.7. Subgrid Scale Parameterizations

Finally, an especially significant concern about adaptive grid air quality modeling is the applicability of subgrid parameterizations to grids with nonuniform resolution and highly refined regions. The issue has not yet been addressed in reported research efforts. Parameterizations for physical processes (e.g., turbulence, cloud processes) must be valid for the refined grid. The dependence of these parameterizations on grid resolution may bring into question their validity across the entire domain if considerable differences in grid resolution are allowed. Furthermore, if resolution is sufficiently increased, some parameterizations might not be required and their inclusion could adversely affect solution accuracy. The concern is also relevant to adaptive grid modeling in other atmospheric realms. For instance, one adaptive grid weather prediction model assigns an adjustment factor, determined by cell area, to each cell and uses this factor to regulate the degree to which the convective parameterization is applied at individual cells (Bacon et al., 2000). Similarly, techniques that integrate dependence on grid resolution into the parameterizations of adaptive grid air quality models may have to be considered.

5.5.3. Shared Conclusions

All adaptive grid air quality modeling applications previously described find that dynamic mesh refinement significantly increases the accuracy of results. Observed differences in simulated concentration fields using adaptive and static grids demonstrate a legitimate need for increased resolution in air quality modeling. Adaptive gridding has consistently proven to be an adequate and highly attractive option to meet increased resolution requirements. Additionally, the different adaptive grid methods reported outperform grid nesting and increase computational efficiency compared to high resolution simulations capable of providing the same level of accuracy. Adaptive grids significantly decrease numerical diffusion while revealing detailed pollutant concentration structures and features that cannot be resolved with static grids, uniform or nested, using comparable computational resources. Decreased errors associated with pollutant levels modeled using adaptive grids can be perceived near emissions sources as well as at considerable downwind distances.

In the adaptive grid applications described, the largest spatial error, and therefore the highest degree of refinement needed to reduce this error, is typically observed at regions with pronounced concentration gradients. Large gradients can be usually found near pollutant sources and along plume edges further downwind. The nonlinear nature of atmospheric chemical transformations further strengthens the case for adaptive gridding. Studies have repeatedly determined that pollutant concentrations subjected to nonlinear chemistry (e.g., ozone, nitrogen oxides) are mesh dependent. Under these circumstances, integrated pollutant concentrations can change significantly when applying grid refinement techniques that can better resolve the chemical processes. As chemical transport models incorporate detailed secondary organic aerosol processes, nonlinear as well, the advantages of adaptive grids may become even more apparent.

Vertical grid adaptation has only been fully incorporated into a single adaptive grid model. Tomlin et al. (2000) find that vertical resolution may be important to resolve

vertical profiles of pollutant sources and consequently determine accurate ground-level concentrations further downwind. Higher resolution may be warranted near inversion heights under unstable conditions. Since increased resolution is typically provided near the surface and mixing heights vary greatly throughout the day, vertical adaptivity may be helpful in capturing relevant concentration gradients above ground (Ghorai et al., 2000). Although refinement is limited to the horizontal plane within the adaptive grid methods implemented into comprehensive chemical transport models, the authors describe extension of the methods along the vertical direction as a plausible and attractive undertaking (Constantinescu et al., 2008; Garcia-Menendez et al., 2010).

Finally, all developers agree that the power of adaptive gridding will become more apparent as resolution of model inputs is increased to better match refined grids. This includes emissions, meteorological fields, and boundary conditions. Accuracy has been seen to improve when applying high resolution emissions (Constantinescu et al., 2008). The significance of coupling adaptive grid air quality models to high resolution weather data has also been mentioned (Constantinescu et al., 2008; Garcia-Menendez et al., 2010; Lagzi et al., 2004). A potential alternative is to operate meteorological and air quality models under the same adapted grid. The coupled modeling approach would allow a weight function determined by any combination of both meteorological and air quality variables to drive grid refinement for both models simultaneously (Garcia-Menendez et al., 2010).

5.6 Additional Applications of Adaptive Grid Modeling in Atmospheric Sciences

As adaptive grid modeling is being explored in air quality modeling, concurrent efforts to integrate the technique into weather prediction and global circulation models have been reported. Attempts to apply adaptive grids in comprehensive meteorological models have been limited with few recent developments. A noteworthy application is the Operational Multiscale Environmental model with Grid Adaptivity (OMEGA) (Bacon et

al., 2000). This numerical weather prediction model operates on a three-dimensional unstructured grid constructed from triangular prisms. Adaptation is carried out by adding or removing vertices at the centroids of cells tagged for refinement, subdividing cells, and restructuring node connections to minimize aspect ratio. An interesting feature of the model is the addition of dispersion modeling. Three distinct atmospheric dispersion techniques are integrated into OMEGA: Eulerian, Lagrangian particle, and probabilistic puff modeling. The techniques simplify pollutant transport by relying on averaged wind fields, parameterizing turbulent diffusion, and neglecting chemical transformation processes. Although these methodologies are not new, their incorporation into an adaptive grid meteorological model is of interest. With their inclusion, OMEGA allows embedded dispersion models to operate under high resolution meteorological fields. Furthermore, adaptation of the meteorological model can be driven by the pollutant plume itself (Bacon et al., 2000). Figure 5.5 illustrates grid adaptation to a plume in OMEGA. In this manner, a coupled meteorological-air-quality model that continuously exchanges data to drive the adaptation is established.

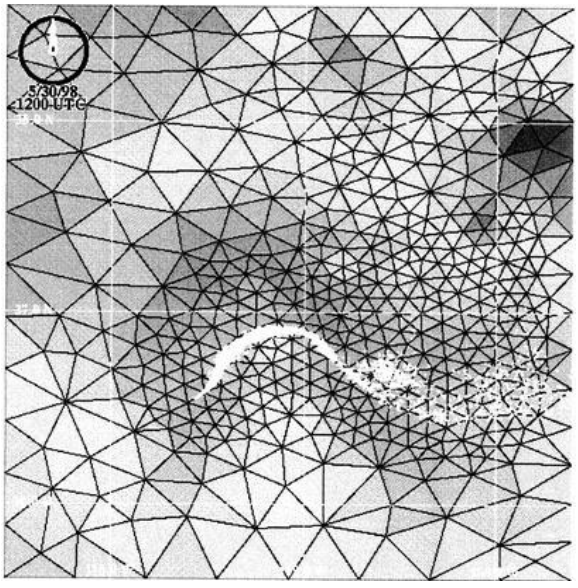

Figure 5.5. OMEGA grid dynamically adapted to a pollutant plume. Reprinted with permission from Bacon et al. (2000).

Much of the progress recently reported pertaining to adaptive grid modeling in atmospheric science involves incorporation of the technique into general circulation models. The motivation to integrate adaptive gridding into global models is largely analogous to that driving incorporation into air quality and weather models: models simulate atmospheric processes covering a wide range of scales and available computational resources are unable to explicitly resolve all processes involved. Therefore, it is not surprising to find that adaptive gridding techniques explored in climate models are frequently equivalent to those applied to air pollution modeling. However, the spatial and temporal scales of interest are very different to those in air quality simulations. In addition, the spherical nature of the global modeling domain and differences in simulated processes result in very different grid refinement requirements.

Nonetheless, future applications of adaptive gridding in air quality modeling may benefit from previous and ongoing efforts to integrate the technique into global models. Hubbard and Nikiforakis (2003) applied the grid refinement technique of Berger and Oliger (1984) previously explored in regional weather modeling, to global atmospheric modeling. Adaptive grid climate modeling on unstructured triangular or tetrahedral based grids has been explored by Behrens et al. (Behrens, 2005; Behrens et al., 2000; Behrens et al., 2005; Lauter et al., 2007). Here, adaptation is achieved by bisecting triangular or tetrahedral elements. Jablonowski et al. explored block-structured adaptive gridding within a global atmospheric model (Jablonowski et al., 2006; Jablonowski et al., 2009; St-Cyr et al., 2008). The grid refinement technique implemented in these applications is similar to that applied to air quality modeling by Constantinescu et al. (2008) and is illustrated in Figure 5.6. Refinement is achieved by organizing the domain into a block structured two-dimensional grid and further dividing blocks tagged for refinement into smaller self-similar units containing a fixed number of cells. Adaptation is allowed to proceed for several levels and each block is solved independently. A refinement

technique applicable to three-dimensional grids based on any geometric element was described by Weller and Weller (2008). The method has been explored on reduced latitude-longitude and hexagonal icosahedral grids (Weller and Weller, 2008), cubed sphere and triangular icosahedral grids (Weller et al., 2009), and polygon based grids (Weller, 2009). Moreover, an interesting approach to adaptation was presented by Weller (2009) where future refinement requirements are predicted at each adaptation step, allowing less frequent grid restructuring and diminished costs associated with restructuring the grid. Predictions are attained by advancing the solution by one adaptation time step on a coarse grid and estimating refinement criteria from this solution to generate a refined grid effective for the entire adaptation step. Additional research efforts exploring atmospheric modeling with unstructured Voronoi tessellations and C-grid discretization have been recently reported (Ringler et al., 2010; Thuburn et al., 2009). These grid generation techniques provide a natural framework for multiscale modeling and could effortlessly incorporate adaptive gridding in the future.

Figure 5.6. Block-structured adaptive grid on a global domain. Reprinted with permission from St-Cyr et al. (2008).

5.7. Concluding Remarks

Adaptive grid methods have not been fully explored in atmospheric modeling. Early attempts in weather prediction did not flourish and this field remained dominated by static nested grid methods. There have been a few recent attempts to integrate adaptive grids into air quality modeling but once again these attempts did not enjoy wide acceptance. Future undertakings should consider several key factors if greater interest in the technique is sought. The prevalence of community-driven models in atmospheric sciences today makes compatibility with existing model frameworks an indispensible requirement for increased use of adaptive gridding methodologies. Additional applications that go beyond typical power plant plume and ozone chemistry simulations are necessary to further demonstrate the worth of dynamic grid refinement. Finally, adaptive grid air quality models will have to be accompanied by equivalent increases to the resolution of emissions and meteorological inputs to truly reach their full potential.

What looks promising for adaptive grids is the presence of a vibrant support by the global climate community who acknowledge reaching a plateau after years of improvement in accuracy, mainly driven by progress in high performance computing. Adaptive grid methods are viewed as a means to reignite model advancement and a long term solution for dealing with the multiscale nature of the climate system (Slingo et al., 2009). The potential benefits of adaptive grid methods in global-scale modeling have been recognized (Weller et al., 2010). The range of scales covered by climate models is vast. For this reason, adaptive gridding might prove most crucial to future climate modeling.

The potential returns of adaptive grids are considerable while the risks are relatively small. The methods have matured through advancements in computational fluid dynamics and wide use, for example, in aerospace engineering applications. Difficulties could be encountered in developing parameterizations for processes that cannot be resolved by adaptive gridding. The problem may eventually dissipate as adaptive grids

continue to provide increased grid resolution. Nonetheless, the issue must be dealt with in the interim. The wide range of scales provided by adaptive grids will necessitate resolution dependent parameterizations and this may appear as a daunting task. However, what is faced by increasing grid resolution uniformly or through grid nesting is the same problem: parameterizations that made sense for coarse grid resolution must be rethought as grid resolution increases. A culture of designing resolution-dependent parameterizations upfront instead of revising the parameterizations every time model resolutions change must develop. For these reasons, development of adaptive grid models is a worthwhile investment.

5.8. References

Bacon, D.P., Ahmad, N.N., Boybeyi, Z., Dunn, T.J., Hall, M.S., Lee, P.C.S., Sarma, R.A., Turner, M.D., Waight, K.T., Young, S.H., Zack, J.W. (2000) A dynamically adapting weather and dispersion model: The Operational Multiscale Environment Model with Grid Adaptivity (OMEGA). Monthly Weather Review 128, 2044-2076.

Baker, T.J. (1997) Mesh adaptation strategies for problems in fluid dynamics. Finite Elements in Analysis and Design 25, 243-273.

Behrens, J. (2005) Adaptive atmospheric modeling: Scientific computing at its best. Computing in Science & Engineering 7, 76-83.

Behrens, J., Dethloff, K., Hiller, W., Rinke, A. (2000) Evolution of small-scale filaments in an adaptive advection model for idealized tracer transport. Monthly Weather Review 128, 2976-2982.

Behrens, J., Rakowsky, N., Hiller, W., Handorf, D., Lauter, M., Papke, J., Dethloff, K. (2005) amatos: Parallel adaptive mesh generator for atmospheric and oceanic simulation. Ocean Modelling 10, 171-183.

Berger, M.J., Oliger, J. (1984) Adaptive mesh refinement for hyperbolic partial-differential equations. Journal of Computational Physics 53, 484-512.

Byun, D., Schere, K.L. (2006) Review of the governing equations, computational algorithms, and other components of the models-3 Community Multiscale Air Quality (CMAQ) modeling system. Applied Mechanics Reviews 59, 51-77.

Carmichael, G.R., Peters, L.K., Saylor, R.D. (1991) The STEM-II regional scale acid desposition and photochemical oxidant model. 1. An overview of moel

development and applications. Atmospheric Environment Part a-General Topics 25, 2077-2090.

Clark, T.L., Farley, R.D. (1984) Severe downslope windstorm calculations in two and three Spatial dimensions using anelastic interactive grid nesting: a possible mechanism for gustiness. Journal of the Atmospheric Sciences 41, 329-350.

Constantinescu, E.M., Sandu, A., Carmichael, G.R. (2008) Modeling atmospheric chemistry and transport with dynamic adaptive resolution. Computational Geosciences 12, 133-151.

Dietachmayer, G.S. (1992) Application of continuous dynamic grid adaption techniques to meteorological modeling. 2. Efficiency. Monthly Weather Review 120, 1707-1722.

Dietachmayer, G.S., Droegemeier, K.K. (1992) Application of continuous dynamic grid adaption techniques to meteorological modeling .1. Basic formulation and accuracy. Monthly Weather Review 120, 1675-1706.

Garcia-Menendez, F., Yano, A., Hu, Y., Odman, M.T. (2010) An adaptive grid version of CMAQ for improving the resolution of plumes. Atmospheric Pollution Research 1, 239-249.

Ghorai, S., Tomlin, A.S., Berzins, M. (2000) Resolution of pollutant concentrations in the boundary layer using a fully 3D adaptive gridding technique. Atmospheric Environment 34, 2851-2863.

Hu, Y., Odman, M.T. (2010) A variable time–step algorithm for air quality models. Atmospheric Pollution Research 1, 229-238.

Hubbard, M.E., Nikiforakis, N. (2003) A three-dimensional, adaptive, Godunov-type model for global atmospheric flows. Monthly Weather Review 131, 1848-1864.

Jablonowski, C., Herzog, M., Penner, J.E., Oehmke, R.C., Stout, Q.F., van Leer, B., Powell, K.G. (2006) Block-structured adaptive grids on the sphere: advection experiments. Monthly Weather Review 134, 3691-3713.

Jablonowski, C., Oehmke, R.C., Stout, Q.F. (2009) Block-structured adaptive meshes and reduced grids for atmospheric general circulation models. Philosophical Transactions of the Royal Society a-Mathematical Physical and Engineering Sciences 367, 4497-4522.

Jones, R.W. (1977) A nested grid for a 3-dimensional model of a tropical cyclone. Journal of the Atmospheric Sciences 34, 1528-1553.

Lagzi, I., Karman, D., Turanyi, T., Tomlin, A.S., Haszpra, L. (2004) Simulation of the dispersion of nuclear contamination using an adaptive Eulerian grid model. Journal of Environmental Radioactivity 75, 59-82.

Lagzi, I., Turanyi, T., Tomlin, A.S., Haszpra, L. (2009) Modelling photochemical air pollutant formation in Hungary using an adaptive grid technique. International Journal of Environment and Pollution 36, 44-58.

Lauter, M., Handorf, D., Rakowsky, N., Behrens, J., Frickenhaus, S., Best, M., Dethloff, K., Hiller, W. (2007) A parallel adaptive barotropic model of the atmosphere. Journal of Computational Physics 223, 609-628.

Miyakoda, K., Rosati, A. (1977) One-way nested grid models - interface conditions and numerical accuracy. Bulletin of the American Meteorological Society 58, 117-117.

Morgan, K., Peraire, J. (1998) Unstructured grid finite-element methods for fluid mechanics. Reports on Progress in Physics 61, 569-638.

Odman, M.T. (1997) A quantitative analysis of numerical diffusion introduced by advection algorithms in air quality models. Atmospheric Environment 31, 1933-1940.

Odman, M.T., Khan, M.N., Srivastava, R.K., McRae, D.S., (2002) Initial application of the adaptive grid air pollution model, in: Borrego, C., Schayes, G. (Eds.), Air Pollution Modeling and its Application XV. Kluwer Academic/Plenum Publishers, New York, pp. 319-328.

Odman, M.T., Russell, A.G. (1994) On local finite-element refinements in multiscale air-quality modeling. Environmental Software 9, 61-66.

Phillips, N.A., Shukla, J. (1973) On the strategy of combining coarse and fine grid meshes in numerical weather prediction. Journal of Applied Meteorology 12, 763-770.

Pleim, J.E., Chang, J.S., Zhang, K.S. (1991) A nested grid mesoscale atmospheric chemistry model. Journal of Geophysical Research-Atmospheres 96, 3065-3084.

Ringler, T.D., Thuburn, J., Klemp, J.B., Skamarock, W.C. (2010) A unified approach to energy conservation and potential vorticity dynamics for arbitrarily-structured C-grids. Journal of Computational Physics 229, 3065-3090.

Skamarock, W., Oliger, J., Street, R.L. (1989) Adaptive grid refinement for numerical weather prediction. Journal of Computational Physics 80, 27-60.

Skamarock, W.C., Klemp, J.B. (1993) Adaptive grid refinement for 2-dimensional and 3-dimensional nonhydrostatic atmospheric flow. Monthly Weather Review 121, 788-804.

Slingo, J., Bates, K., Nikiforakis, N., Piggott, M., Roberts, M., Shaffrey, L., Stevens, I., Vidale, P.L., Weller, H. (2009) Developing the next-generation climate system models: challenges and achievements. Philosophical Transactions of the Royal Society a-Mathematical Physical and Engineering Sciences 367, 815-831.

Srivastava, R.K., McRae, D.S., Odman, M.T. (2000) An adaptive grid algorithm for air-quality modeling. Journal of Computational Physics 165, 437-472.

Srivastava, R.K., McRae, D.S., Odman, M.T. (2001a) Simulation of a reacting pollutant puff using an adaptive grid algorithm. Journal of Geophysical Research-Atmospheres 106, 24245-24257.

Srivastava, R.K., McRae, D.S., Odman, M.T. (2001b) Simulation of dispersion of a power plant plume using an adaptive grid algorithm. Atmospheric Environment 35, 4801-4818.

St-Cyr, A., Jablonowski, C., Dennis, J.M., Tufo, H.M., Thomas, S.J. (2008) A comparison of two shallow-water models with nonconforming adaptive grids. Monthly Weather Review 136, 1898-1922.

Thuburn, J., Ringler, T.D., Skamarock, W.C., Klemp, J.B. (2009) Numerical representation of geostrophic modes on arbitrarily structured C-grids. Journal of Computational Physics 228, 8321-8335.

Tomlin, A., Berzins, M., Ware, J., Smith, J., Pilling, M.J. (1997) On the use of adaptive gridding methods for modelling chemical transport from multi-scale sources. Atmospheric Environment 31, 2945-2959.

Tomlin, A.S., Ghorai, S., Hart, G., Berzins, M. (2000) 3-D Multi-scale air pollution modelling using adaptive unstructured meshes. Environmental Modelling & Software 15, 681-692.

Weller, H. (2009) Predicting mesh density for adaptive modelling of the global atmosphere. Philosophical Transactions of the Royal Society a-Mathematical Physical and Engineering Sciences 367, 4523-4542.

Weller, H., Ringler, T., Piggott, M., Wood, N. (2010) Challenges facing adaptive mesh modeling of the atmosphere and ocean. Bulletin of the American Meteorological Society 91, 105-108.

Weller, H., Weller, H.G. (2008) A high-order arbitrarily unstructured finite-volume model of the global atmosphere: tests solving the shallow-water equations. International Journal for Numerical Methods in Fluids 56, 1589-1596.

Weller, H., Weller, H.G., Fournier, A. (2009) Voronoi, Delaunay, and block-structured mesh refinement for solution of the shallow-water equations on the sphere. Monthly Weather Review 137, 4208-4224.

Zhang, D.-L., Chang, H.-R., Seaman, N.L., Warner, T.T., Fritsch, J.M. (1986) A two-way interactive nesting procedure with variable terrain resolution. Monthly Weather Review 114, 1330-1339.

CHAPTER 6

AN ADAPTIVE GRID VERSION OF CMAQ FOR IMPROVING THE RESOLUTION OF PLUMES

Abstract

Atmospheric pollutant plumes are not well resolved in current air quality models due to limitations in grid resolution. Examples of these include power plant and biomass burning plumes. Adequate resolution of these plumes necessitates multiscale air quality modeling at much finer scales than currently employed and adaptive grids may be the best approach to accurate fine-scale modeling of air pollution dynamics and chemistry. An adaptive grid version of the Community Multiscale Air Quality Model (CMAQ) with all necessary functions for tracking gaseous pollutants and particulate matter has been developed. The model incorporates a dynamic, solution-adaptive grid algorithm and a variable time step algorithm into CMAQ, while retaining the original functionality, concept of modularity, and grid topology.

The adaptive model was evaluated by comparing its performance to that of the standard, static grid CMAQ in simulating particulate matter concentrations from a biomass burning air pollution incident affecting a large urban area. The adaptive grid model significantly reduced numerical diffusion, produced better defined plumes, and exhibited closer agreement with monitoring site measurements. The adaptive grid also allows impacts at specified locations to be attributed to a specific pollutant source and provides insight into air pollution dynamics unattainable with a static grid model. Potential applications of adaptive grid modeling need not be limited to air quality simulation, but could be useful in meteorological and climate models as well.

*A modified version of this chapter has been published in *An adaptive grid version of CMAQ for improving the resolution of plumes*, Atmospheric Pollution Research **2010**, 1, 239-249.

6.1 Introduction

The dynamic and chemical processes of air pollution involve a wide range of scales. While the initial transformation of emissions and dispersion of plumes occur on relatively small scales, long-range transport engages much larger scales. Air quality models rely on their grids for explicit resolution of processes involved; the processes that occur on sub-grid scales are parameterized. Modeling large geographic regions with uniform resolution at the finest relevant scale is beyond the realm of current computers; therefore, regional models generally settle for coarser grid resolution. When emissions or plumes are injected into grid cells coarser in size than characteristic plume dimensions, they instantaneously mix with the contents of the grid cell. Such mixing is unrealistic; it dilutes the plumes and the details of the near-field chemistry are lost. Multiscale models have been proposed to surpass the limitations of single-scale models. Conceptually, a multiscale model blends small scales with large scales and assigns the most appropriate scales to the phenomenon being modeled.

The approaches to multiscale air quality modeling generally fall into one of the following two categories. The first category features static grids that can be nested multiple levels deep for better resolution of finer scale processes. This is the approach taken in the Community Multiscale Air Quality Model (CMAQ) (Byun and Schere, 2006). The second approach involves grids whose resolutions continuously adapt to the needs of a particular phenomenon throughout the simulation. Note that this classification does not distinguish sub-grid modeling as a separate category. Embedding a subgrid scale model into the grid model (e.g., plume-in-grid modeling) is a multiscale modeling technique that can be used both with static grid nesting and dynamic grid adaptations.

In static grid nesting, finer grids (FGs) are nested inside coarser ones (CGs). Multilevel nests can be placed to resolve the plumes of interest; however, as wind direction can change during the simulation, fine resolution must cover the entire area surrounding the emission source (e.g., power plant or industrial facility). There are two

types of grid nesting: one-way and two-way. In one-way nesting, the CG provides boundary conditions to the FG and no feedback is allowed from the FG to the CG; therefore, the CG and FG can be modeled sequentially. CMAQ uses one-way nesting. In two-way nesting, there is full interaction between the grids and all grids must be modeled simultaneously. The biggest limitation of static grid nesting is that resolution and the extent of each grid must be determined *a priori* and remain fixed throughout the simulation. The right choices of scale and coverage must be made at the beginning of the simulation.

In dynamic grid adaptations, the grid resolution changes continuously and automatically to improve the ability of the model to capture detailed dynamics or follow the chemical evolution of plumes. For example, refining the grid where chemical reactivity is high can lead to better characterization of the interactions of pollutant plumes with ambient atmospheres. Similarly, the passage of a front, clouds, and other relevant dynamic features can be better resolved if dynamic adaptations are used. Dynamic adaptive grids were suggested for use in atmospheric modeling a few decades ago, but did not gain widespread acceptance. The use of adaptive grids in air quality modeling is thoroughly discussed in Chapter 5.

Several adaptive grid algorithms were developed specifically for air quality modeling during the last decade. Although these algorithms did not necessarily make their way into functional air quality models, they were quite useful in determining the limitations of alternative approaches. For example, Tomlin et al. developed an unstructured grid algorithm for the purpose of resolving pollutant plumes in the boundary layer (Ghorai et al., 2000; Tomlin et al., 1997; Tomlin et al., 2000). This algorithm could have been linked with an adaptive grid meteorology model that also employs unstructured grids (e.g., (Bacon et al., 2000)) and developed into a transport-chemistry coupled with dynamics modeling system. However, the former did not occur. The reason may be the difficulties involved in transferring existing air pollution modeling

technologies to unstructured grids. On the other hand, the adaptive grid algorithm developed by Srivastava et al. (Srivastava et al., 2000, 2001a, b) is based on structured grids and may be easier to implement in an air quality modeling system.

Although some adaptive grid air pollution models were developed (Constantinescu et al., 2008; Odman et al., 2001; Odman et al., 2002), they were limited to gas-phase chemistry. Prior to this study, no effort has been reported towards the development of an adaptive grid chemical transport model for particulate matter (PM) or the incorporation of any adaptive grid capability into community models. However, dynamic grid adaptations in a community model such as CMAQ can significantly improve modeling of plumes from emission sources such as power plants or biomass burns, and hence the assessment of their air quality impacts.

This chapter continues with a description of how an adaptive grid version of the CMAQ model has been developed based on the adaptive grid algorithm by Srivastava et al. (2000) and the adaptive grid air pollution model by Odman et al. (2001). This is followed by a brief account of the model code testing. The adaptive grid version of CMAQ is then applied to simulate a biomass burning plume and compared to the standard, static grid version in terms of plume resolution and agreement with ground-level observations.

6.2 Model Development Methodology

The purpose of this work is to obtain more accurate solutions from the CMAQ modeling system to better assess the air quality impacts of plumes. The accuracy of the solution of a numerical model can be increased by either using higher order approximations (p-refinement) or by refining the modeling grid. There are two common grid refinement methods: (1) increasing the number of grid elements (h-refinement) and (2) maintaining the same number of grid elements but refining the grid by repositioning

the nodes (r-refinement). In adaptive grid refinement, h- or r-, the objective is to generate an optimal grid with available computational resources for the most accurate solution.

The adaptive grid refinement method used here falls into the r-refinement category. It employs a constant number of grid nodes. An important characteristic of the algorithm is that it utilizes a structured grid that partitions a rectangular domain into *N* by *M* quadrilateral cells. The nodes move throughout the simulation but the topology of the grid remains the same. Each grid node is still connected to the same neighboring nodes and each cell retains the same neighboring cells after movement. However, the length of the links between nodes and the area of the grid cells change. One advantage of retaining the structure of the grid is that the nonuniform grid in the physical space can be mapped onto a uniform grid in the computational space through a coordinate transformation. The solution of partial differential equations that govern atmospheric diffusion is simpler on a uniform grid. Another advantage that cannot be achieved by an unstructured grid is compatibility with CMAQ. Not only can the numerical solution schemes developed for CMAQ be used after the coordinate transformation, but the subgrid parameterizations in CMAQ can be adopted as well (as long as they remain valid within the range of adaptive grid scales). Since these parameterizations assume a certain grid topology, they are generally incompatible with unstructured grids.

The time integration of the governing equations on a dynamic adaptive grid can be viewed as a two-step operation. In the first step, *the solution step*, the grid movement is frozen in time and the equations are solved on this stationary grid. In the second step, *the adaptation step*, the grid nodes are moved through the solution fields obtained from the first step. As a result of the movement of the grid nodes to new locations, it will appear as if fluxes are crossing the faces of the grid cells. Ideally, the adaptation step should be repeated after each solution step owing to the change in resolution requirements. However, since frequent adaptations may be computationally restrictive, it may be practical to apply the adaptation step less frequently than the solution step. A

logical choice was to perform grid adaptation once every output time step as, in CMAQ, the partial solutions for different processes are guaranteed to synchronize before the solution is outputted. However, considering that CMAQ's typical one-hour output time step may be excessively long to achieve efficient adaptation, the output time step was reduced to 15 minutes.

Development of the adaptive grid CMAQ (AG-CMAQ) involved four major tasks: (1) reformulation of governing equations in general curvilinear coordinates; (2) implementation of spatially varying time steps; (3) incorporation of the adaptive grid algorithm; and, (4) consideration of meteorological data and emissions. The first two tasks are related to the solution step. The third and fourth tasks belong to the adaptation step. These four tasks will be described next. The following section ends with a brief account of the code verification procedure.

6.2.1 Governing equations and coordinate transformation

CMAQ is based on the species continuity equation that relates the rate of change of the concentration of species n, c_n, to transport and chemistry as follows:

$$\begin{aligned}\frac{\partial(\gamma c_n)}{\partial t}+\frac{\partial(\gamma U c_n)}{\partial X}+\frac{\partial(\gamma V c_n)}{\partial Y}+\frac{\partial(\gamma\dot{\sigma} c_n)}{\partial \sigma}+\frac{\partial}{\partial X}\left(\gamma K^{XX}\frac{\partial c_n}{\partial X}\right)\\ +\frac{\partial}{\partial Y}\left(\gamma K^{YY}\frac{\partial c_n}{\partial Y}\right)+\frac{\partial}{\partial \sigma}\left(\gamma K^{\sigma\sigma}\frac{\partial c_n}{\partial \sigma}\right)=\gamma R_n+\gamma S_n\end{aligned}, \tag{6.1}$$

where X and Y are the coordinates on a conformal map of Earth and σ is a terrain-following normalized vertical coordinate. Hence, the spherical shape of Earth and the irregularity of its surface already necessitate coordinate transformations, and γ is the Jacobian of these transformations:

$$\gamma=\frac{1}{m^2}\frac{\partial z}{\partial \sigma}. \tag{6.2}$$

Here m is the scale factor of a conformal map projection, i.e., the ratio of the distance on map to distance on Earth. A popular normalized vertical coordinate is sigma-p (pressure)

which is related to the altitude coordinate z as $\partial z/\partial\sigma = p^*/\rho g$, where p^* is the pressure difference between the surface and the top of the domain, ρ is the air density, and g is the gravitational acceleration. In Equation (6.1), U and V are the wind velocity components in the X and Y directions after scaling by m, and $\dot{\sigma}$ is a nondimensional velocity component in the σ direction. K^{XX}, K^{YY} and $K^{\sigma\sigma}$ are the elements of the diagonal turbulent diffusivity tensor with $K^{\sigma\sigma}$ related to vertical diffusivity K^{zz} as:

$$K^{\sigma\sigma} = \left(\frac{\partial\sigma}{\partial z}\right)^2 K^{zz}. \tag{6.3}$$

R_n and S_n are the chemical reaction and emission terms for species n.

One more coordinate transformation was necessary to develop AG-CMAQ, the transformation of the horizontal space from the (X,Y) coordinate system to a curvilinear coordinate system (ξ,η):

$$\begin{aligned}\xi &= \xi(X,Y)\\ \eta &= \eta(X,Y)\end{aligned}. \tag{6.4}$$

Through this transformation, the adaptive grid that is nonuniform in (X,Y) space becomes a uniform grid in (ξ,η) space. The governing equations in (ξ,η,σ) space can be derived from Equation (6.1) above through the use of the chain rule for derivatives:

$$\begin{aligned}&\frac{\partial(Jc_n)}{\partial t} + \frac{\partial\left(Jv^{\xi}c_n\right)}{\partial\xi} + \frac{\partial\left(Jv^{\eta}c_n\right)}{\partial\eta} + \frac{\partial(J\dot{\sigma}c_n)}{\partial\sigma} + \frac{\partial}{\partial\xi}\left(JK^{\xi\xi}\frac{\partial c_n}{\partial\xi}\right)\\ &\quad + \frac{\partial}{\partial\eta}\left(JK^{\eta\eta}\frac{\partial c_n}{\partial\eta}\right) + \frac{\partial}{\partial\sigma}\left(JK^{\sigma\sigma}\frac{\partial c_n}{\partial\sigma}\right) = JR_n + JS_n\end{aligned}. \tag{6.5}$$

In this equation, the new Jacobian, J, is related to γ as

$$J = \left(\frac{\partial X}{\partial\xi}\frac{\partial Y}{\partial\eta} - \frac{\partial Y}{\partial\xi}\frac{\partial X}{\partial\eta}\right)\gamma \tag{6.6}$$

and v^{ξ} and v^{η} are the non-dimensional components of the wind velocity vector in the ξ and η directions related to U and V as

$$\begin{aligned} v^{\xi} &= \frac{\partial \xi}{\partial X} U + \frac{\partial \xi}{\partial Y} V \\ v^{\eta} &= \frac{\partial \eta}{\partial X} U + \frac{\partial \eta}{\partial Y} V \end{aligned} . \tag{6.7}$$

The elements of the turbulent diffusivity tensor $K^{\xi\xi}$ and $K^{\eta\eta}$ can be expressed as

$$\begin{aligned} K^{\xi\xi} &= K^{XX} \left(\frac{\partial \xi}{\partial x} \right)^2 + K^{YY} \left(\frac{\partial \xi}{\partial y} \right)^2 \\ K^{\eta\eta} &= K^{XX} \left(\frac{\partial \eta}{\partial x} \right)^2 + K^{YY} \left(\frac{\partial \eta}{\partial y} \right)^2 \end{aligned} . \tag{6.8}$$

Now that the grid is uniform in (ξ,η) space, it is much easier to solve the Equation (6.5). In fact, since the finite difference stencils in the ξ and η directions are the same as the stencils used in the X and Y directions in CMAQ, the solution algorithms can be taken directly from CMAQ. In addition, the parameterizations that only involve the vertical direction (e.g., cumulus parameterization) are directly applicable if the vertical coordinate is not transformed. The metric derivatives in Equations (6.6), (6.7) and (6.8) are calculated after each grid adaptation step using finite differences at the most appropriate locations (e.g. at the grid nodes or at the centers of the grid cells), stored as global variables, and then passed to various process modules that need them.

6.2.2 Variable time-step algorithm

In CMAQ, Equation (6.1) is solved using a method called process splitting where the rate of change of concentrations in one time step is broken into components associated with each process. These processes, which include advection, diffusion, chemistry, aerosol processes and cloud processes, are applied to the concentration fields sequentially. After all processes are applied for one time step, the solution is complete. The time step used for advancing split processes in CMAQ is determined by the characteristic time for advection. The goal is to complete the process cycle before any material is advected by more than one grid cell distance. This is ensured by selecting a

time step smaller than the grid size divided by the wind speed. This also satisfies the Courant stability condition for explicit advection schemes. Since the grid size is uniform in CMAQ, the maximum wind speed determines the time step for the entire domain. Note that using a time step much smaller than a cell's characteristic time step does not make the solution more accurate; therefore, having a single global time step is computationally inefficient. In AG-CMAQ, the grid size is not uniform and the minimum ratio of grid size to wind speed (i.e. a relatively small grid size and a relatively large wind speed) determines the time step. Since the smallest and largest grid sizes can differ by orders of magnitude, the inefficiency becomes a serious bottleneck. Odman and Hu (2007) developed an algorithm that overcomes the global time step limitation by allowing the use of local time steps.

In the variable time step algorithm, VARTSTEP (Odman and Hu, 2010), every cell is assigned its own local time step, which must be an integer multiple of the smallest time step in the domain and a whole divisor of the model's output time step. For example, if the smallest time step in the domain is 1 minute and the output time step is 15 minutes, the allowable local time steps are 1, 3, 5, and 15 minutes. Considering that the length scales may be as small as 10 m in AG-CMAQ, and with a 10 m s^{-1} wind speed a time step of 1s may be necessary, the lower bound for local time steps was decreased to 1 second. With this adjustment, there is now a much wider range of possible local time steps than in the above example. The model clock time, *t*, is advanced by the minimum time step in the domain. When the clock strikes a multiple of the local time step, the grid concentration is advanced by the local time step by applying the changes resulting from different processes.

Greatest computational savings can be expected in chemistry and aerosol processes that are independent from neighboring cell concentrations because the changes due to those processes can be computed at the frequency of the local time steps. On the other hand, transport processes involve neighboring cell concentrations; therefore, they

must be computed more frequently than the local time step. The transport fluxes from neighboring cells must be kept in reservoirs until the concentrations are updated. This increases the memory requirements with respect to CMAQ by an array equal in size to the concentration array. Horizontal advection in all grid cells is computed at the frequency of the minimum time step in the domain. Chemistry and aerosol processes are computationally more intensive than horizontal advection in CMAQ (Odman and Hu, 2010). As a result, the local time stepping enabled by VARTSTEP makes AG-CMAQ much more computationally efficient than its predecessors (Odman et al., 2001; Odman et al., 2002).

6.2.3 Adaptive grid algorithm

As mentioned before, a simulation with AG-CMAQ has two fundamental steps: the solution step, described above, and the grid adaptation step. The purpose of grid adaptation is to locally increase or decrease grid resolution such that a more accurate solution can be obtained in the following solution step. The solution fields (e.g. concentration) remain unchanged during the adaptation step. However, grid nodes are clustered in regions where finer resolution is needed for an accurate solution.

The grid adaptation methodology used here is based on the Dynamic Solution Adaptive Grid Algorithm described in Srivastava et al. (2000). In the algorithm, the movement of the grid nodes is controlled by a weight function. Grid resolution is increased by clustering the grid nodes around regions where the weight function bears large values. Since the number of nodes is constant, refinement of the grid in some regions of the domain is accompanied by coarsening in other regions where the weight function has smaller values. In this manner, a multiscale grid is obtained where the scales change gradually. Unlike nested grids, there are no fine-to-coarse grid interfaces, which may introduce numerical difficulties due to the abrupt change or discontinuity of grid scales. In practice, the number of grid nodes is selected according to the computational

resources available. By automatically distributing the grid nodes throughout the modeling domain the adaptive grid algorithm attempts to optimize the use of computational resources during the simulation.

The weight function must be able to determine where grid should be clustered for a more accurate solution. A linear combination of the errors in concentrations of various chemical species makes an ideal weight function because it will assume large values where the errors are large. Adaptation weight scan be estimated as

$$w = \sum_n \alpha_n \nabla^2 c_n \,, \tag{6.9}$$

where w is the weight function, ∇^2 , the Laplacian, is a measure for the numerical error in c_n, and α_n is a coefficient that adjusts the weight of the numerical error in species n with respect to the others. The different chemical mechanisms used in CMAQ all have a large number of species. Each one of these species may have very different resolution requirements. Therefore, no single set of α_n can guarantee accurate solutions for all applications. Here, the focus was on PM emissions from biomass burning; consequently, all α_n terms were set to zero, except for those from primary PM species. In applications involving secondary pollutants, such ozone or secondary organic aerosols, the proper choice of α_n may not be as obvious and may require some experimentation. For example, a weight function combining nitrogen oxides (NOx), volatile organic compounds (VOCs) and ozone is likely to produce the best grid for capturing ozone formation. Odman et al. (2002), Khan (2003), and Constantinescu et al. (2008) tried weight functions with different combinations of α_n for NOx, VOC, and ozone, in applications to urban and power plant plumes. For two-dimensional grid adaptation, such as that described in this chapter, concentrations at the surface, or any other layer, as well as vertical column totals may be used in Equation (6.9).

Using the weight function, the new position of the grid node i, $\vec{P}_i^{\,new}$, is calculated as follows:

$$\vec{P}_i^{new} = \sum_{k=1}^{4} w_k \vec{P}_k \Big/ \sum_{k=1}^{4} w_k \ . \tag{6.10}$$

Here, $\vec{P}_i^{new}$, $k = 1,\ldots,4$ are the original positions of the centroids of four grid cells that share the grid node i in the horizontal plane and w_k is the value of the weight function at each centroid. New grid coordinates are stored into a three-dimensional array and passed as an argument to all process modules.

The movement of grid nodes in a steady concentration field results in fluxes crossing the boundaries of the grid cells. In this respect, grid adaptation is similar to advection where the grid boundaries are fixed but the field is moving due to wind velocity. Alternatively, the problem can be approached by observing that after adaptation each grid cell encloses a different portion of the domain, hence a different plot of the concentration field. Therefore, cell-average concentrations must be recomputed. This is similar to interpolation. Since interpolation is numerically equivalent to advection (Smolarkiewicz and Grell, 1992), either way of thinking is acceptable. Here, a high-order accurate and monotonic advection scheme known as the piecewise parabolic method (Colella and Woodward, 1984) was used to determine the concentrations of grid cells after adaptation.

Grid adaptation is an iterative process that continues until an optimal grid is found. Note that the concentration field must be redistributed (i.e., interpolated as described above using the advection scheme) to the new grid locations and the weight function must be recalculated after every iteration. The grid is considered to have converged when the new node positions in Equation (6.10) are the same, within a preset tolerance, as the original positions. A very small tolerance may lead to a large number of iterations. On the other hand, a large tolerance may not yield adequate grid resolution to minimize numerical error. After testing with alternative tolerance levels, the decision to stop iterating was applied when the movement of any grid node was less than 5% of the

minimum distance between the node in question and the four nodes to which it is connected along the horizontal plane.

6.2.4. Meteorological data and emissions

After the grid adaptation, meteorological data and emissions are needed on the new grid locations for the next solution step. For meteorological data, an ideal solution would be to have a meteorological model that can operate on the same adaptive grid and run in parallel with AG-CMAQ. The weight function that drives grid adaptations can include functions of meteorological variables such as vorticity. Such an adaptive grid meteorological model could also resolve local circulations that cannot be detected by static grid meteorological models, even at very fine grid resolutions. An adaptive grid version of the Penn State/NCAR Mesoscale Model (MM5) has been developed based on the Dynamic Solution Adaptive Grid Algorithm to predict optical turbulence in the upper atmosphere (Xiao et al., 2006). However, at the time of this study, that model was still under evaluation for applications within the boundary layer. In the absence of an adaptive grid meteorological model, the best available option was to obtain weather data from a high-resolution, static-grid model, store it in a uniform grid input file at 15-minute frequency and, when needed in AG-CMAQ, interpolate onto the adaptive grid. The interpolation weights were calculated after each grid adaptation step and stored as global variables, in the same manner as the metric derivatives.

The processing of emissions is computationally expensive, requiring relocation of various emission sources in the adapted grid cells. Khan et al. (2005) developed efficient search and intersection algorithms for emissions processing. Here, all emissions are treated either as foreground or background emissions. For example, if AG-CMAQ is being used to resolve a biomass burning plume, the emissions from that burn are considered to be in the foreground, while all other emissions (e.g. power plant, industrial, traffic, and biogenic emissions) are in the background. If the foreground emissions are

from a stack (e.g., a power plant), the position of the stack must be relocated on the grid as the cell containing the stack may have changed after grid adaptations. For foreground emissions from an area source (e.g. a forest fire) the area of the source must be intersected with the adaptive grid. Since the focus is usually on a few foreground sources, these search and intersection operations are not very intensive. In order to avoid higher computational costs associated with processing of emissions, background emissions are all merged and mapped onto a uniform high-resolution *emissions grid*. Each adaptive grid cell intersects with a number of emissions grid cells. The polygonal intersections of emissions grid cells with adaptive grid cells are calculated and stored as global variables after the grid adaptation step. When emissions are needed during the solution step, the fluxes are read from the emissions input file and apportioned to the adaptive grid cells using these polygonal intersections as described in Odman et al. (2002).

6.2.5 Code verification

The development of AG-CMAQ was a major undertaking. In addition to adding the adaptive grid related modules, important modifications had to be made to the base CMAQ code. However, special care was taken to remain faithful to the original modularity concept. Several rounds of reviews were conducted critically examining the code and confirming it reflected the intent of the methodology. Finally, carefully designed tests were executed to complete the verification of the AG-CMAQ code.

Two of those code verification tests were most useful. In the first test, results from a standard, static grid CMAQ simulation were compared to those obtained from AG-CMAQ without activating any grid adaptation. The measure of success in this test would be the similarity of results from the adaptive grid simulation to the benchmark. Emissions data and model inputs corresponding to a prescribed burn performed at Ft. Benning, Georgia on April 9, 2008 were used in the simulations. Further details about this fire are included in Chapter 2. The results from the application of AG-CMAQ without adaptation

were practically the same to those from the static grid CMAQ, except for very small and random differences, mostly in biogenic organic and nitrate aerosol concentrations (< 0.1 μg m^{-3}). A second verification test was carried out to observe the performance of AG-CMAQ with grid adaptation in a simulation of the same prescribed burn. In this test, to refine the grid around the fire plume in AG-CMAQ, fine particulate matter ($PM_{2.5}$) concentration was used as the adaptation variable. Modeled surface-level $PM_{2.5}$ concentration fields are shown in Figure 6.1. The results from AG-CMAQ were as expected: grid resolution was increased in the regions of highest $PM_{2.5}$ concentration. In the area of highest resolution, grid cell size was reduced down to approximately 100 m × 100 m from the initial grid dimensions of 1.3 km × 1.3 km. A reduction in the artificial dispersion of the plume, typical of photochemical models, was also evident in the adaptive grid simulation.

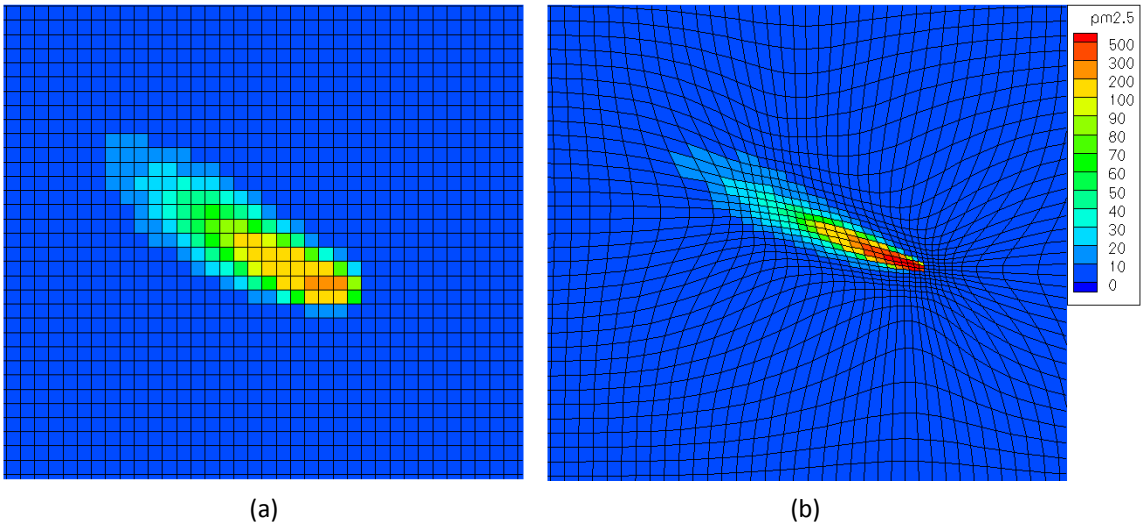

Figure 6.1 Comparison of $PM_{2.5}$ concentrations (μg m^{-3}) at Fort Benning, Georgia (U.S.A.) during a prescribed burn on April 9, 2008: (a) standard CMAQ with 1.33 km grid resolution, (b) with a dynamically adapting mesh, AG-CMAQ. Reprinted with permission from Odman et al. (2010).

6.3. Model Evaluation Results and Discussion

In previous studies, the adaptive grid algorithm was evaluated using problems with increasing complexity and relevance to air quality modeling. Starting with pure advection tests (Srivastava et al., 2000), idealized reactive flow (Srivastava et al., 2001a) and plume dispersion cases (Srivastava et al., 2001b) were simulated using the Dynamic Solution Adaptive Grid Algorithm. The ability of the algorithm to track multiple urban and power plant plumes was also demonstrated (Khan et al., 2005). In all these applications, the adaptive grid solution was more accurate than the static, uniform grid solution with the same number of grid nodes. Here, the algorithm was evaluated in AG-CMAQ with a regional-scale air quality simulation that involves a biomass burning event.

Pollution plumes caused by prescribed burning are excellent examples of highly concentrated events occurring at a finer, local scale with an impact that transitions into a larger, regional scale downwind. In prescribed burns, smoke plumes typically develop at scales below those suitable for existing photochemical models due to limitations in grid resolution. In the AG-CMAQ application described in the following section a large prescribed burn affecting a large urban area is simulated. However, AG-CMAQ can be applied to any type of pollution plume and is not limited to those resulting from prescribed burns or forest fires. The model evaluation included in this work compares the performance of AG-CMAQ and a standard static grid version of CMAQ. Differences in the simulations were determined from surface-level pollutant concentrations and three-dimensional visualizations of modeled plumes. Additionally, modeled concentrations are compared to measurements from 6 monitoring stations affected during the smoke incident.

6.3.1. Modeling application

To evaluate model performance, the Atlanta smoke incident of February 28, 2007 was simulated on fixed and adaptive grids. The episode is further described in Chapter 3. In short, air quality in the Atlanta metropolitan area was impacted by heavy smoke from prescribed burns on this day with hourly $PM_{2.5}$ concentrations recorded at monitoring sites throughout the area escalating to nearly 150 $\mu g\ m^{-3}$ and hourly ozone concentrations increasing by up to 30 ppb (Lee et al., 2008). The dramatic increase in pollution levels has been mainly attributed to two prescribed burns approximately 80 km southeast of Atlanta at the Oconee National Forest and Piedmont National Wildlife Refuge. The smoke episode was initially simulated at 4 km resolution in Hu et al. (2008). Subsequent simulations are discussed in Chapters 3 and 4. Since smoke from prescribed burns was detected at multiple monitoring sites, this event provides a unique opportunity to evaluate AG-CMAQ and compare its performance to a standard CMAQ simulation.

The modeling framework described in Chapter 2 was applied to complete air quality simulations. The evaluation simulation is similar to the base case simulation considered in the sensitivity analyses included in Chapters 3 and 4. The Weather Research and Forecasting model (WRF, version 2.2) was used to simulate meteorology. A 12 km resolution WRF simulation covering the Southeastern U.S. was completed and used to provide boundary conditions to a nested 4 km grid simulation over Georgia. The modeling domains included 13 vertical layers. A projected 2002 "typical year" inventory developed for the Southeastern U.S. was processed with the Sparse Matrix Operator Kernel Emissions model (SMOKE, version 2.1) to prepare emissions from non-fire sources. Biomass burning emissions were estimated by the Fire Emission Production Simulator (FEPS) using information collected and after the burns, including area burned, fuel moisture and fuel consumption characteristics. Local meteorology and fire data were used to estimate plume rise with the Daysmoke model. The number of updraft cores in Daysmoke was set to 6 despite the large area of the burns, primarily because of the mass

ignition techniques employed and hot burning temperatures. Fire-related emissions were vertically injected into CMAQ grid cells using hourly layer-fraction estimates. At the hour when burn emissions peaked, about 75% of the plume fell into layer 8 of CMAQ (out of 13 total), between 1,090 and 1,865 m above the ground.

6.3.2. Results

The simulation was initiated at 21:00 UT on February 27 and finalized at 5:00 UT on March 1. Grid adaptation commenced at 15:00 UT on February 28 consistent with initial emissions from the Oconee National Forrest and Piedmont National Wildlife Refuge fires. Grid refinement in AG-CMAQ was driven by $PM_{2.5}$ concentrations. Figure 6.2 shows $PM_{2.5}$ concentrations throughout the modeling domain at 4:45 UT on March 1 after full plume development from both the AG-CMAQ and standard CMAQ simulations. Visual inspection of the modeled $PM_{2.5}$ surface-level concentration fields provides evidence of significant differences between the adaptive grid and static grid simulations. The artificial dilution effect commonly present in gridded photochemical models appears to decrease when applying the adaptive grid. The smoke plumes drawn with AG-CMAQ appear better defined and pollutant concentrations remain higher near plume cores. Most significantly perhaps, plumes from the two ongoing prescribed burns can be distinctly observed when applying an adaptive grid. By using a static grid, the plumes cannot be distinguished from each other and appear as a single thicker plume. In this case the results from AG-CMAQ provide a clearer prediction of changes to local air quality and pollutant dispersion.

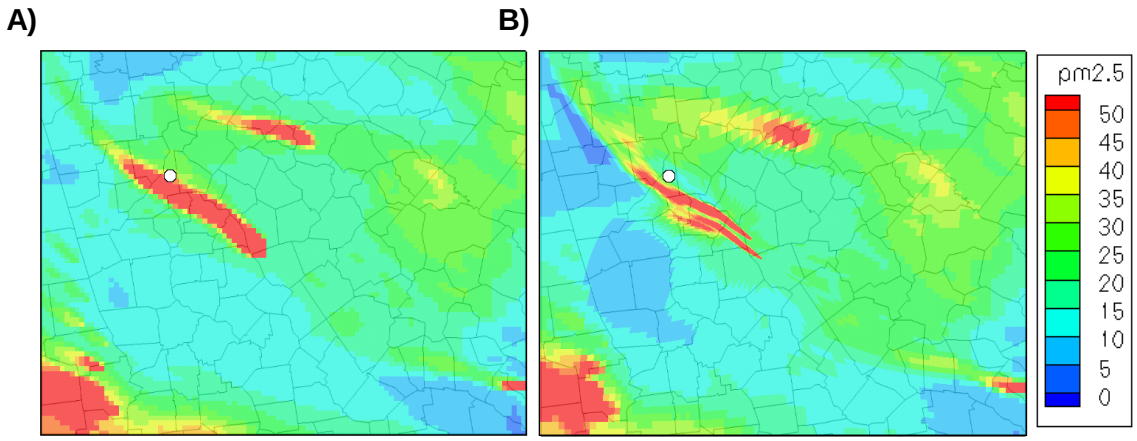

Figure 6.2. Simulated surface-level $PM_{2.5}$ concentrations (μg m^{-3}) over Georgia at 4:45 UT on March 1, 2007 using A) static grid CMAQ and B) AG-CMAQ. The location of Atlanta is denoted by the white circle.

The analysis of simulated results was extended beyond surface layer concentrations to include pollutant concentrations and plume dynamics aloft. Figure 6.3 shows a three-dimensional plot of $PM_{2.5}$ concentrations which includes concentrations at the surface-level and domain boundaries, as well as the three-dimensional iso-surfaces defined by a constant $PM_{2.5}$ concentration equal to 50 μg m^{-3}. The viewer position in the plots is facing the northwestern corner of the domain with plumes blowing in the direction of Atlanta. A comparison of the results produced by CMAQ and AG-CMAQ with the use of three-dimensional visualizations provides insight into differences between the simulations not evident from simple surface-level concentration fields. Two differences between both model simulations are most striking. As was observed from the surface-level concentrations plots, the plumes from both targeted prescribed burns are undistinguishable and appear as a single merged plume using CMAQ results. However, the results from AG-CMAQ allow plumes from each prescribed burn to be distinctly observed. Unlike the static grid simulation, AG-CMAQ allows impacts from smoke plumes at specified locations to be attributed to a specific prescribed burn. It is also apparent that with the static grid simulation a significant portion of the smoke plume initially bifurcates from the main body of the plume directed towards Atlanta due to

upper-level wind shear and heads north at a higher altitude (Figure 6.3A). This bifurcation is not perceived from surface-level concentration fields and more importantly is not present in the AG-CMAQ simulation. The detachment of a plume fragment could partially explain CMAQ's under-prediction of pollutant concentrations at monitoring sites.

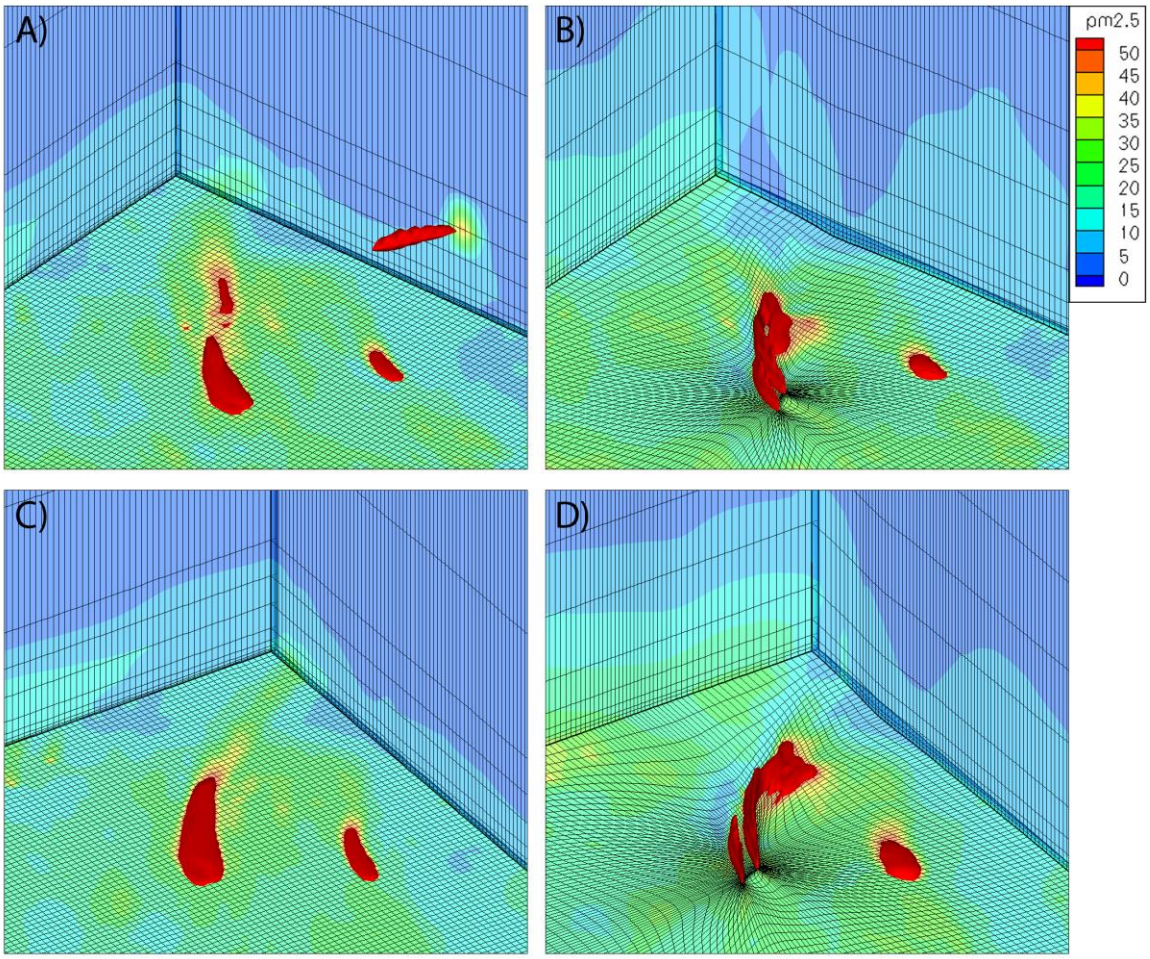

Figure 6.3. Three-dimensional visualization of smoke plumes and $PM_{2.5}$ concentrations ($\mu g\ m^{-3}$) on March 1, 2007 at 0:30 UT using A) static grid CMAQ and B) AG-CMAQ, and at 2:15 UT using C) static grid CMAQ and D) AG-CMAQ.

Modeled concentrations from both static grid CMAQ and AG-CMAQ simulations were compared to observations at several air quality monitoring sites in the Atlanta metropolitan area that experienced a significant increase in $PM_{2.5}$ concentrations during

the event. Results from both simulations are plotted along with hourly measurements at six monitoring sites in Figure 6.4. All sites are concentrated around the city of Atlanta with exception of the McDonough monitoring station located about 40 km away, halfway between the city of Atlanta and the location of the prescribed burns. The tendencies of modeled and observed concentrations at the sites considered are generally similar except at the McDonough site. At all sites, excluding McDonough, results from the static grid CMAQ simulation consistently underpredict maximum $PM_{2.5}$ concentrations by 58-70% of measured values. Additionally, the CMAQ results at these sites exhibit two distinct concentration peaks unlike the monitoring station observations. The simulation with AG-CMAQ results in higher peak concentration at all locations, other than McDonough, by 27-40% relative to the maximum static grid CMAQ concentration predictions.

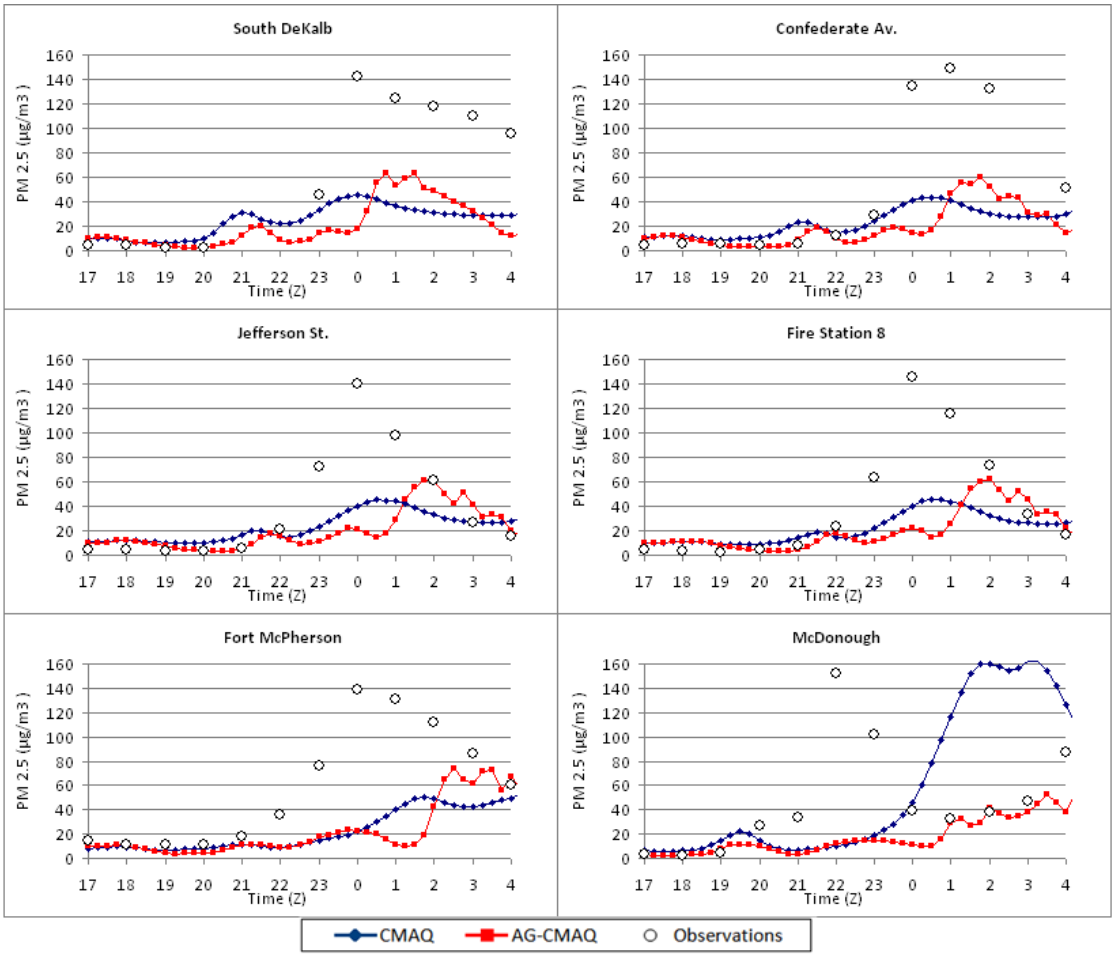

Figure 6.4. Modeled $PM_{2.5}$ concentrations ($\mu g\ m^{-3}$) using static grid CMAQ and AG-CMAQ along with observed concentrations at the South DeKalb, Confederate Avenue, Jefferson Street, Fire Station 8, Fort McPherson, and McDonough air quality monitoring sites.

The prominence of the double peak behavior observed in the static grid results is lessened by using AG-CMAQ as results show a stronger concentration increase at a single major concentration spike. However, a delay of approximately one hour in concentration peaks is observed in the AG-CMAQ simulation with respect to static grid results which exhibit timing more consistent with station observations. Table 1 presents a statistical comparison of model error for static grid CMAQ and AG-CMAQ simulations relative to monitoring site observations.

Table 6.1. Model error metrics for CMAQ and AG-CMAQ relative to $PM_{2.5}$ observations at the Jefferson Street (JST), Confederate Avenue (CFA), McDonough (MCD), South DeKalb (SDK), Fort McPherson (FTM), and Fire Station 8 (FS8) monitoring sites and their averages.

	Mean Error ($\mu g/m^3$) $\frac{1}{N}\sum_{i=1}^{N}\lvert Cm_i - Co_i\rvert$		**Mean Normalized Error** $\frac{1}{N}\sum_{i=1}^{N}\left\lvert\frac{Cm_i - Co_i}{Co_i}\right\rvert$		**Normalized Mean Error** $\frac{\sum_{i=1}^{N}\lvert Cm_i - Co_i\rvert}{\sum_{i=1}^{N} Co_i}$		**Mean Fractional Error** $\frac{1}{N}\sum_{i=1}^{N}\frac{\lvert Cm_i - Co_i\rvert}{\left(\frac{Co_i + Cm_i}{2}\right)}$	
	CMAQ	***AG-CMAQ***	***CMAQ***	***AG-CMAQ***	***CMAQ***	***AG-CMAQ***	***CMAQ***	***AG-CMAQ***
JST	21.9	21.7	114.1%	71.4%	65.4%	65.0%	78.0%	58.3%
CFA	28.9	29.4	82.8%	57.0%	66.4%	67.5%	66.5%	58.3%
MCD	47.2	27.6	131.3%	58.6%	111.8%	65.3%	92.5%	64.3%
SDK	39.0	40.5	94.9%	70.1%	68.5%	71.0%	85.7%	78.6%
FTM	32.2	33.3	48.6%	52.3%	60.6%	62.7%	69.7%	74.4%
FS8	23.2	23.8	97.0%	83.4%	63.8%	65.4%	72.5%	65.0%
Avg.	32.1	29.4	94.8%	65.5%	72.7%	66.2%	77.5%	66.5%

Cm: Modeled Concentration, *Co*: Observed Concentration Measurement, *N*: Number of Concentration Observations

A closer look at the surface-level concentration fields along with the location of the six monitoring sites can explain some of the features observed in the time series plots. Four of the sites, South Dekalb, Confederate Av., Jefferson St., and Fire Station 8, are located in this order along a straight path downwind of the prescribed burns. Correspondingly, all increases in $PM_{2.5}$ concentrations recorded for these sites occur following the same timing pattern from the station closest to the prescribed burns to the furthest. Figure 6.5A shows surface-level concentrations and monitoring site locations from the static grid simulation at 22:30 UT on February 28. The simulated plume appears fragmented into two segments. The initial segment is responsible for the first of two concentration peaks observed in the CMAQ results. However, the initial plume segment has a tangential impact on all stations, leading to smaller concentration increases. The southwesternmost station (Fort McPherson) remains practically unaffected. The larger concentration peaks are caused by the more direct impact from the second plume segment. The plume segmentation observed in the CMAQ simulation is caused by the upper-level bifurcation previously described. Although an interruption in the modeled plume is apparent with CMAQ results, no distinction between smoke plumes from the different prescribed burns is appreciable. Figure 6.5B shows surface-level concentrations and monitoring site locations from the AG-CMAQ simulation also at 22:30 UT. From these results no plume segmentation can be observed and plumes from both prescribed burns are clearly distinct. Once again, the earliest impact of the plume at monitoring sites is tangential, and avoids the Fort McPherson site.

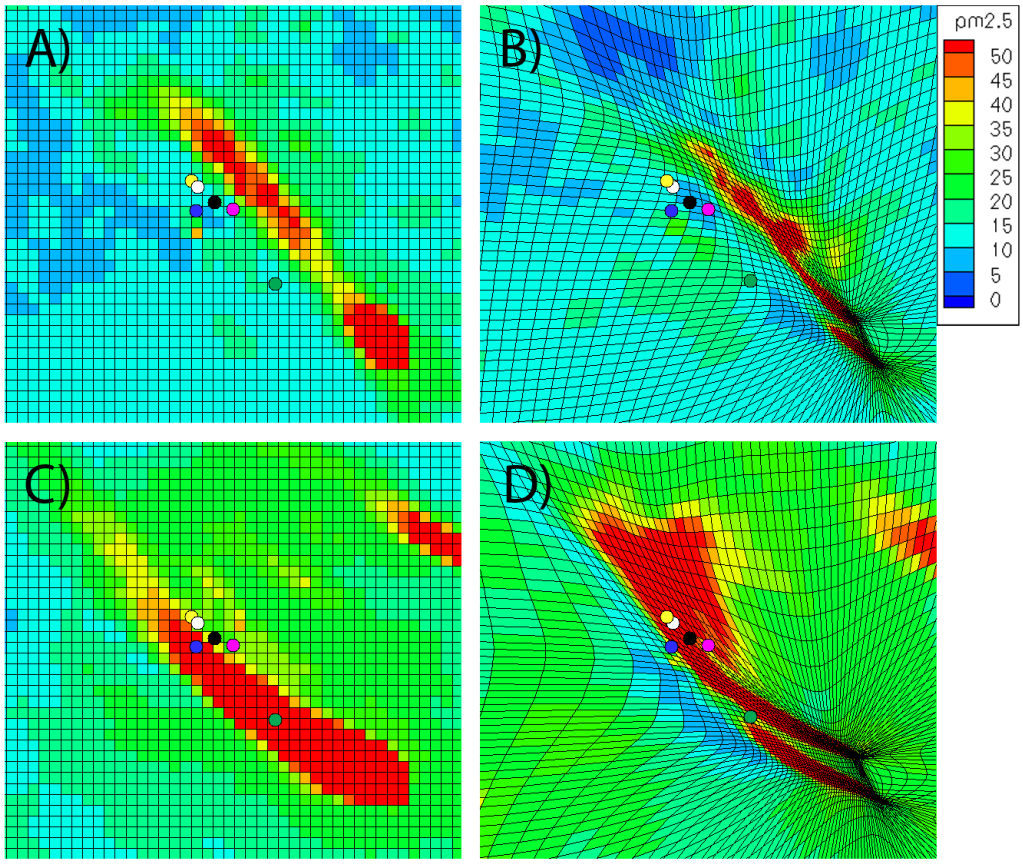

Figure 6.5. Simulated $PM_{2.5}$ concentrations (μg m^{-3}) on February 28, 2007 at 22:30 UT using A) static grid CMAQ and B) AG-CMAQ, and on March 1, 2007 at 02:00 UT using C) static grid CMAQ and D) AG-CMAQ. The locations of the McDonough (green), South DeKalb (pink), Confederate Avenue (black), Fort McPherson (blue), Jefferson Street (white), and Fire Station 8 (yellow) air quality monitoring sites are indicated by the colored circles.

Similar plots at 02:00 UT on March 1 for CMAQ and AG-CMAQ simulations are presented in Figures 6.5C and 6.5D respectively. The AG-CMAQ simulation indicates that the major modeled concentration peak is attributable to the prescribed burn farthest north at the Oconee National Forest. This conclusion cannot be derived from the static grid CMAQ results. The southernmost station at McDonough also merits special attention. While nested between plumes in Figure 6.5D, the site is affected by both plumes at different instances during the AG-CMAQ simulation. This may explain the site's unique double concentration peak recorded in the station measurements. If indeed

these observations correspond to distinct hits from different plumes, such behavior can only be deduced with the increased resolution provided by the adaptive grid model. However, the initial hit recorded in the observations at the McDonough site is not apparent in the model's predictions as the smoke plume is oriented excessively to the east of the site.

6.3.3. Discussion

We believe that differences in simulated concentration fields produced by the static grid and adaptive grid models reflect the improved reproduction of plume dynamics and decrease in artificial dilution that was achieved through grid refinement. Nevertheless, the consistent underprediction of maximum $PM_{2.5}$ concentrations observed from a static grid simulation, although ameliorated, persists throughout the adaptive grid simulation. It is likely that model inputs and processes unrelated to grid resolution, including the underestimation of fire-induced volatile organic compound emissions and secondary organic aerosol formation, are largely responsible for the differences between modeled results and measurements (Lee et al., 2008). Uncertainties in plume rise, mixing layer height, and prescribed burn emission factors all contribute to the error in modeled pollutant concentrations and should be addressed in an attempt to achieve results more consistent with site observations.

It is also clear that the surface-level concentrations are quite sensitive to wind direction and speed inputs derived from meteorological models. The sensitivity to winds becomes even greater when plumes are better defined, as in the adaptive grid simulation. Small changes in wind direction can greatly change the impact plumes have on surface-level pollutant concentrations at specified locations. The performance of Eulerian chemical transport models will continue to be constrained by the limitations in fine-scale wind predictions inherent to meteorological models. To address this concern in the future, the grid refinement methodology in AG-CMAQ could be applied in meteorological

models to develop numerical weather prediction systems that can effectively adapt to air pollutant concentrations. Such adaptation would require continuous input of pollutant concentrations from the air quality model into the meteorological model. Thus, coupled air quality and meteorological adaptive grid models that operate simultaneously at finer scales and continuously exchange feedback may provide an ideal platform to simulate atmospheric plumes.

Finally, the bifurcation observed in the three-dimensional visualization of the static grid simulation results may indicate the importance of vertical resolution in achieving more accurate results. An adaptive grid algorithm that includes refinement of the model's vertical layering would allow full grid adaptation across a three-dimensional domain and may prove useful in simulating plume dynamics at even greater levels of detail. Extension of grid adaptation into the vertical dimension could also be useful in resolving cloud processes.

6.4. Conclusions

An adaptive grid air pollution model (AG-CMAQ) has been developed by integrating a dynamic, solution-adaptive grid algorithm into CMAQ. The model can efficiently refine the grid in response to any defined simulation variable or parameter. Although adaptive grid air pollution models have been previously explored, AG-CMAQ is unique in its capacity to model particulate matter and the first built onto an existing community model. At this time, adaptive grid modeling could potentially be the best approach to multiscale modeling of air pollution dynamics and chemistry.

The adaptive grid model produces results that were practically equal to those obtained from a standard, static grid CMAQ simulation when grid adaptation was disabled. The model effectively increased grid resolution in response to pollutant concentrations when adaptation was applied. AG-CMAQ performance was evaluated by simulating an air pollution incident affecting the Atlanta metropolitan area caused by two

prescribed burns. The evaluation showed that AG-CMAQ successfully reduced the artificial diffusion inherent to chemical transport models and produced better defined plumes compared to a fixed grid CMAQ simulation. Additionally, AG-CMAQ allowed both prescribed burn plumes to be distinctly observed and the impacts at specific locations to be attributed to a particular burn. AG-CMAQ more accurately predicted $PM_{2.5}$ concentrations with respect to observations than the fixed grid CMAQ simulation at most monitoring station locations affected during the incident. The mean fractional error was reduced by 15% on average in the adaptive grid simulation, indicating better agreement with site observations.

The results of this study indicate that the adaptive grid model may provide understanding of air quality and atmospheric dynamics beyond that attainable through a static grid simulation. However, our evaluation shows that despite the improvement, AG-CMAQ continued to under-predict observed $PM_{2.5}$ concentrations. It is likely that the error is partially attributable to processes unrelated to grid resolution within the air quality modeling system. Among these, the ability of meteorological models to simulate fine-scale and short-term variability in winds may be of greatest concern.

Adaptive grids are a tool that could prove useful for various applications beyond plume simulation. Grid refinement driven by reactivity may provide insight into atmospheric chemistry. The need for improved fine-scale wind modeling could be addressed by applying adaptive gridding within numerical weather prediction models. Adaptive mesh modeling is currently being discussed as a tool applicable to climate models to focus on small-scale processes that cannot be resolved in existing models. Some have suggested that adaptive grid models may provide the only means of resolving these small-scale processes within a single model (Weller et al., 2010). The potential benefits that could be attained through dynamic grid refinement in atmospheric simulations with chemical transport models are only briefly explored in this study. However, adaptive grids will likely lead to additional and greater advantages not

necessarily restricted to air quality modeling, but encompassing different geophysical models as well.

6.5. References

Bacon, D.P., Ahmad, N.N., Boybeyi, Z., Dunn, T.J., Hall, M.S., Lee, P.C.S., Sarma, R.A., Turner, M.D., Waight, K.T., Young, S.H., Zack, J.W. (2000) A dynamically adapting weather and dispersion model: The Operational Multiscale Environment Model with Grid Adaptivity (OMEGA). Monthly Weather Review 128, 2044-2076.

Byun, D., Schere, K.L. (2006) Review of the governing equations, computational algorithms, and other components of the models-3 Community Multiscale Air Quality (CMAQ) modeling system. Applied Mechanics Reviews 59, 51-77.

Constantinescu, E.M., Sandu, A., Carmichael, G.R. (2008) Modeling atmospheric chemistry and transport with dynamic adaptive resolution. Computational Geosciences 12, 133-151.

Ghorai, S., Tomlin, A.S., Berzins, M. (2000) Resolution of pollutant concentrations in the boundary layer using a fully 3D adaptive gridding technique. Atmospheric Environment 34, 2851-2863.

Hu, Y.T., Odman, M.T., Chang, M.E., Jackson, W., Lee, S., Edgerton, E.S., Baumann, K., Russell, A.G. (2008) Simulation of air quality impacts from prescribed fires on an urban area. Environmental Science & Technology 42, 3676-3682.

Khan, M.N., (2003) Development and application of an adaptive grid air quality model. Georgia Institute of Technology, Atlanta, GA.

Khan, M.N., Odman, M.T., Karimi, H.A. (2005) Evaluation of algorithms developed for adaptive grid air quality modeling using surface elevation data. Computers, environment and urban systems 29, 718-734.

Lee, S., Kim, H.K., Yan, B., Cobb, C.E., Hennigan, C., Nichols, S., Chamber, M., Edgerton, E.S., Jansen, J.J., Hu, Y., Zheng, M., Weber, R.J., Russell, A.G. (2008) Diagnosis of Aged Prescribed Burning Plumes Impacting an Urban Area. Environmental Science & Technology 42, 1438-1444.

Odman, M.T., Hu, Y. (2010) A variable time-step algorithm for air quality models. Atmospheric Pollution Research 1, 229-238.

Odman, M.T., Hu, Y.T., McRae, D.S., Goodrick, S.L., Liu, Y.Q., Achtemeier, G.L., Naeher, L.P., (2010) Predicting the Regional Air Quality Impacts of Prescribed Burns, in: Steyn, D.G., Rao, S.T. (Eds.), Air Pollution Modeling and Its Application XX, pp. 189-193.

Odman, M.T., Khan, M.N., McRae, D.S., (2001) Adaptive grids in air pollution modeling: Towards an operational model, in: Gryning, S., Schiermeier, F.A. (Eds.), Air pollution modeling and its application XIV. Kluwer Academic/Plenum Publishers, New York, pp. 541-549.

Odman, M.T., Khan, M.N., Srivastava, R.K., McRae, D.S., (2002) Initial application of the adaptive grid air pollution model, in: Borrego, C., Schayes, G. (Eds.), Air Pollution Modeling and its Application XV. Kluwer Academic/Plenum Publishers, New York, pp. 319-328.

Srivastava, R.K., McRae, D.S., Odman, M.T. (2000) An adaptive grid algorithm for air-quality modeling. Journal of Computational Physics 165, 437-472.

Srivastava, R.K., McRae, D.S., Odman, M.T. (2001a) Simulation of a reacting pollutant puff using an adaptive grid algorithm. Journal of Geophysical Research-Atmospheres 106, 24245-24257.

Srivastava, R.K., McRae, D.S., Odman, M.T. (2001b) Simulation of dispersion of a power plant plume using an adaptive grid algorithm. Atmospheric Environment 35, 4801-4818.

Tomlin, A., Berzins, M., Ware, J., Smith, J., Pilling, M.J. (1997) On the use of adaptive gridding methods for modelling chemical transport from multi-scale sources. Atmospheric Environment 31, 2945-2959.

Tomlin, A.S., Ghorai, S., Hart, G., Berzins, M. (2000) 3-D Multi-scale air pollution modelling using adaptive unstructured meshes. Environmental Modelling & Software 15, 681-692.

Weller, H., Ringler, T., Piggott, M., Wood, N. (2010) Challenges facing adaptive mesh modeling of the atmosphere and ocean. Bulletin of the American Meteorological Society 91, 105-108.

Xiao, X., McRae, D., Hassan, H., Frank, R., George, J., (2006) Modeling Atmospheric Optical Turbulence, 44th AIAA Aerospace Sciences Meeting and Exhibit. American Institute of Aeronautics and Astronautics.

CHAPTER 7

A THREE-DIMENSIONAL REFINEMENT ADAPTIVE GRID ALGORITHM FOR EULERIAN AIR QUALITY MODELS

Abstract

Adaptive grid methods can be used to advance the multiscale capabilities of Eulerian chemical transport models and attain grid resolutions unprecedented in regional-scale air quality modeling. Previous efforts to explore the use of adaptive grids in air quality models have been limited to horizontal adaptation or simplified models. Here, a three-dimensional fully adaptive grid algorithm designed for Eulerian models is presented. The algorithm allows vertical refinement yet retains a grid's original structure, enhancing compatibility with existing air quality models. Initial advection tests evaluating the algorithm's functionality and potential to better capture concentration gradients in atmospheric plumes are included. Additional research needs and recommendations for complete implementation into operational air quality models are discussed.

7.1 Introduction

Air quality models can provide valuable insight into the processes that determine air pollution levels and are important atmospheric research tools. Currently, regional-scale air quality models are widely used to guide environmental policy (Rao et al., 2010). Present-day Eulerian chemical transport models include state-of-the-science representations of chemical and physical processes and are capable of simulating multiple pollutants across extensive domains. However, the spatial scales of atmospheric processes relevant to air quality modeling differ by several orders of magnitude. At this

time, the spatial resolution of comprehensive Eulerian air quality models continues to be limited by high computational demand and limited system resources.

Multiscale modeling is a practical approach to simulate different spatial scales within a single modeling framework. Adaptive grids are an attractive method to enhance the multiscale capabilities of grid-based air quality models. The technique is used to increase solution accuracy by dynamically refining the modeling grid in response to a model variable or parameter. Several efforts attempting to apply adaptive gridding in air quality models have been previously reported (Constantinescu et al., 2008; Srivastava et al., 2000; Tomlin et al., 1997). These are discussed extensively in Chapter 5. Mesh moving (r-refinement) methods may be best suited for grid adaptation in Eulerian models designed to operate on structured grids. For instance, an r-refinement algorithm has been introduced into to the Community Air Quality modeling system (CMAQ) (Garcia-Menendez et al., 2010). Implementation of the adaptive grid method into this operational air quality model is described in Chapter 6.

Nearly all adaptive grid air quality modeling has been limited to horizontal grid refinement. Vertical adaptation has only been reported in a few simulations using an unstructured mesh enrichment (h-refinement) technique (Ghorai et al., 2000; Tomlin et al., 2000). These studies highlight the importance of vertical grid resolution to resolve vertical pollutant profiles and capture concentration gradients at the edge of the boundary layer or near inversions. Vertical adaptivity has not yet been applied in current operational models. However, full three-dimension grid adaptation continues to be an attractive possibility for comprehensive air quality models. This may be particularly true for simulations involving concentrated pollutant plumes penetrating into the free troposphere. Examples of these include fire-related smoke plumes that rise above the boundary layer and long-range pollution transport in the free troposphere (Banta et al., 1992; Liang et al., 2004). In simulations attempting to replicate atmospheric phenomena at high altitudes, where vertical grid resolution typically coarsens, vertical refinement

may be an effective mechanism to better resolve concentrated plumes. In addition, as three-dimensional adaptive grid modeling increases the spatial scales available to regional-scale models, subgrid treatments and embedded models designed to capture the small-scale physical and chemical dynamics of atmospheric plumes may become unnecessary.

Here a three-dimensional adaptive grid algorithm designed for grid-based chemical transport models is described. The r-refinement algorithm includes vertical adaptation and builds on the horizontal method described in Chapter 6. The four-step algorithm is explained in in the following section. A coordinate transformation necessary to use existing solution algorithms on irregular grids is described in Section 7.3. In Section 7.4., functionality and advection tests carried out within the CMAQ framework are discussed. Finally, recommendations relevant to achieving full three-dimensional adaptation in current operational air quality models are included at the end of the chapter.

7.2 Three-dimensional adaptation algorithm

The three-dimensional adaptive grid method described herein extends on the two-dimensional algorithm presented in Srivastava et al. (2000) and implemented into CMAQ in Garcia-Menendez et al. (2010). The method relies on an r-refinement technique. Grid nodes are allowed to freely move across the three-dimensional modeling domain to regions calling for increased resolution. However, the total number of nodes and their connectivity remain constant throughout the simulation. Grid adaptation is achieved applying an iterative process. The procedure consists of four key operations: (1) estimating a three-dimensional weight field; (2) grid node repositioning in relation to the weight field; (3) redistribution of concentration fields onto the newly adapted grid; and (4) examining grid convergence criteria to continue or terminate the iterative process. Figure 7.1 shows the steps included in the adaptive grid algorithm; each operation is further discussed below.

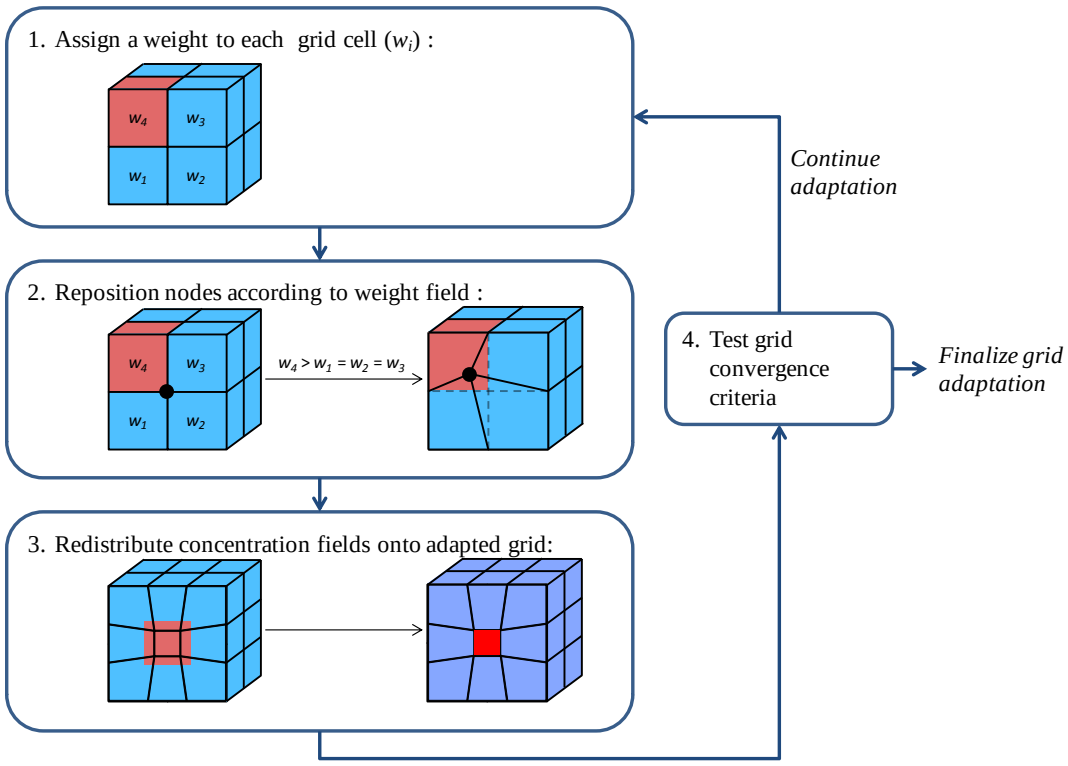

Figure 7.1. Steps of the three-dimensional adaptive grid algorithm

7.2.1 Refinement weighting

The basis of any adaptive grid algorithm is an estimate of solution error on a gridded spatial domain. Adaptation should be aimed at modifying a grid's structure to reduce resolution-derived error and increase model accuracy. A refinement criterion that that efficiently points toward solution error is a key component of any adaptation algorithm. In the algorithm described herein, node movement is driven by a three-dimensional weight field quantified for each individual grid cell (included as step 1 in Figure 7.1). The weights, *w*, may be a function of any model variable or parameter. However, in air quality modeling, refinement criteria have always been based on atmospheric concentration fields. In previously reported adaptive grid algorithms, solution error has been quantified using concentration gradients between adjoining cells (Ghorai et al., 2000), first- and second-order concentration approximations of local

concentrations (Tomlin et al., 1997), and numerical estimates of the curvature in pollutant concentrations (Constantinescu et al., 2008; Srivastava et al., 2000).

In the three-dimensional adaptive grid algorithm described in this chapter, a discrete approximation of the Laplacian is used to evaluate numerical error and assign adaptation weights to each grid cell. As in the two-dimensional algorithm described in Garcia-Menendez et al. (2010), adaptation weights are estimated for each cell as

$$w = \left| \nabla^2 c \right|, \tag{7.1}$$

where the Laplacian, ∇^2, is approximated using a seven-point stencil derived from the gridded concentrations, c, of any atmospheric species. A combination of species or pollutants can also be used. For the adaptation tests and applications described in this chapter, fine particulate matter ($PM_{2.5}$) concentrations, estimated from the sum of various fine aerosol model species, are used to estimate weights following Equation 7.1.

In Cartesian coordinates, $\nabla^2 c$ is given by

$$\nabla^2 c = \frac{\partial^2 c}{\partial x^2} + \frac{\partial^2 c}{\partial y^2} + \frac{\partial^2 c}{\partial z^2} \tag{7.2}$$

and can be numerically approximated from a discretized concentration field at each cell centroid as

$$(\nabla^2 c)_{i,j,k} \approx \frac{c_{i+1,j,k} - 2c_{i,j,k} + c_{i-1,j,k}}{\Delta x^2} + \frac{c_{i,j+1,k} - 2c_{i,j,k} + C_{i,j-1,k}}{\Delta y^2} + \frac{c_{i,j,k+1} - 2c_{i,j,k} + c_{i,j,k-1}}{\Delta z^2} \tag{7.3}$$

where i , j and k are indices for the three-dimensional grid's columns, rows and layers. In an adaptive grid algorithm, the discrete Laplacian approximation can be calculated using the air quality model's conformal map and terrain following coordinates (e.g. X, Y, σ) or the curvilinear computational coordinate system (e.g. ξ, η, ζ) further discussed in Section 7.3. Differing from the two-dimensional weight function used in Garcia-Menendez et al. (2010), within a three-dimensional formulation, the use of an air quality's original coordinate system may be complicated by dissimilar horizontal and vertical coordinates.

This is the case in CMAQ, where a normalized vertical coordinate, sigma-pressure (σ), is used. The computational domain is uniform in space and features unit grid spacing ($\Delta\xi$, $\Delta\eta$, $\Delta\zeta = 1$), reducing the numerical approximation of the Laplacian magnitude to

$$\left|(\nabla^2 c)_{i,j,k}\right| \approx \left|6c_{i,j,k} - (c_{i+1,j,k} + c_{i-1,j,k} + c_{i,j+1,k} + c_{i,j-1,k} + c_{i,j,k+1} + c_{i,j,k-1}\right|. \quad (7.4)$$

The estimate in uniform computational space can be related back to the model's initial nonuniform domain by including cell volume, V, in the adaptation weight function

$$w_{i,j,k} = \left|(\nabla^2 c)_{i,j,k}\right| \times V_{i,j,k}^{\ e_1}, \quad (7.5)$$

where the parameter e_1 can be used to adjust the weight of each grid cell with respect to its size. Setting e_1 to a value greater than 0 diminishes a cell's weight as it becomes smaller, while using a negative e_1 value further promotes refinement of fine resolution regions. The ideal e_1 level largely depends on the modeling application and error indicator being applied to drive refinement. In the simulations carried out in this work, effective three-dimensional adaptation was achieved by setting e_1 to 0. Selecting an e_1 less than 0 usually led to excessive refinement, while values greater than 0 caused undesirable oscillations in vertical adaptation.

A few additional considerations were taken into account in the weight function formulation. Fewer points are included in stencils used to approximate the Laplacian at grid cells along the domain boundaries. Smoothing procedures are applied to weight fields to avoid abrupt transitions in grid resolution. Weight fields are normalized with respect to the maximum weight of every adaptive grid iteration. A minimum value, w^{min}, is added onto each estimated weight. To conserve the nonuniform vertical layering typically used in air quality models, w^{min} is a function of the cell's vertical layer. The thickest vertical layer, usually that furthest from the surface, is assigned a domain-wide minimum allowable value at the start of the simulation. In the simulations described in this chapter this value was set to 0.001. The magnitude of w^{min} is inversely related to a vertical layer's initial thickness and increases as layers become thinner. In this manner,

grid structures that concentrate vertical resolution near the ground are preserved under homogeneous w fields. The final normalized and vertically adjusted weight used to drive adaptation, $w^{adj\text{-}norm}$, ranges from 0 to 1 and is estimated for each grid cell as

$$w_{i,j,k}^{adj-norm} = \frac{\frac{w_{i,j,k}}{w^{max}} + w_k^{min}}{w^{adj,max}}, \tag{7.6}$$

where w^{max} is the domain-wide maximum unadjusted weight and $w^{adj,max}$ is the maximum unnormalized adjusted weight. Figure 7.2 shows examples of final smoothed three-dimensional $w^{adj\text{-}norm}$ fields estimated from blank and single-cell-value concentration fields.

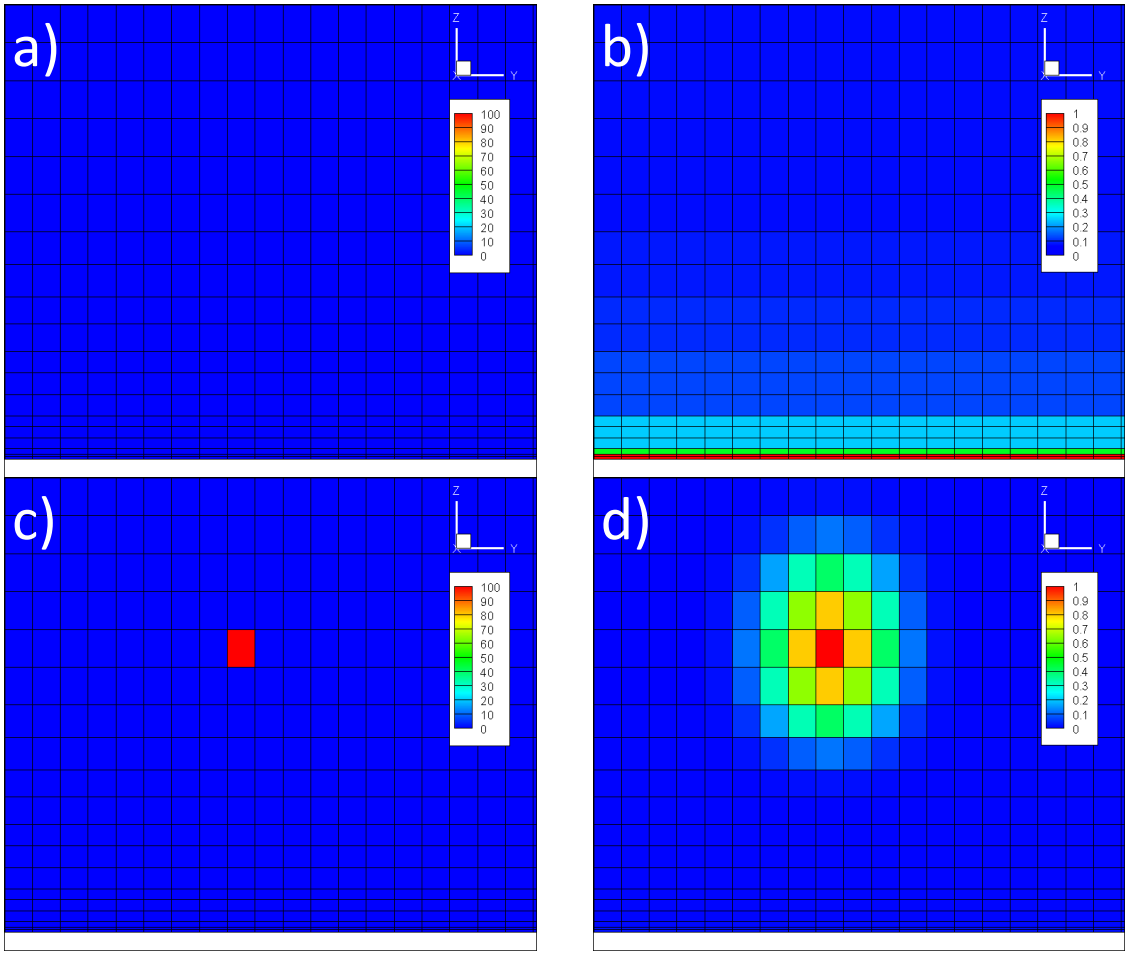

Figure 7.2. Side view of the $w^{adj\text{-}norm}$ fields (b and d) estimated from (a) blank and (c) single-cell-value concentration fields (μg m^{-3}).

7.2.2 Grid movement

In the adaptive grid algorithm, resolution refinement is achieved by repositioning grid nodes with respect to a three-dimensional adaptation weight field. The technique is designed to cluster nodes at high-weight regions within a modeling domain, thereby reducing the resolution-associated error. Node movement in the three-dimensional algorithm extends on the horizontal adaptation method described in Garcia-Menendez et al. (2010). Following the weight function calculation described in Section 7.2.1, the computational grid is restructured by repositioning nodes with respect to the weight field. The process is included as the second step in Figure 7.1. The new location of each node is determined from the weight and centroids of the eight cells that share the node. Using CMAQ's (X,Y,σ) coordinate system, a node's new position is given by

$$\begin{aligned} X_{i,j,k}^{new} &= \sum_{n=1}^{8} w_n X_n^{cent} \Big/ \sum_{n=1}^{8} w_n \\ Y_{i,j,k}^{new} &= \sum_{n=1}^{8} w_n Y_n^{cent} \Big/ \sum_{n=1}^{8} w_n \\ \sigma_{i,j,k}^{new} &= \sum_{n=1}^{8} w_n \sigma_n^{cent} \Big/ \sum_{n=1}^{8} w_n \end{aligned} \quad , \tag{7.7}$$

where $X_{i,j,k}^{new}$, $Y_{i,j,k}^{new}$, $\sigma_{i,j,k}^{new}$ are the coordinates for node *i ,j, k* after adaptation, X_k^{cent}, Y_k^{cent}, σ_k^{cent} are the coordinates at the centroids of the node's adjoining grid cells (n=1-8) and w_n is the weight assigned to each of these cells. The formulation prevents nodes from crossing cell borders and moving into nonadjoining cells, therefore retaining grid connectivity and allowing the use of local interpolation algorithms in redistribution procedures, as further discussed in Section 7.2.3. Grid nodes at domain boundaries are only allowed to reposition themselves along the boundary and nodes at domain corners are kept fixed.

The grid movement technique described by Equation 7.7 allows full three-dimensional grid adaptation within a modeling domain. In air quality models, unconstrained three-dimensional adaptation may be impractical due to the nature of the solution algorithms and parameterizations applied. In CMAQ, for instance, vertical mixing and cloud processes are parameterized and treated for each stack of cells. Parameterized vertical processes such as these may be difficult to transform into a curvilinear computational coordinate system (ξ, η, ζ) and process on an irregular grid. Vertically constraining horizontal adaptation allows the processes to be retained in the adaptive grid model. In a vertically constrained adaptation algorithm, horizontal resolution only changes along the horizontal plane, maintaining cell area constant throughout each stack. The constraint is placed on the adaptation scheme by using a two-dimension weight field , w^{2D}, to drive horizontal node repositioning, as in the two dimensional algorithm described in Garcia-Menendez et al. (2010). Using this technique, $X_{i,j,k}^{new}$ and $Y_{i,j,k}^{new}$ remain fixed along *k* and are given by

$$\begin{aligned} X_{i,j,k}^{new} &= \sum_{k=1}^{4} w_n^{2D} X_n^{cent} \Big/ \sum_{n=1}^{4} w_n \\ Y_{i,j,k}^{new} &= \sum_{k=1}^{4} w_n^{2D} Y_n^{cent} \Big/ \sum_{n=1}^{4} w_n \end{aligned} , \tag{7.8}$$

where X_n^{cent} and Y_n^{cent} are coordinates at the centroids of the node's adjoining grid cells along a horizontal grid layer (*n*=1-4) and w_n^{2D} is the two-dimensional weight assigned to each vertical stack of cells. Single-layer concentrations, at the surface or above, as well as column totals can be used to estimate w_n^{2D}. Figure 7.3 compares side views of unconstrained and vertically constrained adaptation driven by the same weight field. While unconstrained three-dimensional adaptation is more efficient and provides greater flexibility, vertically constrained adaptation may still achieve the algorithm's objective of dynamically restructuring grids to reduce the error related to model resolution.

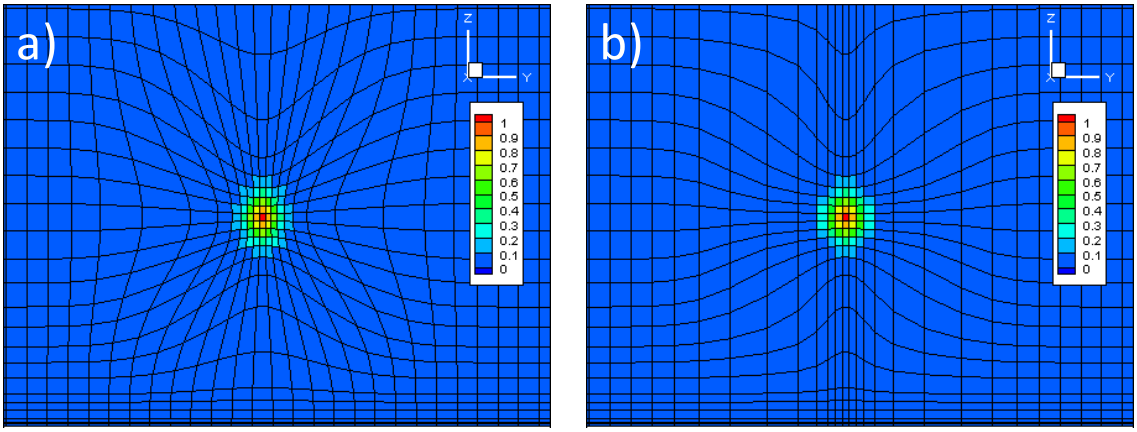

Figure 7.3. Side view of grid response to a normalized weight field using (a) unconstrained adaptation and (b) vertically constrained adaptation.

7.2.3 Concentration field redistribution

An important component of any adaptive grid algorithm is a redistribution procedure to estimate solution fields on a new grid after nodes are repositioned, shown as step 3 in Figure 7.1. In an iterative adaptation procedure the computational cost associated with the algorithm may be largely attributable to solution field redistribution (Garcia-Menendez and Odman, 2011). Local interpolation algorithms can be used to redistribute concentration fields if the adaptation is small and nodes are repositioned within the original volume of adjoining cells (i.e. nodes do not cross cell boundaries). This is the case for the grid repositioning technique described in Section 7.2.2. However, all solution fields must be redistributed after every adaptation iteration and in doing so may be significantly diffused. Global interpolation algorithms can redistribute solution fields onto any grid, which allows redistribution of the initial concentration fields onto every grid generated in an iterative adaptation algorithm.

For adaptive grid methods, global interpolation presents several significant advantages over local schemes. The numerical diffusion associated with continuously redistributing concentration fields by repeatedly applying a local interpolation scheme in an iterative adaptation algorithm may be significantly reduced with a global interpolation

scheme. Additionally, the use of global interpolation only requires that the variables included in the weight function calculation (e.g. $PM_{2.5}$) be interpolated during each adaptive grid iteration. All other solution fields can be redistributed onto the finalized grid once node repositioning has stopped, leading to important computational savings compared to local interpolation. In mesh enrichment (h-refinement) adaptive grid methods, it may be possible to redistribute solution fields using simple global interpolation algorithms. In r-refinement methods, however, geometric intersection algorithms must be used to redistribute fields if grid cells do not remain rectangular prisms. Two-dimensional r-refinement methods may still rely on relatively simple global intersection algorithms. However, three-dimensional r-refinement algorithms require elaborate intersection schemes which may be dependent on computationally-intensive search algorithms. The complexity of intersection algorithms applicable to three-dimensional adaptive grid methods largely counters the computational benefits of global interpolation schemes compared to local schemes.

In Garcia-Menendez et al. (2010), local interpolation is used to horizontally redistribute concentration fields by applying a high-order accurate and monotonic advection scheme. Similarly, in the three-dimensional adaptive grid algorithm a local interpolation algorithm is included. Redistribution is carried out by estimating an apparent velocity at the faces of each grid cell after adaptation and using them in an advection scheme to update concentration fields. Apparent velocities are calculated at each node as

$$\begin{aligned} v_{i,j,k}^{X^*} &= \left(X_{i,j,k}^{new} - X_{i,j,k}^{old}\right)/\Delta t \\ v_{i,j,k}^{Y^*} &= \left(Y_{i,j,k}^{new} - Y_{i,j,k}^{old}\right)/\Delta t \\ v_{i,j,k}^{\sigma^*} &= \left(\sigma_{i,j,k}^{new} - \sigma_{i,j,k}^{old}\right)/\Delta t \end{aligned} \quad , \tag{7.9}$$

where $X_{i,j,k}^{old}$, $Y_{i,j,k}^{old}$, $\sigma_{i,j,k}^{old}$ are the coordinates for node *i,j,k* prior to displacement and Δt is an arbitrary time interval. The apparent velocities are transformed into curvilinear

computational coordinates (ξ,η,ζ) using the metric derivatives between the coordinate systems as follows,

$$\begin{aligned} v_{i,j,k}^{\xi*} &= \frac{\partial \xi}{\partial X} v_{i,j,k}^{X*} + \frac{\partial \xi}{\partial Y} v_{i,j,k}^{Y*} + \frac{\partial \xi}{\partial \sigma} v_{i,j,k}^{\sigma*} \\ v_{i,j,k}^{\eta*} &= \frac{\partial \eta}{\partial X} v_{i,j,k}^{X*} + \frac{\partial \eta}{\partial Y} v_{i,j,k}^{Y*} + \frac{\partial \eta}{\partial \sigma} v_{i,j,k}^{\sigma*} \\ v_{i,j,k}^{\zeta*} &= \frac{\partial \zeta}{\partial X} v_{i,j,k}^{X*} + \frac{\partial \zeta}{\partial Y} v_{i,j,k}^{Y*} + \frac{\partial \zeta}{\partial \sigma} v_{i,j,k}^{\sigma*} \end{aligned} \quad . \tag{7.10}$$

Transformed apparent velocities are then used to estimate fluxes along ξ, η, and ζ by applying the piecewise parabolic method advection scheme (Colella and Woodward, 1984) to each row, column and stack of cells. Concentrations for each cell are recomputed using the fluxes at each face and the ratio between the original and new cell volumes.

7.2.4 Grid convergence

The final step in the iterative adaptive grid algorithm, included in Figure 7.1 as step four, is a test of grid *convergence* to either continue or terminate adaptation. Refinement control has been an important component of all previously reported adaptive grid applications in air quality modeling (Garcia-Menendez and Odman, 2011). Ideally, grid adaptation would cease after an equal level of solution error is achieved across the full domain, a concept described as error equidistribution (Baker, 1997). However, depending on the weight function and redistribution algorithm selected for the adaptive grid algorithm, reaching equidistribution may be difficult or unfeasible. Additionally, excessive refinement may offset the computational benefits of adaptive gridding without significantly increasing model accuracy further.

In an iterative r-refinement adaptive grid method, the convergence criteria may take the form of minimum grid movement or a maximum number of adaptation procedures (Garcia-Menendez et al., 2010). The use of a volume-weighted error estimate, such as Equation 7.5, or a global interpolation redistribution scheme may facilitate grid

convergence. However, satisfactory adaptation may be efficiently attained by using simpler algorithms and grid convergence criteria. In the simulations included within this chapter, a minimum displacement of 10% for grid nodes with respect to initial cell spacing and an upper limit of 5 adaptation iterations were selected as refinement criteria. When the displacement of all nodes drops below the minimum movement criteria or the maximum number of iterations is reached, adaptation is halted and the grid is finalized. The model solution is then advanced in time using the restructured grid.

7.3 Coordinate transformation

An important advantage of r-refinement, or mesh moving, methods over other adaptive grid techniques is that throughout the entire simulation the total number of grid cells is constant and their connectivity remains intact. Frequently, Eulerian air quality models operate on structured grids (e.g. CMAQ), allowing data to be organized into rectangular matrices. In these models, the solution algorithms included are commonly designed for structured grids specifically. Thus, r-refinement, which allows a grid to remain structured after adapting, may be especially practical when adaptive gridding is applied to current chemical transport models. However, the solution algorithms may have also been explicitly developed for uniform grids and may not be directly applicable to nonuniform grids. A coordinate transformation capable of converting a nonuniform grid in physical space into a uniform grid in computational space can be used to overcome this limitation.

In adaptive grid modeling, a local coordinate transformation from the model's original space into a boundary-conforming curvilinear coordinate system can be applied. The transformation is achieved after establishing a unique correspondence between the coordinate systems by defining and normalizing the values at cell boundaries for each location, every time the grid is restructured. The model's original coordinates are

transformed into a curvilinear computational coordinate system (ξ, η, ζ) that features unit dimensions for each cell and allows the grid to regain uniformity, as shown in Figure 7.4.

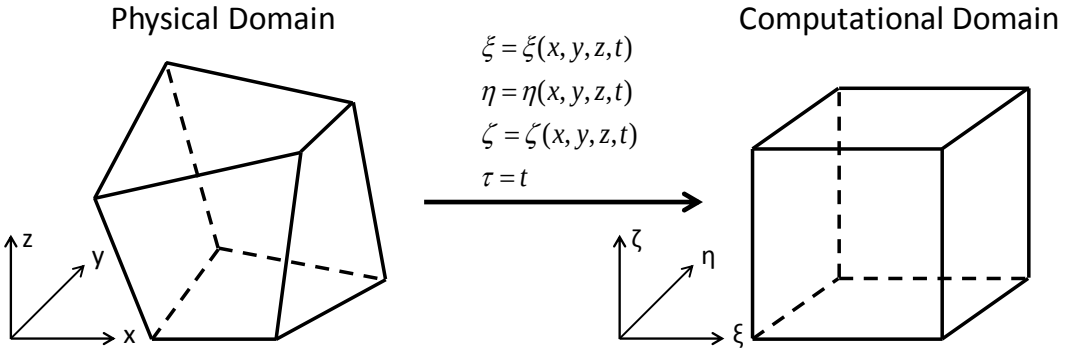

Figure 7.4. Grid cell transformation from Cartesian (x, y, z, t) to boundary-conforming curvilinear coordinates (ξ, η, ζ, τ).

To use a model's original solution algorithms on the uniform computational domain, the coordinate transformation must be applied to the system's governing equations. Chemical transport models rely on dividing the atmosphere into discrete grid cells and solving a species continuity equation, describing the rate of change of a chemical species' concentration with respect to time, to estimate future atmospheric concentrations. In Cartesian coordinates, conservation of mass for each species can be expressed as

$$\frac{\partial c_n}{\partial t} + \frac{\partial (u c_n)}{\partial x} + \frac{\partial (v c_n)}{\partial y} + \frac{\partial (w c_n)}{\partial z} + \frac{\partial}{\partial x}\left(K^h \frac{\partial c_n}{\partial x}\right) + \frac{\partial}{\partial y}\left(K^h \frac{\partial c_n}{\partial y}\right) + \frac{\partial}{\partial z}\left(K^v \frac{\partial c_n}{\partial z}\right) = e_n + r_n \quad , \tag{7.11}$$

where c_n is the concentration of species n changing in time, t, u, v, and w are the wind velocity components in the x, y, and z directions, K^h and K^v are horizontal and vertical turbulent diffusion coefficients, e_n is the volumetric emission rate of n, and r_n is a chemical reaction rate for n. Equation 7.11 considers atmospheric advection, turbulent

diffusion, emissions and chemical transformation processes. To transform the equation into uniform computational space, a set of curvilinear coordinates is defined as

$$\begin{aligned} \xi &= \xi(x,y,z,t) \\ \eta &= \eta(x,y,z,t) \\ \zeta &= \zeta(x,y,z,t) \end{aligned} . \tag{7.12}$$

The species continuity equation on curvilinear coordinates can be derived by numerically manipulating Equation 7.11 and is expressed as

$$\begin{aligned} &\frac{\partial(Jc_n)}{\partial t} + \frac{\partial\left(Jv^{\xi}c_n\right)}{\partial \xi} + \frac{\partial\left(Jv^{\eta}c_n\right)}{\partial \eta} + \frac{\partial\left(Jv^{\zeta}c_n\right)}{\partial \zeta} \\ &+ \frac{\partial}{\partial \xi}\left(K^{\xi\xi}\frac{\partial(Jc_n)}{\partial \xi}\right) + \frac{\partial}{\partial \eta}\left(K^{\eta\eta}\frac{\partial(Jc_n)}{\partial \eta}\right) + \frac{\partial}{\partial \zeta}\left(K^{\zeta\zeta}\frac{\partial(Jc_n)}{\partial \zeta}\right) = Je_n + Jr_n \end{aligned} , \tag{7.13}$$

where v^{ξ}, v^{η}, and v^{ζ} are the are the wind velocity components in the ξ, η, and ζ directions, $K^{\xi\xi}$, $K^{\eta\eta}$, and $K^{\zeta\zeta}$ are the turbulent diffusion coefficients along ξ, η, and ζ, and J is the Jacobian of the transformation given by

$$\begin{aligned} J = &\frac{\partial x}{\partial \xi}\frac{\partial y}{\partial \eta}\frac{\partial z}{\partial \zeta} - \frac{\partial x}{\partial \xi}\frac{\partial z}{\partial \eta}\frac{\partial y}{\partial \zeta} + \frac{\partial y}{\partial \xi}\frac{\partial z}{\partial \eta}\frac{\partial x}{\partial \zeta} \\ &- \frac{\partial y}{\partial \xi}\frac{\partial x}{\partial \eta}\frac{\partial z}{\partial \zeta} + \frac{\partial z}{\partial \xi}\frac{\partial x}{\partial \eta}\frac{\partial y}{\partial \zeta} - \frac{\partial z}{\partial \xi}\frac{\partial y}{\partial \eta}\frac{\partial x}{\partial \zeta} \end{aligned} . \tag{7.14}$$

The nondimensional wind velocity components can be estimated from the original velocity terms using the metrics of the transformation as

$$\begin{aligned} v^{\xi} &= \frac{\partial \xi}{\partial x}u + \frac{\partial \xi}{\partial y}v + \frac{\partial \xi}{\partial z}w \\ v^{\eta} &= \frac{\partial \eta}{\partial x}u + \frac{\partial \eta}{\partial y}v + \frac{\partial \eta}{\partial z}w \\ v^{\zeta} &= \frac{\partial \zeta}{\partial x}u + \frac{\partial \zeta}{\partial y}v + \frac{\partial \zeta}{\partial z}w \end{aligned} . \tag{7.15}$$

As the transformed curvilinear coordinate system remains orthogonal, diffusive transport is reduced to the nondimensional diagonal elements of the turbulent diffusivity tensor which can be obtained from

$$
\begin{aligned}
K^{\xi\xi} &= K^h\left(\frac{\partial \xi}{\partial x}\right)^2 + K^h\left(\frac{\partial \xi}{\partial y}\right)^2 + K^v\left(\frac{\partial \xi}{\partial z}\right)^2 \\
K^{\eta\eta} &= K^h\left(\frac{\partial \eta}{\partial x}\right)^2 + K^h\left(\frac{\partial \eta}{\partial y}\right)^2 + K^v\left(\frac{\partial \eta}{\partial z}\right)^2 \\
K^{\xi\xi} &= K^h\left(\frac{\partial \zeta}{\partial x}\right)^2 + K^h\left(\frac{\partial \zeta}{\partial y}\right)^2 + K^v\left(\frac{\partial \zeta}{\partial z}\right)^2
\end{aligned}
\qquad (7.16)
$$

The metrics of the transformation included in Equations 7.15 and 7.16 are given by

$$
\begin{aligned}
\frac{\partial \xi}{\partial x} &= J^{-1}\left(\frac{\partial y}{\partial \eta}\frac{\partial z}{\partial \zeta} - \frac{\partial z}{\partial \eta}\frac{\partial y}{\partial \zeta}\right) \qquad & \frac{\partial n}{\partial x} &= J^{-1}\left(\frac{\partial y}{\partial \zeta}\frac{\partial z}{\partial \xi} - \frac{\partial z}{\partial \zeta}\frac{\partial y}{\partial \xi}\right) \\
\frac{\partial \xi}{\partial y} &= J^{-1}\left(\frac{\partial z}{\partial \eta}\frac{\partial x}{\partial \zeta} - \frac{\partial x}{\partial \eta}\frac{\partial z}{\partial \zeta}\right) \qquad & \frac{\partial n}{\partial y} &= J^{-1}\left(\frac{\partial z}{\partial \zeta}\frac{\partial x}{\partial \xi} - \frac{\partial x}{\partial \zeta}\frac{\partial z}{\partial \xi}\right) \\
\frac{\partial \xi}{\partial z} &= J^{-1}\left(\frac{\partial x}{\partial \eta}\frac{\partial y}{\partial \zeta} - \frac{\partial y}{\partial \eta}\frac{\partial x}{\partial \zeta}\right) \qquad & \frac{\partial n}{\partial z} &= J^{-1}\left(\frac{\partial x}{\partial \zeta}\frac{\partial y}{\partial \xi} - \frac{\partial y}{\partial \zeta}\frac{\partial x}{\partial \xi}\right)
\end{aligned}
\qquad (7.17)
$$

$$
\begin{aligned}
\frac{\partial \zeta}{\partial x} &= J^{-1}\left(\frac{\partial y}{\partial \xi}\frac{\partial z}{\partial \eta} - \frac{\partial z}{\partial \xi}\frac{\partial y}{\partial \eta}\right) \\
\frac{\partial \zeta}{\partial y} &= J^{-1}\left(\frac{\partial z}{\partial \xi}\frac{\partial x}{\partial \eta} - \frac{\partial x}{\partial \xi}\frac{\partial z}{\partial \eta}\right), \\
\frac{\partial \zeta}{\partial z} &= J^{-1}\left(\frac{\partial x}{\partial \xi}\frac{\partial y}{\partial \eta} - \frac{\partial y}{\partial \xi}\frac{\partial x}{\partial \eta}\right)
\end{aligned}
$$

and are approximated at each grid node using a seven-point stencil of neighboring nodes.

In CMAQ, the system is solved using horizontal coordinates on a conformal map of the earth and a normalized terrain-following vertical coordinate (e.g. sigma-pressure). This transformation can be included in the Jacobian defined in equation 7.14 as

$$
J = \left(\begin{array}{l}
\dfrac{\partial x}{\partial \xi}\dfrac{\partial y}{\partial \eta}\dfrac{\partial \sigma}{\partial \zeta} - \dfrac{\partial x}{\partial \xi}\dfrac{\partial \sigma}{\partial \eta}\dfrac{\partial y}{\partial \zeta} + \dfrac{\partial y}{\partial \xi}\dfrac{\partial \sigma}{\partial \eta}\dfrac{\partial x}{\partial \zeta} \\
-\dfrac{\partial y}{\partial \xi}\dfrac{\partial x}{\partial \eta}\dfrac{\partial \sigma}{\partial \zeta} + \dfrac{\partial \sigma}{\partial \xi}\dfrac{\partial x}{\partial \eta}\dfrac{\partial y}{\partial \zeta} - \dfrac{\partial \sigma}{\partial \xi}\dfrac{\partial y}{\partial \eta}\dfrac{\partial x}{\partial \zeta}
\end{array}\right)\left(\frac{1}{m^2}\frac{\partial z}{\partial \sigma}\right), \qquad (7.18)
$$

where m is a map scale factor for the conformal map projection and σ is the transformed vertical coordinate. Equation 7.13 in curvilinear coordinates therefore retains the same

form as CMAQ's original governing equations and the model's solution algorithms can be directly applied in the transformed computational space.

7.4 Functionality Evaluation

The CMAQ modeling system (version 4.7.1) (Byun and Schere, 2006) was used as a platform to verify the functionality of the three-dimensional adaptation algorithm described in Section 7.2. CMAQ simulates several atmospheric processes, including advection, diffusion, deposition, chemistry, aerosol dynamics, and cloud processes. The model is designed as a modular system, with individual atmospheric processes simulated by distinct science modules. This allows users to focus on specific processes. However, the model is constructed under the assumptions of structured and horizontally uniform grids. Additionally, CMAQ is designed to operate on grids that remain fixed throughout the simulation. Implementing an adaptation algorithm into CMAQ requires that major changes be made to the model's original code and coordinate transformations be applied to the process modules included in a simulation. Several tests were carried out to corroborate that the three-dimensional adaptation algorithm performed in accordance with the method's intent. One test is described below.

To verify the functionality of the three-dimensional algorithm, adaptation was used to simulate the advection of a pollutant puff under a three-dimensional wind field generated with the Weather Research and Forecasting Model (Skamarock et al., 2008). Horizontal grid spacing was initially set to 4 km × 4 km and the modeling domain was divided into 34 vertical sigma-pressure layers increasing in depth from the ground up to approximately 20 km above. A $PM_{2.5}$ puff was instantaneously injected into a single grid cell in layer 15 of the modeling domain, 2500 m above the ground. Figure 7.5 illustrates the grid's response to the pollutant puff being advected across the domain. In the figure, the puff is depicted as a three-dimensional iso-surface bounded by constant $PM_{2.5}$ concentration equal to 10 $\mu g\ m^{-3}$. Within the plots, intersecting grid planes along *X* and *Y*

are shown at different times and include grid lines and predicted concentrations along each plane. The surface grid is also included. The puff crosses the intersection as it is advected from its initial position behind the grid planes towards the viewer. Three-dimensional adaptation is apparent in the sequence: grid cells along the *X* and *Y* planes are initially regular and uniform; while the puff crosses the intersection, grid resolution is refined around the puff; as the puff moves beyond the plane intersection, refinement persists prior to returning to the original grid configuration. The simulation demonstrates that the adaptive grid performs as expected by refining both horizontal and vertical resolution in response to pollutant concentrations.

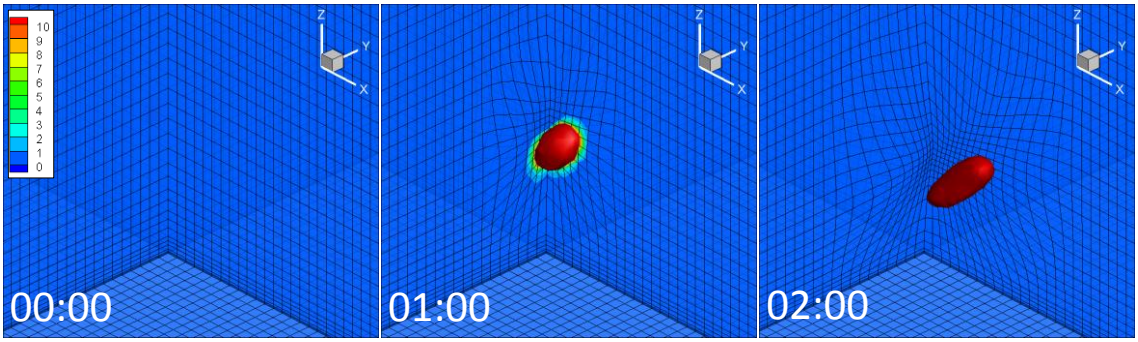

Figure 7.5. Pollutant puff shown as a three-dimensional iso-surface bounded by $PM_{2.5}$ concentration equal to 10 μg m^{-3} crossing an intersection of *X* and *Y* grid planes. Grid lines and $PM_{2.5}$ concentrations (μg m^{-3}) along the planes are also included.

The evolution of the grid as it dynamically adapts to the puff is further apparent later in the simulation. Figures 7.6 and 7.7 provide additional visualizations of grid adaptation 4 hours into advection of the puff. At this time, the puff has been significantly deformed and elongated by wind shear. Figure 7.6a shows a side view of a *Y* grid plane intersecting the puff along *X* and σ. The $PM_{2.5}$ concentration contour lines included in Figure 7.6a indicate the areas with the largest concentration gradients and curvature. In Figure 7.6b, showing the same grid plane, a three-dimensional iso-surface representing the pollution puff and grid cells along the plane are included. Three-dimensional grid

refinement concentrated around high concentration gradients, in agreement with the weight function formulation described in Section 7.3.1, is apparent.

Dynamic adaptation to the puff simultaneously refines both horizontal and vertical grid resolution. Adaptation in each direction is depicted in Figure 7.7. Here again, a side view of the modeling domain shows the pollutant puff as a constant concentration iso-surface 4 hours after release. The viewer position is rotated by 90˚ with respect to Figure 7.6, the puff moving towards the viewer. In addition, a series of X and σ grid planes, along with the grid lines on each plane, are included in Figures 7.7a and 7.7b respectively. Each plane shows a unique response. In Figure 7.7b, for instance, σ grid planes near the surface respond by moving nodes upwards towards the pollution, while planes initially above the puff relocate nodes to lower altitudes. In general, the adaptive grid algorithm acted as expected during the test, concurrently refining horizontal and vertical grid resolution in response to concentration gradients.

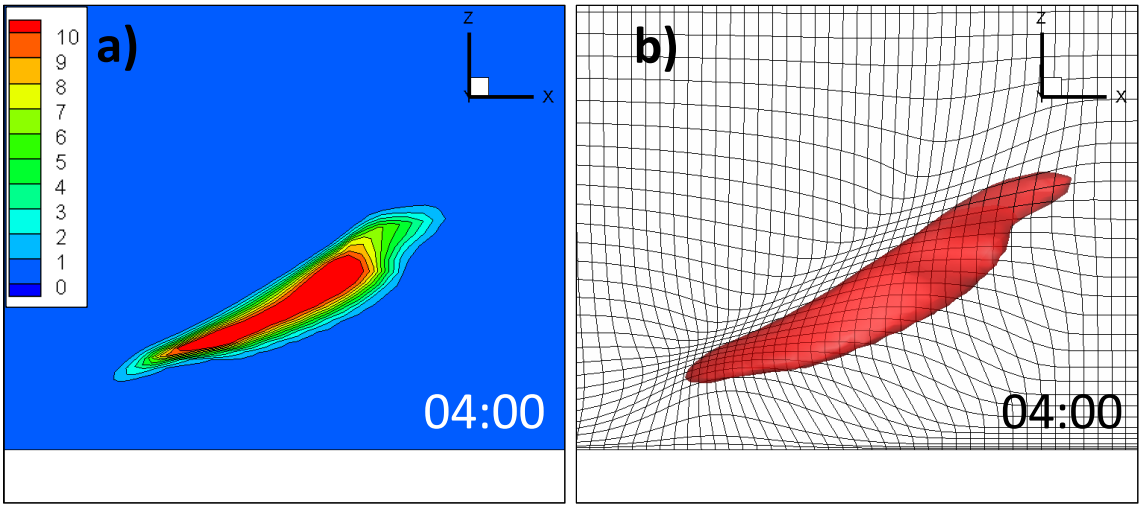

Figure 7.6. Y grid plane intersecting the pollutant puff 4 hours after release showing (a) $PM_{2.5}$ concentrations (µg m^{-3}) and contour lines and (b) grid lines and a three-dimensional 1 µg m^{-3} iso-surface.

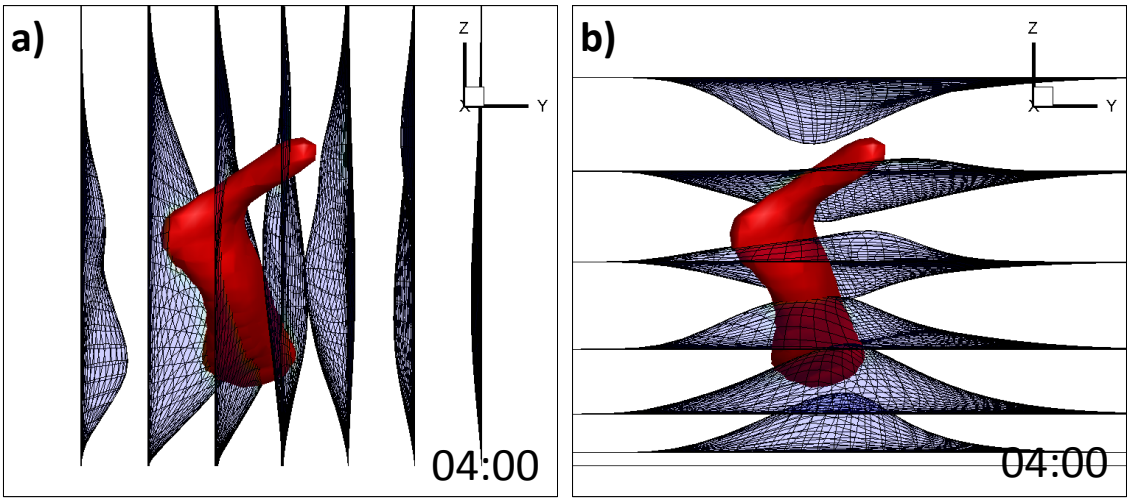

Figure 7.7. Three-dimensional 1µg m^{-3} iso-surface of $PM_{2.5}$ concentrations 4 hours after release of pollutant puff. A series of (a) *X* grid planes and (b) σ grid planes are also shown.

7.5 Advection of a pollutant puff

A test similar to one described in in section 7.4 was used to simulate the transport of a pollutant puff within a wind field and compare the results produced under fixed and adaptive grids. Here an elemental carbon (EC) pollutant puff was instantaneously injected into a WRF-generated wind field approximately 2000 m above the ground. The grids initially featured 4 km horizontal grid resolution and 34 vertical layers extending up to 20 km. The pollutant was injected into a single 4 × 4 km grid cell, approximately 400 m tall. The emissions instantaneously increased EC concentration within the cell to 1000 µg m^{-3}. Pollutant dispersion was simulated for several hours. No initial concentrations or additional emissions sources were included and only horizontal and vertical advection were modeled. In the simulations, the puff rapidly dispersed as it was advected across the wind field. Figure 7.8 shows three-dimensional visualizations of the puff at different times as it traveled within the fixed and adaptive grids. The initial EC concentration quickly dropped. However, under the adaptive grid, the puff remains more compact and better defined. Ten hours into the simulation significant differences are evident in the

modeled puffs. The variation reflects the decrease in numerical diffusion achieved by the adaptive grid through grid refinement.

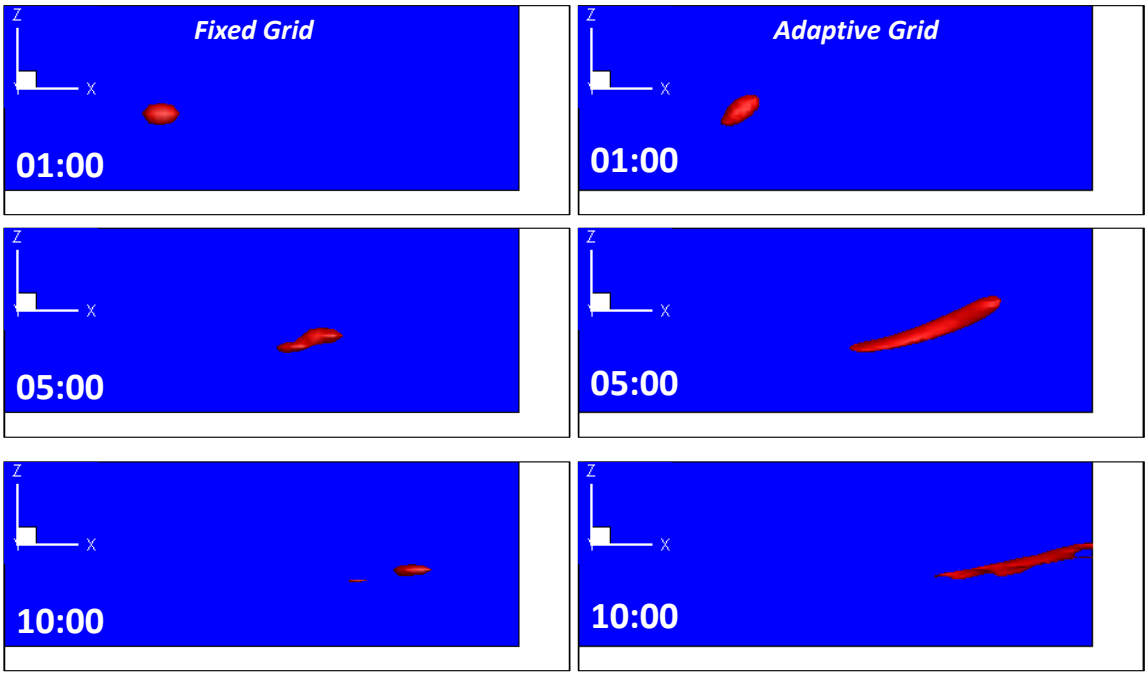

Figure 7.8 Side view of three-dimensional iso-surfaces defined by EC concentration equal to10 μg m^{-3} in fixed and adaptive grid simulations ,1, 5, and 10 hours after the puff is released.

Figure 7.9 compares the decrease in maximum EC concentrations simulated on fixed and adaptive grids during the 6 hours following the puff's release. In all simulations, the initial EC concentration falls abruptly after emissions are injected. Nevertheless, the drop is attenuated by the adaptive grid. In addition, 6 hours into the simulation the maximum concentration estimated in the adaptive grid simulation (54 μg m^{-3}) is twice as large as that predicted using a fixed grid (27 μg m^{-3}). Figure 7.9 also shows the maximum concentrations predicted by adapting with greater intensity. An adaptive grid simulation using 10 adaptation iterations as a grid convergence criterion for the procedure described in Section 7.2 is compared to the original simulation limited to 5 iterations. Although the initial decrease in maximum EC concentration was further

reduced by increasing grid refinement, peak simulated concentrations eventually fell below the concentrations predicted using less adaptation iterations. Finally, the results of a simulation using the vertically constrained adaptive grid algorithm described in Section 7.2.2 are also shown in Figure 7.9. The predictions generated with the constrained and unconstrained methods are very similar. Figure 7.10 compares grid adaptation using the vertically constrained and unconstrained approaches and further confirms the likeness in modeled concentrations.

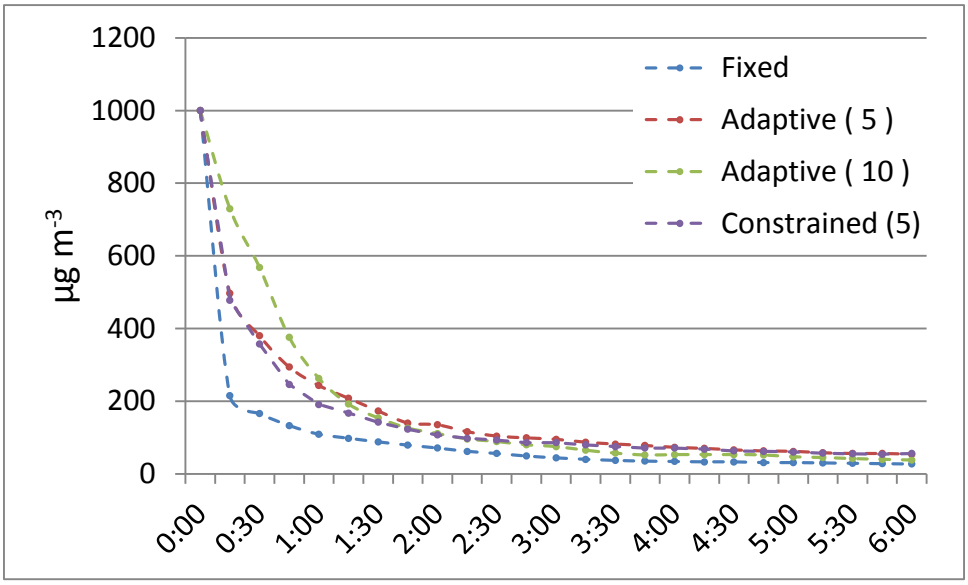

Figure 7.9 Maximum EC concentration predicted by a fixed grid simulation, adaptive grid simulations with 5 and 10 adaptation iterations, and a vertically constrained adaptive grid simulation with 5 iterations.

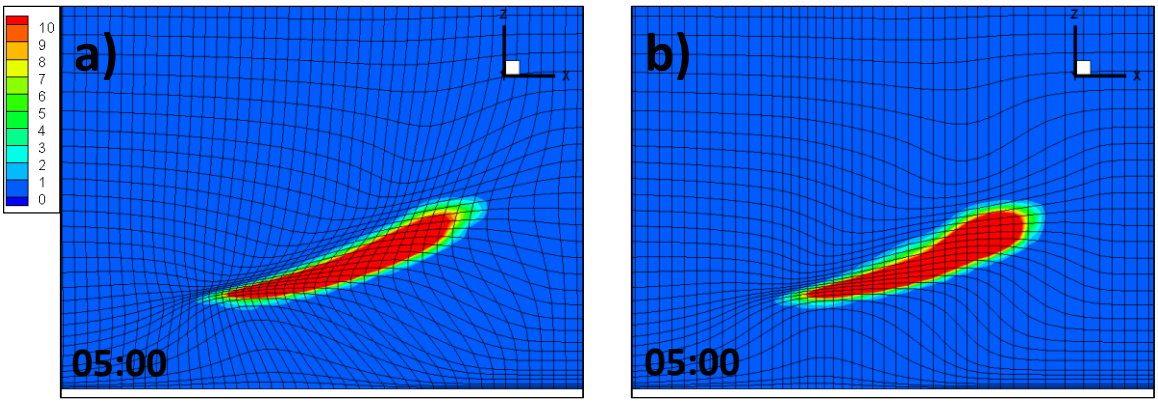

Figure 7.10 *Y* grid plane intersecting the pollutant puff 5 hours after release, simulated with (a) unconstrained three-dimensional adaptation and (b) vertically constrained adaptation. EC concentrations (μg m^{-3}) and grid lines along the planes are also shown.

7.6 Advection of a continuous point source

To further examine the performance of the three-dimensional adaptive grid algorithm, advection of a continuous point source was modeled under fixed and adaptive grids. EC was continuously emitted at a rate of 2500 g s^{-1} into a single grid cell 2000 m above the ground. The simulation used the vertically constrained adaptation algorithm and the same model configuration applied in the puff advection test described in section 7.5, with 4 km ×4 km initial horizontal grid resolution and 34 vertical layers. No other emission sources were included. Initially, the point source was advected under a uniform field of 5 m s^{-1} southeasterly winds. Figure 7.11 shows the pollutant plume simulated with fixed and adaptive grids. Under a uniform wind field, the advection simulation would ideally produce a highly concentrated plume traveling directly northwest and eventually reach steady-state conditions. However, numerical diffusion dilutes the pollutant concentrations as the plume travels across a finite resolution grid. Numerical diffusion has a larger impact on the pollutant plume in the fixed grid simulation, leading to lower concentrations downwind of the point source. In contrast, a highly concentrated plume develops under the adaptive grid. Although the earliest emissions released on the

adaptive grid are numerically diffused by the grid's initial coarse resolution, the grid rapidly refines along the advection trajectory and is better able to capture the continuous plume. Similarly, the adaptive grid can improve representations of emissions sources subjected to vertical transport. Figure 7.12 compares adaptive and fixed grid simulations of the continuous EC point source advected directly upwards by a uniform 0.3 m s^{-1} vertical wind field. Here again three-dimensional refinement retains higher concentrations along the plume centerline and reduces numerical diffusion.

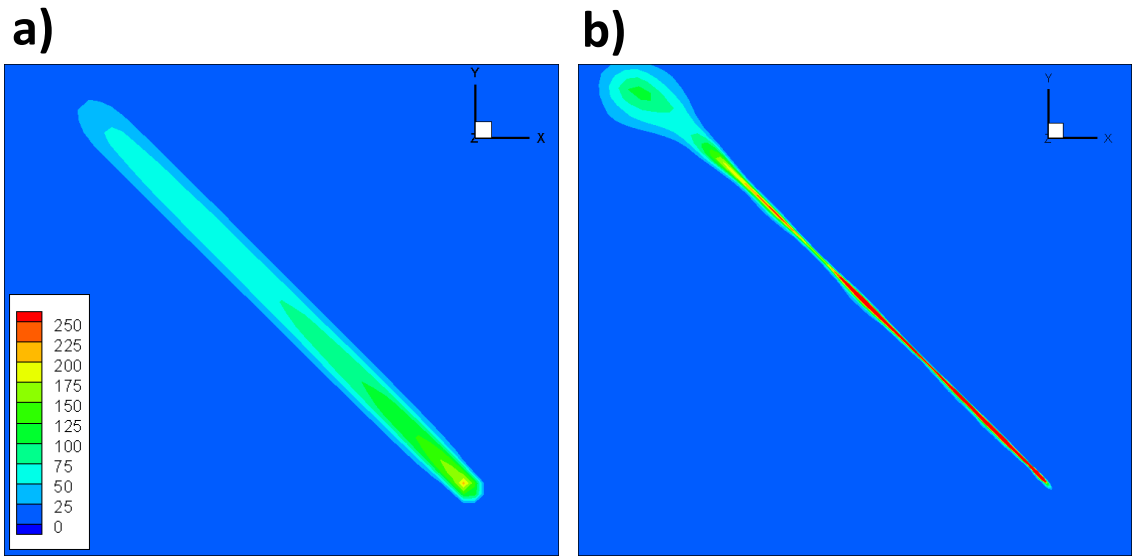

Figure 7.11 Aerial view of EC concentrations (µg m^{-3}) predicted in layer 15 of the modeling domain under uniform southeasterly wind field 11 hours after the start of emissions using (a) fixed grid and (b) adaptive grid.

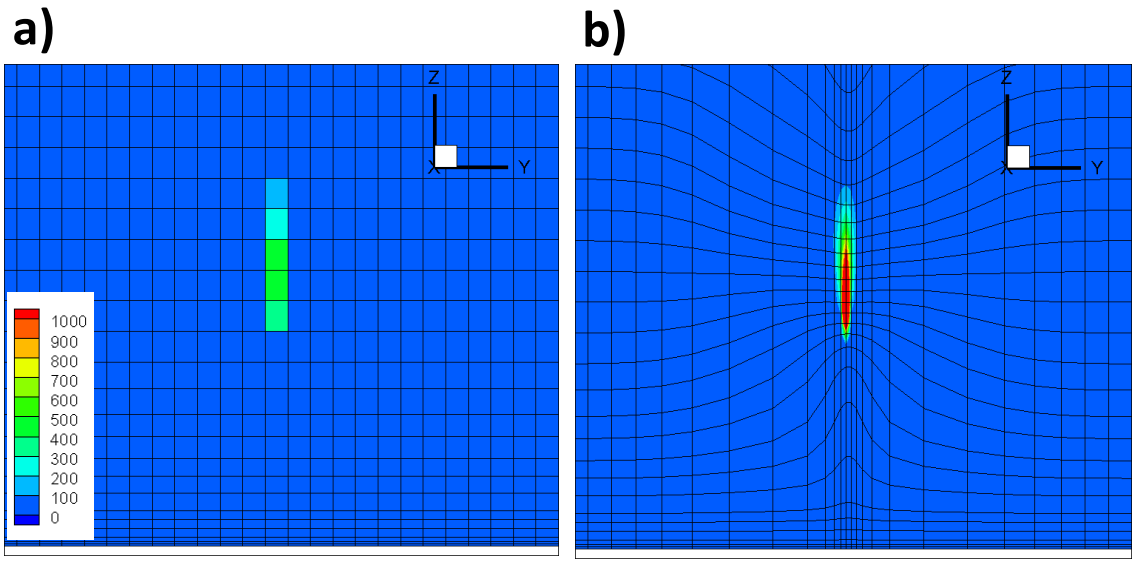

Figure 7.12 Side view of EC concentrations (μg m^{-3}) predicted under uniform vertical wind field 1 hour after the start of emissions using (a) fixed grid and (b) adaptive grid.

Advection of the point source emissions was also simulated on a WRF-generated three-dimensional wind field. Figure 7.13 and 7.14 contrast the pollutant plumes generated using fixed and adaptive grids. Six hours after the initial release of emissions, significant differences between the simulations are apparent from the three-dimensional iso-surfaces included in figure 7.13. Here again emissions in the adaptive grid simulation are initially diffused as refinement begins. However, adaptation quickly leads to a highly concentrated pollution plume. In the fixed grid simulation, the model generates a uniformly shaped plume as emissions are consistently subjected to numerical diffusion. The strong influence of grid adaptation on pollutant concentrations is clear near the point source. Figure 7.14 compares the initial 20 km of the simulated plumes. Like in the uniform wind field simulation, the adaptive grid captures higher concentrations and drastically reduces numerical diffusion. However, the effect is short-lived as high concentrations are dispersed by winds after traveling for a brief period.

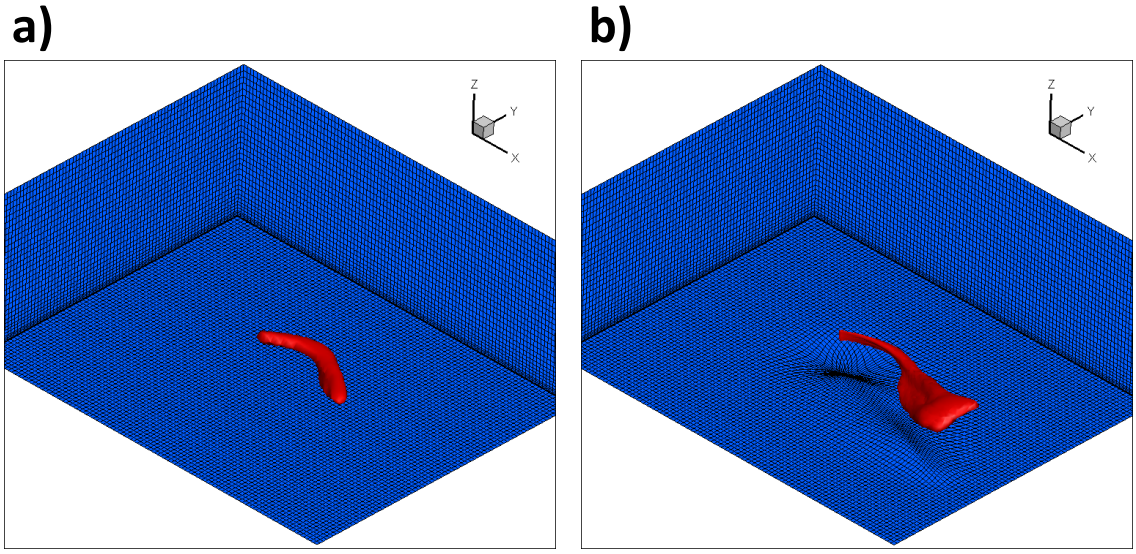

Figure 7.13 Three-dimensional iso-surfaces bounded by EC concentration equal to 10 µg m^{-3} simulated 6 hours after the start of emissions using (a) fixed grid and (b) adaptive grid.

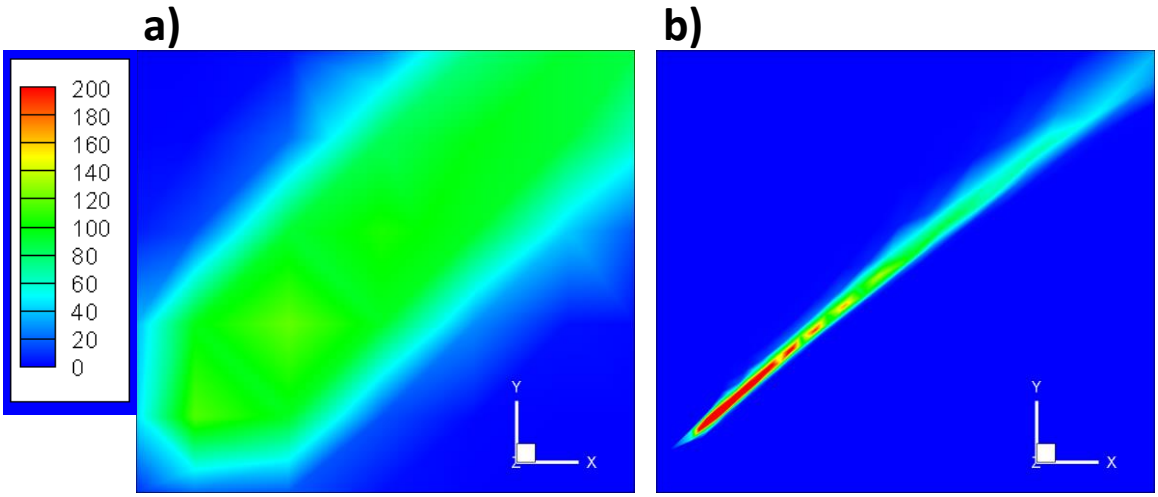

Figure 7.14 Aerial views of EC concentrations (µg m^{-3}) predicted 8 hours after the start of emissions approximately 2000 m above the ground using (a) fixed grid and (b) adaptive grid.

7.7 Discussion and Recommendations

A three-dimensional adaptive grid algorithm applicable to Eulerian air quality models has been described. The mesh-moving algorithm may be especially well-suited

for chemical transport models developed under the assumption of structured grids. Additionally, a coordinate transformation can be used to apply solution algorithms designed exclusively for uniform or symmetrical grids on an irregular refined grid. The three-dimensional algorithm is the first adaptive grid method designed for regional-scale air quality models to simultaneously refine horizontal and vertical grid resolution. Atmospheric simulations featuring concentrated plumes in the free troposphere, as well as plumes near inversions or the top of the boundary layer, would especially benefit from three-dimensional adaptation. Furthermore, the algorithm can refine grids down to very high resolutions and may aid in ultimately eliminating subgrid scale treatments and embedded models, designed to capture small-scale processes relevant to atmospheric plumes, from regional-scale chemical transport models.

A vertically constrained adaptive grid algorithm was also described. In future attempts to apply the adaptation algorithm in air quality modeling, vertically constraining adaptation is highly recommended. In the simulations explored within this chapter, the vertically constrained algorithm produced results that were very similar to those obtained with unconstrained three-dimensional adaptation. However, important advantages are associated with the vertically constrained method, including compatibility with process treatments designed for stacks of cells and simpler interpolation and redistribution procedures. The benefits of vertically constrained adaptation appear to substantially outweigh the costs associated with reduced adaptation flexibility.

The advection tests carried out in this study demonstrate the potential of adaptive grid modeling to capture concentration gradients from concentrated plumes that are lost in fixed grid simulations. The ability of adaptive grid models to replicate detailed gradients and reduce the artificial mixing associated with coarse grids may improve the treatment of nonlinear processes in chemical transport models. However, adaptive grid simulations will continue to be constrained by the resolution and accuracy of the meteorological data used in air quality modeling. High-resolution meteorological fields

commensurate with the resolution of the air quality modeling grid are needed to replicate small-scale dynamics. As long as coarse resolution meteorological fields are used in adaptive grid air quality modeling, the benefits of grid refinement may be limited to more accurate nonlinear processes and reduction of numerical diffusion.

The use of global interpolation algorithms in solution field redistribution procedures is highly recommended for future applications of three-dimensional grid refinement. Global interpolation would greatly benefit three-dimensional adaptive grid simulations for three key reasons: (1) artificial diffusion associated with local interpolation algorithms, such as the one used in this study, is eliminated; (2) the computational demand of solution redistribution operations in iterative methods may be significantly reduced; and (3) grid convergence and optimal grid configurations are more efficiently realized. In the advection simulations carried out in this study, most of the computational burden imposed by the adaptive grid algorithm was related to solution redistribution operations with local interpolation algorithms. Grid convergence in the iterative adaptation process was hard to achieve and frequently relied on programmed constraints to halt adaptation. Excessive refinement was an important concern in several test simulations, but may be difficult to avoid with the current formulation of the adaptive grid algorithm if a local interpolation scheme is applied.

Most importantly, the benefits of grid refinement can be largely negated by local interpolation algorithms that continuously diffuse solution fields in iterative adaptation methods. In the two-dimensional adaptive grid simulations carried out in Garcia-Menendez et al. (2010), grid refinement improved modeling predictions in spite of the use of a local interpolation algorithm. However, in the three-dimensional adaptive grid advection simulations described in this work local interpolation of concentration fields significantly hindered model performance and rendered the use of the model's horizontal and vertical diffusion modules unfeasible. Although, a complex global interpolation algorithm may be needed to carry out the solution field redistribution operations required

by a three-dimensional adaptive grid algorithm, the procedure can be significantly simplified by applying vertically constrained adaptation. In future attempts to apply the three-dimensional adaptive grid algorithm in air quality simulations the use of global interpolation algorithms along with vertically constrained adaptation is highly recommended. By applying these methods, full implementation of three-dimensional adaptation in air quality models will take a significant step forward.

7.8 References

Baker, T.J. (1997) Mesh adaptation strategies for problems in fluid dynamics. Finite Elements in Analysis and Design 25, 243-273.

Banta, R.M., Olivier, L.D., Holloway, E.T., Kropfli, R.A., Bartram, B.W., Cupp, R.E., Post, M.J. (1992) Smoke-Column Observations from Two Forest Fires Using Doppler Lidar and Doppler Radar. Journal of Applied Meteorology 31, 1328-1349.

Byun, D., Schere, K.L. (2006) Review of the governing equations, computational algorithms, and other components of the models-3 Community Multiscale Air Quality (CMAQ) modeling system. Applied Mechanics Reviews 59, 51-77.

Colella, P., Woodward, P.R. (1984) The piecewise parabolic method (PPM) for gas-dynamical simulations. Journal of Computational Physics 54, 174-201.

Constantinescu, E.M., Sandu, A., Carmichael, G.R. (2008) Modeling atmospheric chemistry and transport with dynamic adaptive resolution. Computational Geosciences 12, 133-151.

Garcia-Menendez, F., Odman, M.T. (2011) Adaptive Grid Use in Air Quality Modeling. Atmosphere 2, 484-509.

Garcia-Menendez, F., Yano, A., Hu, Y., Odman, M.T. (2010) An adaptive grid version of CMAQ for improving the resolution of plumes. Atmospheric Pollution Research 1, 239-249.

Ghorai, S., Tomlin, A.S., Berzins, M. (2000) Resolution of pollutant concentrations in the boundary layer using a fully 3D adaptive gridding technique. Atmospheric Environment 34, 2851-2863.

Liang, Q., Jaegle, L., Jaffe, D.A., Weiss-Penzias, P., Heckman, A., Snow, J.A. (2004) Long-range transport of Asian pollution to the northeast Pacific: Seasonal

variations and transport pathways of carbon monoxide. Journal of Geophysical Research-Atmospheres 109.

Rao, S.T., Galmarini, S., Puckett, K. (2010) Air Quality Model Evaluation International Initiative (AQMEII): Advancing the State of the Science in Regional Photochemical Modeling and Its Applications. Bulletin of the American Meteorological Society 92, 23-30.

Skamarock, W.C., Klemp, J.B., Dudhia, J., Gill, D.O., Barker, D.M., Duda, M.G., Huang, X.-Y., Wang, W., Powers, J.G., (2008) A description of the Advanced Research WRF version 3, Tech. Note, NCAR/TN-475+STR. Natl. Cent. for Atmos. Res., Boulder, Colorado, USA.

Srivastava, R.K., McRae, D.S., Odman, M.T. (2000) An adaptive grid algorithm for air-quality modeling. Journal of Computational Physics 165, 437-472.

Tomlin, A., Berzins, M., Ware, J., Smith, J., Pilling, M.J. (1997) On the use of adaptive gridding methods for modelling chemical transport from multi-scale sources. Atmospheric Environment 31, 2945-2959.

Tomlin, A.S., Ghorai, S., Hart, G., Berzins, M. (2000) 3-D Multi-scale air pollution modelling using adaptive unstructured meshes. Environmental Modelling & Software 15, 681-692.

CHAPTER 8

SUMMARY OF CONCLUSIONS AND FUTURE RESEARCH DIRECTIONS

8.1 Conclusions

Eulerian chemical transport models are an attractive option to simulate the transport and transformation of fire emissions. However, current regional-scale systems may be ineffective as an air quality forecasting tool when applied to simulate regional-scale transport of fire-related smoke. This may be especially true for simulations involving long- or regional-scale smoke transport from multiple wildfires over a prolonged period. To varying degrees, several elements of the modeling system contribute to the errors in simulated pollutant concentrations, including fire-related emissions, meteorological inputs, grid resolution, and the vertical distribution of fire emissions.

Significant uncertainties are associated with fire emissions estimates and their distribution on gridded modeling domains. $PM_{2.5}$ concentrations predicted by a regional-scale air quality model in simulations attempting to replicate fire-related air quality episodes are highly sensitive to plume rise, and more specifically to emissions injection altitude relative to the boundary layer. The model predictions are also responsive to the horizontal and temporal distribution of fire emissions on gridded domains. In addition to representative estimates of emitted mass, effectively modeling smoke transport with chemical transport models depends on an accurate spatiotemporal allocation of emissions.

Uncertainty in meteorological fields derived from numerical weather prediction systems can propagate strongly through atmospheric chemical transport models and may

constrain their ability to replicate the effects of wildland fires on air quality. Fire-related air quality predictions from a regional-scale air quality model proved to be extremely sensitive to meteorological fields. For such an application, model performance largely depends on the accuracy of wind inputs. More importantly, simulated pollutant concentrations displayed large sensitivities to variations in wind fields well within the uncertainty range of numerical weather prediction systems. Errors associated with wind data may account for large discrepancies frequently detected between observed and predicted $PM_{2.5}$ concentrations. Normalized errors in simulations attempting to predict the regional impacts of fires on $PM_{2.5}$ concentrations could be as high as 100% due to inaccuracies in wind data. In the simulation of a severe fire-related air quality episode, the influence of uncertainty in wind inputs on concentration predictions substantially outweighed the effect of all other sources of error identified, including uncertain emission rates. This suggests that fire-related regional-scale air quality simulations are limited by the performance of existing numerical weather models. Additionally, as air quality modeling moves towards finer grid resolution, errors associated with meteorological inputs can be expected to constrain accuracy even further.

Adaptive grid modeling is an appealing method to simulate atmospheric plumes in chemical transport models, including fire-related emissions. An adaptive grid algorithm was implemented in the Community Air Modeling System (CMAQ). The algorithm allows dynamic, solution-adaptive grid refinement that can efficiently modify resolution in response to any variable or parameter. In an evaluation simulation aiming to reproduce smoke transport from two controlled fires to an urban area, the adaptive grid algorithm reduced artificial diffusion, produced better defined plumes, and led to more accurate $PM_{2.5}$ concentrations with respect to observations. Additionally, a three-dimensional adaptive grid algorithm capable of simultaneously refining horizontal and vertical grid resolution was presented. Extremely fine grid resolution can be achieved using this grid refinement method. In initial advection tests, the three-dimensional

algorithm was able to efficiently increase grid resolution along concentration gradients and capture features of elevated emissions that were rapidly lost in fixed grid simulations. Ongoing development and refinement of the three-dimensional adaptive grid algorithm would greatly benefit from replacing local interpolation schemes with global interpolation algorithms. Beyond improved predictions of fire-related impacts on air quality, adaptive grid modeling may improve understanding of atmospheric processes.

8.2 Future Research Directions

8.2.1 Simulating the air quality impacts of wildland fires with two-way coupled meteorology-air quality models

The strong influence of meteorological data on air quality predictions from simulations attempting to replicate the effects of fires with regional-scale chemical transport models was extensively discussed in Chapter 5. The modeling system used throughout this work, described in Chapter 2, uses one-way coupling between a meteorological model and the system's chemical transport model. In the past, the feedback of air pollution to atmospheric dynamics has been regularly ignored by air quality modelers. However, the impacts of atmospheric concentrations on weather, by altering the radiation budget and cloud formation, are also accepted (Grell and Baklanov, 2011). The feedback to meteorology may be particularly important in simulations centered on wildland fires, where high aerosol loads could lead to significant changes in planetary boundary layer height, photolysis rates, and temperature profiles. The effects of fires on these meteorological variables would subsequently influence air quality predictions. In addition, heat released by fires may directly affect microscale meteorology.

Recently, operational systems that allow two-way coupled air quality and meteorological modeling have become available, either as meteorological models that

include an air quality component or as coupled independent models that continuously exchange feedback. The Weather Research and Forecasting model coupled with chemistry (WRF-Chem) simultaneously simulates meteorology and the transport and transformations of trace gases and aerosols (Grell et al., 2005) and has been used to explore the effects of fire emissions on weather forecasts (Grell et al., 2011). WRF-Chem simulations investigating the influence of fire emissions on ozone photochemistry have also suggested that two-way coupling may be necessary to better predict the air quality impacts of large fires (Jiang et al., 2012). Similarly, the latest release of the Community Multiscale Air Quality modeling system (CMAQ) enables two-way coupling between CMAQ's chemical transport model and the Weather Research and Forecasting model (WRF) (Wong et al., 2012). Two-way coupled systems offer an extremely interesting framework to carryout simulations investigating fire-related plumes. Through online modeling, it may be possible to capture the effects of fires on smoke transport and plume rise. The benefits of two-way coupling would likely be heightened in high-resolution air quality simulations. Smoke episode simulations, diagnostic model evaluations, and uncertainty analyses similar to those undertaken here should be carried out under a two-way coupled framework to gain additional insight into fire-related air quality impacts and improve the ability of chemical transport models to replicate the phenomenon.

8.2.2 Adaptive grid modeling beyond smoke transport

Here, adaptive grid air quality modeling is used to simulate smoke transport from wildland fires. The analyses completed focused on primary fine aerosol emissions and mostly ignored chemical transformations. However, high resolution may greatly improve the representation of chemical transformations in simulations involving concentrated plumes. Simulations exploring the impacts of fires on ozone concentrations or secondary organic aerosol formation would benefit from adaptive grid refinement. The assumption of immediate and complete mixing within grid cells made by chemical transport models

may lead to errors in estimated chemical reaction rates. For power plant or industrial stacks, plume-in-grid models embedded within chemical transport models have been used to better simulate fine-scale mixing and concentration gradients. However, a highly refined grid could lead to improved estimates of chemical transformation rates. The influence of high-resolution on the chemical evolution of fire-related emissions predicted by chemical transport models should be further explored with adaptive gridding. Beyond wildland fires, adaptive grid models may be especially advantageous in simulations of industrial and urban pollution plumes. In simulations with highly concentrated and reactive pollutants, the advantages of adaptive grid refinement could be substantial.

8.2.3 Simulating the long-range transport of pollutants with adaptive grid models

The simulations within this work have focused on regional-scale transport of relatively short-lived plumes. Additionally, the analyses have mostly centered on transport within the planetary boundary layer. However, plumes may displace air pollutants on a global scale. For instance, intercontinental transport of pollution has been identified for emissions from North America impacting air quality over Europe (Li et al., 2002) and East Asian emissions impacting air pollution levels in North America (Jaffe et al., 1999). Furthermore, advection in the free troposphere is an important mechanism in long-range transport of pollution (Liang et al., 2004).

Global chemical transport models have been used to simulate the air quality impacts of emissions transported over large scales (Fairlie et al., 2007; Wild and Akimoto, 2001; Yienger et al., 2000). Simulations of this nature could greatly benefit from high-resolution adaptive grid techniques such as those discussed in this work. Adaptive grid air quality models may reach their full potential in long-range plume simulations for a number of reasons: grid resolution in global or hemispheric simulations is further constrained by computational resources; vertical resolution in chemical transport models is typically coarser in the free troposphere than the boundary layer; and

spatial and temporal scales are substantially larger. Under these conditions, the ability of chemical transport models to capture atmospheric plumes may be significantly limited. Adaptive gridding in regional-scale air quality models should be applied to explore pollutant transport across the largest scales applied to these systems and atmospheric plumes lofted into the free troposphere. Additionally, the implementation of adaptive grid methods in established global chemical transport models remains an attractive prospect.

8.2.4 A rectangular three-dimensional adaptive grid algorithm

The adaptive grid algorithm applied in this work uses an r-refinement (mesh-moving) method, which allows nodes to reposition while retaining grid structure. Alternatively, h-refinement methods modify the structure of a grid by changing the number of cells, yet allow refinement to occur into self-similar elements or cells with specific geometries. As discussed in Chapter 5, advantages and drawbacks are associated with implementing either method into operational Eulerian air quality models. Still, neither method has achieved widespread acceptance by air quality modeling communities.

A major limitation of the h-refinement approach is that current air quality modeling systems generally use solution algorithms designed for structured grids. Modifying the procedures within existing models to allow simulations on unstructured grids would be a major undertaking and entail extensively redesigning a model. On the other hand, r-refinement may be incompatible with existing solution algorithms designed to operate on uniform or rectangular grids. As described in this work, the restriction may be overcome by applying a coordinate transformation. However, fully transforming the numerical solution schemes included in the model is not a simple task and may not be possible for all processes or parameterizations. In addition, redistribution and interpolation operations on nonuniform grids with irregular cells may be complex and

computationally intensive, especially for three-dimensional refinement, largely negating the benefits provided by the adaptive grid model.

An adaptive grid method that may be practical within current operational air quality models is a *rectangular* r-refinement algorithm. The method combines advantages of r- and h-refinement algorithms previously explored in air quality models and is illustrated in Figure 8.1. The rectangular algorithm would operate by dynamically repositioning grid lines instead of nodes. By doing so, the structure and topography of a grid stay intact, grid cells remain symmetrical, and orthogonality is preserved. Compared to other adaptive grid methods, refinement in rectangular adaptation is more rigid. However, the advantages of the method may outweigh the loss in flexibility. The algorithm is compatible with numerical schemes designed for structured grids. No coordinate transformation is necessary for existing solution algorithms. These must simply include the capability to handle nonuniform grids, which remain symmetrical and orthogonal. Redistribution and interpolation operations on rectangular grids are simpler and their computational demand is minor compared to nonrectangular r-refinement methods. Furthermore, global interpolation algorithms may be effortlessly applied to redistribute solution fields, further decreasing the computational burden of the algorithm and easing weight and grid convergence calculations. A rectangular adaptive grid algorithm, although less elegant and more restrictive, may still provide efficient refinement and fulfill its purpose of increasing solution accuracy. More importantly, the simplicity of the method and congruity with well-established chemical transport models may encourage air quality modeling communities to finally adopt adaptive gridding.

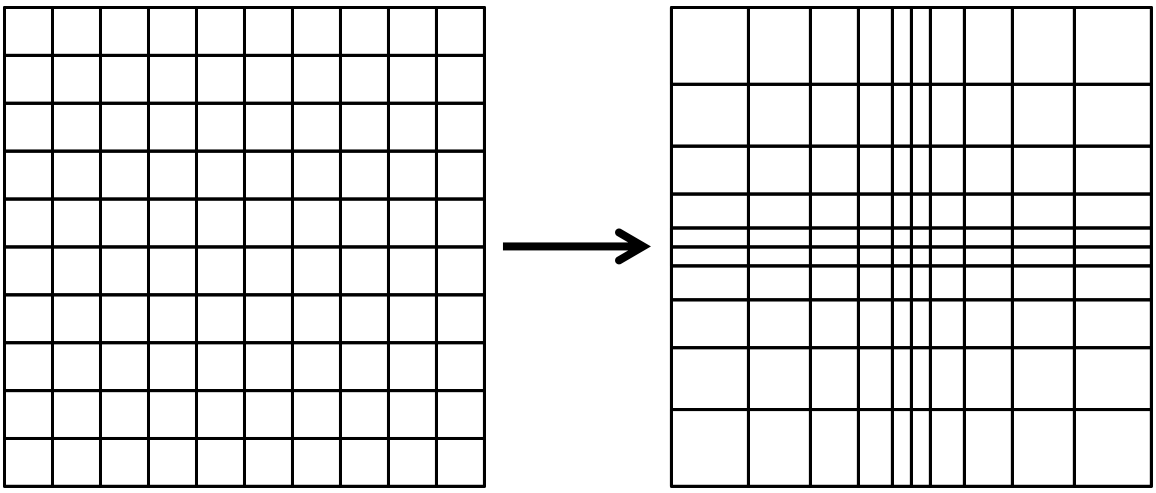

Figure 8.1. Rectangular r-refinement.

8.3 References

Fairlie, T.D., Jacob, D.J., Park, R.J. (2007) The impact of transpacific transport of mineral dust in the United States. Atmospheric Environment 41, 1251-1266.

Grell, G., Baklanov, A. (2011) Integrated modeling for forecasting weather and air quality: A call for fully coupled approaches. Atmospheric Environment 45, 6845-6851.

Grell, G., Freitas, S.R., Stuefer, M., Fast, J. (2011) Inclusion of biomass burning in WRF-Chem: impact of wildfires on weather forecasts. Atmospheric Chemistry and Physics 11, 5289-5303.

Grell, G.A., Peckham, S.E., Schmitz, R., McKeen, S.A., Frost, G., Skamarock, W.C., et al. (2005) Fully coupled "online" chemistry within the WRF model. Atmospheric Environment 39, 6957-6975.

Jaffe, D., Anderson, T., Covert, D., Kotchenruther, R., Trost, B., Danielson, J., et al. (1999) Transport of Asian air pollution to North America. Geophysical Research Letters 26, 711-714.

Jiang, X., Wiedinmyer, C., Carlton, A.G. (2012) Aerosols from Fires: An Examination of the Effects on Ozone Photochemistry in the Western United States. Environmental Science & Technology 46, 11878-11886.

Li, Q.B., Jacob, D.J., Bey, I., Palmer, P.I., Duncan, B.N., Field, B.D., et al. (2002) Transatlantic transport of pollution and its effects on surface ozone in Europe and North America. Journal of Geophysical Research-Atmospheres 107.

Liang, Q., Jaegle, L., Jaffe, D.A., Weiss-Penzias, P., Heckman, A., Snow, J.A. (2004) Long-range transport of Asian pollution to the northeast Pacific: Seasonal variations and transport pathways of carbon monoxide. Journal of Geophysical Research-Atmospheres 109.

Wild, O., Akimoto, H. (2001) Intercontinental transport of ozone and its precursors in a three-dimensional global CTM. Journal of Geophysical Research-Atmospheres 106, 27729-27744.

Wong, D.C., Pleim, J., Mathur, R., Binkowski, F., Otte, T., Gilliam, R., et al. (2012) WRF-CMAQ two-way coupled system with aerosol feedback: software development and preliminary results. Geosci. Model Dev. 5, 299-312.

Yienger, J.J., Galanter, M., Holloway, T.A., Phadnis, M.J., Guttikunda, S.K., Carmichael, G.R., et al. (2000) The episodic nature of air pollution transport from Asia to North America. Journal of Geophysical Research: Atmospheres 105, 26931-26945.